Subcontract NP-1

WANL-TME-1506
30 September 1966

Westinghouse Astronuclear Laboratory

A REVIEW OF NERVA FLIGHT SAFETY SOURCE TERM INFORMATION

(TITLE UNCLASSIFIED)

[redacted]

Subcontract NP-1

WANL-TME-1506

30 September 1966

Westinghouse Astronuclear Laboratory

A REVIEW OF NERVA FLIGHT SAFETY SOURCE TERM INFORMATION

(TITLE UNCLASSIFIED)

Doc
17.c

[redacted]

Prepared by:
W.S.Brown
J.M.Bridges, Supervisor
Physical Sciences
Nuclear Systems Applications

[redacted]

DISTRIBUTION OF THIS DOCUMENT IS UNLIMITED

TABLE OF CONTENTS

BLANK PAGE

TABLE OF CONTENTS (CONTINUED)

TABLE OF CONTENTS (CONTINUED)

TABLE OF CONTENTS (CONTINUED)

LIST OF ILLUSTRATIONS

LIST OF ILLUSTRATIONS (CONTINUED)

LIST OF ILLUSTRATIONS (CONTINUED)

LIST OF TABLES

BLANK PAGE

LIST OF TABLES (CONTINUED)

CHAPTER 1.0

SUMMARY

This document is a status report on the NERVA Source Term Program, which is part of the overall ROVER Flight Safety Program. This latter program has as its purpose the evaluation of the potential radiological safety problems arising from an in-flight abort of a nuclear propelled rocket vehicle and the development of safety countermeasures which will be effective in minimizing these problems. A number of governmental agencies and industrial organizations have participated in the ROVER safety studies. The Source Term Program is concerned with the correlation of the information pertaining to the radiological safety problems resulting from re-entry and earth impaction of radioactive materials generated during flight operations of NERVA-type nuclear rocket engines. Such information encompasses the following topic areas: accident models and flight failure probabilities of nuclear powered rocket vehicles, the amount and distribution of radioactive debris on the Earth's surface in the event of an in-flight failure, evaluation of flight safety countermeasure systems, interactions of radioactive debris with man and evaluation of the resulting radiological effects, and probable radiation exposure of the world population resulting from nuclear rocket flight operations. "Source Term" reports summarizing this information have been periodically issued. This document summarizes the source term studies and flight safety work performed in the period from September 1964 to September 1966.

The following statements and conclusions are based on the information presented in this report:

1. Estimation of the fission product inventory of the fuel debris impacting the Earth's surface in the event of flight failure, requires the consideration of various fission product loss mechanisms and the operational and post-operational history of the reactor. Fission product losses from the fuel can occur by diffusion, corrosion, and re-entry burnup. Under normal (design) operating conditions total loss of fission products from NERVA reactors by diffusion and corrosion mechanisms will probably not exceed 5 percent of the total inventory

generated. Loss of coolant or reactor excursion accidents would result in significant loss of fission product inventory by diffusion due to the high core temperatures reached. Loss of fission products from fuel fragments by atmospheric burnup and ablation during re-entry is dependent on the size of the fragments. Particles smaller than about 1/32 inch have a maximum of 50 percent burnup with burnup percentage decreasing for larger sized particles.

2. The source term due to neutron activation of the structural and metallic components of a NERVA engine is small in comparison with that due to fission products from the fuel materials. Thus the contribution of activation products to the total radioactive source strength of re-entering debris can be neglected in a safety analysis without introducing significant uncertainties in the analysis.

3. The nature of an in-flight accident and the probability of vehicle system failures during flight must be known in order to define the probable radiation exposures to the population resulting from that accident. Examination of possible flight accident events for an NRX-type engine lead to the selection of a loss-of-coolant situation as being the most severe credible malfunction situation. Based on the present design concept for the NERVA (5000 Mw) reactor, there do not appear to be any flow accident situations different from the NRX reactor other than loss-of-coolant to the tie tubes. However, there is still a need for detailed examination and identification of malfunction situations and evaluation of the response of the flight system to such malfunctions.

4. Conservative estimates have been made of the nuclear stage reliability for hypothetical flight missions powered by NRX and NERVA sized engines. These reliability estimates were used to derive a function defining the probability of failure per second during the entire time interval of nuclear powered flight for these missions. These probability functions were used in the safety analysis of these missions to predict expected population radiation dose exposures.

5. If no major countermeasure action is taken following an in-flight loss-of-coolant accident (a "passive" re-entry situation), an NRX-type reactor will spontaneously disassemble due to post-operational heating effects. Axial core support is lost within 20 to 30 seconds due to melting of the tie rods. The lateral core support system fails at about 160 seconds after the loss-of-coolant accident. Under tumbling conditions, fuel elements could be ejected out the nozzle. Between 150 to 550 seconds after loss-of-coolant, tne core support plate is incapable of supporting any loads. During final re-entry, when the re-entry vehicle encounters maximum aerodynamic heating and loading, complete disassembly will occur, with burnup and failure complete at about 95,000 feet altitude.

6. The NERVA (5000 Mw) reactor should maintain its integrity under loss-of-coolant conditions for substantially longer time periods than the NRX based on the present conceptual NERVA design. The effective lifetime of the lateral support system will be determined by the lifetime of the beryllium reflector. Design features of the NERVA reactor to insure integrity for extended time periods under loss-of-coolant conditions are currently under study.

7. Conceptual auxiliary thrust systems (ATS) appear feasible to insure a safe disposal of a failed radioactive nuclear engine. This can be accomplished by either dumping the engine into deep ocean waters or by boosting the engine into a long-lived Earth orbit thereby extending time of radioactive decay to an acceptable value. The conceptual ATS design utilizes multiple solid-propellant rocket motors mounted on the instrument unit at the forward end of the hydrogen propellant tank of the nuclear stage. Use is made of the thrust obtained by controlled dumping of the liquid hydrogen propellant remaining in the NERVA propellant tank. The successful use of an ATS system assumes integrity of the

reactor up to and during the time of application of the auxilliary thrusting action. Therefore, reactor integrity following loss-of-coolant accidents must be assured if the ATS system is to be a successful safety countermeasure.

3. An explosive destruct test of a full scale mockup of a NERVA-NRX reactor has provided the best available data on the expected fragmentation of the reactor core that would result from use of an explosive destruct countermeasure. The detonation of four in-place projectiles located in each quadrant of the core yielded a non-isotropic spatial distribution of the core debris. The measured distribution of fragment numbers, mass, size, velocity, and spatial location have been used to predict the Earth impact patterns of core debris resulting from application of an in-flight explosive destruct countermeasure. Analyses have shown that for a critical 10 second time interval of a NERVA sub-orbit start trajectory in which a failure would result in African impact under passive re-entry conditions, explosive destruct utilized during the first four seconds of the interval could result in all debris impacting in the ocean. However, this avoidance of land deposition of the debris can be accomplished only if the destruct action is initiated over a very narrow range of reactor attitudes. For failure times later than the first four seconds, some land impact of debris will occur regardless of reactor attitude.

9. Fragmentation of the NERVA core by a self-induced nuclear excursion offers a potential safety countermeasure technique. Experimental and analytical studies performed to date indicate that for a reactor period of 0.6 msec or less, there exists a definite threshold in the energy required to fragment NERVA fuel material, and that this threshold lies somewhere in the range of 1.7×10^{15} to 5×10^{15} fissions per gram U-235. This threshold is reduced with increasing fuel temperature. The current design of the NERVA and NRX reactors do

not appear to have the inherent capability of undergoing such excursions as the result of a reactor malfunction. Additional studies are needed to determine the mechanical feasibility and engineering problems associated with the reactivity insertion requirements.

10. Evaluation of the radiological safety problems originating from nuclear rocket engine debris requires information on the interaction of the radioactive debris with man and the manner and extent to which absorbed ionizing radiation is distributed in man. Suitable analytical models have been developed for use within the ROVER safety program which define the probabilities of exposure of a receptor to the debris. Also, specialized radiological dose models have been derived for calculating either gamma ray exposures or the beta and gamma dose delivered from contact with a debris particle.

11. Safety analyses have been made for three hypothetical nuclear vehicle flight missions. The relative effectiveness of safety countermeasures to enhance the safeness of the mission is quantitatively expressed in terms of the maximum possible and the expected (probable) number of persons in the general population exposed to specified radiation dose levels. A direct comparison of population exposures received under passive re-entry conditions and for the destruct and ouxiliary thrust system countermeasures is not possible because different dose exposure models and analysis conditions were used. Preliminary analyses comparing explosive destruct and nuclear (self) destruct countermeasures, indicate that the whole body gamma dose exposures from nuclear destruct may be fifty times greater than those exposures resulting from explosive destruct. This analyses is based on presently available data which may not represent the final requirements for nuclear destruct or may not adequately reproduce the conditions that exist with a flight configuration system. Thus this comparison between the two destruct countermeasures cannot be evaluated with a high degree of confidence.

CHAPTER 2.0
INTRODUCTION

Nuclear safety plays a particularly important role in the utilization of space nuclear propulsion systems. As a result, since its inception considerable attention has been paid to safety within the ROVER program. The safety effort has been primarily directed toward two major areas: (1) evaluation of the potential radiological safety problems arising from a flight mission abort, and (2) the development of safety countermeasures which will serve to minimize these problems. A number of governmental agencies and industrial organizations have participated in the ROVER safety effort. Because of the broad range of information generated within the program, it was deemed desirable to issue periodical Source Term Reports to summarize the work pertinent to the ROVER Flight Safety Program. The designation "Source Term" has been used to describe these reports because of the importance of the radioactive source strength in assessing radiobiological safety problems arising from in-flight failure of a nuclear propulsion system.

The previous Source Term Report was issued September 1964[1]* and reviewed the accomplishments of the ROVER Flight Safety Program to that date. This present document summarizes the work accomplished in the program since the last report, and in particular, uses much of the information published in a series of volumes entitled "ROVER Flight Safety Preliminary Review".[2]

It is hoped that this document will serve as a guide or source book to ROVER Program contractors and others to summarize the present status of flight safety source term information. In addition it provides a compilation of references where more detailed source term information is available. The information included in this report is limited to work items pertinent to the definition and evaluation of radiological hazards resulting from the re-entry and earth impaction of radioactive materials generated during flight operations of NERVA type nuclear rocket engines. The information related to such items as ground handling safety, astronauts and crew safety, disposal of spent rocket engines and mission capabilities is not included, unless specifically related to earth re-entry hazards.

* References are given at the end of each chapter.

BLANK PAGE

2.1 REFERENCES

1. Westinghouse Astronuclear Laboratory, NERVA Source Term Program, WANL-TNR-178, Pittsburgh, Pennsylvania, September 1964 (CRD)

2(a) Lockheed Missiles and Space Company, and the George C. Marshall Space Flight Center, Safety Analysis Report - Evaluation of Destruct and Auxiliary Thrust Systems, Volume I, April 1966 (CRD)

(b) Westinghouse Astronuclear Laboratory and the Space Nuclear Propulsion Office, Cleveland, Safety Analysis Report - Evaluation of Passive Re-entry approach, Volume II, September 1965 (CRD)

(c) Space Nuclear Propulsion Office, Cleveland, Summary Report - Nuclear Rocket Countermeasures, Volume III
Part A - Program Report on the Anti-Criticality Poison Wire System, Westinghouse Astronuclear Laboratory; September 1965 (CRD)
Part B - Post Operational Destruct System, Picatinny Arsenal; December 1965 (CRD)
Part C - The Self-Destruct Concept for Post-Operational ROVER Reactor Disposal, Los Alamos Scientific Laboratory; April 1966 (CRD)

(d) U. S. Naval Radiological Defense Laboratory and Nuclear Utility Services, Safety Analysis Report - Radiological Considerations in Nuclear Flight Safety, Volume IV April 1966 (CRD)

(e) Los Alamos Scientific Laboratory, Summary Report - Safety Neutronics for ROVER Reactors, Volume V, October 1965 (CRD)

CHAPTER 3.0

SOURCE TERM DUE TO FISSION PRODUCTS

The fission products that are generated and retained in the reactor fuel provide the major source of radioactivity arising from the operation of a nuclear powered rocket. In order to quantitatively evaluate the source strength of this fuel material, it is necessary to consider the means by which the fission products may be lost from the fuel both during and after reactor operation. The fission product inventory of the fuel debris that impacts on the Earth's surface will depend upon many factors including: reactor operating time, fuel element characteristics, high core temperatures attained in the event of off-design operation, reactor malfunctions or accident occurrence, and the physical state and size of re-entering fuel debris. This section defines various mechanisms and operational modes that affect the fission product source term, and summarizes the experimental and analytical work that has been performed to quantitatively evaluate this source term.

3.1 FACTORS IN EVALUATION OF THE FISSION PRODUCT INVENTORY

The analytical estimation of the fission product inventory remaining in the fuel at any time depends on the accuracy of the mathematical model(s) used for the calculations in representing the actual build-up and loss mechanisms. The build-up and radioactive decay of fission products are calculated using data on the fission yields and decay rates of the various isotopes. Loss mechanisms include diffusion of fission products out of the fuel matrix, corrosion of the graphite fuel by the high temperature hydrogen, and re-entry burnup. The following paragraphs summarize the analytical techniques and the experimental data that have been accumulated in the ROVER flight safety program to estimate quantitatively the fission product activity of NERVA fuel following reactor operation. The application of this data to predict the fission product source term for NERVA reactors following normal or malfunctional operations is given in Section 3.2.

3.1.1 Generation of Fission Product Inventory

The equations for calculating the fission product inventory in a reactor due to fissioning of U^{235} are straight-forward but complex. The production and decay of a particular nuclide is considered to be a combination of the direct formation of the nuclide by fission, and the formation by production and decay of its precursors in the same mass chain. Because of the complexity of the calculations, the equations are usually programmed for high speed digital computer solution.

A number of computer programs are reported in the literature for calculation of fission product abundances and decay energies[1-8]. Within the ROVER Flight Safety Program, data on the U^{235} fission yields and decay chains issued by the U.S. Naval Radiological Defense Laboratory[9] have been used as the standard for calculating fission product abundances. Reference 9 details ninety comprehensive fission chain diagrams, and presents data on fission yields, half lives, and branching ratios for 505 U^{235} fission product nuclides. Also, data are tabulated presenting the activity build-up in curies/megawatt for each of the 505 nuclides for reactor operating times of 1 second to 60 minutes, and post-shutdown inventories for reactor runs of 1, 5, 30, and 60 minutes at 42 post-shutdown times from shutdown to 10^9 seconds. A description of the computer program used by NRDL to calculate fission product abundances has recently been issued[10].

Private industries working within the ROVER Flight Safety Program have developed their own special purpose fission product abundance codes for use within larger computer programs utilized for analysis of nuclear rocket safety. Westinghouse Electric Corporation originally developed its Fission Product Inventory Program (FPIP)[11] to accommodate up to 499 nuclides. Since decay energy spectra data were not available for many nuclides, the program was later revised to include 273 nuclides, with the library data updated to be consistent with that of Reference 9. This revised program has been incorporated into the WANL Source Term Computer Program[12]. A comparison of the results between the 499 and 273 nuclide programs was shown in Reference 13. The 273 nuclides have recently been reduced to 254 nuclides in order to be consistent with the FIPDIF program (See Section

3.1.2.1 below). The library was shortened by deleting very short half-life nuclides from several decay chains without significantly affecting the results. Lockheed Missiles and Space Company has developed their Fission Product Inventory Code (FPIC)[14, 15] which is used as a subroutine in their Nuclear Flight Executive Program[15]. The FPIC program uses a library of 123 nuclides and is similar to the WANL modified FPIP program in that it not only calculates fission product abundances. but also the gamma and beta energy decay rates plus the integrated number of disintegrations, integrated gamma MEV, and integrated beta MEV over any desired time period. NUS Corporation uses its fission product abundance program, FLYASH, in conjunction with a program for Nuclear Rocket Safety Evaluation (NURSE II)[16]. The values of the library constants used in this program are in agreement with the USNRDL standards.

A comparison of the nuclide abundance computer programs of USNRDL, WANL, and LMSC was made in March, 1965 to determine any disagreement in the results of the three programs. The abundances of 55 radiobiologically significant fission products were calculated for a 10-minute run time at 1000 MW, at decay times varying from 10^3 to 10^8 seconds. The results[17] showed nearly perfect agreement between the WANL and NRDL results. THE LMSC results showed some inconsistencies, with the LMSC results generally higher (by a factor of two in a few cases) than the NRDL results. However, the variations were not considered sufficient to introduce significant errors in the interpretation of radiobiological effects. A comparison between the WANL and LMSC results for the gamma energy rate (MEV/sec) and the integrated gamma energy (MEV) showed relative differences of about 15 percent and 5 percent respectively.

As indicated above, the WANL and LMSC computer programs calculate the beta and gamma decay energies of the fission product mixtures as well as the individual nuclide abundances. The gamma energy release rate is divided into seven standard gamma energy groups as follows:

Group	Gamma Energy Range (MEV)
1	0 to 0.40
2	0.41 to 0.90
3	0.91 to 1.35
4	1.36 to 1.80
5	1.81 to 2.20
6	2.21 to 2.60
7	> 2.60

The units of the gamma energy rate are MEV/sec, which is directly related to dose rate. The utilization of gamma decay energy in calculation of gamma doses is discussed in Chapter 7.0.

Similarly, the WANL modified FPIP program calculates the beta energy release rate in five energy groups: 0 to .25, 0.26 to 0.75, 0.76 to 1.25, 1.26 to 1.75, and greater than 1.75 MEV. These energy groups only approximate the true average or expected beta energies of the fission product mixtures since the assumption is made in the program that the average energy of a beta emitter is one-third the maximum beta energy (beta spectrum end point energy). A computer code has been recently developed by NRDL[18] which computes the composite beta spectra and average energies of fission product mixtures by summing the spectra of the individual nuclides weighted according to their abundances. Graphs of the beta spectra for individual negatron emitters have been published by NRDL[19]. A report on the spectra of positron emitters is in preparation by NRDL[20].

In conclusion, there are many computer programs available that accurately calculate the fission product inventories and decay energies as a function of operating time and decay time. However, since mechanisms other than radioactive decay can reduce the fission product inventory of NERVA fuel, use of these programs alone cannot completely define the fission product source term of any fuel debris that re-enters and impacts on the Earth. The inventory losses by other mechanisms are discussed in the subsequent paragraphs.

3.1.2 Mechanisms that Reduce the Fission Product Inventory

Several mechanisms exist for NERVA reactors in which the fission product inventory may be reduced from that generated due to the fissioning process and normal radioactive decay. Loss mechanisms can occur both during reactor operation and in the time period following reactor shutdown. The fission product losses incurred during reactor operation depend mainly on the fuel characteristics and fuel temperatures reached. Loss following reactor shutdown is largely dependent on core after heat temperatures, and the size of the fuel debris re-entering the Earth's atmosphere. The following paragraphs describe the results of studies to define the mechanisms that may reduce the fission product inventory of NERVA fuel. The quantitative reduction expected under different operational conditions is described in Section 3.2.

3.1.2.1 Fission Product Diffusion

Experiments show that certain fission products will diffuse from NERVA fuel at temperatures above 3200°R (1500°C) (silver as low as 1000°C), and the diffusion rate increases sharply above 4632°R (2300°C). The fuel temperatures expected in the NERVA reactor will exceed the 3200°R critical temperature in the exit half of the core and will reach temperatures of about 4460°R (2200°C) at the exit end of the core. In the case of reduced coolant flow or loss-of-coolant due to some malfunction or accident, considerably higher fuel temperatures could be reached. Thus it becomes necessary to determine the extent of diffusion in order to predict the core fission product inventory.

The diffusion of fission product nuclides through a solid matrix is a complex physico-chemical process, whose absolute rate cannot be predicted from a theoretical basis. It is necessary to experimentally measure the diffusion rates of the fission products. During the past three years an extensive program has been in progress to experimentally measure the diffusion rates of the fission products in NERVA fuel. The purpose of these studies is to determine the release of fission products from NERVA fuel as a function of time, temperature, geometry, and environment. The work has progressed in three major areas: (1) experiments to determine the magnitude of fission product release for times and temperatures characteristic

of normal reactor operations, (2) experiments to determine the magnitude of fission product release for times and temperatures that might be expected under accident conditions, and (3) development of means for using the experimental data to predict fission product release for future operations of NERVA reactors under both accident and normal operating conditions. These studies have application for both the flight safety and the ground testing programs of the NRX/XE and NR/NE reactors. For the latter case, the diffusion data have been used to predict the radioactivity released in the effluent gas[21]. The results of the experimental diffusion studies have been documented in a series of comprehensive reports[22-27]. The major results and conclusions from the work performed to date are summarized below.

Fuel Samples Used for Diffusion Measurements. Laboratory measurements of fission product diffusion are made on two basic categories of NERVA fuel samples: (1) samples cut from new fuel elements which are irradiated in an experimental reactor facility, and then subjected to a controlled thermal heating cycle simulating NERVA operating conditions. Following the heating, the fuel is radiochemically analyzed to measure loss of specific nuclides by diffusion; (2) samples cut from the radioactive fuel elements removed from the NRX reactors following full-power testing. Radiochemical analysis of these samples is performed to determine diffusion losses that occurred during reactor operation.

For those experiments involving samples of category 1, four different types of fuel have been utilized. Each of these fuel types represents a different possible diffusion path for the fission product nuclide to escape from the fuel. The four types of samples and their designation are as follows:

1. Type II Fuel. This is a sample cut from the as fabricated fuel with unlined cooling channels, and consists of 100μ-diameter UC_2 beads having a 25μ coating of laminar pyrolytic graphite dispersed homogeneously in a graphite matrix.
2. Type II - NbC Fuel. This is a sample of the Type II fuel which is completely coated with a 2-mil thickness of the NbC coated via a vapor deposition process. This coating represents the barrier through which the fission products must diffuse if escape is to be via the NbC coated coolant channels in full size NERVA fuel elements.

3. Type III Fuel. This is a sample of Type II fuel which has been intentionally heated to 2500°C in vacuum for 30 minutes prior to irradiation. This thermal pretreatment results in degradation of the pyrolytic coating surrounding the fuel bead accompanied by migration of the UC_2 into the graphite matrix. In Type III fuel, the tendency for diffusion is enhanced, since the pyrolytic carbon coating is no longer present to act as a diffusion barrier. Similar thermal degradation could occur in a NERVA reactor in the event of a malfunction or accident condition which caused a reduced or loss of cooling to the core thereby overheating the fuel. Experiments have shown that degradation of the pyrocarbon coating is a time and temperature dependent phenomenon. Irradiated fuel held at 2200°C for 15 minutes shows evidence of degradation as measured by an increased release rate of gross gamma activity[26]. Improved fuel beads with triple laminar pyrographite coatings show enhanced diffusion when held at 2350°C for as little as 5 minutes[28], although photomicrographs show that the fuel bead and coating are still intact with no visible evidence of UC_2 migration into the graphite matrix. Fuel held at 2500°C for 30 minutes, Type III fuel, is completely degraded with complete loss of pyrocarbon as evidenced by photomicrographs.

4. Type III - NbC Fuel. This is a sample of the Type II - NbC fuel which has been irradiated, and then subjected to temperatures above 2200°C to produce degradation of the pyrocoating.

A schematic illustration of the four possible diffusion paths in NERVA fuel, corresponding to these four fuel sample types is shown in Figure 3-1.

Additional fuel samples have been prepared recently to simulate the reactor components and geometry. These samples are defined as unit cells[26], and resemble the geometry of a NERVA fuel cluster assembly to provide identical diffusion path lengths for fission product release. This unit cell is a cluster of 4-inch long segments of NERVA fuel held together with a modified tie rod assembly. The fuel element cluster is contained in a hollow graphite cylinder three inches in diameter.

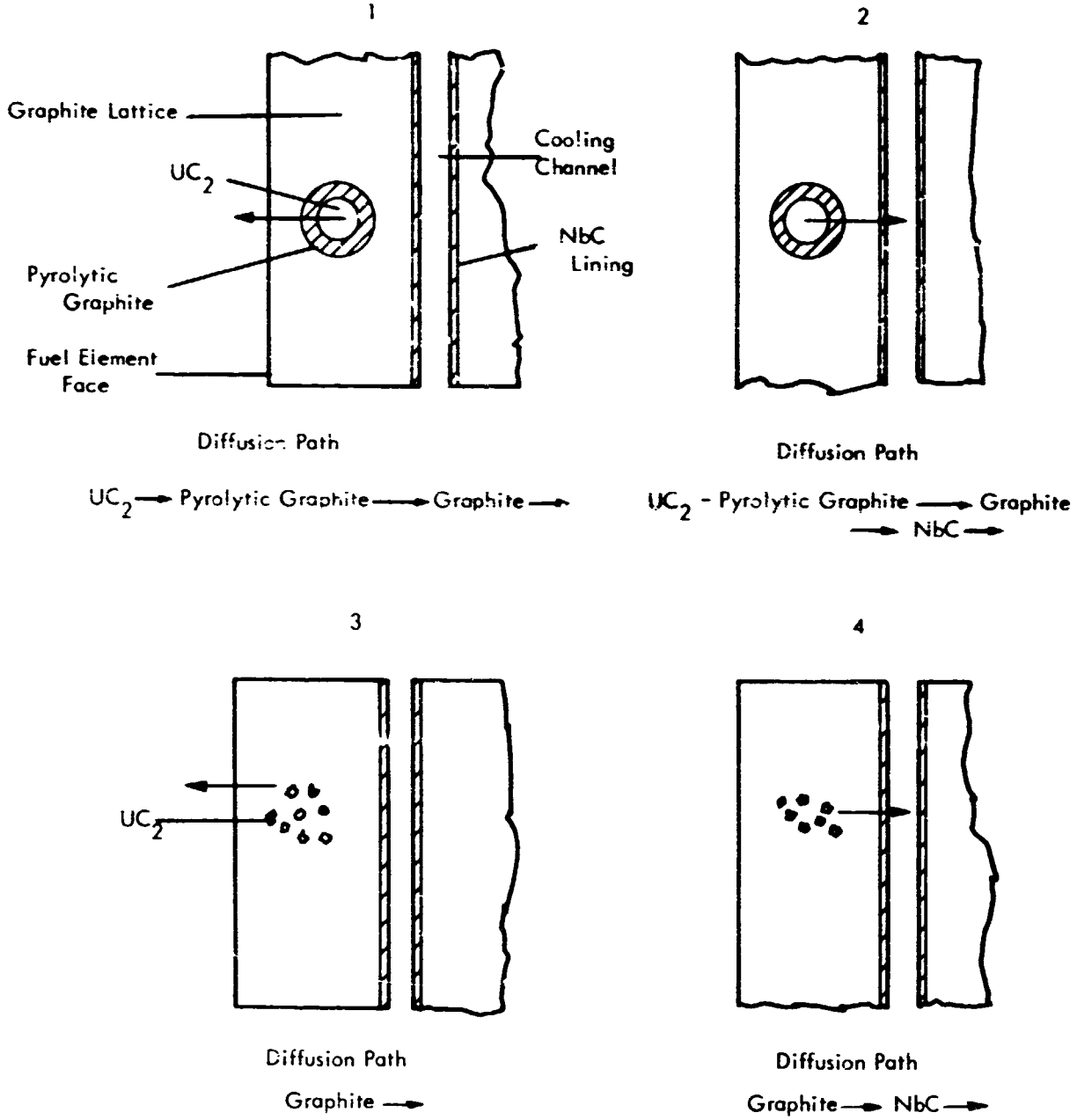

Figure 3-1. Fission Product Diffusion Paths in UC_2 Fuel

Fuel samples for post-operational analysis of the NRX reactors were taken if possible from fuel elements spaced in a radial line from the core center to the periphery. The radioactive elements were sectioned and 1/4-inch slices were taken at several axial locations. The slices near the inlet end of the core were used as control samples since temperatures were no greater than 900°C, and hence suffered no loss of fission products by diffusion. The weight and activity of each fuel element slice were measured, the fuel was dissolved by a technique to insure no loss of fission products, and the solution was diluted to standard volume for subsequent radiochemical analysis.

Experimental Procedure. The fuel samples were 1/4-inch diameter by 1/4-inch high cylinders machined from NERVA fuel elements, or were merely 1/4-inch slices from a fuel element. These samples were irradiated in the GETR, the TREAT reactor, or the reactor at the Westinghouse Reactor Evaluation Center, Waltz Mill, Pa. Following the irradiation, the samples were heated in a vacuum of 10^{-4} mm Hg at temperatures ranging from 3190°R (1500°C) to 5350°R (2700°C) for time intervals up to 30 minutes. A description of the apparatus used for heating these samples is given in References 23 and 24.

The radiochemical analysis results of the heated samples are compared with that of an unheated control sample to determine the extent of release by diffusion of a given fission product nuclide. It is not necessary to analyze for all 254 fission product nuclides comprising the fission product inventory since it is assumed that the diffusion rates of all isotopes of the same chemical element are equal and since 97 percent of the inventory can be represented by 20 elements. The elements and their contribution to the total fission product activity are shown in Table 3-1. In addition to the elements shown in the table, radiochemical analysis has been performed on silver and cadmium which are rapid diffusers.

Results

1. Type II and Type II - NbC. The complete results of diffusion experiments on the uncoated samples are given in Reference 23; results on the NbC coated samples are given in Reference 24.

TABLE 3-1

FISSION PRODUCT ELEMENTS OF INTEREST TO THE DIFFUSION PROGRAM

	Element	Percent Contribution 0 Time After 10 Min Reactor Operation	Percent Contribution 24 hr After 10 Min Reactor Operation
2.	Sr	8.14	6.04
3.	Rb	8.12	0.71
4.	Kr	7.70	1.60
5.	Zr	7.19	6.71
6.	Y	6.19	17.21
7.	Sb	6.18	0.76
8.	Cs	6.02	0.02
9.	Xe	5.89	13.32
10.	I	4.74	15.47
11.	Br	4.37	0.30
12.	Ba	4.29	0.88
13.	Te	3.67	3.34
14.	Ce	3.59	5.69
15.	La	3.41	3.19
16.	Te	2.85	2.60
17.	Mo	2.61	3.19
18.	Sn	1.25	0.01
19.	Pr	0.46	3.75
20.	Ru	0.10	0.75
		$\sum$96.7	$\sum$98.9

The NbC coating had an inhibiting effect on the release of most fission products. A comparison between the release of various fission products from uncoated and NbC coated Type II fuel is given in Figure 3-2. The reduction in release varies from 17 percent for Sr^{89} to 57 percent for Y^{91} for samples heated at 2200°C for five minutes. An overall reduction of 46 percent was found for the gross release of the fission product inventory.

2. Type III and Type III - NbC Fuel. Complete data on the release of fission products from Type III fuel are given in Reference 24. For most nuclides there was a greater release from Type III fuel than Type II. However, no release of Mo^{99} or Zr^{95} was found under the most severe test conditions, 2300°C for 30 minutes. Conversely, Ag^{111}, Sr^{89}, and Ba^{140} were completely released during the same test conditions.

The difference in the release fractions for the two fuel types is shown in Figure 3-3. The most significant differences in release between the two fuel types were for Sn^{125}, Te^{129}, and I^{131}. In Type II fuel, no release of these nuclides occurred at 1800°C, whereas, appreciable release occurs for all three nuclides in Type III fuel at this temperature. It has been determined that diffusion from Type III fuel can be represented by assigning the elements to one of eleven diffusion groups.

Complete data on the release fractions of fission products from Type III - NbC are given in Reference 26. For most nuclides there was an inhibiting effect on the release from these coated samples as compared with uncoated samples heated under similar conditions. A comparison between the release from coated and uncoated Type III fuel is shown in Figure 3-4. The reduction in release varied from 4.5 percent for Sr^{89} to 60.2 percent for La^{140}, for samples heated at 2400°C for 5 minutes. Te^{129} was an exception to the general trend; for this nuclide greater release was obtained with coated rather than uncoated samples. This may be due to exchange problems in radiochemical analyses. There is no reason for NbC to enhance tellurium release.

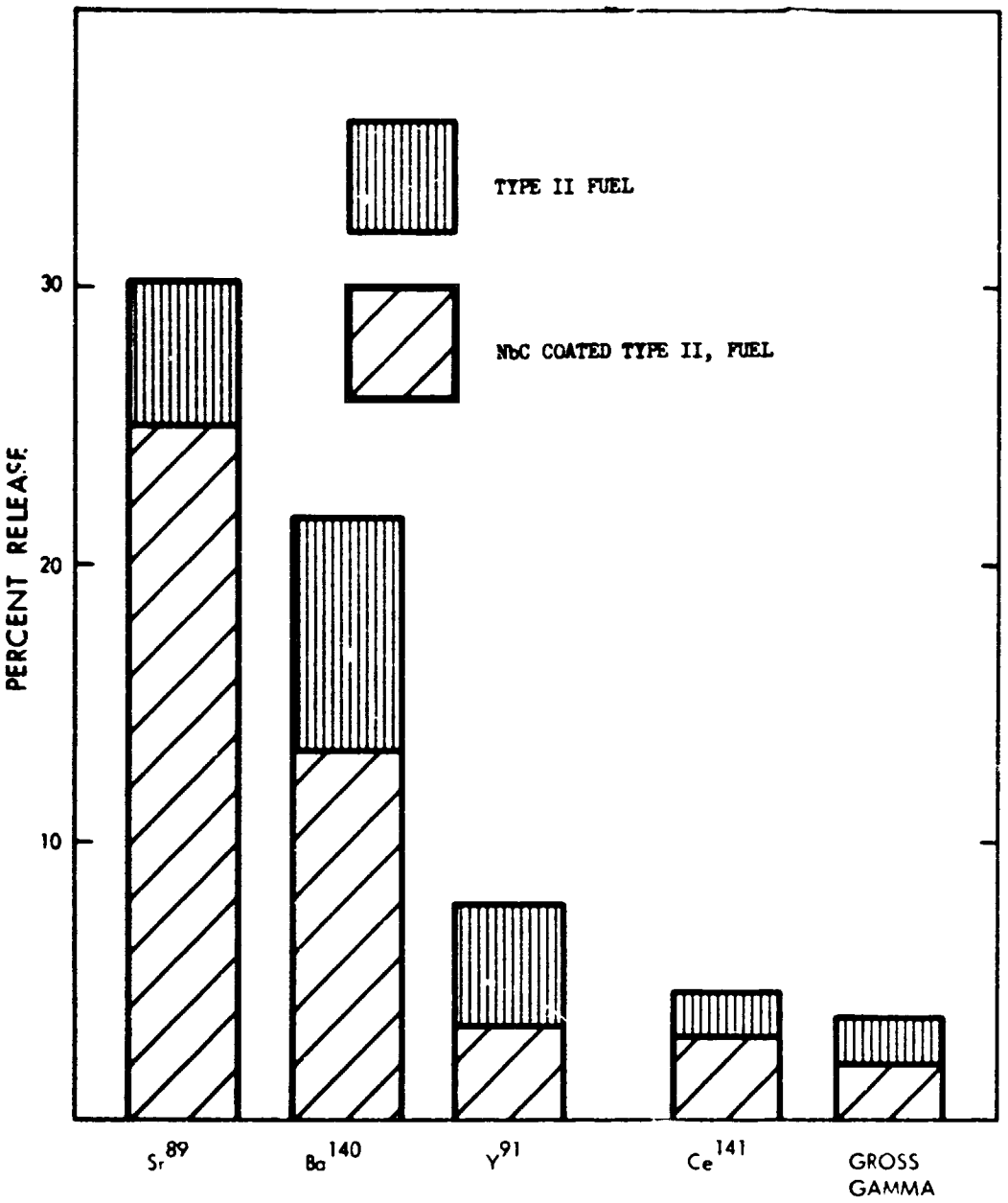

Figure 3-2. Comparison of Fission Product Release from Type II Fuel and NbC Coated Type II Fuel 2200°C for Five Minutes

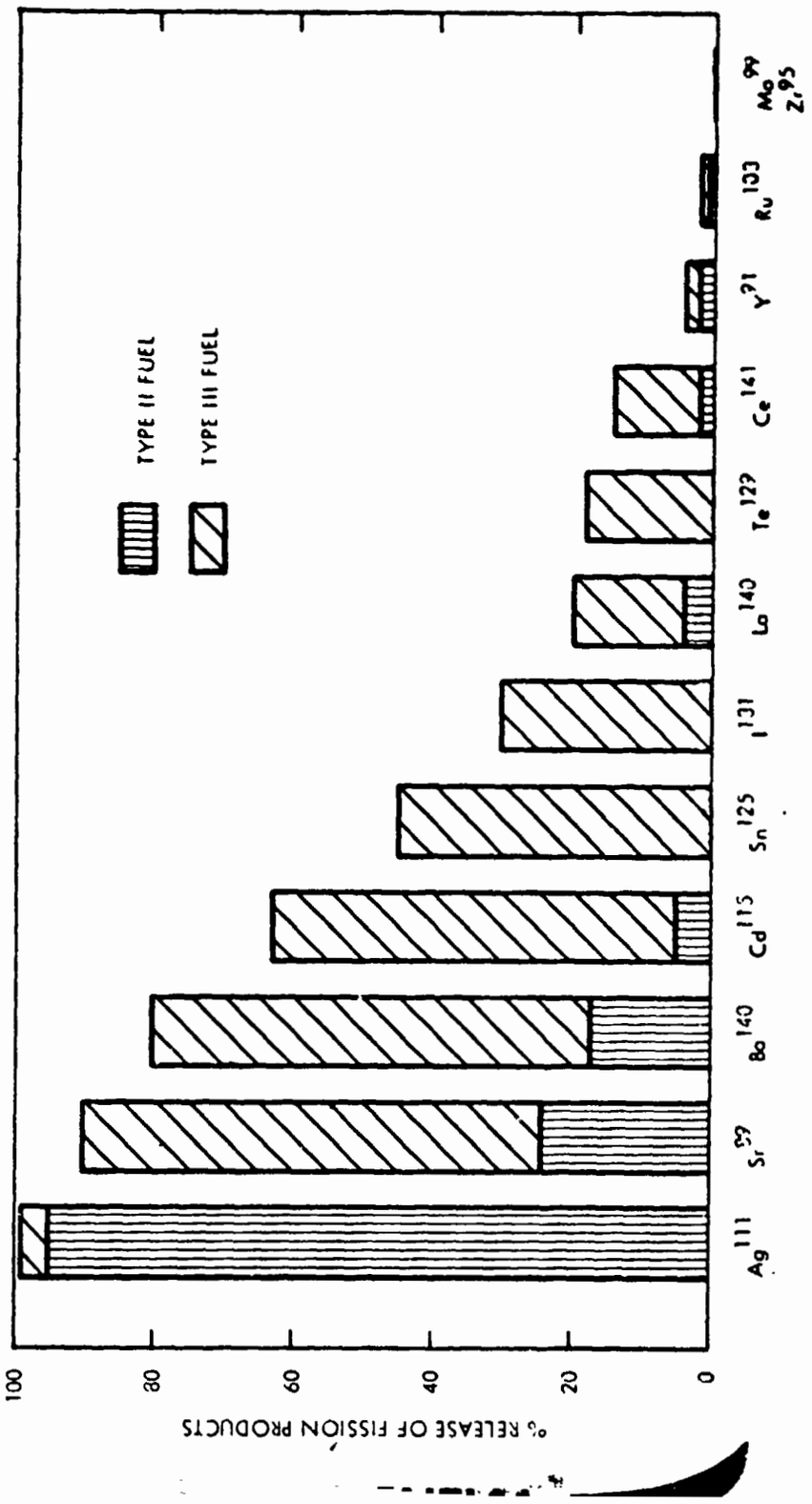

Figure 3-3. Percent of Fission Nuclides Released from Types II and III Fuel at 1800°C in 30 Minutes

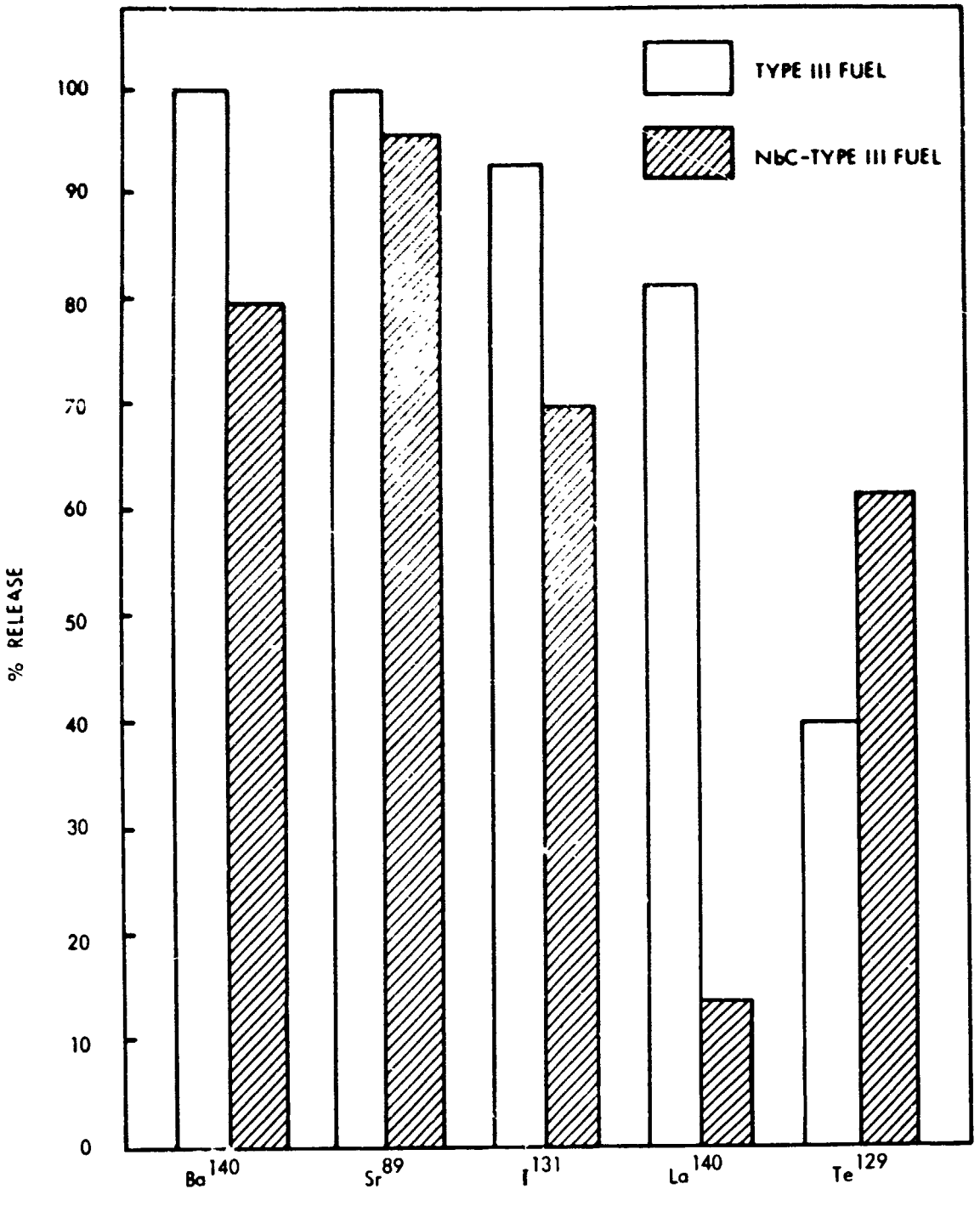

Figure 3-4. Comparison of Release of Fission Products from Types III and NbC Type III Fuels, at 2400°C, 15 Minutes

3. Unit Cell Experiments. Complete data on the release of individual isotopes during these experiments are given in Reference 26. The average Sr^{89} fractional release was 0.92 and 0.96 for 30 minutes at 2300°C and at 2450°C, respectively. The corresponding Ba^{140} releases were 0.67 and 0.65. Other isotopes showed less release. The gross gamma inventory release was 0.29 and 0.26, respectively. In general it appears that release from the 1/4- and 1/2-hexagonal fuel elements (used in the unit cell to fill out the circular geometry) was greater than from the regular hexagonal elements. There are some indications that release rate of Sr^{89} from the unit cell is similar to the release rate from Type III - NbC fuel. It has been concluded[26] that further unit cell experiments are necessary to obtain adequate data to describe release of fission products from the NERVA reactor under loss-of-coolant conditions.

Analysis of Diffusion Data. In order to obtain rate constants which describe the fractional release as a function of time, the release data for each isotope were empirically fitted to an exponential function:

$$f = e^{-Dt}$$

where

f = fraction of the nuclide concentration retained

D = diffusion rate constant in seconds^{-1}

t = time in seconds.

The release data for $Ce^{141,144}$, Y^{91}, La^{140}, Te^{129}, and I^{131} are well represented by the above equation. Figure 3-5[24] shows a typical plot of fraction retained versus time for Y^{91} in Type III fuel. However, the data for Cs^{137}, Sn^{125}, Sr^{89}, Ba^{140}, and Xe^{133} indicate that diffusion appears to be a two-step process, with an initial fast release followed by a slow release which increased slightly with time. The nuclide retention as a function of time can be represented as:

$$f = Ge^{-D_1 t} + (1 - G)e^{-D_2 t}$$

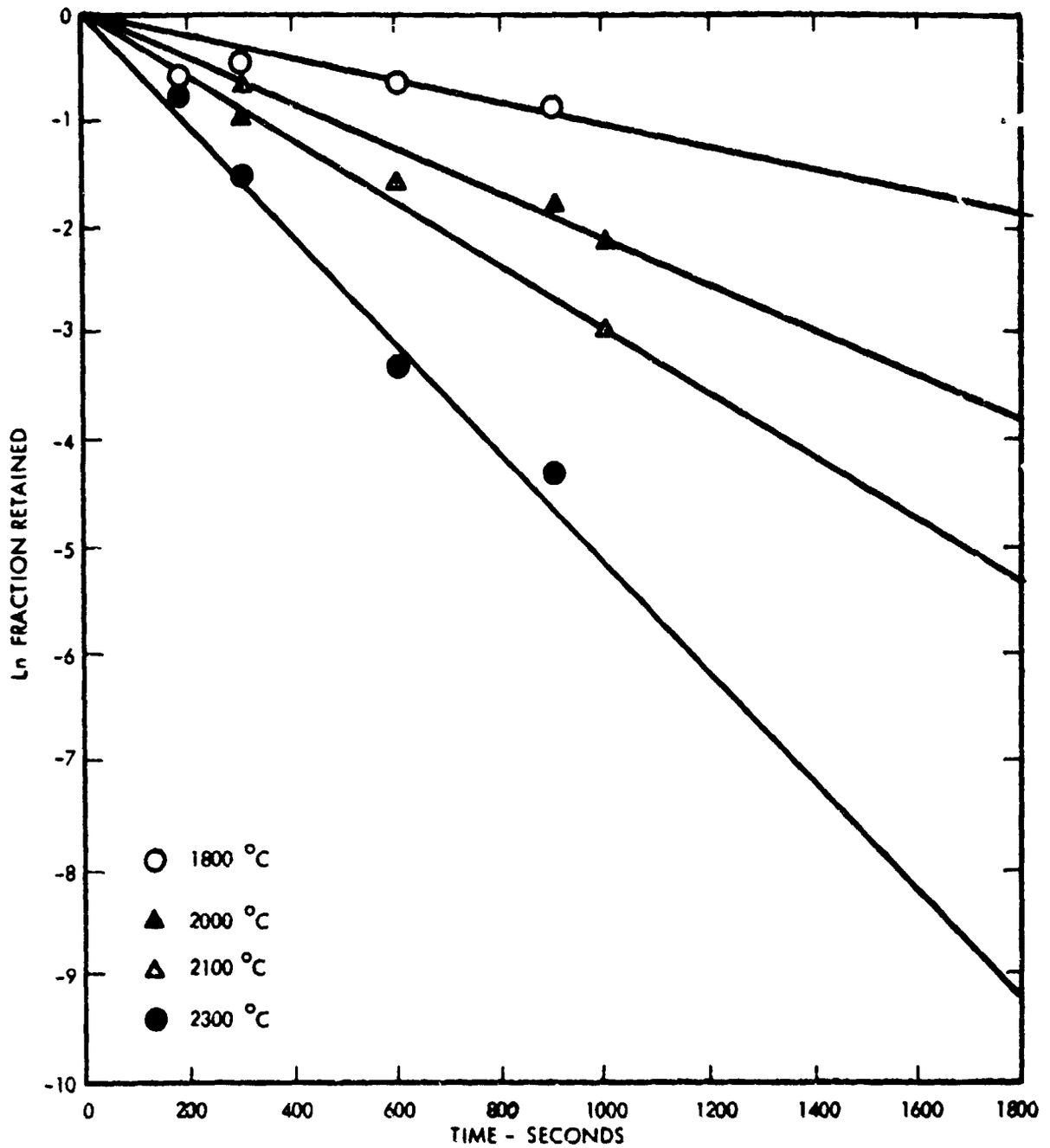

Figure 3-5. Y^{91} Diffusion in Type III Fuel

where

f = the total fraction of the nuclide concentration retained

t = time

G = the fraction of the nuclide concentration which diffuses at a fast rate characterized by the rate constant D_1

1 - G = the fraction of the nuclide concentration which diffuses at a slow rate characterized by the rate constant D_2.

A similar mode for nuclide release has been reported by Zumwalt[29]. For Ba and Sr, the fast diffusing fraction was 14.8 percent. For xenon, 10.6 percent diffuses at an initial fast rate while the remaining 89.4 percent diffuses at a slower rate. A typical plot showing the two step release for Ba^{140} is shown in Figure 3-6[24]. The rate constants, D, for all nuclides adhere to the Arrhenius Equation:

$$D = D_o e^{-\frac{E}{RT}}$$

where

D_o = an experimental constant with dimensions of reciprocal time

E = the activation energy in calories per mole

R = the gas constant, calories/mol-deg

T = the temperature in degrees Kelvin

A typical plot of relationship for Sn^{125} in NbC coated Type II fuel is shown in Figure 3-7[25]. A tabulation of the values for D_o and E/R for Type II, Type II - NbC and Type III fuels is given in Reference 25; the values for Type III - NbC are tabulated in Reference 26.

Analytical Prediction of Diffusion. An analytical model has been developed utilizing the experimentally determined diffusion rate equations to predict the extent of fission product diffusion occurring under a variety of operational and post-operation conditions. This program, FIPDIF[30], calculates the fission product inventory which remains in the core and that which is released to the surroundings for any given power and temperature profile.

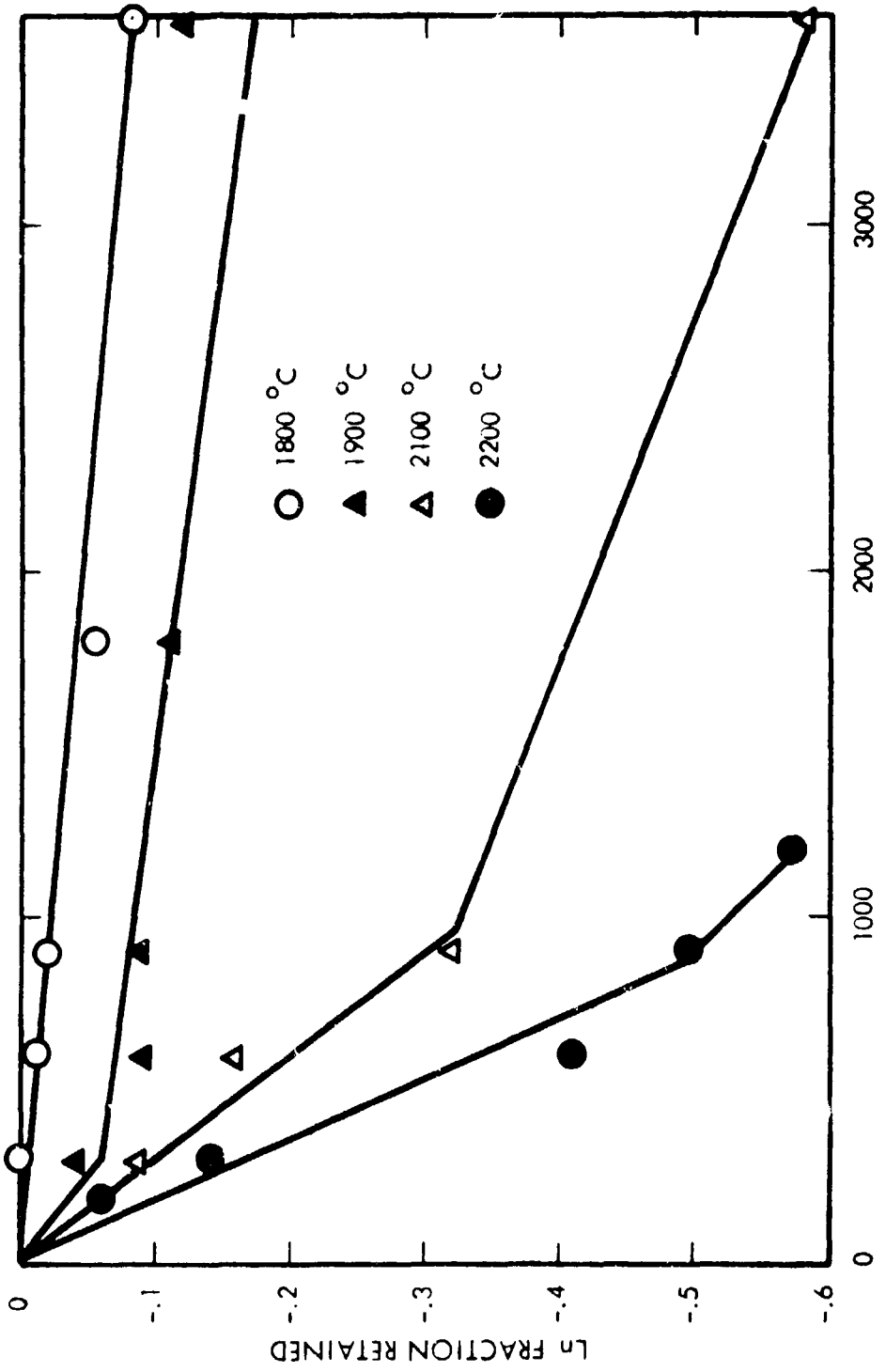

Figure 3-6. Ba^{140} Diffusion in NbC Coated Type II Fuel

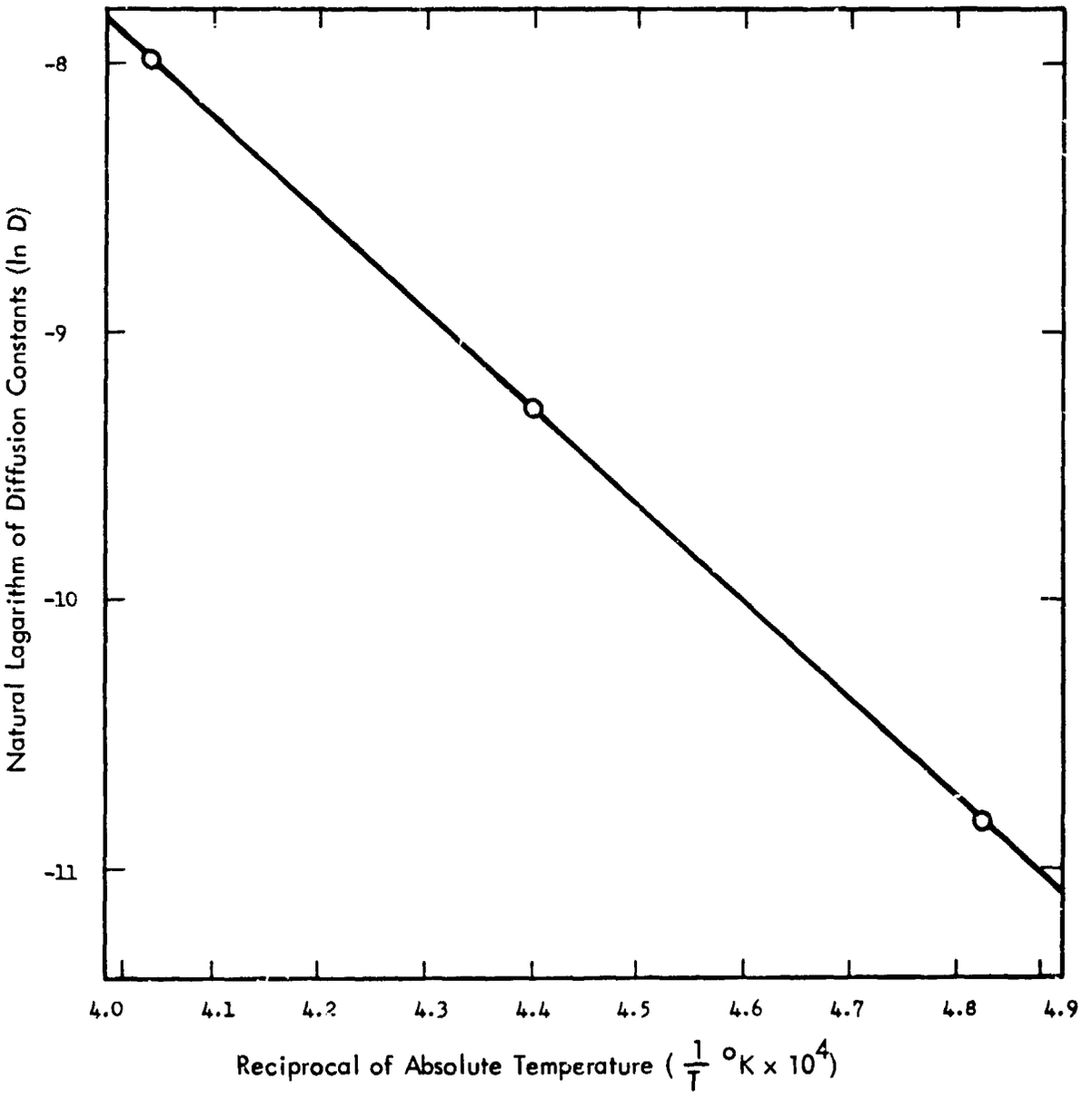

Figure 3-7. Arrhenius Relationship for Sn^{125} in NbC Coated Type II Fuel

In its present form it can be used to simulate a reactor startup-run-shutdown profile consisting of as many as 40 time intervals. These time intervals may be of any desired length. During each time interval, a power level and temperature are specified for each of as many as ten axial core sections. The core sections are disc shaped with a radius of 45.2 cm. They may be of any desired thickness. At the conclusion of any or all of the specified time intervals, the following data may be printed out:

1. Remaining fission product inventory in each core section and/or total core inventory of each isotope.
2. Curies of each isotope which have diffused from each section and/or total curies of each isotope which have diffused from the core.

FIPDIF is an integral code which solves the two basic differential equations:

$$\frac{dN_i}{dt} = PG_i\gamma_i - \lambda_i N_i - D_i N_i - \sum_{j=1}^{i-1} B_{j\longrightarrow i}\lambda_j N_j$$

where

N_i = number of atoms of isotope (i) in the given core section

P = power level in the core section (fissions second)

γ_i = fission yield of isotope (i)

λ_j = decay constant of isotope (j) which is a precursor of isotope (i)

$B_{j\longrightarrow i}$ = branching ratio for the production of isotope (i) from a precursor (j)

D_i = diffusion constant (characteristic of the isotope and the temperature of the core section)

G_i = a factor which is used to account for the faster diffusion of the fraction of some nuclides which are deposited externally to the fuel beads by recoil

and

$$\frac{dL_i}{dt} = D_i N_i$$

where

L_i = number of atoms of isotope (i) which have diffused from the core section.

Values used for the diffusion coefficients of the various isotopes were those obtained experimentally as described in the preceding paragraph. Provisions have been made in the program to incorporate the diffusion coefficients for both the Type II (normal) and Type III (degraded) fuel, thereby permitting calculation of fission product diffusion at elevated temperatures. A comparison of the predicted fission product release from the NRX reactor tests, as calculated by the FIPDIF program, with the measured release as determined by radiochemical analysis is discussed in Section 3.2.1.

The FIPDIF program has no provisions for the calculation of temperature variation due to heat transfer from core section to core section or to the reactor components and the atmosphere. A computer program, NOFLOW[31], is capable of generating temperature profiles in various components of the NERVA reactor, but does not have the ability to reflect losses of the fission product inventory by diffusion, and thereby does not accurately calculate the decay heat source. Therefore, in order to reflect the loss of fission product decay heat in the core temperature calculations, and the effect of changing core temperature on diffusion, FIPDIF and NOFLOW have been combined into a linked program[32]. This linked program is particularly applicable where high core temperatures are produced as for an accident in which loss-of-coolant occurs. Further details on the coupled NOFLOW-FIPDIF program and the expected diffusion losses occurring under loss-of-coolant conditions are discussed in Section 3.2.2.

3.1.2.2 Fuel Element Corrosion

In the NERVA reactor, under full power operating conditions, the fuel elements are exposed to a temperature range of about 30°C at the inlet end to as high as 2200°C at the exit (nozzle) end of the reactor. Over a substantial portion of this temperature range, the graphitic fuel elements would be rapidly consumed by the chemical reaction of carbon with hydrogen to produce methane and acetylene. In order to minimize the extent to which these reactions occur (called hydrogen corrosion) a NbC coating is applied to those surfaces of the fuel elements which are exposed to hydrogen flow. The present design calls for the coolant channels and the external surfaces at the exit end of the element to be coated. The NbC coating is applied in a batch process by vapor deposition at 1900°C. The coating thickness varies from approximately 0.4 mils thick at the cold (inlet end of the coolant channels) to approximately 3.0 mils thick at the hot end of the channels.

Fuel elements from each coating batch are hydrogen corrosion tested under temperature conditions more severe than expected for full power NERVA operation in order to verify that the coating operation has produced a coating which is capable of affording adequate protection to the fuel element. This corrosion testing also serves two other important purposes: (1) to characterize and understand the general hydrogen corrosion test behavior of fuel elements in order to predict behavior in reactor operation, and (2) to identify those coating characteristics which result in observed behavior and those characteristics which lead to improved behavior.

The results of corrosion testing of fuel elements made for the NRX reactors have been documented in References 33, 34, and 35 and corrosion tests on the LASL Phoebus 1 elements are documented in Reference 35. The observations and measurements of fuel element corrosion following the NRX reactor ground tests are documented in References 36, 37, and 38.

To determine the reduction in fission product inventory of the fuel due to corrosion, information on the loss of fuel from the matrix must be known. In the laboratory corrosion tests and in the post-operational examination of the fuel elements, direct measurements of the UC_2 lost from the fuel by corrosion have not been made. However, there is evidence

that UC_2 and fuel beads have been lost from the core during reactor operation. Radioactive particulate samples were recovered from the ground following the NRX/EST test at distances of 1000 feet to 4.7 miles from the reactor. Metallographic, radioactivity assay, and electron probe analyses were made on this particulate material[21]. The results of analysis of this material indicated that all but one of the particles contained uranium, and the radioactivity was due to fission product activity not activation product activity. The particles appeared to be from fuel element fragments, with the uranium in the form of both oxide and carbide in the particles. In some, the presence of small pieces of NbC indicated flaking of the fuel element bore coat. The larger particles exhibited irregular configurations, and the smaller particles were spherical. The size of some of the particles indicates that rather large (> 500μ) pieces of fuel matrix or non-fueled graphite were torn away.

Additional evidence of loss of fission product activity by "corrosion mechanism" during operation of the NRX/EST and NRX-A5 tests has been obtained by analysis of particulate matter collected on filters mounted on aircraft which flew through the reactor effluent cloud[21, 41]. Analysis of these aircraft filter samples shows the presence of Mo^{99}. Laboratory experiments indicate that neither Mo^{99} nor its precursors Zr^{99} and Nb^{99} are released from NERVA fuel by diffusion at temperatures up to 2600°C. Thus the presence of Mo^{99} in the effluent cloud is an indicator of uranium fuel bead loss by corrosion because Mo^{99} would be present only in uranium fuel beads. Extensive radiochemical analyses have been made on these effluent cloud samples to determine the contributions by diffusion and corrosion to the total fission product release. The results of these analyses are summarized in Reference 21, and reveal that during experimental plans EP-IV and EP-IVA of the NRX/EST test, the corrosion mechanism accounted for 44.8 and 59.8 percent, respectively, of the total gross gamma radioactivity released. Further data on the measured loss of fission products by both diffusion and corrosion mechanisms are given in Section 3.2.1.

3.1.2.3. Re-Entry Burnup of Fuel Material

Another means of reducing the fission product inventory of re-entering core fragments involves the burnup of this debris during the re-entry process. Assuming uniform distribution of the UC_2 in the graphite matrix, as the mass of a re-entering particle decreases, the fission product inventory associated with this mass loss will be diminished in direct proportion.

A complete summary of the analytical and experimental work performed up to 1964 to evaluate NERVA fuel re-entry burnup was published in the previous NERVA Source Term Report[13]. No significant additional work within the Rover Program has been published since that time. The major results of the work reported in Reference 13 are abstracted below for the sake of completeness of this document.

Analytical Evaluation of Burnup. Analytical models, developed by both General Electric[42] and Westinghouse[43], have been programmed for digital computer solution of re-entry burnup. The models are based on theoretical considerations of the rate of graphite oxidation under the flow regions encountered during atmospheric re-entry. Results of the two programs vary somewhat, with the Westinghouse model yielding a greater percentage of burnup than the G. E. Model. A comparison of the probable reasons for the divergence of results between the two programs is given in Reference 13. The basic difference in the analyses lies in the assumption of which of the several graphite oxidation steps is rate controlling.

The amount of burnup that occurs depends on particle size, re-entry angle at the top of the atmosphere, and particle velocity. For cases of interest in ROVER Flight Safety, the re-entry angle will be small (< 10 degrees), and the effect of varying re-entry angle can be neglected. Also, the particle velocity will differ little from the orbital velocity at re-entry altitude. If these parameters are neglected, re-entry burnup of small NERVA fuel graphite particles can be represented by a single curve, as shown in Figure 3-8. These data are based on the Westinghouse burnup model, and are derived from the WEREC computer program[43]. The data of Figure 3-8 are used by LMSC in their Nuclear Flight Executive Program for NERVA destruct analysis[44]. The WANL Source Term Computer Program utilizes the WEREC program as a subroutine, and therefore calculates the extent of fuel burnup for the actual re-entry trajectory.

Experimental Evaluation of Burnup. A series of experiments were performed by WANL to determine oxidation rates of graphite under simulated re-entry conditions[43, 45]. The tests were conducted in a plasma-jet facility, and were confined to examining oxidation under continuum and transition flow conditions. The experimentally determined oxidation rates showed good agreement with the theoretically calculated rates.

Figure 3-8. Re-entry Burnup Survival as a Function of Particle Diameter[44]

The addition of metallic additives to the graphite did little to enhance re-entry burnup[46]. Irradiated samples of NERVA fuel were also tested under simulated re-entry conditions[47] and this work indicated that irradiation does not affect the rate of oxidation of re-entering graphite. It can be concluded from both the analytical and experimental studies, that the reduction in the source term of re-entering fuel debris will be a maximum of about 50 percent, and appreciably less than this for particles greater than 1/16-inch diameter.

A potentially greater loss of fission products from NERVA fuel by re-entry burnup and ablation following a nuclear (self) destruct action has been postulated by LASL[48]. Examination of fuel samples and graphite fragments of unfueled support elements and reflector fragments following the KIWI-TNT experiment has shown evidence of condensation of fission products on the surfaces of these fragments, rather than pressure penetration of the fission products during the excursion. Thus, if the fission products primarily reside on the fragment surfaces, even a 10 percent ablation weight loss may be very effective in reduction of the fission product inventory of the debris impacting on the earth.

3.2 FISSION PRODUCT INVENTORY FOR DIFFERENT MODES OF REACTOR OPERATION

It was shown in Section 3.1 that the fission product inventory generated during NERVA reactor operation could be diminished by several mechanisms depending on the operational and post-operational history of the reactor. This section defines the expected losses in the fission product inventory under normal and abnormal reactor operating conditions. With the prediction of such losses, it then becomes possible to define the source term of the fuel debris that impacts on the earth.

3.2.1 Normal Operations

"Normal" reactor operation refers to that operational mode in which the reactor is operated at or very near its design conditions of power, temperature, coolant flow, etc; that is, operation in which no deliberate or known off-design conditions, abnormality, or malfunction exist. Experimental measurements of the fission product losses that occurred with each test of the NRX series of reactors were conducted from the start of hot testing. Although some operational abnormalities were experienced during this test series, the operations, in general, are indicative of normal reactor operations and provide an excellent basis for the determination of expected fission product losses under normal reactor operating conditions.

As the technology of the NERVA reactor advances and as improved fuel performance is obtained, the fission product loss by corrosion and diffusion mechanisms under normal operations is expected to be less than that experienced to date in the NRX test series. The measured and predicted (by the FIPDIF code) losses of fission products for each of the NRX tests are summarized in the following paragraphs.

3.2.1.1 NRX-A2 and NRX-A3 Tests

The results of radiochemical analyses to measure the loss of fission products from the NRX-A2[24] and NRX-A3[25, 26] tests are summarized in Table 3-2. The predicted values of release as calculated by the FIPDIF program at the time of the test are also shown in this table. FIPDIF calculations using diffusion constants for both uncoated and NbC coated Type II fuel were made for the NRX-A3 test. As can be seen, the calculated data using the Type II - NbC constants more closely agrees with the experimental data, leading to the conclusion that the primary path for diffusion is through the NbC lining into the cooling channels. Type II - NbC constants had not been determined at the time of the NRX-A2 test, and the prediction for the NRX-A2 test using these constants has not been made.

The data of Table 3-2 were determined by post-mortem radiochemical analyses on fuel samples only - aircraft effluent samples were not available. There is some uncertainty in these measurements, since the amount of activity released is based on small differences in large numbers. Both reactors were run at essentially identical steady state conditions of power and temperature, and similar fission product releases would be expected. On this basis, the 12 percent difference in the measurement of the gross gamma activity released (1.02 and 0.9 percent for the A2 and A3, respectively) represents fair precision. Since effluent samples were not available, it is not possible to define the fraction of the total release due to corrosion. The predicted results assume all loss was by diffusion.

3.2.1.2 NRX/EST (NRX-A4) Test

The NRX/EST reactor was operated in February - March 1966 according to five experimental plans (EP) at various power levels. Only the last two runs, EP-IV and EP-IV A were conducted at full power for a significant time (approximately 15-1/2 and 13-1/2 minutes, respectively). The number of fissions produced in the fuel during EP-IV and EP-IV A

TABLE 3-2

COMPARISON OF PREDICTED FISSION PRODUCT RELEASE FROM NRX-A2 AND NRX-A3 WITH RADIOCHEMICAL ANALYSES

		NRX-A2 Percent Release		NRX-A3 Percent Release		
Mass Chain Number	End Product Nuclide	Radiochemical Analysis	Predicted With Type II Diffusion Constants	Radiochemical Analysis	Predicted With Type II Diffusion Constants	Predicted With Type II - NbC Diffusion Constants
81	Sr	0.0	0.54	1.30	3.92	1.61
91	Y	4.82	4.93	2.60	5.20	2.80
95	Zr	1.93	1.56	3.10	2.45	0.66
115	Cd	18.67	1.45	30.0		39.0
131	I	1.66	1.15	1.80	2.52	0.80
137	Cs	-	-	0.00	0.12	0.00
140	Ba	1.32	2.03	1.90	8.64	1.0
141	Ce	1.54	2.85	-	-	-
144	Ce	0.94	0.06	-	-	-
Gross Gamma Inventory		1.02	1.24	0.09	-	1.60

TABLE 3-3

COMPARISON OF MEASURED AND PREDICTED RELEASE OF FISSION PRODUCTS FROM NRX/EST EP-IV

Nuclide	Percent Total Release Based On Radiochemical Analyses	Percent Corrosion Release	Percent Diffusion Release	Predicted Percent Release Based On Type II "Uncoated" Fuel Diffusion Constants	Predicted Percent Release Based On Type II - NbC Diffusion Constants
Sr^{89}	2.28	0.65	1.63	1.27	0.23
Sr^{91}	2.06	0.65	1.41	6.19	3.74
Y^{91}	2.19	0.12	2.34	2.73	1.64
*Sr^{92}	2.46	0.65	1.54	7.72	4.49
Y^{93}	1.78		1.13	7.27	3.19
Zr^{95}	2.06		1.41	1.19	0.32
Zr^{97}	1.84		1.19	0.02	0.01
Mo^{99}	0.65		0.00	0.00	0.00
Ag^{111}	36.21		35.5	8.19	8.19
Cd^{115}	60.55		59.9	46.10	46.10
Sn^{125}	8.09		7.44	3.45	0.46
Sb^{127}	6.50		5.85	7.44	1.06
I^{131}	2.71		2.06	2.20	.38
Te^{132}	1.20		0.55	1.22	.11
I^{133}	1.17	0.65	0.52	0.34	.02
*I^{135}	0.65	0.12	0.53	0.26	.02
Cs^{137}	<0.97	0.65	<0.32	0.20	0.01
Ba^{140}	1.57		0.92	5.57	0.65
Ce^{141}	1.73		1.08	4.16	0.50
Ce^{143}	2.30		1.65	1.75	0.45
Ce^{144}	2.05		1.40	0.52	0.16
GROSS GAMMA	1.45		0.80	2.10	0.42

*NTO Analysis

TABLE 3-4

COMPARISON OF MEASURED AND PREDICTED RELEASE OF FISSION PRODUCTS FROM NRX/EST EP-IV A

Nuclide	Percent Total Release Based On Radiochemical Analyses	Percent Corrosion Release	Percent Diffusion Release	Predicted Percent Release Based On NbC Diffusion Constants	Predicted Percent Release Based On "Uncoated" Fuel Diffusion Constants
Sr^{89}	12.12	4.41	7.71	2.56	5.65
Sr^{91}	9.02	4.41	4.61	6.40	10.83
Y^{91}	12.25	4.41	7.84	2.19	3.72
*Sr^{92}	15.96	10.30	5.66	6.14	10.15
Y^{93}	8.84	4.41	4.43	4.68	9.74
Zr^{97}	6.59		2.18	0.01	0.05
Ag^{111}	46.30		41.89	16.90	16.90
Cd^{115}	63.60		59.19	46.53	46.53
Sn^{125}	16.92		12.51	1.26	5.17
Sb^{127}	10.53		6.12	2.09	8.47
I^{131}	9.46		5.05	0.55	2 [illegible]
Te^{132}	5.32		.91	0.40	1.78
I^{133}	6.25		1.84	0.32	2 18
Cs^{137}	7.12		2.71	0.15	0 41
Ba^{140}	8.84		4.43	2.27	5.43
Ce^{141}	9.68		5.27	1.25	4.49
Ce^{144}	11.23		6.82	0.75	1.87
Zr^{95}	7.48		3.07	0.44	
Mo^{99}	4.4		0.00	0.0	0.0
GROSS GAMMA	7.36		2.95	0.46	2.32

* NTO Analysis

was approximately 54 percent (27 percent each) of the total fissions produced during the entire power operation of the reactor.

The results of the measured and predicted fission product releases for EP-IV and EP-IV-A are summarized in Tables 3-3 and 3-4 respectively[21]. These data are based on radiochemical analyses of particulate material collected on filters from the effluent cloud during each EP. The release due to corrosion is based on the results of Mo^{99} analyses as described in Section 3.1.2.2 and is shown in the tables. The amount of fission products lost by diffusion is the difference between the total release and the corrosion release. The predicted release by diffusion mechanism as calculated by the FIPDIF program is also shown in these tables.

Tables 3-3 and 3-4 show that the corrosion mechanism can account for a significant portion of the total radioactivity release. The percent of total radioactivity released due to corrosion during each of the experimental plans is tabulated in Table 3-5; for many nuclides, corrosion release accounted for over 50 percent of the total activity released.

The data of Tables 3-3 and 3-4 show that the measured fission products released by diffusion are greater than the predicted diffusion using the Type II- NbC diffusion constants, which indicates that the fuel elements lost some of the bore coating. However, for the EP-IVA the actual release by diffusion was greater than the maximum predicted, even with uncoated fuel diffusion constants. A possible explanation may be due to the higher temperature reached in the peripheral elements caused by the large control drum angle reached near the end of the test.

3.2.1.3 NRX-A5 Test

Post-mortem radiochemical analyses on the NRX-A5 fuel elements has not been completed, and therefore, final data on measured release of activity is not available. However, preliminary data on the release during EP-III and EP-IV, as determined from effluent samples, has been reported[49] and are summarized in Table 3-6. These data show that the corrosion mechanism accounted for only a small fraction of the total release in EP-III, but that in EP-IV, the release of fission products by corrosion was approximately equal to that released by diffusion. These data are preliminary in that they are based on the assumption that 50 percent of fission cadmium is released to the effluent cloud. The actual cadmium release will be determined by post-mortem analysis, and it is necessary to define the fraction of the effluent

TABLE 3-5

PERCENT OF TOTAL RADIOACTIVITY RELEASE DUE TO CORROSION IN EP-IV AND EP-IV A

NUCLIDE	EP-IV	EP-IV A
Sr^{89}	28.5	35.4
Sr^{91}	31.5	48.9
Sr^{92}	4.9	64.5
Y^{91}	29.6	36.0
Y^{93}	35.6	50.0
Zr^{95}	31.6	59.0
Zr^{97}	35.4	67.0
Mo^{99}	100.0	100.0
Ag^{111}	1.75	9.55
Cc^{115}	1.07	6.92
Sn^{125}	8.1	26.1
Sb^{127}	10.0	41.7
Te^{132}	54.0	82.8
I^{131}	24.0	46.5
I^{133}	55.5	70.5
I^{135}	18.5	---
Cs^{137}	67.0	61.8
Ba^{140}	41.5	50.0
Ce^{141}	37.6	45.6
Ce^{143}	28.2	---
Ce^{144}	31.7	39.2
Gross Gamma	44.8	59.8

TABLE 3-6

MEASURED FISSION PRODUCT RELEASE FROM NRX-A5

NUCLIDE	EP-III CLOUD SAMPLE % OF TOTAL INVENTORY RELEASED			EP-IV CLOUD SAMPLE % OF TOTAL INVENTORY RELEASED		
	TOTAL	CORROSION	DIFFUSION	TOTAL	CORROSION	DIFFUSION
Ba^{140}	0.118	0.003	0.115	3.79	1.64	2.15
Sr^{91}	0.278	0.003	0.275	4.17	1.64	2.53
Sr^{89}	0.946	0.003	0.943	6.37	1.64	4.73
Zr^{97}	0.006	0.003	0.003	6.44	1.64	4.80
Zr^{95}	0.051	0.003	0.048	7.22	1.64	5.58
Cd^{115}	50.0	ASSUMED		50.0	ASSUMED	
Mo^{99}	0.003	0.003	0.000	1.64	1.64	0.00
Ag^{111}	27.5	0.003	27.5	30.4	1.64	28.8
Sb^{127}	1.84	0.003	1.84	6.67	1.64	5.03
I^{131}	0.907	0.003	0.904	1.70	1.24	0.46
I^{133}	0.398	0.003	0.295	0.82*	1.24	--
Te^{132}	0.627	0.003	0.624	1.89	1.64	0.25
GROSS GAMMA	0.276	0.003	0.273	3.50	1.64	1.86

* Less I^{133} was found than corrosion indicated.

'All of above data is preliminary and is based on an assumed 50% Cd release.)

cloud sampled[21]. Cadmium release in the NRX/EST test was about 60 percent. Thus, if this same release occurred in the NRX-A5 test, the values of Table 3-6 would increase by a factor of 6/5.

Comparison of the NRX-A5 results with those of the NRX/EST shows that the total gross gamma released by NRX-A5 was approximately 50 percent of that released by NRX/EST. Predicted gross gamma release by diffusion using Type II - NbC diffusion contstants for NRX-EP-III agreed with the measured release by diffusion. The predicted gross gamma release by both corrosion and diffusion for NRX-A5 EP-IV was only 25 percent higher than the total measured release.

3.2.1.4 Conclusions

Experimental measurements of the fission product release from the NRX-A2 through NRX-A5 reactors have shown that the gross gamma radioactivity release expected under normal operating conditions is in the range of 1 to 7 percent of the fission product inventory generated during operating times at full power to about 17 minutes. For the larger release rates, corrosion of the fuel elements contributes about one-half to the total release. This extent of corrosion is considered unacceptable for future NERVA reactors. With the development of an improved fuel, it is expected that corrosion losses (and diffusion losses) will be reduced. In order to obtain the desired core life of up to 60 minutes at full power, it is reasonable to assume that the maximum release by corrosion will not exceed 4 to 5 percent of the total fission product inventory generated. For presently envisioned missions utilizing a NERVA engine, single operating periods of the engine will probably not exceed 30 minutes. For operating times equal to or less than this, it is conservatively estimated that total losses of fission products by both diffusion and corrosion will probably not exceed 5 percent of the total inventory generated. Thus the inventory will be at least 95 percent of the theoretical inventory if no diffusion or corrosion losses occur. Estimates of biological dose and dose rate calculations based on a source activity known within 5 percent accuracy are considered acceptable. Thus, it can be concluded that for evaluation of the source term upon re-entry of the reactor or core fragments following normal reactor operations, the loss of fission products from the core during the reactor operating period can be neglected.

3.2.2 Malfunction or Accident Conditions

Reactor malfunctions or accidents may lead to conditions which will produce abnormally high core temperatures, thereby enhancing loss of fission products by diffusion. Accident and malfunction situations which have been investigated in the NERVA program are discussed in Chapter 5.0. The accidents which will result in the greatest loss of fission products are loss-of-coolant and nuclear excursions. The predicted inventory losses that would occur under these two accident conditions are discussed below. Detailed discussion on the response of the NERVA system to loss-of-coolant accidents and nuclear excursions are presented in Sections 6.2 and 6.5, respectively.

3.2.2.1 Loss-of-Coolant

In the event of a loss-of-coolant accident, the nuclear core will attain high temperatures, and diffusion of fission products results. The present discussion is limited to consideration of in-flight accidents. Hence, the dispersion of these gaseous fission products outside the Earth's sensible atmosphere, does not pose any particular biological or ecological safety problem. In fact, the loss of fission products at high altitudes will enhance NERVA flight safety as a result of the fact that the fission product inventory of the remaining core material which may eventually re-enter the Earth's biosphere will be reduced accordingly. This section describes the computer program used to predict fission product loss under loss-of-coolant conditions and presents typical analytical predictions.

NOFLOW-FIPDIF Analytical Model for NRX. The digital computer program NOFLOW-FIPDIF[32] was produced by linking modified versions of two other programs - NOFLOW[31] and FIPDIF[30]. The first program, NOFLOW, describes the post-operational thermal response of an NRX reactor subsequent to a loss-of-coolant accident. This program takes into account two basic energy sources - heat deposition due to fission power and heat deposition due to fission product decay. The analytical model divides the nuclear reactor into a number of components and component sections. (This model is described in Section 6.2.1.1.) Temperatures of these component sections are evaluated as a function of time after loss-of-coolant by performing a thermal balance involving the aforementioned energy sources and the thermal losses and gains arising from conduction and radiation.

The FIPDIF computer program is concerned with the loss of fission products from the NERVA core via a diffusion mechanism. Since the physical and mathematical models involved in the diffusion process were described in Section 3.1.2.1, they will not be repeated here. However, it should be re-emphasized that the rate and, hence, the extent of fission product diffusion is strongly temperature-dependent; the rate increases exponentially with fuel temperature.

Obviously, these two computer programs must be coupled in order to predict core temperatures and the magnitude of fission product losses subsequent to loss-of-coolant. While the core temperatures predicted by NOFLOW depend to a large extent upon the decay of fission product in the fuel, the loss of fission products from the core predicted by FIPDIF and, hence, the quantity remaining, depend on the temperature of the core. Thus, by linking both programs, meaningful estimates of fission product losses and of core temperatures may be made. The coupled program is described in detail elsewhere[32]; a brief description of the program follows.

Since both NOFLOW and FIPDIF each required more than two-thirds of the available computer storage space, it was necessary to separate their computational functions into two links of a chain program and to use a third link to accept input data and to perform initializing operations. The program operates as follows:

1. Input is read into Link I. Here values for required constants are set and initial values of variables are determined for both Link II and III.
2. Control is then transferred to Link III (the FIPDIF program) which evaluates the fission product inventory during normal operation. By taking into account the core operating temperature profiles and appropriate diffusion constants it evaluates both the inventory released and that retained under operational conditions. Finally, during this step of the operation, Link III evaluates the rate at which the fission product decay is decreasing when loss-of-coolant occurs.
3. Control is then transferred to Link II (NOFLOW) which calculates temperatures of reactor components for a series of time steps. The fission product decay energy used in these calculations is approximated by using the decay power at shutdown and

the value of the rate of decrease of decay power as calculated in Link III. Temperature change calculations are continued until any given core section changes temperature by 400°R. Time weighted core section temperatures and power levels are evaluated for the length of time that control was maintained in Link II (ΔT_2).

4. Control is once again transferred to Link III where the change in fission product inventory during the time step, ΔT_2 is calculated. Evaluation of the fraction of inventory retained in the core and that released to the environment are included in these calculations. Finally, a decay power is calculated based on the total inventory remaining in the core.

5. Link II is then used to calculate the core temperature changes for one step (DELT).

6. This information is transferred to Link III which evaluates the decay powers in the core at the middle of the time step (DELT) using the value of the temperature change calculated in step 5 above. The value of rate of decrease of decay power is then evaluated using the decay power evaluated at the end of step 4 and that calculated at the midpoint of DELT.

The program continues to evaluate reactor temperatures and fission product inventories by repeating steps 3 through 6 until the accident simulation is completed. Then control is transferred to Link I which causes power and temperature histories to be written on the output tape.

Diffusion Results for NRX. The magnitude of the fission product diffusion experienced under loss-of-coolant conditions will depend largely upon the temperatures experienced under these conditions and on the length of time the core remains integral subsequent to the occurrence of the accident. Once disassembly occurs, fuel material cools rapidly as a result of thermal radiation to the environment and diffusion ceases.

Figure 3-9 shows typical core temperatures predicted for the core midplane of an NRX reactor as a function of time after loss-of-coolant for a number of operational periods ranging from 63 to 1450 seconds. The shutdown reactivity was 2 percent, corresponding to that anticipated for a complete loss of hydrogen flow with no movement of the control drums. As may be seen, an initially rapid increase in core temperatures occurs in all cases followed by a rapid drop in temperature when sublimation of the graphitic fuel material commences.

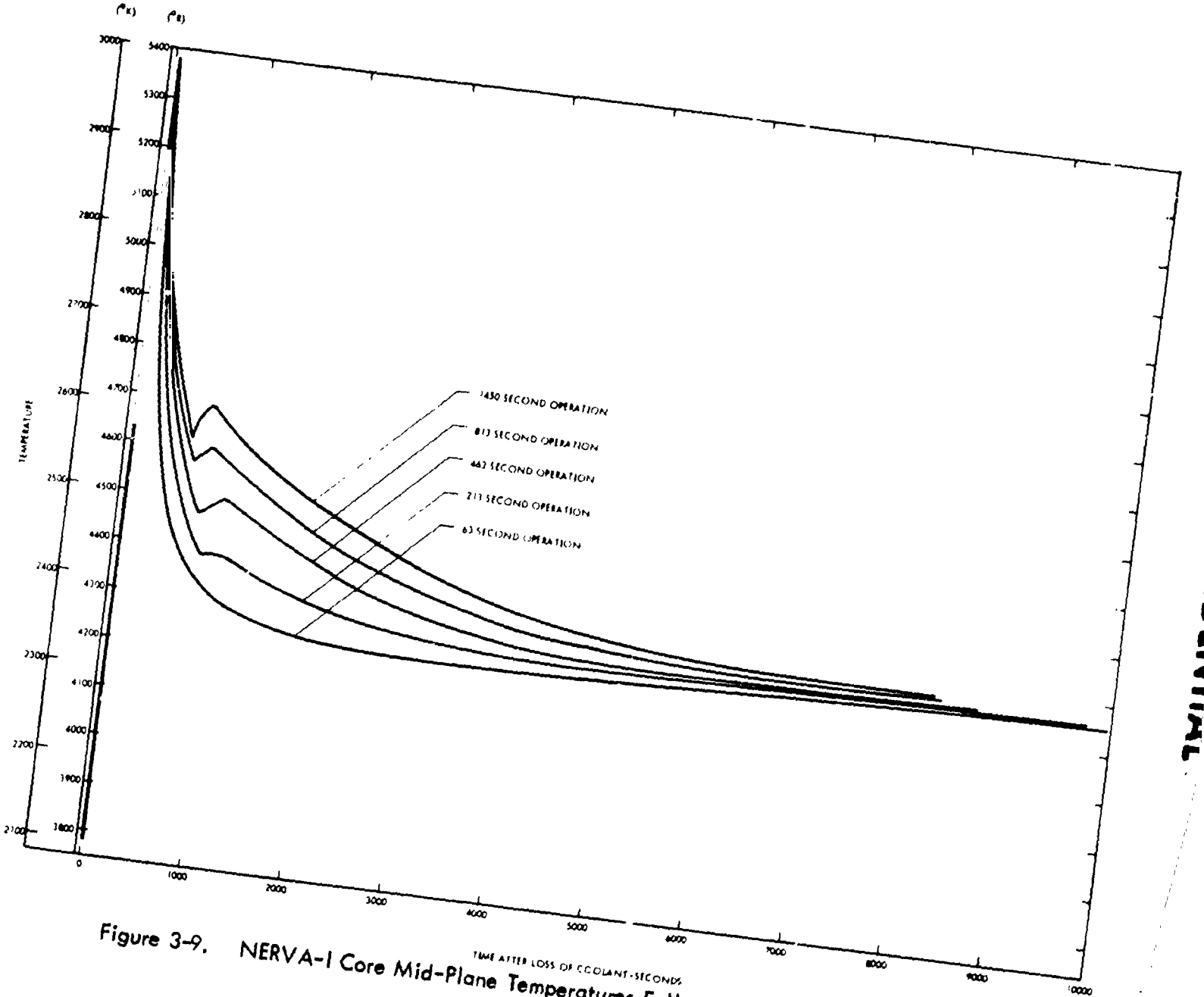

Figure 3-9. NERVA-1 Core Mid-Plane Temperatures Following Loss-of-Coolant

In addition it may be observed that the magnitude of the core temperature increases with increasing operating time. These high temperatures serve as a driving force to diffuse fission products from the core.

The length of time during which the core remains integral subsequent to loss-of-coolant depends on the integrity of the two systems supporting the reactor core, i.e. the axial support systems and the lateral support system. In the NRX reactor, the former consists of tie rods running axially through the reactor core and supported above the core dome end by an aluminum core support plate. The rods are made of Inconel-X and have a stainless steel sleeve. NOFLOW-FIPDIF analyses indicate that these will melt for all operating periods within 20 to 30 seconds after a loss-of-coolant accident, leaving the core with no axial support. All remaining core support must be imposed by the lateral support system. In the NRX reactor the lateral support system consists, in part, of stainless steel leaf springs supported by an aluminum bracket which is attached to the graphite inner reflector by two aluminum retainer screws. Since aluminum has the lowest yield temperature (1260°R), when the spring assembly reaches this temperature, it is expected that lateral support to the core will be lost. For the NRX reactor, NOFLOW-FIPDIF indicates that the entire lateral support system will be lost within 155 to 160 seconds after loss-of-coolant occurs, independent of operating time. Once this happens, the entire core is left without restraining forces and disassembly is expected to occur upon the application of any appreciable force at the core. Even minor centrifugal forces, such as those experienced by a vehicle tumbling in orbit, should be sufficient to eject fuel elements from the reactor. (For a more detailed discussion of the disassembly mode of a spent reactor, see Reference 50 or Chapter 6.0 of this report.)

In order to report the inventory remaining and that diffused from the fuel, it is necessary to select a particular reference time. This might be, for example, the time at which the element is ejected from the core, i.e. when diffusion ceases. Perhaps, a more meaningful reference time from a flight safety point of view would be that time at which the elements impact the Earth's surface subsequent to in-flight failure. To present data in this context it is necessary to hypothesize a mission and to select failure times along the mission profile. For each failure time, a disassembly time would be evaluated,* and the re-entry time of resultant

* As noted earlier in this section, the NRX disassembly time would occur about 160 seconds after loss-of-coolant accident - a value which is independent of operating time.

debris would be assessed. This re-entry time would determine the extent of fission product decay subsequent to the time at which diffusion ceases (i.e. at disassembly).

For the purpose of this report, fission product diffusion will be viewed in terms of the latter context - i.e. in terms of the inventory present at time of ground impact. For discussion purposes, the reference mission selected will involve start-up of an NRX powered nuclear stage in a 100 mm-orbit. In this mission the reactor operates 1450 seconds until injection energy for a 70-hour lunar transfer is achieved. The flight details on this particular mission (designated as Mission Model I) are summarized in Section 8.2. If a loss-of-coolant accident occurs during reactor operation, the reactor will eventually disassemble and the ejected fuel elements will remain in orbit, until the energy of the orbiting body is overcome by atmospheric drag forces. When this occurs the element will re-enter the Earth's atmosphere and will constitute a potential radiological safety problem. The later in the mission that the failure occurs, the longer the ejected element will remain in orbit. Figure 3-10 shows the orbital lifetime of an ejected fuel element as a function of engine operating time. The time abscissa in this figure is shown in terms of time after launch; however, if it is kept in mind that for the mission under discussion,the nuclear reactor starts up at 588 seconds after launch, then Figure 3-10 can be readily interpreted in terms of engine operating time. It is apparent from an examination of this figure that the orbital lifetime of a fuel element increases rapidly with engine operating time. The orbit lifetime of the reactor shell without the fuel elements is also shown in Figure 3-10.

Table 3-7 shows the inventory at ground impact for a single fuel element for four selected times after start-up when loss-of-coolant occurs, i.e., 63, 263, 463, and 613 seconds after engine start-up. This table shows the inventories in terms of curies/element for ten selected isotopes and the total inventory per element. Inventories are given for the situation in which no diffusion occurs and also for the case in which diffusion does take place for the 160 second time period after loss-of-coolant, during which the core is restrained by some load-bearing component, i.e. the lateral support system. As may be seen, diffusion will reduce the total fuel inventory about 30 percent. If additional time were allotted for diffusion, i.e. if the lateral support system did not fail so early during the post-accident history, it is expected that additional reduction in inventory would occur.

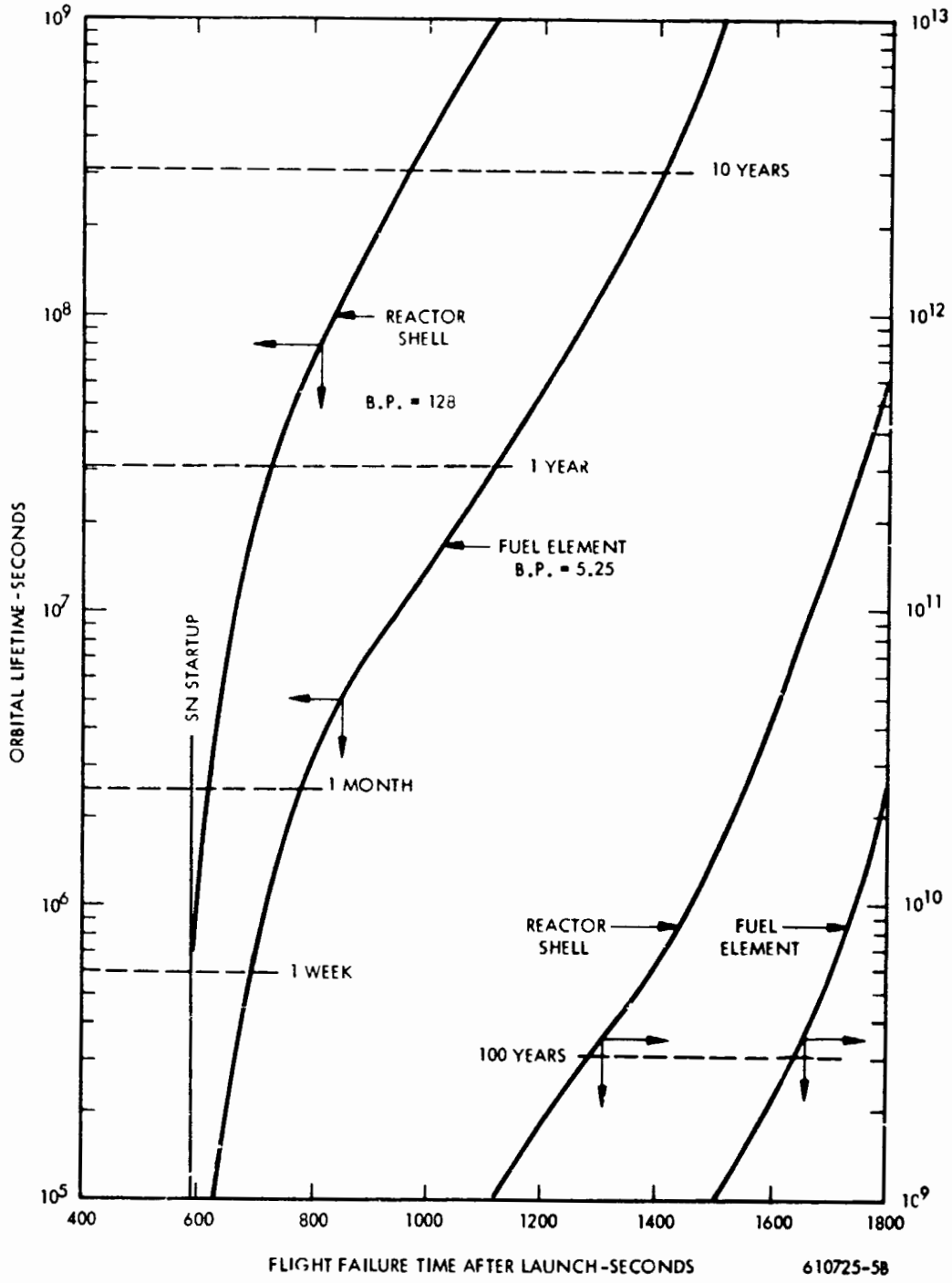

Figure 3-10. Orbital Lifetime of NERVA-I Reactor Shell and Fuel Elements During Mission Model I as a Function of Flight Failure Time After Launch

CONFIDENTIAL

TABLE 3-7

ACTIVITY OF SELECTED FISSION PRODUCTS IN NRX FUEL ELEMENT AT GROUND IMPACT

MISSION MODEL I (100 NM ORBIT START)

Activity of NRX Fuel Element at Ground Impact (curies/element)

Isotope	Reactor Operating Time to Loss-of-Coolant = 63 Seconds			Reactor Operating Time to Loss-of-Coolant = 263 Seconds			Reactor Operating Time to Loss-of-Coolant = 463 Seconds			Reactor Operating Time to Loss-of-Coolant = 613 Seconds		
	With Diffusion	Without Diffusion	Percent Reduction	With Diffusion	Without Diffusion	Percent Reduction	With Diffusion	Without Diffusion	Percent Reduction	With Diffusion	Without Diffusion	Percent Reduction
Sr^{90}	1.58×10^{-4}	7.18×10^{-4}	78.0	1.37×10^{-3}	6.05×10^{-3}	77.4	2.05×10^{-3}	1.12×10^{-2}	81.7	2.32×10^{-3}	1.48×10^{-2}	84.3
Y^{90}	6.29×10^{-5}	2.84×10^{-4}	77.8	1.37×10^{-3}	$60\ 5\times10^{-3}$	77.4	2.05×10^{-3}	1.13×10^{-2}	81.8	2.32×10^{-3}	1.48×10^{-2}	84.3
Y^{93}	9.40×10^{-2}	8.27×10^{-1}	88.6	0.0	0.0	--	0.0	0.0	--	0.0	0.0	--
Ru^{106}	1.45×10^{-3}	1.45×10^{-3}	0	1.10×10^{-2}	1.10×10^{-2}	0	1.51×10^{-2}	1.51×10^{-2}	0	9.44×10^{-3}	9.44×10^{-3}	0
Sn^{125}	4.44×10^{-5}	1.27×10^{-3}	96.5	4.88×10^{-6}	1.68×10^{-4}	97.1	3.31×10^{-11}	1.19×10^{-9}	97.2	0.0	0.0	--
Te^{129m}	2.14×10^{-3}	5.65×10^{-3}	62.1	6.31×10^{-3}	1.66×10^{-2}	62.1	4.96×10^{-4}	1.31×10^{-3}	62.1	3.42×10^{-7}	8.00×10^{-7}	62.0
I^{131}	1.91×10^{-1}	3.94×10^{-1}	51.5	1.55×10^{-2}	2.88×10^{-2}	46.2	1.42×10^{-8}	2.49×10^{-8}	43.0	0.0	0.0	--
I^{133}	1.37	2.23	38.6	0.0	0.0	--	0.0	0.0	--	0.0	0.0	--
Ba^{140}	3.47×10^{-1}	6.10×10^{-1}	43.11	1.77×10^{-1}	2.43×10^{-1}	27.16	3.70×10^{-5}	4.74×10^{-5}	21.9	1.53×10^{-14}	1.92×10^{-14}	20.3
Ce^{144}	1.81×10^{-2}	2.66×10^{-2}	32.0	1.40×10^{-1}	1.96×10^{-1}	28.57	1.74×10^{-1}	2.44×10^{-1}	28.7	8.74×10^{-2}	1.22×10^{-1}	28.4
Total *	1.72×10^{1}	2.47×10^{1}	30.3	3.17	4.89	35.2	9.86×10^{-1}	1.48	33.4	2.56×10^{-1}	3.87×10^{-1}	33.8

*Sum of activities of 254 most important fission products.

Diffusion for NERVA. The previous discussion was limited to a consideration of the 1100 MW NRX reactor. In-flight application of a nuclear vehicle may be accomplished by using the 5000 MW NERVA reactor. To date, no estimates of post-operational diffusion have been made for this reactor. However, some post-operational heating histories have been obtained and are reported in Section 6.2. While it is not yet possible to predict the magnitude of fission product diffusion for NERVA under loss-of-coolant conditions, some inferences may be made regarding the magnitude of this diffusion in comparison with that for the NRX reactor.

In the NRX reactor, core integrity was maintained for about 160 seconds after loss-of-coolant. At this time the aluminum brackets which are components of the lateral support system failed. The core was then left in a non-restrained condition, and ejection of fuel elements was predicted. In the case of NERVA the structure of the lateral support system was extensively changed. Leaf springs attached to the graphite inner reflector are no longer used. In NERVA, the lateral support forces are transmitted to the core by segmented graphite seals acted on by graphite plungers which are supported by Inconel springs recessed into the beryllium reflector structure. For a 30-second operating period, it appears that some lateral support will be maintained indefinitely in the event of loss-of-coolant. For a 500-second operating period, lateral support will endure for at least 1500 seconds[51]. With much longer periods of reactor integrity predicted, it is expected that the amount of post-operational fission product diffusion occurring for the NERVA reactor will be greater than that anticipated for the NRX reactor.

3.2.2.2 Nuclear Excursions

In the event the NERVA (or NRX) reactor undergoes a nuclear excursion, it is expected that large quantities of gaseous fission products will be released to the environment. A nuclear excursion may be of two types - destructive or non-destructive. If the excursion is non-destructive, the primary result will be overheating of the core and simultaneous fission product diffusion. In fact, the consequences of a non-destructive excursion will be essentially the same as those accompanying a loss-of-coolant accident. For both the NERVA and NRX reactors, it appears that the only types of excursions which may occur accidentally are those of the non-destructive variety[52].

However, from a safety countermeasure point of view, it may be both feasible and desirable to induce a destructive nuclear excursion.* Such an excursion will serve both to fragment the core into a multitude of small particles and to release fission products. The mechanism of release in this case will differ considerably from that existing under either operational or loss-of-coolant conditions. When fission products are released from the core under the latter conditions, the mechanism of release involves diffusion of the pertinent elements or their ionic derivatives through the graphitic matrix. If the fuel is in a bead form surrounded by a pyro-graphite coating, then release will also involve diffusion of the species through this coating. In the event of a destructive nuclear excursion, it is expected that the primary effect will involve liquefaction of the uranium carbide fuel within the bead structure, rapidly followed by mechanical rupturing of the beads and concomitant fragmentation of the nuclear core[48]. With the uranium carbide in a liquid state, the mechanism of fission product release will be one of evaporation of the fission products from the liquified fuel. The results of several experimental programs have demonstrated the magnitude of release accompanying a nuclear excursion.

TREAT Experiments. The first experiments to assess the magnitude of fission product release during a NERVA excursion involving beaded fuel were those performed at the TREAT reactor at Idaho[53]. In these tests the percentage release of Xe^{133}, I^{131}, and Te^{132} was determined as a function of sample transient energy. The percent release is defined as follows:

$$\text{Percent Release of Nuclide X at } t_s = A_R/A_1 \times 100\%$$

t_s = time after transient when nuclide was separate from its sample environment

A_R = the activity of the nuclide released to sample environment at time t_s

A_1 = calculated activity of nuclide X in the test sample at time t_s, assuming no loss

Iodine release ranged from 0.09 percent at 390 cal/g (900°C) to 10.5 percent at 1870 cal/g (3200°C); xenon release, from 0.08 percent at 390 cal/g to 9.6 percent at 1870 cal/g (3200°C); tellurium release, fr .08 at 390 cal/g to 4.8 percent at 1870 cal/g.

* Excursion mechanisms are discussed in more detail in Section 6.5.

These release data are based on radiochemical analyses performed 2 to 7 days after the transient experiment took place. Thus, it was not necessarily these isotopes which were lost during the transient but rather their precursors in the radioactive decay schemes which were vaporized. In the case of I^{131}, the release fraction measured several days after the transient will depend upon the quantities of Sb^{131}, Te^{131}, and Te^{131m} released during the transient; for Xe^{133} the measured release fraction will be a function of I^{133} and Te^{133} release fractions; while Te^{132} measured release fraction will depend on Sn^{132} and Sb^{132} releases. Because of the delay time required in performing the radiochemical analyses, it is virtually impossible to use these data to evaluate the fractional release occurring during actual transient condition. Fuel damage in the tests consisted of degradation of the fuel bead coatings along with migration of uranium carbide into the graphite matrix. However, no actual fuel fragmentation was observed -- a result believed to be due to the long transient periods (40 m sec) used in these tests. Thus, it is not possible to ascertain whether or not the fission product release in these series of experiments was the result of an evaporation or a diffusion mechanism.

KIWI-TNT. With the performance of the KIWI-TNT experiment, it was possible to assess the magnitude of fission product release occurring under actual destructive excursion conditions. In this full scale nuclear transient test an energy release of 3.1×10^{20} fissions was obtained in a transient period of 0.65 milliseconds[52, 48]. Considerable core fragmentation was observed with the largest degree occurring in the core center where the fission density was highest.

Radiochemical analyses of the KIWI-TNT cloud showed that about 66 percent of the least volatile fission products Mo^{99} and Nd^{147} were found in the cloud subsequent to the test[54]. Larger fractions of most other fission products were found with about 50 percent of the core fuel.

In addition, it was found that radioactive isotope deposition occurred on non-fueled graphite structural components. However, analyses showed that these isotopes resided primarily on the components surfaces. It was concluded by LASL as a result of this test, that in a destructive excursion "almost all of the fission products would be released as vapor with a portion recondensing on cooler fragments".[48]

3.3 REFERENCES

1. General Electric Co., Aircraft Nuclear Propulsion Division, Fission Product Decay Gamma Energy Spectrum, APEX-134, Evandale, Ohio, 153 (U).

2. Blomeke, J. O., and M. F. Todd, Uranium-235 Fission Product Production as a Function of Thermal Neutron Flux, Irradiation Time, and Decay Time, ORNL-2127, December 1958 (U).

3. Clark, F. H., Decay of Fission Product Gammas, NDA-27-29, December 1954 (U).

4. Burrell, M. O., G. F. Duncan, and J. F. Perkins, The Computation of Gamma Activity and Related Effects from the Cyclic Operation of a U-235 Reactor, Lockheed Georgia Company, Nuclear Report-39, August 1958 (U).

5. Perkins, J. F. and R. W. King, Energy Release from the Decay of Fission Products, Nuc. Sci. Eng. 3, 726, (1958) (U).

6. Speigler, P., Energy Release from Decay of Fission Products, USAEC Report NAA-SR-Memo-4126, July 1959 (U).

7. Griffin, J., Beta Decays and Delayed Gammas from Fission Fragments, LA-2811, December 1962 (U).

8. Engle and Fisher, Energy Time Dependence of Delayed Gamma from Fission, LAMS-2642, July 1962 (U).

9. Kochendorfer, D. B., Calculated Activities of U-235 Fission Products for Very Short Nuclear Reactor Operation, USNRDL-TR-757, Volume I and II, June 18, 1964 (U).

10. Hogan, M. A., et al., A Computer Program for Calculating Fission Product Abundance, USNRDL-TR-921, October 15, 1965 (U).

11. Call, D. W., Fission Product Inventory Program, WANL-TME-537, September 1963 (U).

12. Brown, W. S., WANL Source Term Program Status Report, WANL-TME-796, Volume II, May 1964 (U).

13. Westinghouse Astronuclear Laboratory, NERVA Source Term Program, (U), WANL-TNR-178, Pittsburgh Pennsylvania, September 1964 (CRD).

14. Lockheed Missiles and Space Company, Nuclear Flight Executive Program, Nuclear Vehicle Flight Safety Study, Phase III Report, LMSC-A-304973, January 1964 (U).

15. Lockheed Missiles and Space Company, Nuclear Flight Executive Program Operating Manual, LSMC-A824882, July 15, 1966 (U).

16. Couchman, M.W., NURSE-II Nuclear Rocket Safety Evaluation Code for the CDC-3600, NUS-249, NUS Corporation, September 1965 (U).

17. U.S. Naval Radiological Defense Laboratory, Radionuclide Abundance Results of Intercomparison, USNRDL Code 908 Memo to Radiological Effects Working Group, March 1, 1965 (U).

18. Hogan, O.L., et al., BETA SPECTRA II. Spectra of Individual Negatron Emitters, USNRDL-TR-802, December 16, 1964 (U).

19. Hogan, O.L. and M. A. Hogan BETA SPECTRA I. Fortran Program for Composite Spectra, USNRDL-TR-1033, March 28, 1966 (U).

20. Hogan, O.L., BETA SPECTRA IV. Spectra of Individual Positron Emitters, (U. S. Naval) Radiological Defense Laboratory - (to be published).

21. Grandy, G.L., et al, Effluent Studies on NRX/EST, WANL-TME-1476, July 1966 (CRD).

22. Rymer, G. T., Henninger, W. A., and Grandy, G. L., The Release of Fission Products from UC_2 Graphite Fuels, WANL-TME-542, August 1963 (CRD).

23. Rymer, G. T., et al, Interim Report on the Release of Fission Products from NERVA Fuel, WANL-TNR-162, July 1, 1964 (CRD).

24. Rymer, G.T., et al, Interim Report on Fission Product Release from NERVA During Post Irradiation Thermal Anneals and During the NRX-A2 Test, WANL-TME-1165, May 1965 (CRD).

25. Rymer, G.T., et al, Interim Report on the Experimental Investigation of Fission Product Diffusion, WANL-TME-1294, September 1965 (CRD).

26. Rymer, G.T., et al, Progress Report on the Experimental Investigation of Fission Product Diffusion, WANL-TME-1402, March 1966 (CRD).

27. Rymer, G. T., et al, An Examination of the Mechanism of Fission Product Release from NERVA, Classified Paper Presented at AIAA Second Propulsion Joint Specialist Conference, Colorado Springs, Colorado, June 13, 1966 (CRD).

28. Personal Communication, G. T. Rymer and G. L. Grandy, WANL, to W. S. Brown, September 1966.

29. Zumwalt, L. R., et al, Fission Product Release from Monogranular UC_2 Particles, Nuclear Science and Engineering, Vol. 21, pages 1 to 12 (1965).

30. Cleary, J. D. and G. T. Rymer, Interim Report on Fission Product Diffusion Code (FIPDIF), WANL-TME-958, September 1964 (CRD).

31. Trammel, M. R., Analysis of the Effect of Post Operational Heat on a NERVA Reactor, WANL-TME-957, October 1, 1964 (CRD).

32. Cleary, J. D., W. C. McCune, M. R. Trammel, The Coupled NO FLOW-FIPDIF Computer Program, WANL-TME-1224, July 1965 (CRD).

33. Blinn, M. B. and G. R. Kilp, The Hydrogen Corrosion Behavior of NERVA Fuel Elements, Classified Paper Presented at AIAA Propulsion Joint Specialist Conference, Colorado Springs, Colorado, June 1965 (CRD).

34. Blinn, M. B., Hydrogen Corrosion Testing of NERVA Reference Fuel, WANL-TNR-129, January 1964 (CRD).

35. Lyon, L. L., et al, Evaluation of Advanced Phoebus-NERVA Fuel Elements Under Simulated Reactor Conditions, presented at AIAA Second Propulsion Joint Specialist Conference, Colorado Springs, Colorado, June 13, 1966 (CRD).

36. Westinghouse Astronuclear Laboratory, Post-Operational Examination of NRX-A2 Fuel Elements, WANL-TME-1122, April 1965 (CRD).

37. Simmons, C. R., et al, Post-Operational Examination of NRX-A3 Fuel Elements, WANL-TME-1333, February 11, 1966 (CRD).

38. Simmons, C. R. and R. A. Fiore, Preliminary Post-Test Observations on NRX-A4 Fuel Elements, Classified Paper Presented at AIAA Second Propulsion Joint Specialist Conference, Colorado Springs, Colorado, June 13, 1966 (CRD).

39. Westinghouse Astronuclear Laboratory, NERVA Source Term Estimates - Presentation at Cleveland, July 1, 1966, WANL-TME-1468, July 1966 (CRD).

40. Davidson, S. L. and P. J. Richard, Fuel Element Bore Weight Loss Code and its Application to NERVA Core Design, WANL-TME-1344, January 1966 (CRD).

41. Personal Communication, G. L. Grandy to W. S. Brown, WANL, September 1966.

42. Engel, M. J., et al, The Effects of Atmospheric Re-Entry on Graphite Particles, General Electric Company, Missiles and Space Division, DIN: 214 - L28F, January 1964 (U).

43. Bridges, J. M., H. G. Hargrove, and D. Hoecker, Summary Report of the Theoretical, Analytical, and Experimental Studies Performed in the Investigation of the Re-Entry Burn-up of NERVA Fuel, WANL-TNR-135, September 1963 (U).

44. Lockheed Missiles and Space Company, ROVER Flight Safety Program Preliminary Review, Vol. I - Safety Analysis Report - Evaluation of Destruct and Auxiliary Thrust Systems, LMSC-A778908, Sunnyvale, California, March 30, 1966.

45. Bridges, J. M., Experimental Study of the Re-Entry Oxidation of NERVA Fuel, WANL-TNR-072, October 1962 (CRD).

46. Bridges, J. M., G. T. Rymer, and M. E. Korposh, Results of Plasmajet Test of Fueled Materials Containing Additives, WANL-TME-602, November 1963 (U).

47. Grandy, G. L. and R. N. Pinchok, Investigation of the Fission Product Diffusion and Burnup Characteristics of NERVA Fuel Under Re-Entry Conditions, WANL-TME-739, April 1964 (CRD).

48. Los Alamos Scientific Laboratory, ROVER Flight Safety Program - Preliminary Review - Volume III C - Summary Report, The Self Destruct Concept for Post-Operational ROVER Reactor Disposal, RFS-425, April 1966 (Also LA-3535-MS).

49. Westinghouse Astronuclear Laboratory, Fission Product Release NRX-A5, letter to B. P. Helgeson, SNPO-Nevada, July 22, 1966.

50. Westinghouse Astronuclear Laboratory, ROVER Flight Safety Program - Preliminary Review, Vol. II - Safety Analysis Report - Evaluation of Passive Re-entry Approach, WANL-TNR-209, Pittsburgh, Pa., September 30, 1965.

51. Trammell, M. R. and W. C. McCune, Evaluation of the Thermal Response of Three Proposed Reactor Designs to Post-Operational Heat Conditions, WANL-TME-1431, June 1, 1966 (CRD

52. Los Alamos Scientific Laboratory, ROVER Flight Safety Program - Preliminary Review, Vol. V - Summary Report, Nuclear Rocket Safety Neutronics, Los Alamos, New Mexico, September 30, 1965, RFS-376.

53. Simmons, C. R., M. A. Vogel, and A. Boltax, Transient Irradiation Experiments on NERVA Fuel Material, WANL-TNR-157, December 1963.

54. Bryant, E. A., J. E. Sattezahn and G. F. Wagner, Radiochemical Measurements on KIWI-TNT, LA-3290, May 1965.

CHAPTER 4.0

SOURCE TERM DUE TO NEUTRON ACTIVATION

The previous discussion in Chapter 3.0 was concerned with the inventory associated with radioactive fuel material. In addition to this source of radioactivity, there will exist in the reactor, materials which have become radioactive as the result of neutron activation. The purpose of this chapter is to examine the source term associated with activated non-fueled components, to compare the activity of these components with that of NERVA fuel, and to review the experimental and analytical work performed to assess the re-entry ablation characteristics of these materials.

4.1 MATERIALS ACTIVATION OF METALLIC REACTOR COMPONENTS

Calculation of the source strength resulting from neutron activation of all the structural components in the NRX reactors has been documented in the NERVA source term report[1] and in a comprehensive activation analysis report[2]. The former document has included comparisons of the activation product radioactivity with the fission product activity including comparison of radiobiological hazards from re-entering fuel and structural materials debris. Major results and conclusions from that report are summarized below. Stepher - and Planisek[2] provide extensive data and curves on the gamma activity (MEV/sec- ; and gamma dose rates from all NRX-A2 components as a function of decay time following reactor operation for 1.77×10^5 megawatt seconds. The data is applicable to other reactor operating times by direct proportionin of the integrated power.

The relative contributions of each of the activated structural materials and of the fuel to the total beta and gamma activity source strength of the NRX reactors are summarized in Table 4-1[1]. Activity of components fabricated from the four metals shown in the table comprises essentially all of that arising from neutron activation. The contribution from other materials was investigated but found to be negligible. For example, although there is c considerable mass of beryllium present, the total gamma and beta energy source originating from the beryllium comprises less than 0.1 percent of the total activity due to the four materials shown in the table.

TABLE 4-1

CONTRIBUTION OF STRUCTURAL MATERIALS AND FISSION PRODUCTS TO TOTAL SOURCE STRENGTH OF NERVA REACTOR

Time After Shutdown (Hr)	Inconel-X	Stainless Steel	Aluminum	Titanium	Fission Products
		Gamma Energy, Percent			
0	0.01	0.13	0.61	0.02	99.23
0.5	0.03	0.81	0.05	0.002	99.11
1	0.06	1.59	0.08	0.001	98.26
2	0.13	3.27	0.16	0.001	96.44
10	0.14	1.85	0.21	0.006	97.79
24	0.03	0.36	0.10	0.001	99.51
168	0.13	0.68	0.01	0.008	99.19
720	0.52	2.43	0	0.002	97.05
4320	1.47	10.83	0.002	0.005	87.68
8760	1.41	20.64	0.005	0.006	77.94
43800	0.42	51.66	0.02	0.009	47.90
87600	0.30	40.14	0.02	0	59.55
		Beta Energy, Percent			
0	0.02	0.16	0.07	0.04	99.72
0.5	0.02	0.75	0.05	0.008	99.17
1.0	0.04	1.17	0.07	0.01	98.72
2	0.09	2.24	0.12	0.009	97.54
10	0.06	0.91	0.16	0	98 86
24	0.008	0.31	0.14	0	99.53
168	0.008	0.64	0.002	0	99.35
720	0.03	2.38	0.001	0	97.59
4320	0.05	0.71	0	0	99.23
8760	0.03	0.69	0	0	99.28
43800	0.04	0.18	0.001	0	99.77
87600	0.06	0.17	0.001	0	99.77

The data of Table 4-1 show that for periods up to one year (8760 hr) after shutdown, activity from the fission products accounts for 78 percent or greater of the total gamma energy source. For times greater than one year after shutdown, gamma activity due to stainless steel becomes significantly greater, but is still less than the fission product activity even after 10 years decay. It can be concluded that the contribution of the activation products to the total source term inventory is not significant.

4.1.1 Re-Entry Hazards from Activation Products

Although the total inventory of activation products is small in comparison with the total activity due to fission products, it is of interest to define specific radiological safety problems that may exist resulting from re-entry of neutron activated structural materials. The source term from activation products associated with passive re-entry of an NRX and NERVA engine has been described[3]. The NERVA Source Term Program report[1] describes the source strength of small particles that could originate from an explosive destruct countermeasure and could introduce a possible ingestion hazard. It also presents a description of contamination of ocean waters by activating products. A brief summary of these findings as reported in those documents is given below.

4.1.1.1 Passive Re-entry

Passive re-entry behavior of the NRX and NERVA reactor following a loss-of-coolant accident from earth orbit startup and sub-orbit startup of the reactor has been described in Reference 3. Following the loss-of-coolant accident, the reactor core disassembles, and under tumbling conditions, the fuel elements, filler strips, nozzle, lateral support system, and cluster plates are lost from the reactor vehicle in space. The remaining reactor shell is then comprised basically of the pressure vessel, dome, core support plate, beryllium reflector, and shield. The source strength of this shell upon ultimate re-entry and impact on earth is a function of flight failure time (length of reactor operating time) and the subsequent re-entry time (decay time) to earth impact. Calculations of the gamma source strength of this shell due to neutron activation have been calculated for

failures from both orbit start and sub-orbit start missions, and are shown graphically in Figures 4-1 and 4-2, respectively. For comparison purposes, the gamma source strength of a single NRX fuel element is also shown in these figures. For the 100-nautical mile orbit start case it can be seen from Figure 4-1 that the activation products source strength of the entire NRX reactor shell at no time is significantly greater than the source strength from a single fuel element, and is, in fact, less than that from a single element for a failure occurring during the majority of flight time. For the sub-orbit start case, early failures will result in predictable impact locations, with short re-entry times (15 minutes to 1 hour) of the reactor shell. Thus, the activity will be considerably greater than that due to failure from orbit start. It is seen from Figure 4-2 that the gamma source strength of the reactor shell is about eight to twelve times greater than the source strength of a single fuel element for land impact locations. Expected gamma doses to the general population from the 1626 fuel elements impacting in Africa have been calculated[3]. The addition of the equivalent of 8 to 12 fuel elements (from the source strength of the activation products) to the total of 1626 elements would have only a minor effect on the expected population exposures. Passive re-entry analyses were also made for the NERVA (5000 Mw) reactor following failure from startup in 263 nautical mile earth orbit[3]. Because of the long orbit lifetimes of the reactor shell due to the high altitude start, the maximum activation products source strength of the reactor shell was about one-tenth of that shown in Figure 4-1. For failure times later than about 60 seconds after startup, the source strength of a single NERVA fuel element greatly exceeds the reactor shell source strength.

4.1.1.2 Small Particle Consideration

An NRX reactor mission was assumed in which the reactor was started sub-orbitally, followed by nine minutes full power operation and then destructed immediately by a high explosive charge. The beta and gamma source strengths for 1000-micron diameter spherical particle of the structural materials and of a fuel element were calculated at the time of ground impact of the particle, and for decay times up to 10 years thereafter. The 1000-micron particle was chosen as the maximum diameter of an ingestible particle.

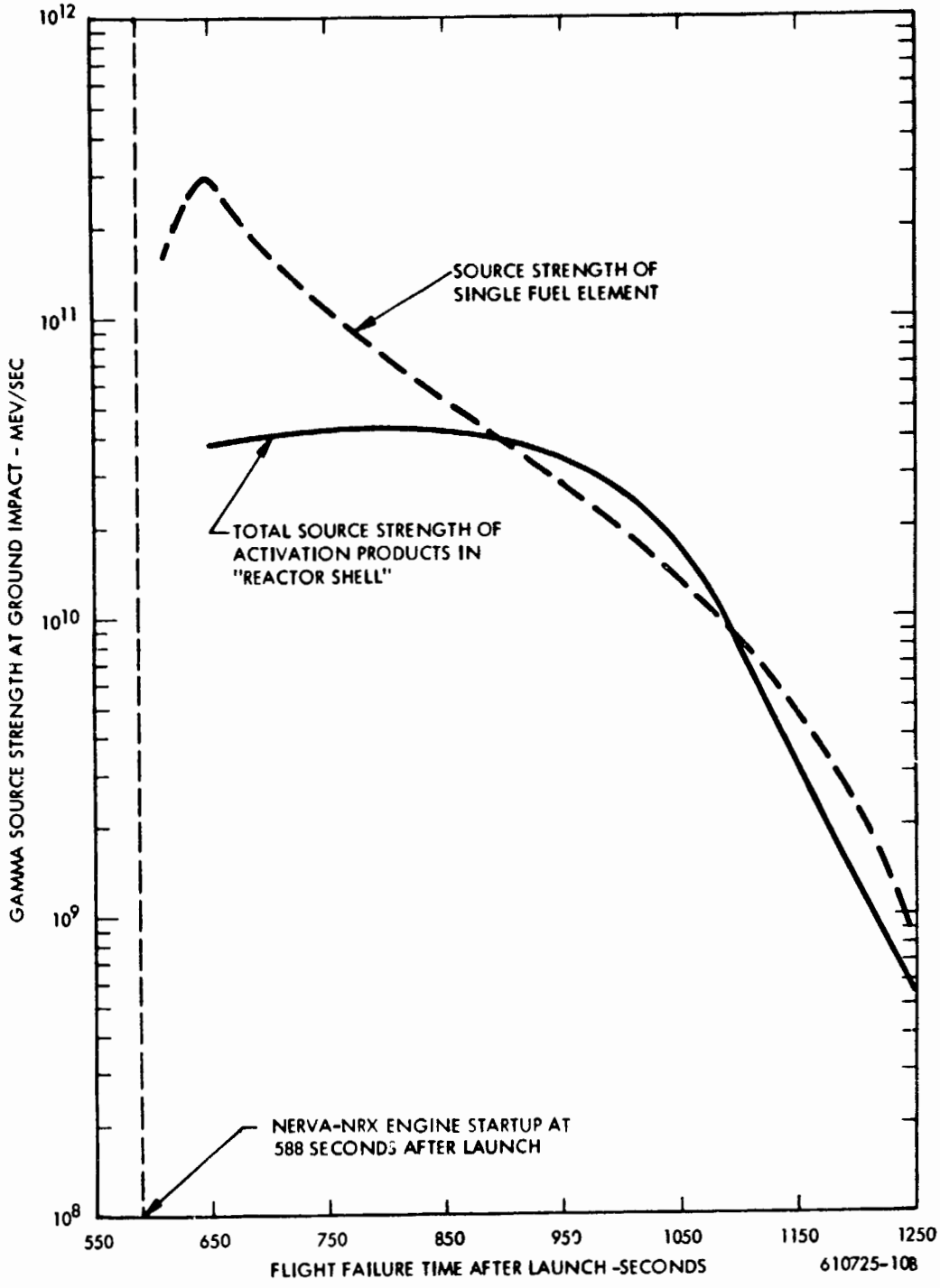

Figure 4-1. Gamma Source Strength of Activation Products and a Single Fuel Element on the Earth's Surface, 100 Nautical Mile Orbit Startup of NRX Type Engine

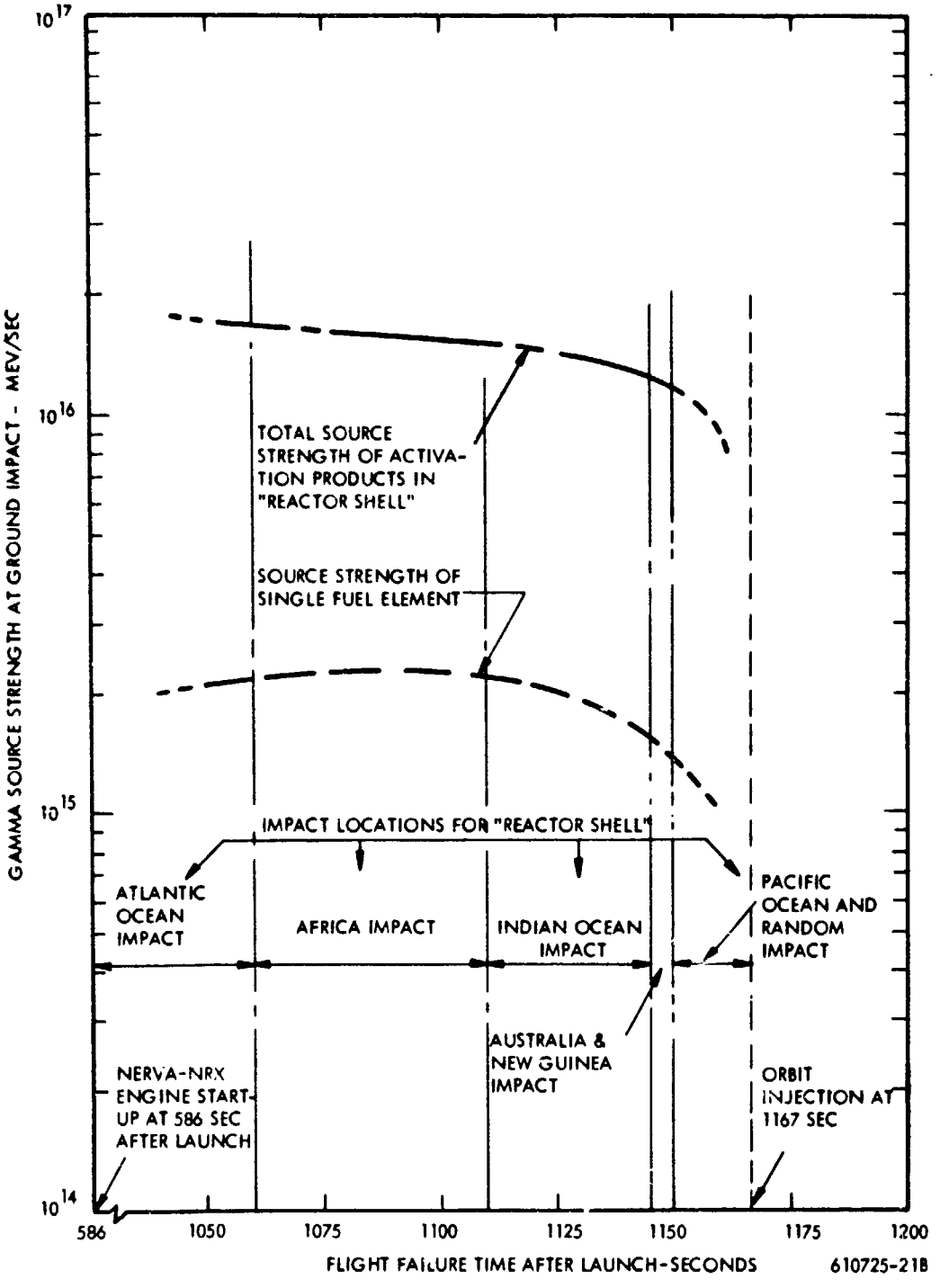

Figure 4-2. Gamma Source Strength of Activation Products and a Single Fuel Element on Earth's Surface, Sub-orbit Startup of NRX Type Engine

The results of these calculations showing the beta energy decay rate are illustrated in Figure 4-3. The beta energy curve is shown because it gives the beta particle emissions from an ingested particle that are of greatest concern. Comparison of the curves in Figure 4-3 reveals that the beta source strength of a fuel particle (due to fission products) always exceeds the activity of a stainless steel or Inconel particle by a factor of 50 to 100. The gamma source strength curves[1] are similar to those of Figure 4-3, with the exception that after one year decay, the fission product activity is about equal to that of the stainless steel and Inconel. Since the beta dose is controlling for ingested particles, the conclusion can be made that the dose received from an ingested particle of activated structural material would be insignificant in comparison with the dose received from an equal volume sized particle of fuel material. This conclusion is based on the reasonable assumption that both particles are insoluble during the residence time within the body.

4.1.1.3 Contamination of Ocean Waters

An evaluation has been made of the extent of contamination of ocean waters by radioactive structural materials resulting from destructive action of an NRX sized reactor[1]. The model used assumed that explosive destruct action occurred following nine minutes power operation from a suborbital start of the reactor. A simplified dispersion model assuming isotropic scattering of the debris was used. The activity at the point of maximum ocean surface particle density was used, and the particles were assumed to be dissolved or dispersed in the water only one meter deep. The activity of the water was calculated after 12 hours from time of destruct. The 12 hours can be considered to include settling time of the particles and residence time in the ocean. The 12 hour period is assumed to be the minimum time possible for the radioactive material to enter the human food chain.

The results of these calculations are summarized in Table 4-2. This table lists the concentration in microcuries per milliliter for 24 different radionuclides formed by neutron activation of NERVA structural materials. These 24 radionuclides comprise greater than 99.9 percent of the total activity originating from stainless steel, Inconel-X, aluminum, and titanium after 12 hours decay. The total concentration of each nuclide is compared with the maximum permissible concentration of radioisotopes in sea water[4] and with the maximum

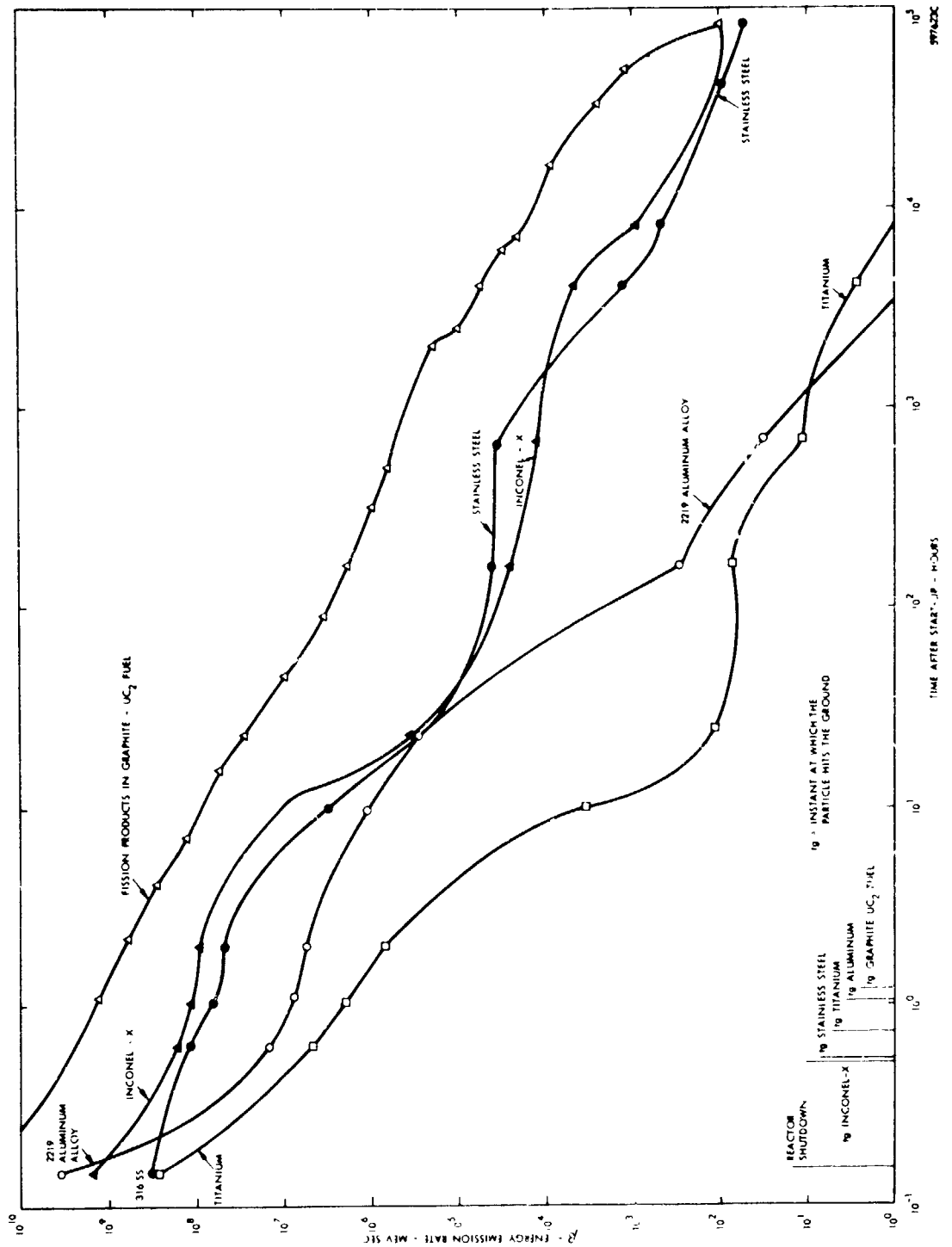

Figure 4-3. Total β Energy Emission Rate of a 1000 μ Diameter Particle of Structural Materials and NERVA Fuel Following Sub-orbital Start with 9 Minutes Full Power Operation (1120 MW) Followed by Destruct

TABLE 4-2

CONTAMINATION OF OCEAN WATER BY RE-ENTRY OF RADIOACTIVE NRX REACTOR STRUCTURAL MATERIALS

Nuclide		Sea Water Activity, μc/ml					Permissible Concentration	
Symbol	t-1/2	316 Stainless Steel	Inconel-X	2219 Aluminum	Titanium (Including Pressure Vessel)	Total	Sea Water[4] MPCC (μc/ml)*	Drinking Water[5] MPC (μc/ml)
Na^{24}	15 h		2.8×10^{-10}	6.0×10^{-8}	9.2×10^{-10}	6.3×10^{-8}		3×10^{-5}
Si^{31}	2.6 h	2.7×10^{-8}	2.2×10^{-10}			2.7×10^{-8}		2×10^{-4}
P^{32}	14.3 d	2.7×10^{-10}				2.7×10^{-10}	2.8×10^{-9}	2×10^{-5}
Sc^{46}	84 d				5.9×10^{-11}	5.9×10^{-11}		4×10^{-5}
Sc^{47}	3.4 d				6.6×10^{-11}	6.6×10^{-11}		9×10^{-5}
Sc^{48}	44 h				4.1×10^{-10}	4.1×10^{-10}		3×10^{-5}
Cr^{51}	28 d	5.8×10^{-8}	1.6×10^{-8}			7.4×10^{-8}	2.0×10^{-7}	2×10^{-3}
Mn^{54}	314 d	3.2×10^{-10}	5.0×10^{-11}			3.7×10^{-10}	6.7×10^{-9}	1×10^{-4}
Mn^{56}	2.6 h	2.3×10^{-6}	4.0×10^{-7}	7.8×10^{-7}		3.5×10^{-6}		1×10^{-4}
Fe^{59}	45 d	5.5×10^{-10}	2.2×10^{-11}			5.7×10^{-10}	3.0×10^{-9}	5×10^{-5}
Co^{57}	267 d	5.8×10^{-10}	3.6×10^{-9}			4.2×10^{-9}	5.0×10^{-8}	4×10^{-4}
Co^{58M}	9 h	5.0×10^{-7}	3.1×10^{-7}			8.1×10^{-7}		2×10^{-3}
Co^{58}	71 d	7.3×10^{-10}	4.4×10^{-8}			4.5×10^{-8}**	1.0×10^{-8}	9×10^{-5}
Co^{60}	5.3 y	7.3×10^{-10}	5.3×10^{-10}			1.3×10^{-9}	5.0×10^{-9}	3×10^{-5}
Ni^{63}	92 y	8.1×10^{-11}	1.5×10^{-10}			2.3×10^{-10}		3×10^{-5}
Ni^{65}	2.6 h	9.0×10^{-9}	1.5×10^{-8}			2.4×10^{-8}		1×10^{-4}
Cu^{64}	12.9 h		4.2×10^{-8}	7.0×10^{-6}		7.0×10^{-6}**	6.0×10^{-9}	2×10^{-4}
Nb^{97}	72 m	3.6×10^{-12}				3.6×10^{-12}		9×10^{-4}
Mo^{99}	66 h	2.4×10^{-7}				2.4×10^{-7}		4×10^{-5}
Sn^{113}	118 d				4.8×10^{-11}	4.8×10^{-11}	4.5×10^{-7}	8×10^{-5}
Sn^{121}	25 h				1.4×10^{-8}	1.4×10^{-8}		
Sn^{123}	125 d				5.9×10^{-11}	5.9×10^{-11}		
Sn^{125}	9.4 d				8.1×10^{-11}	8.1×10^{-11}		2×10^{-5}
Ta^{182}	115 d	1.3×10^{-8}				1.3×10^{-8}	4.0×10^{-7}	4×10^{-5}

* Assuming sea water density of 1 gm/cc.

** Exceeded MPCC.

permissible concentration in drinking water[5]. Blank values in the table indicate there is no data available for these radioisotopes in References 4 and 5.

Additional structural materials of the engine not considered in this analysis (nozzle, piping, etc.) would add to the inventory. However, these additional materials have a low specific activity because of their relatively greater distance from the core and thus they are exposed to neutron fluxes which are at least two orders of magnitude lower than the materials in the reactor. Consequently, these additional materials would contribute only slightly to the specific activity of the sea water.

It is concluded from the results of Table 4-2 that contamination of ocean waters from radioactive debris of the structural materials of the NERVA engine does not pose a significant radiological hazard. Two nuclides, Co^{58} and Cu^{64}, exceed the MPCC for sea water. However, these values are not considered to be hazardous. The assumptions made on the distribution of the radioisotopes in the ocean water are extremely conservative. Most certainly, the debris would not remain in water at only one meter depth, but the larger particles would settle to the bottom. In addition, these metal particles are insoluble, and it is extremely conservative to consider that these materials would be uniformly dispersed or dissolved in the waters within a 12-hour period. Therefore, the most likely concentrations of the radioisotopes in the sea water would probably be several orders of magnitude less than that shown in Table 4-2.

Contamination of ocean waters by fission products from the fuel has been estimated by the NUS Corporation.[8] They assumed a nuclear excursion corresponding to 3×10^{20} fissions (10^4 Mw-seconds), with 100 percent release and solubility of fission products into the ocean water. Two initial sea water volume sources were considered, 10 meter and 100 meter diameters and 10 meter depths, with subsequent dilution calculated by a two-dimensionally symmetric diffusion equation. Peak concentrations of individual fission product nuclides were calculated at 10^3 minutes and 10^4 minutes after the excursion. Fission products with concentration in excess of MPCC at 10^3 minutes were Zr^{95}, Ru^{103}, Sn^{125}, I^{131}, Ba^{140}, [illegible], Ce^{141} and Ce^{144}. At one week (10^4 minutes) all fission products with the exception of Ru^{103} were below MPCC values. However, any evaluation of the radiological importance of these nuclides in relation to human exposure must include consideration of such factors, as the

physical state, stable element configuration, and biological half-life of the fission products. With consideration of these factors plus the additional decay and diffusion at one week, the hazard to man from fission products via the marine environment appears to be small.

4.1.2 Conclusions

On the basis of the information presented in this section, it can be concluded that the source term due to neutron activation products is small in comparison with that due to the fission products from the fuel material. Thus, in performing radiological safety analyses for NERVA reactor systems, the contribution of activation products to the total radioactive source strength of re-entering debris, can be neglected without introducing significant uncertainties in the analysis.

4.2 RE-ENTRY ABLATION OF REACTOR COMPONENTS

It appears that the potential radiological safety problems associated with activated reactor components will be of considerably less consequence than those associated with NERVA fuel. However, in order to examine the problems associated with the re-entry of metallic components, it is necessary to assess the degree to which these materials will ablate during the re-entry process.

4.2.1 Experimental Results

The ablation behavior of the following materials was examined in an experimental plasmajet facility consisting of aluminum 6061-T6, aluminum alloy 2219-T852, titanium A110-At, stainless steel 304-A, Inconel-X750, and beryllium[6]. The samples were tested in the form of one-half inch hemispheres. The experimental conditions involved stagnation pressures ranging from 0 00423 to 0.177 atm. and stagnation enthalpies ranging from 800 to 12,500 Btu/lb. As a result of this study the following conclusions were made:

1. The ablation of aluminum, aluminum alloy, and titanium is governed entirely by the melting process; i.e., the energy required to ablate is simply equal to:

$$Q_m = W \int_{T_i}^{T_m} C_p dT + \Delta H_m$$

where:

Q_m = the heat required to ablate a material, cal

W = the weight of a given sample, g

C_p = the heat capacity function, cal/°C-g.

T_i = initial temperature of the material, °C

T_m = melting temperature of the material, °C

ΔH_m = the heat of melting, cal/g

2. In the case of titanium and stainless steel the presence of a thick, tenacious oxide coat on the samples inhibits ablation. However on pre-oxidized stainless steel samples, where cracks and spalling of the oxide layer are evident, the ablation process is accelerated.
3. Rates of oxidation of all materials studied in the plasmajet system, appear, at least in a quantitative sense, to be similar to those obtained by investigators using static systems.
4. The ablation of Inconel-X and stainless steel at high heating rates is similar to that of aluminum, aluminum alloy and titanium.

In addition, it was observed that: (1) At low heating rates, Inconel-X and stainless steel underwent a phenomenon which was termed "incomplete ablation". Incomplete ablation was attributed to a change in sample geometry which changed the total heating rate to the sample and a change in position of the stagnation point which diminished the heating rate to the sample. (2) The ablation of beryllium required more heat than was predicted theoretically. The reasons advanced for this phenomenon were that the heating rate to the sample was lowered as a result of a change in sample geometry during ablation and/or a change in the position of the stagnation point (see 1 above), and a phase change may have occurred in the temperature range 1240-1260°C.

4.2.2 Advanced Ablation Theories

It appears as a result of the above studies that a simple melting model might serve to explain the ablation process for a wide variety of metals. However, sufficient anomalies existed that it seemed desirable to examine ablation from a more exact theoretical model. A model of this type has been proposed[7].

The model examines the interaction between the gaseous hypersonic boundary layer and the liquid layer of the ablating body. In the model, the conditions at the outer edge of the gaseous boundary layer are determined by the properties of the gas behind the shock. Similarly, the properties of the solid determine the boundary conditions at the solid-liquid interface. The model matches five quantities at the gas-liquid interface; i.e., temperature, tangential velocity, mass transfer, heat transfer, and shear stress. Numerical solutions have been obtained for both the gas and liquid boundary layer equations for the high Reynolds number hypersonic laminar flow regime. A thorough description of this mathematical model and its derivation are given in Reference 7.

4.3 REFERENCES

1. Westinghouse Astronuclear Laboratory, NERVA Source Term Program, WANL-TNR-178, Pittsburgh, Pa., September 1964 (CRD).

2. Stephenson, L.D. and F. Planisek, NRX-A2 Activation Analysis Report, WANL-TME-804, August 1964 (CRD).

3. Westinghouse Astronuclear Laboratory, ROVER Flight Safety Program Preliminary Review, Vol. II, Safety Analysis Report - Evaluation of Passive Re-entry Approach, Pittsburgh, Pa., WANL-TNR-209, September 30, 1965 (CRD).

4. National Academy of Sciences, National Research Council, Disposal of Low Level Radioactive Waste into Pacific Coastal Waters, NAS-NRC Publication 985, Washington, D.C., 1962 (U).

5. U. S. Department of Commerce, Maximum Permissible Body Burdens and Maximum Permissible Concentrations of Radionuclides in Air and in Water for Occupational Exposure, National Bureau of Standards Handbook 69, Washington, D.C., June 5, 1959 (U).

6. Pinchok, R.N. and J.M. Bridges, An Experimental Investigation of the Re-entry Behavior of Metal and Alloys, WANL-TNR-192, December 1964 (U).

7. Gilbert, Leon M. and Sinclaire M. Scala, Analysis of the Hypersonic Re-Entry of the NERVA Nuclear Rocket - II.B. The Hypersonic Ablation of Metals, General Electric Co., Missile and Space Division, DIN:214-228F, September 1965.

8. NUS Corporation, Environmental Safety Aspects of Nuclear Rocket Flight Operations, Annual Progress Report, NUS-179, Washington, D. C., June 1964 (U).

CHAPTER 5.0

ACCIDENT AND PROBABILITY MODELS FOR NUCLEAR POWERED FLIGHT VEHICLE SYSTEMS

In the event of an in-flight failure involving a nuclear powered engine system, the vehicle may fail to complete its mission objectives. One consequence of such an occurrence would be the eventual re-entry of radioactive debris to the Earth's biosphere. The time required for such re-entry could range from about fifteen minutes if failure occurred during the sub-orbital portion of the flight to years in case the accident took place during the orbital phase of operation. However, the source term of re-entering debris will depend to a large extent upon the type of accident which occurs and the post-accident behavior of the system. In order to evaluate source terms, a definition of potential accidents and their effect on the flight system is required. In addition, the definition of accident models is required for the assessment of the practicality of utilizing post-accident countermeasures and for the evaluation of the efficacy of such countermeasures in reducing source terms. However, in order to view accident data in a realistic light, it is also necessary to examine these accidents in terms of failure probabilities.

5.1 ACCIDENT MODEL DEFINITION

The process used in the selection of an accident model may follow two approaches. In the first approach, a maximum credible accident is selected for analysis. Other accident types are identified but are eliminated from analysis in terms of being either incredible or of lesser consequence than the maximum credible one. Once this accident model is identified, the radiobiological consequences associated with the particular accident situation may be assessed. If such consequences pose no safety problem, it follows that accidents of lesser magnitude are also safe.

The second approach involves a more detailed examination of the individual malfunction situations which might conceivably lead to entire flight system failure. Once system malfunctions are identified, the response of the system to the malfunction may be evaluated by the use of appropriate analog computer programs. In many cases it may be found that the system itself may serve to compensate for a given malfunction. If it does not, appropriate design changes or countermeasures may be included in the system to prevent the given

malfunction from leading to mission abort. In the event that neither design changes nor countermeasures may be found to alleviate the consequences of a given malfunction situation, it becomes necessary to perform a safety analysis associated with the malfunction. Post-accident behavior must be evaluated, source terms must be assessed, and finally the degree of interaction of the radioactive debris with the Earth's populace must be determined.

The primary virtue of this latter approach arises from the fact that the probability of an accident occurring may be based on the reliability estimates generated during system design and testing. If a malfunction is found to lead to mission abort, then failure mode analyses and reliability data may be used to determine the probability of its occurrence. Moreover, the examination of system response subsequent to malfunction will aid in the development of techniques to prevent system failures. Such detailed accident examination will require participation and cooperation of all major reactor/system/vehicle contractors.

5.1.1 NRX Accident Model

In recently published safety analyses reports[1, 2], a loss-of-coolant accident model was chosen as a basis for subsequent safety analyses. The approach used in selecting this particular accident situation resembled most closely that used in determining a maximum credible accident. A number of postulated accident situations were considered and the consequences of each situation to the flight system were either postulated or examined analytically. In all cases it appeared that the accident situations would lead either to loss-of-coolant or to some accident situation less severe in its consequences. A more detailed failure mode analysis tended to support the conclusion that most postulated failure modes would lead to this malfunction situation.[3] Table 5-1 summarizes the accident types and events considered in these safety analysis studies.

5.1.2 Preliminary NERVA Accident Model

Since the issuance of the aforementioned reports, considerable work has been performed in developing the design of a 5000 MW reactor, NERVA. The development of this system is, to a large extent, still in the design stage, and it is not possible at present to perform the detailed malfunction studies required for the definition of accident models. However, a preliminary examination of the NERVA flow system appears to be merited to determine the applicability of a loss-of-coolant accident model to NERVA.

TABLE 5-1

SUMMARY OF ACCIDENTS

Type of Accident	Accident Event	Accident Model Chosen
Thrust Misalignment	1. Gimbal Hardover 2. SN Guidance and Control Loss 3. Failure of Roll Control Jets	Reactor Intact Until Re-Entry
Neutronic Systems Failure	1. Excursions at Startup Control Drum Runout Accidental Hydrogen Insertion with Drums Full-In 2. Excursion Under Steady State Operation Control Drum Runout Accidental Increase in Hydrogen Density	Loss-of-Coolant in all Cases
Loss-of-Coolant	1. Failure of the Turbine Drive 2. Nozzle Burn Through at the Hot Bleed Port 3. Premature Closure of the Tank Shut-off Valve 4. Failure of the Emergency Coolant Valve to Open Following a Fault Condition 5. Coolant Line Breakage	Loss-of-Coolant in all Cases
Other Accidents	1. Failure to Startup 2. Spontaneous Structural Failure of the Reactor 3. Spontaneous Structural Failure of the Stage 4. Loss of Communications 5. Undefined Multiple Simultaneous Failures	Eliminated-No Hazard Eliminated-Incredible Loss-of-Coolant Reactor Intact Eliminated-Incredible

Figure 5-1 is a schematic of the NERVA flow system, and is similar in all respects to the NRX flow system, except in terms of the tie tube supply system. The NERVA reactor[4] will contain counterflow tie tubes, and as a result, will contain two parallel reactor coolant paths upstream of the reflector outlet. The main feed line will supply coolant flow to the nozzle and thence to the reactor as was done in the NRX series. The second coolant line branches off the pump discharge line upstream of the nozzle tube inlet. This flow, which will serve to cool the counterflow tie tubes, passes through a tie tube control valve (TTCV) which serves to regulate the coolant flow rate. The tie tube coolant line enters the pressure vessel head and is distributed around the shield to the tie tube supply plenum. Individual support tie tubes are then cooled from this plenum. The discharge from the tie tubes enters an effluent plenum which is open at the periphery to the reflector outer plenum. Here the tie tube discharge flow joins the nozzle coolant (i.e., main reactor flow). The two flows are mixed here and during their flow through the shield pass, plena, and support plate. The total coolant then passes through the core and is either exhausted through the nozzle or passes through the hot turbine bleed to the turbine power control valve, then through the turbine from which it is then exhausted.

Since the system does resemble that employed in the NRX reactor, the conclusion that loss-of-coolant is a probable accident situation for the NERVA reactor appears valid. Thus the following failures could lead to loss-of-coolant to the reactor:

1. Failure of the turbine power control valve,
2. Nozzle burn through at the hot bleed port,
3. Premature closure of the tank shut-off valve, and
4. Coolant line breakage.

However, the inclusion of the tie tube coolant system does impose one additional problem. In the event the tie tube control valve closed during operation, coolant to these tubes would cease. The tie tubes could conceivably yield or melt thus removing axial support from the system at a time when coolant was flowing through the remainder of the core. The consequence of such an accident situation in terms of core disassembly would appear to be conceivably different from that arising in the event of complete loss-of-coolant to the total core subassembly. To prevent such an eventuality, the TTCV will be bypassed by an orificed

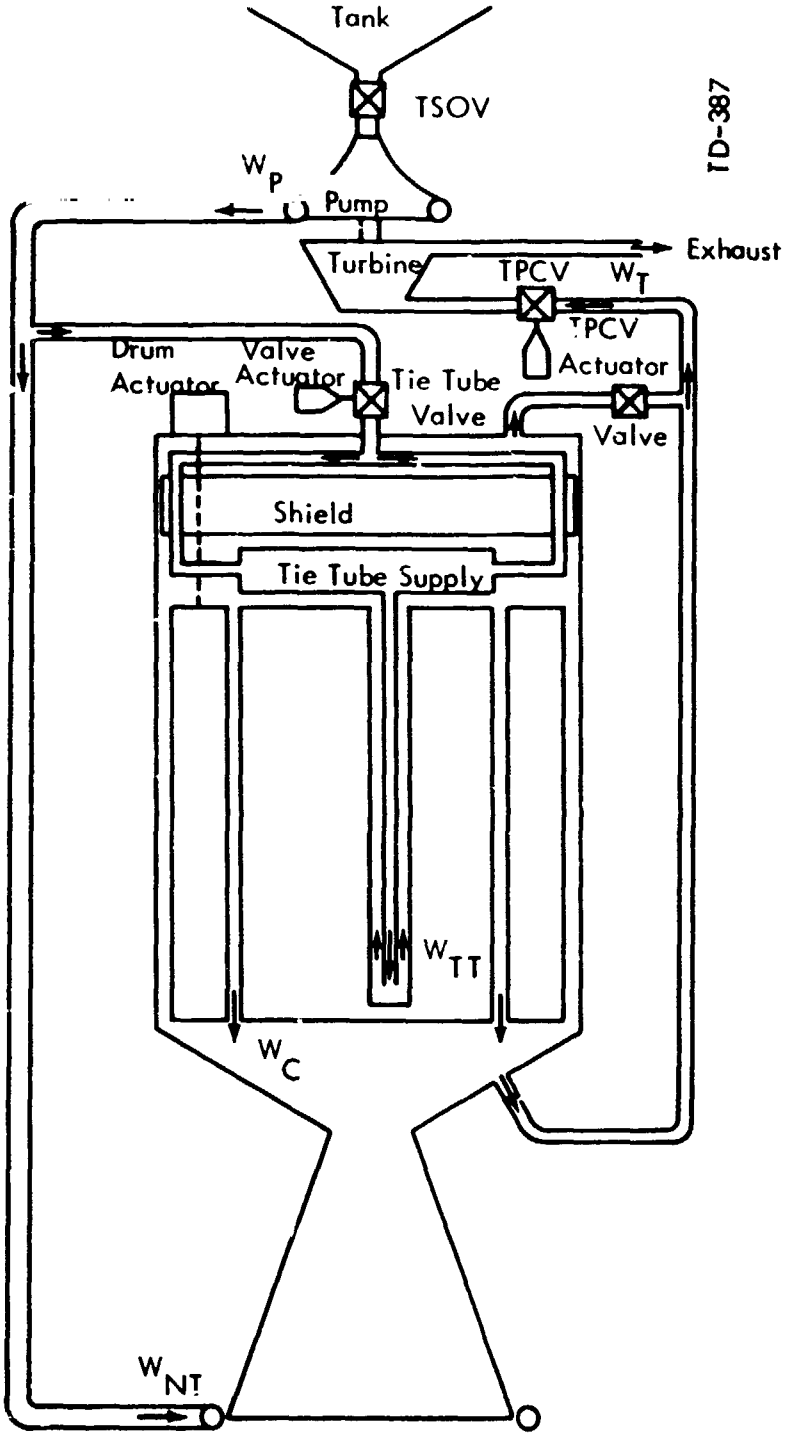

Figure 5-1. NERVA Engine Schematic

line which will deliver 10 lb/sec flow in the event the TTCV closes during operation. Thus, the inclusion of a separate support system does not appear to introduce any flow accident situations different from those considered for the NRX reactor.

5.2 RELIABILITY AND FAILURE PROBABILITY

It is not possible to establish with any accuracy the reliability or probability of failure for a flight system that does not yet exist as hardware. However, certain generalizations can be made based on experience with similar systems, thus providing a conservative "best estimate" of reliability parameters. Lockheed Missiles and Space Company has made estimates of the nuclear stage reliability for specific flight missions powered by NRX and NERVA engines.[1] These estimates have been made in the context that nuclear rocket technology is continuously evolving, and the estimates are conservative representing reasonable examples of what a nuclear stage can be expected to achieve. These Lockheed estimates have been used as the basis for calculating failure probabilities in the safety evaluations of passive re-entry[2] and safety evaluations of explosive destruct and auxiliary thrust system[1] for selected flight missions of NERVA. A summary of the Lockheed reliability estimates and failure probability models that have been used in the ROVER program is presented below.

5.2.1 Mission Reliability Estimates

It has been assumed that the reliability of the first two chemical stages is 1.0; that is, only those flights reaching the point of nuclear stage startup are considered. The reliability estimates are conservatively assigned on the basis of the early operational period of nuclear rocket vehicles. Early operational values apply to the first block of vehicles subjected to actual flight after the successful completion of development, Preliminary Flight Rating Test (PFRT), and qualification testing. A later operational phase identifies that period of vehicle evolution in which the reliability growth curve has attained reasonable stability.

Nuclear stage reliability depends on the mission, reflecting in part the difficulty of the mission profile, such as whether engine shutdown and re-start are required, guidance and attitude requirements, etc. LMSC has made reliability estimates for the three mission models analyzed in the preliminary review of ROVER flight safety. The three mission models are summarized in Chapter 8.0 of this report. Each of the basic functions that must be performed

by the nuclear stage in order to attain mission success is assigned reliability estimates. Reliability estimates are also made for each of the basic functional modes for engine operation. These estimates are presented in Table 5-2[1].

5.2.2 Failure Probability Functions

The probability of failure at any time during the mission can be calculated by using the data of Table 5-2. Basically, this is accomplished by dividing the mission flight profile into discrete time increments representative of the various engine and stage functional modes. Then by applying the reliability estimates for each function, a cumulative reliability for each time increment can be calculated for the entire stage. The failure probability is then determined by subtracting the cumulative reliabilities for each time increment. The derivation of the failure probability by this technique is described in Reference 5. The probability of failure during any of the time increments is considered constant, and the instantaneous failure rate can then be defined as the probability of failure per second. This failure rate is a discontinuous step function that has a constant value over selected time increments for each mission.

TABLE 5-2

MISSION MODEL RELIABILITY ESTIMATES

MS-N Stage Function Reliability Estimates

MS-N Stage Function	Stage Reliability MM I and III	MM II
Separation	1.00	0.980
Guidance	0.935	0.940
Attitude Control	0.945	0.950
Nuclear Engine Operation	0.800	0.800

Engine-Operation Reliability Estimates for Basic Functional Modes

Engine Function		
Sub-Power Start	0.9500	0.980
Start Transient	0.9000	0.930
Operation (full duration)	0.9356	0.9427
Shutdown		0.960
Cooldown		0.970

A typical failure rate curve (failure probability rate function) for a 72-hour lunar mission utilizing the NERVA engine started in earth orbit at 263 nautical miles, as calculated by LMSC,[1] is shown in Figure 5-2. Since many systems come into use at the time of second stage separation and startup of the NERVA engine, the failure probability rate is highest during the first few seconds of operation. The integral of the failure rate probability function between any two values of powered flight time gives the probability that a failure event would have occurred within that time interval. Expressed mathematically, the failure probability is:

$$F_p(t) = \int_{t_1}^{t_2} p(t)\, dt$$

where $p(t)$ = the vehicle failure rate probability function

$F_p(t)$ = the probability of occurrence of a failure event within the time interval t_1 to t_2

The failure rate functions have been used in the safety analysis of nuclear vehicle flight missions in order to predict the expected population dose exposures[1, 2]. Further discussion on the application of the failure rate functions is presented in Chapter 8.0.

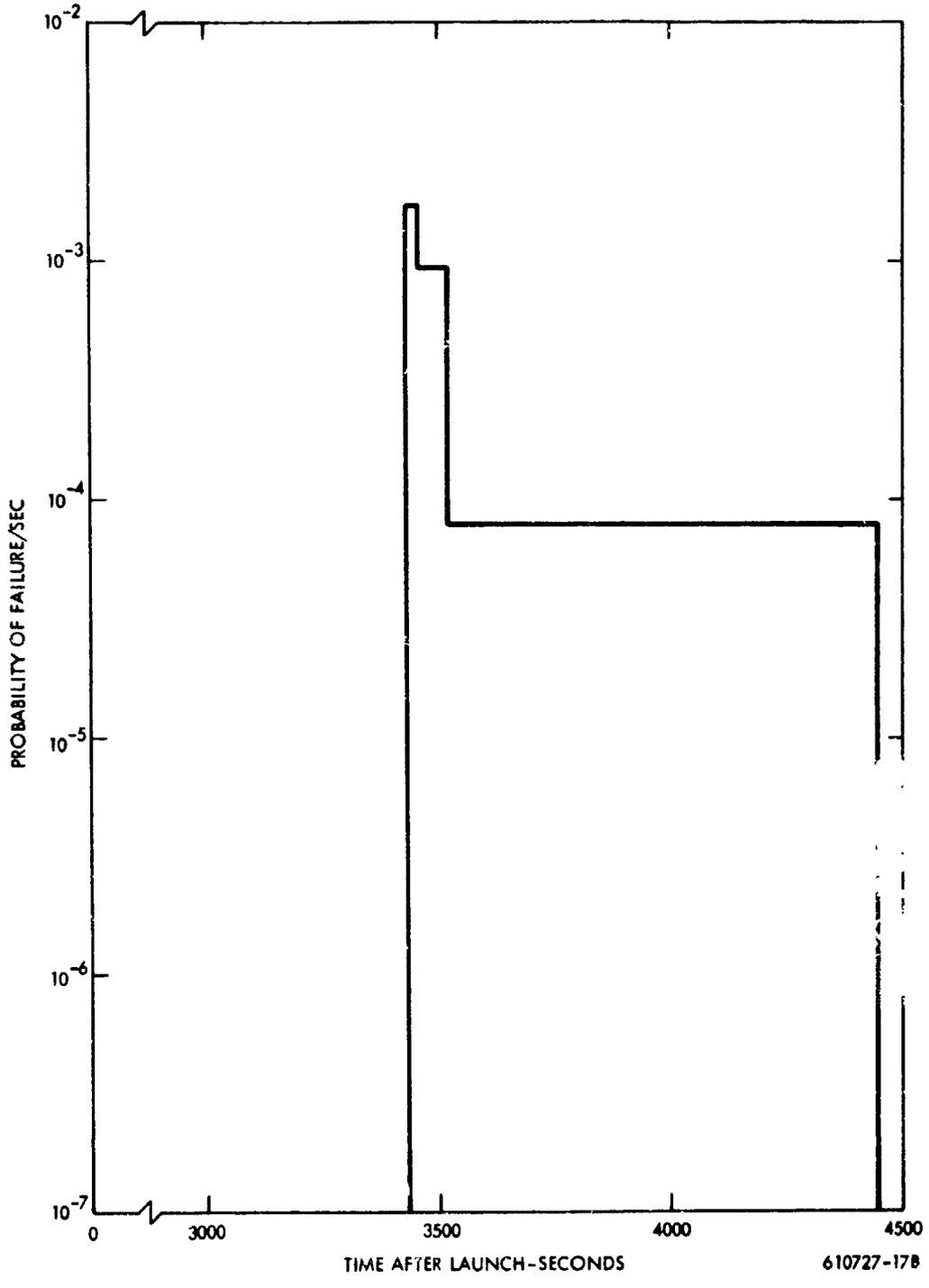

Figure 5-2. Mission Failure Probability Rate Function - Mission Model III

5.3 REFERENCES

1. Lockheed Missiles and Space Company, ROVER Flight Safety Program Preliminary Review. Vol. I, Safety Analysis Report - Evaluation of Destruct and Auxiliary Thrust Systems, LMSC A778908, March 30, 1966(CRD).

2. Westinghouse Astronuclear Laboratory, ROVER Flight Safety Program Preliminary Review, Vol. II, Safety Analysis Report - Evaluation of Passive Re-Entry Approach, WANL-TNR-209, September 1965 (CRD).

3. Contreras, W., NERVA Core Sub-Assembly Flight Safety Failure Mode Analysis, WANL-TME-1206, July 1965 (CRD).

4. Westinghouse Astronuclear Laboratory, NERVA II Conceptual Design Report, WANL-TME-1315, October 1965 (CRD).

5. Lockheed Missiles and Space Company, Nuclear Vehicle Flight Safety - Summary Report for Phases I and II, LMSC-B061396, Sunnyvale, California, July 31, 1963 (CRD).

CHAPTER 6.0
COUNTERMEASURE SYSTEMS

In order to provide the maximum safety to an operational nuclear powered flight vehicle, suitable safety systems must be incorporated into the nuclear propulsion system design. Prior to startup of the nuclear stage, the safety problems associated with the nuclear system are quite similar to those existing for any rocket vehicle, unless the nuclear reactor were to undergo a nuclear excursion. To prevent such a contingency, an anti-criticality poison system has been studied for inclusion in the NERVA flight engine design. In the event that flight system failure were to occur after reactor startup, the possibility exists that the radioactive material generated during reactor operation will re-enter the earth's biosphere, thereby, posing a potential radiobiological safety problem. If such an event does occur, a decision must be made as to what subsequent course of action must be pursued. A number of alternatives are presently under consideration. The simplest of these would involve taking no major action and allowing the reactor to re-enter passively. Alternatively, safety countermeasures may be employed whereby specific action is taken to insure safe disposal. Such action may range from application of auxiliary thrust to produce a controlled impact location or boost to long-life orbit to the deliberate destruction of the reactor into a multitude of small fragments, all of which would hopefully pose no radiological safety problems. This section summarizes the analyses and experimental work performed to date on proposed safety systems currently under study.

6.1 ANTI-CRITICALITY POISON WIRE SYSTEM (ACPS)

Prior to start-up of the SN stage the reactor has no fission power inventory; however, if a nuclear excursion were to occur, a fission product inventory would be generated, and the potential of a radiological hazard would exist. A number of possible accidents which could lead to such a reactor transient have been identified, and include:[1]

1. Core implosion within the liquid detonating region of a C-5 booster fire explosion.

   Water accidents involving high velocity water injection in the core from water impact, or complete water reflection from core immersion (no water in core).

3. Core deformation from land impact.

4. Liquid hydrogen injection in the core through pump malfunction.

5. Gross control drum "runout malfunction".

In order to prevent this type of accident an in-flight poison wire system was designed[2]. This system will maintain the reactor subcritical in the event of all the above accident situations, from assembly to just prior to engine startup.

6.1.1 System Description

6.1.1.1 Wires

The wire material and structure selected, depend upon the type of accident situations and environments which the engine system may encounter. To be an effective countermeasure the wire must be capable of: resisting the high temperatures associated with launch pad fires, remaining pliable at low temperature so that wire removal may be accomplished under orbital flight conditions, and being insoluble in sea water for long periods of time to prevent poison removal in the event of a loss of coolant accident.

Analyses indicated that boron would be an effective element in maintaining the reactor subcritical under accident conditions. In order to obtain the boron in a form which is both insoluble in sea water and of a high melting point, it was decided to make the wires of boron carbide (B_4C). To reduce the weight of poison material required, the B_4C should be prepared from the B^{10} isotope. If 80 to 90 percent enrichment is employed, then the number of wires required to obtain a given poisoning effectiveness is reduced to about one-third the number needed with natural boron.

Since it is necessary to keep the wires flexible at low temperatures and to prevent core and nozzle damage upon removal of the wire, the B_4C wires must be coated. Figures 6-1 and 6-2[2] show cross-sectional and longitudinal views of the proposed poison wire design. This design consists of a B_4C center surrounded by nylon shrinkable tubing, which is in turn enclosed by a braided fiberglass tube and covered with a Teflon sheath. Flexibility can be achieved if the wires are broken into 1/8-inch segments and if fiberglass braid is used in the poison stick encasement as a means of transmitting tensile forces through the length of the wire. This fiberglass braid is not only flexible and strong, but is also resistant to high

Figure 6-1. Cross-sectional View of Poison Wire

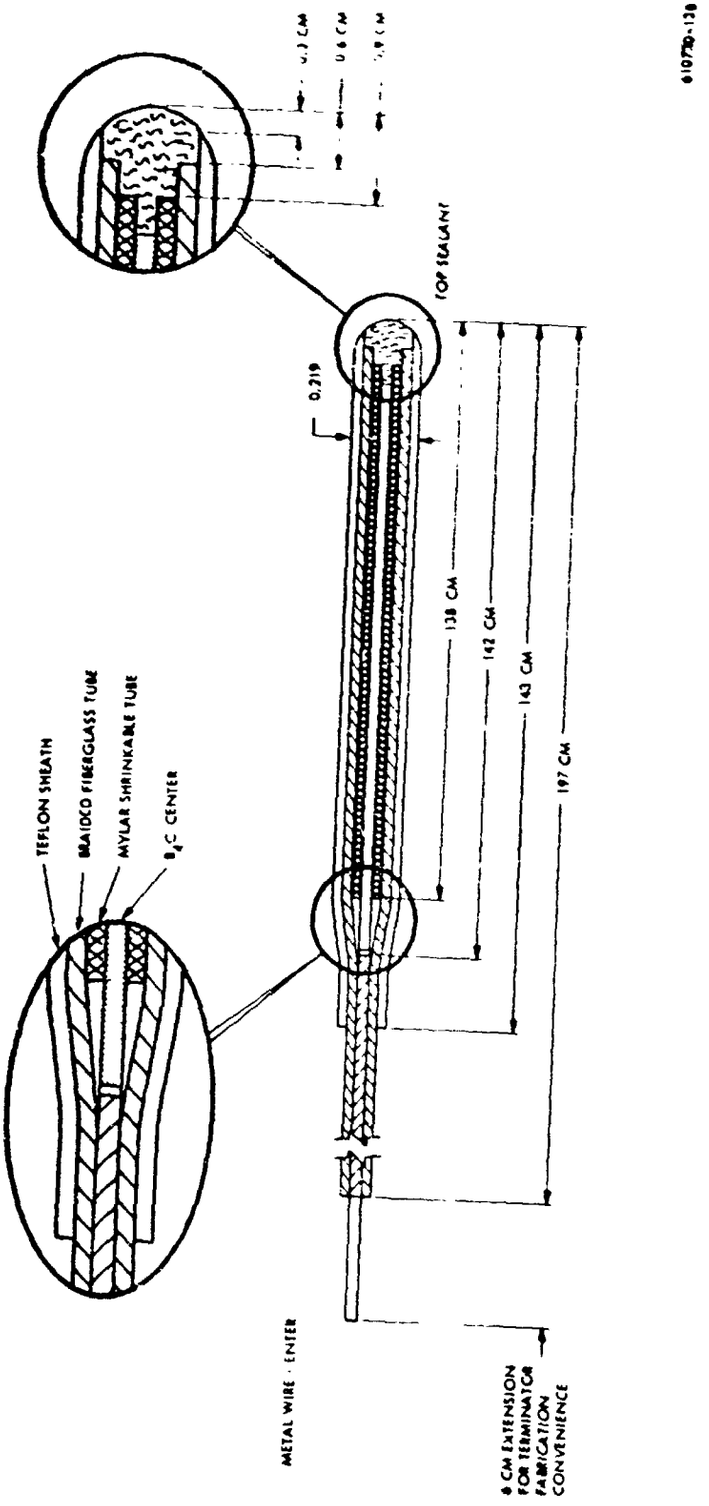

Figure 6-2. Longitudinal View of Poison Wire

temperatures. The outer surface of the prototype poison wire is a Teflon sheath which is shrunk over the fiberglass braid. The low friction coefficient of Teflon minimizes resistance to forces applied during withdrawal of wires from the reactor. Moreover, this Teflon coating serves to prevent the release of poison material through openings in the fiberglass wall.

Reactivity calculations have been performed to determine the total number and the distribution of wires required for effective poisoning[3]. Results indicate an essentially uniform wire distribution with approximately 10 wires per fuel cluster. For convenience in assigning wires to fuel clusters, the nominal number of wires required to establish a bundle was set at ten. In these bundles of ten wires the terminus ends of individual wires are joined, and the integrated bundle is attached to the wire withdrawal system.

6.1.1.2 ACPS System

Figure 6-3 shows a preliminary conceptual design for the ACPS system[2] which is basically a mechanical spring actuated system, but uses a pneumatic motor to initiate wire extraction. It operates on the principle of relative movement of an inner and outer cylinder and the mass momentum generated by instantaneous release of pre-compressed springs. Figure 6-3 shows the placement of this system within the nozzle where a protective foam material will prevent nozzle damage. In this system the wire bundles are connected to a retainer plate via a terminal link. This plate is locked into place by actuator-controlled locks in a guide cylinder that is mounted in the the divergent section of the nozzle. Upon actuation by a telemetry signal, the retainer plate and poison wire are withdrawn from the core by a pneumatic motor connected to the retainer plate via a spring steel wire extraction tape. When the piston to which the retainer plate is attached reaches the end of its travel in the guide cylinder, it hits a proximity switch which shuts off the pull mechanism and induces a telemetry signal which indicates to a ground station that the wires have been extracted and stored. A ground telemetry signal then arms the removal mechanism of the inner locking tube latch. Following this, appropriate release mechanisms are activated, and the entire system is released from the nozzle along with the protective foam materials. The entire operational sequence lasts 10 seconds and occurs just before SN startup.

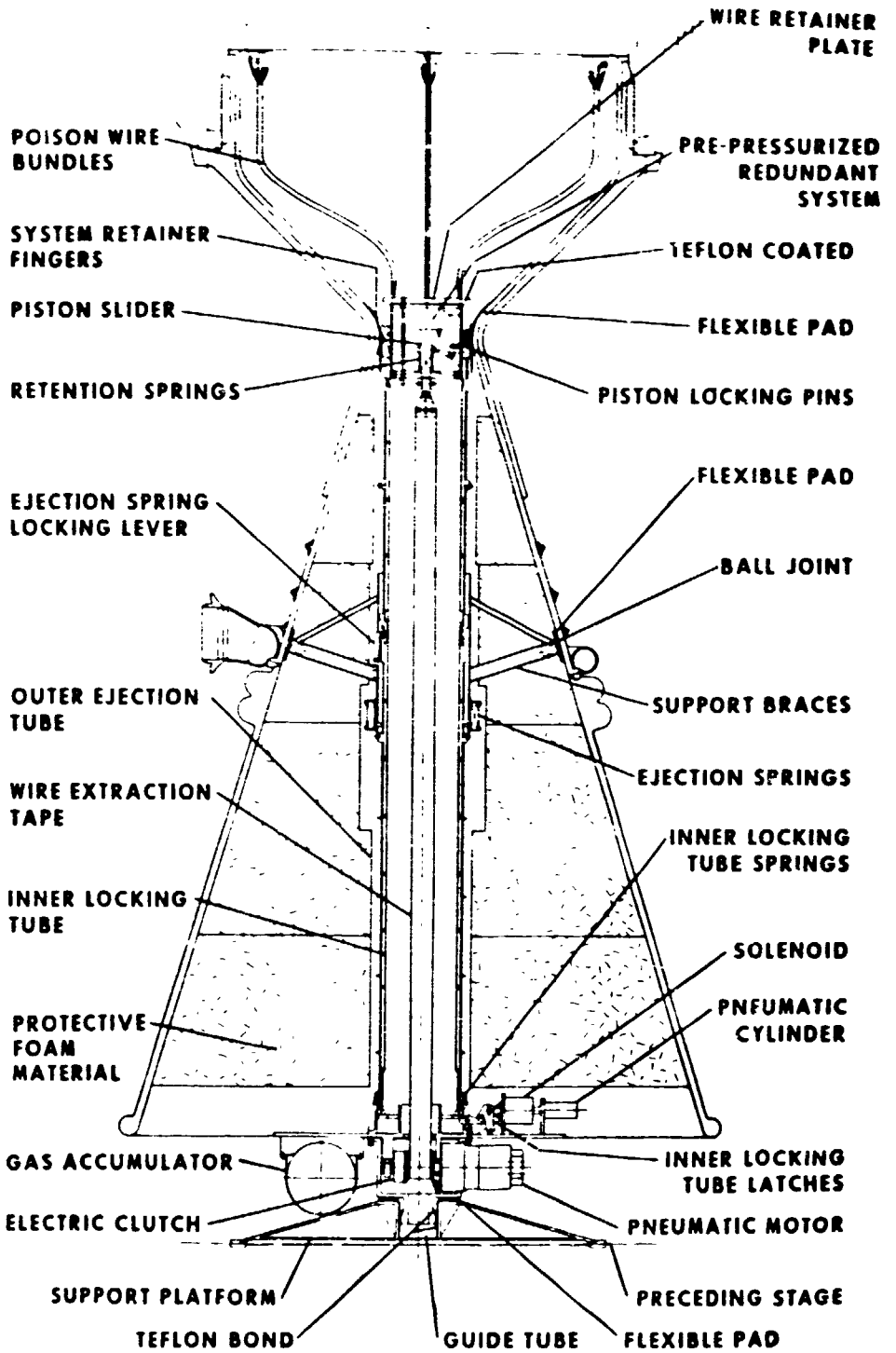

Figure 6-3. Preliminary Conceptual Design for the ACPS

6.1.2 Neutronic Considerations

In order to evaluate the total number of wires required to maintain the core subcritical in the event of an accident situation, a parametric study was performed to determine the effect of changing B_4C density, wire diameter, and number of wires on reactivity under a water flooded condition. This is considered to be a worst accident case. The reactivity of a water flooded reactor was determined to be 1.59 k_{eff}. A reactor reactivity of 0.95 k_{eff} was considered to provide an adequate shutdown margin. The following results were obtained for the 1100 Mw NRX reactor:

1. Reactivity variation is relatively insensitive to $B_4{}^{10}C$ density over the range 80 to 90 percent theoretical.
2. A ten percent change in the number of wires in the range 2000 to 2200 wires results in about a 0.04 reactivity change.
3. A change in wire diameter from 0.137 cm to 0.157 cm results in about 0.08 reactivity change.
4. Two thousand wires, containing 85 percent theoretical density $B_4{}^{10}C$ of 0.147 cm diameter, uniformly distributed throughout the core are adequate to maintain the fully flooded reactor at or below a reactivity of 0.95.

Pre-assembly experimental (PAX) reactor critical tests were conducted to determine the worth of poison wires. Experimentally determined wire worth at the center of the reactor was 5.3 to 6.0 cents each with a dry reactor, and 9.2 to 13.9 cents each for a water flooded reactor (water simulated with polyethylene rods). Calculated worth for wires in the same position was 4.0 cents each in a dry reactor and 6.9 to 9.3 cents in a flooded reactor. These tests indicate the flooded reactor calculations to be somewhat conservative. It appears that 2000 wires will be more than sufficient to maintain a water flooded reactor subcritical.

6.2 PASSIVE RE-ENTRY

The term "passive re-entry" refers to a course of action wherein no major countermeasure is applied subsequent to an in-flight failure of a nuclear stage. The only positive measure that will be taken is to separate the reactor, pressure vessel, and nozzle from the

remainder of the nuclear stage. Under such passive conditions, the fate of this re-entry vehicle becomes a function of the operating history before abort, of the subsequent behavior of the reactor system following failure, and of the natural phenomena associated with atmospheric re-entry at hypersonic velocities.

6.2.1 Post-Accident Reactor Status

The discussion of passive re-entry will be confined to consideration of an accident situation involving total loss-of-coolant to the reactor (Section 5.1). To assess the efficacy of passive re-entry as a post-failure course of action, it is necessary to examine the effect of this loss-of-coolant accident on reactor integrity. The ultimate source term associated with debris will depend to a large extent upon the ability of the reactor to withstand post-operational heating. If the reactor has such capability then the following advantages exist:

1. An ATS system may be utilized to control impact location of a failed reactor. This condition is of particular importance in the event of failure during the sub-orbital portion of a flight trajectory when the spent reactor or reactor debris may impact on land. Use of an ATS system will allow for deep ocean disposal of the radioactive debris. However, the use of such a device is predicated on the condition that the reactor can withstand the forces associated with thrust application.
2. Advantage may be taken of the longer orbital lifetime associated with an intact reactor as compared with that of an individual fuel element. (For the NRX reactor the lifetime of a reactor in orbit will be about 27 times greater than that of a single fuel element in the same orbit.) This enhanced orbital lifetime allows time for additional fission product decay and will ultimately serve to reduce the fission product inventory of re-entering debris.
3. Fission product diffusion will take place during the time period the reactor suffers high core temperatures, subsequent to loss-of-coolant as long as the reactor remains integral. Once disassembly

occurs fuel elements will be released to the local environment where they will cool rapidly. Diffusion will then cease. Thus, the longer the reactor maintains integrity, the longer will diffusion take place and the smaller will be the inventory of reactor debris which eventually re-enters the biosphere.

On the basis of the above potential advantages associated with maintaining a reactor intact, it is obvious that an assessment of the response of a reactor to post operational heating is mandatory.

6.2.1.1 The NRX Reactor

The post-operational heating response of an NRX reactor may be evaluated by using either the NOFLOW[4] or the NOFLOW-FIPDIF[5] computer programs. Both codes consider two sources for the post operational heating of the reactor: fission power and the power resulting from fission product decay. However, in addition, the NOFLOW-FIPDIF program takes into account the reduction of fission product inventory in the core as a result of isotope diffusion at high core temperatures.

A schematic of the geometric model of the NRX reactor used in post operational heating analyses is shown in Figure 6-4. For computing post-operational temperatures, each component was considered to be composed of an arbitrary number of axial segments. The following types of heat transfer modes and energy generation and loss terms were considered:

1. Axial conduction from each segment of each component to adjacent segments.
2. Radial conduction from the core through the pyrographite tiles surrounding the core to the graphite filler strips.
3. Conduction from the core through the pyrographite sleeve surrounding each tie rod.
4. Radiation from the core exit face to each nozzle segment.
5. Radiation from the core inlet face to the core support plate.
6. Radiation from the core support plate to the shield second pass.
7. Radiation from the graphite filler strips to the graphite reflector.

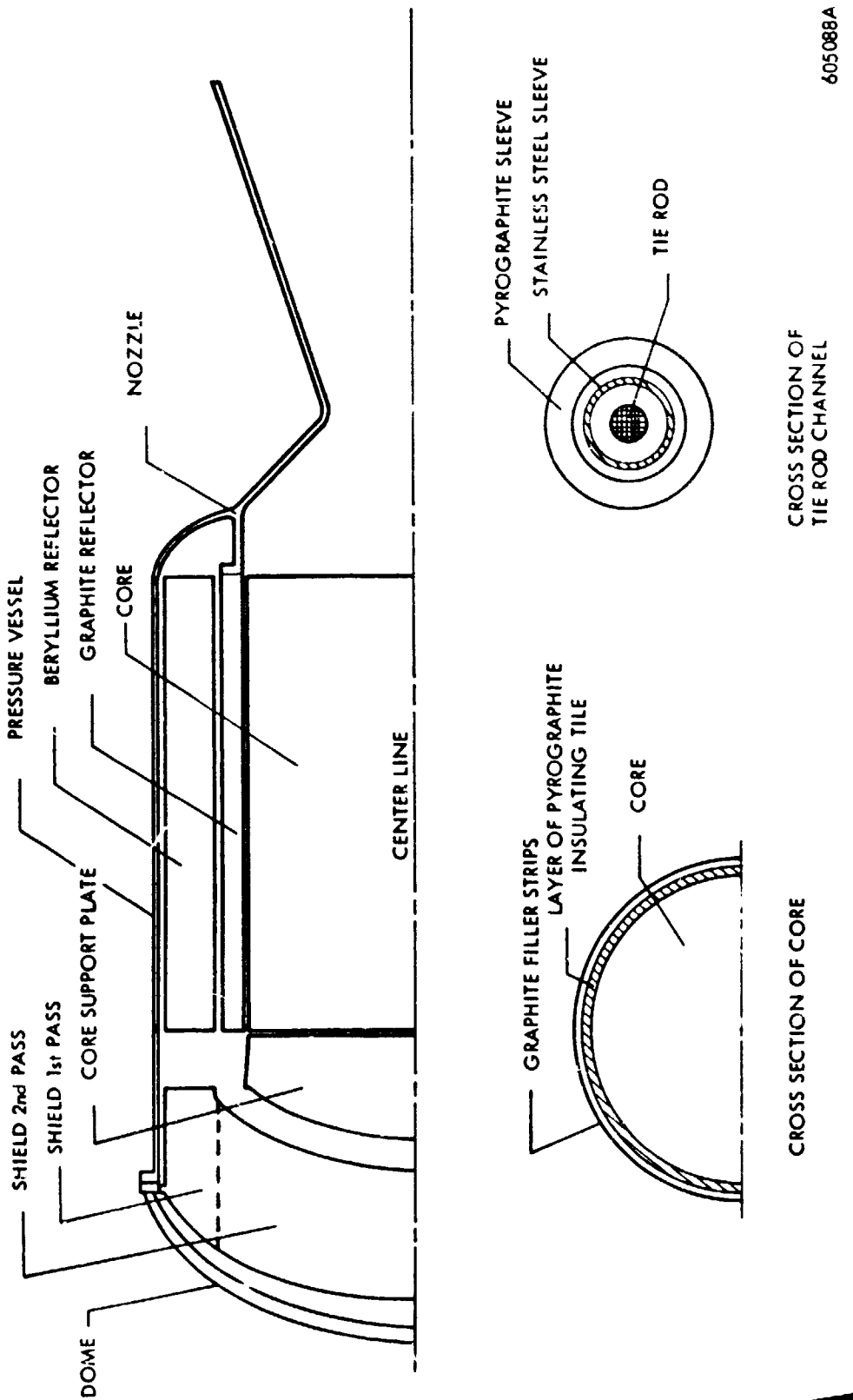

Figure 6-4. Geometric Model of NERVA-NRX Reactor

8. Radiation from the graphite reflector to the beryllium reflector.
9. Radiation from the beryllium reflector to the pressure vessel.
10. Radiation losses from the pressure vessel and pressure vessel dome to the environment.
11. Radiation losses from the nozzle backing to the environment.
12. Nuclear energy deposited in each segment of each component.
13. Radiation transfer from the pyrographite sleeve to the steel sleeve in the tie rod channel.
14. Radiation transfer from the steel sleeve to the tie rod.
15. Energy conducted from the nozzle flange to the lower pressure vessel flange.
16. Energy losses due to melting of tie rods.
17. Energy losses due to sublimation of graphite.

From the point of view of the reactor itself maintaining integrity, the thermal response of the two core support systems - axial and lateral - are of particular importance. The axial support system consists of 289 Inconel tie tubes attached to the core support plate. These tubes run axially through the core and hold the entire core assembly in compression under the pressure drop experienced during normal operation. The lateral support system consists of 324 spring-plunger assemblies attached to the graphite inner reflector of the NRX reactor. It has been designed to withstand a 4 g lateral acceleration. The plungers which are made of graphite bear on graphite seals along the length of the core. Stainless steel springs bear on the plungers, and these springs are attached to the outer face of the inner reflector by aluminum brackets and aluminum retainer screws. Figure 6-5 illustrates this spring assembly. Of all the materials used in the assembly, aluminum has the lowest yield temperature (1260°R). Once aluminum reaches this temperature, the load bearing capabilities of the lateral support system will be lost.

Post-operational heating analyses of the NRX reactor have indicated that both of these support systems will be lost shortly after the loss-of-coolant accident; the axial support system will fail first. All tie rods in the core melt within 20 to 30 seconds after failure.

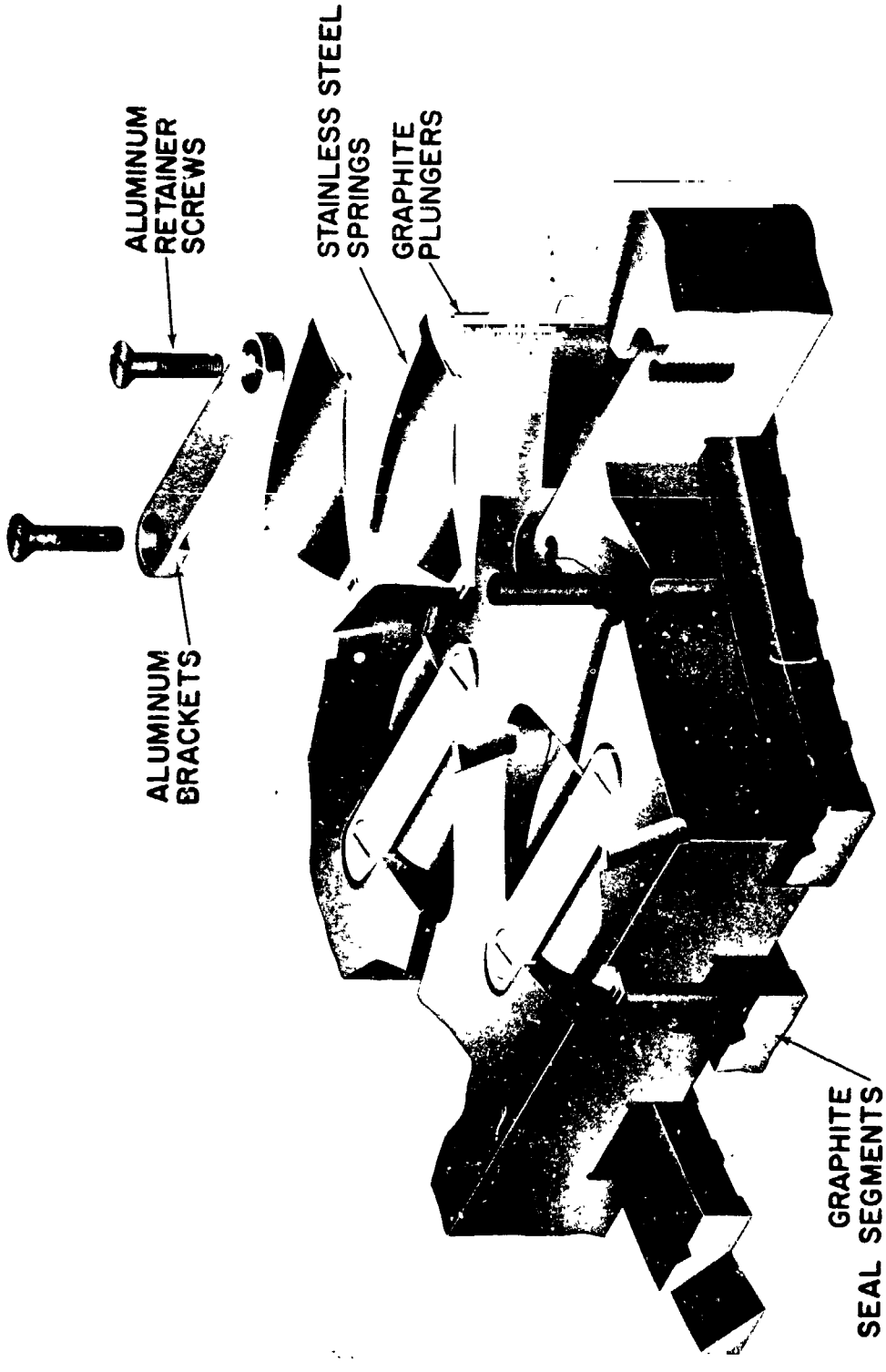

Figure 6-5. Lateral Support System - NRX Reactor

Because of the rapid thermal degradation of these components, no time-temperature histories are shown. The lateral support system survives longer. At about 160 seconds after failure this support system reaches the yield temperature of aluminum - 1260°R at the core exit.*

With the loss of these two load bearing components, the NRX core is left in an essentially non-restrained condition. The only force left to retard element ejection from the core is the frictional force between the faces of adjacent graphite fuel elements. If some force, such as the centrifugal force associated with a tumbling vehicle, is applied to the reactor, it is quite possible that element ejection will commence. An analysis was performed to evaluate this possibility[6]. It was found, allowing for frictional forces between elements, that ejection of all fuel elements from the reactor would be accomplished within about 4400 seconds after loss of all core support if the reactor were tumbling as slowly as one degree per second about its three principal axes. Faster tumbling rates would gut the reactor of its fuel elements even more rapidly. Thus, it appears that the failure of the support systems of the NRX reactor would lead to eventual core disassembly and that the long orbital lifetimes associated with a spent intact reactor could not be achieved. Moreover, fission product diffusion will cease once disassembly is accomplished.

The other component which plays an important role in the passive re-entry approach is the core support plate. This component, located at the dome end of the core is a perforated aluminum forging with a diameter of 38.5 inches and varies in thickness from 4.12 inches at the edge to 6.0 inches at the center. The tie tubes are attached to the core support plate. The importance of the core support plate arises from the function it serves in the event an Auxiliary Thrust System (ATS) is utilized (Section 6.3). If an ATS is used, it could be applied in such a direction that all thrust loads will be borne by the dome end of the reactor, and the core support plate would become the primary load bearing component. In the event this component has overheated to such an extent that it can support no loads, it is to be expected that fuel elements will be ejected from the dome end of the reactor upon ATS application.

---

* The core is coolest at its exit end, thus the last springs to fail will be located here. Springs at the core midplane (the hottest section) will have failed earlier.

Figure 6-6 shows typical post-operational temperature responses for the NRX core support plate. Since this plate is relatively thick, a large temperature gradient across it is expected. Therefore, the analysis considered the plate to consist of four axial sections of equal dimensions and calculated the temperature responses of the four sections. The temperature histories for these regions are shown in Figure 6-6.

On the basis of these histories, it is apparent that core support plate failure will occur, since aluminum can support no load after it reaches a temperature of 1260°R. For purposes of identifying the maximum time that the core support plate could be effective in providing support to the core assembly, it has been assumed that this limit is reached when the section of the plate nearest the core (location 4 in Figure 6-6) has actually reached the melting temperature (1680°R) and when location 3 has reached 1260°R. When this occurs, the remainder of the plate is at very high temperatures and can support little or no applied loads.

Figure 6-7 shows the temperature of location 3 as a function of time after loss-of-coolant, for several operating periods ranging from 63 to 1450 seconds. Examination of this figure shows that the support plate can serve as an effective structural member for a maximum of 550 seconds after loss-of-coolant in the case of a 63-second operating period. For a 1450-second operating period, the plate will be capable of supporting loads for only about 150 seconds after loss-of-coolant accident.

Based on the above thermal analyses, it appears that an NRX reactor will disassemble rapidly after a loss-of-coolant accident. Moreover, it appears that ATS can be applied only during the time period shortly after the accident occurs.

6.1.1.2 The NERVA Reactor

The NRX just discussed will be utilized only under ground test conditions. The actual flight reactor is designated as NERVA; this reactor, presently sized at 5000 Mw, is basically quite similar to the NRX model in overall design concept. However, several of its design features are quite different from those of the NRX, and as a result, the post-operational thermal response of NERVA may be substantially changed from that for NRX.

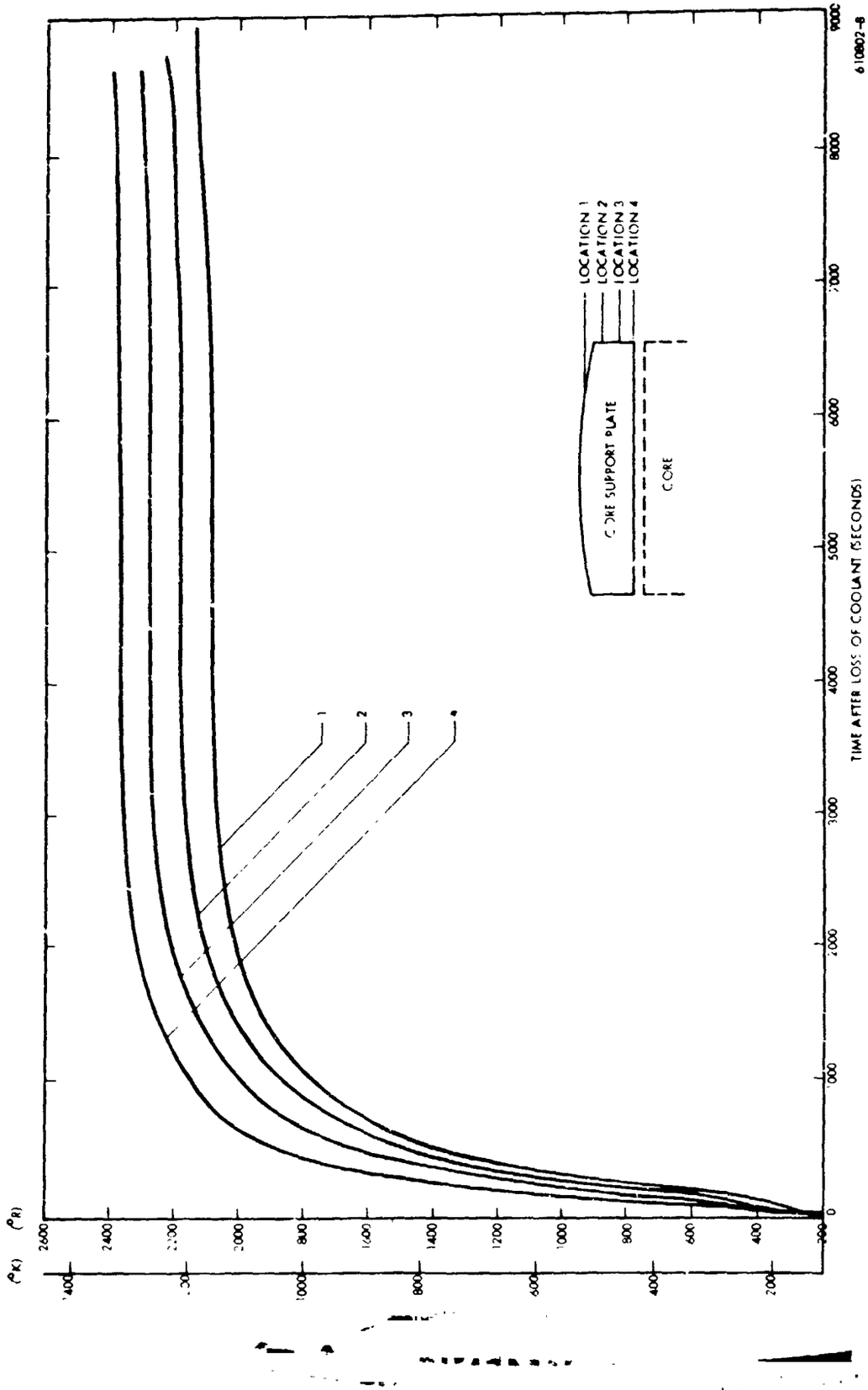

Figure 6-6. NERVA-NRX Core Support Plate Temperature Following Loss of Coolant (463 Seconds Reactor Operation Time)

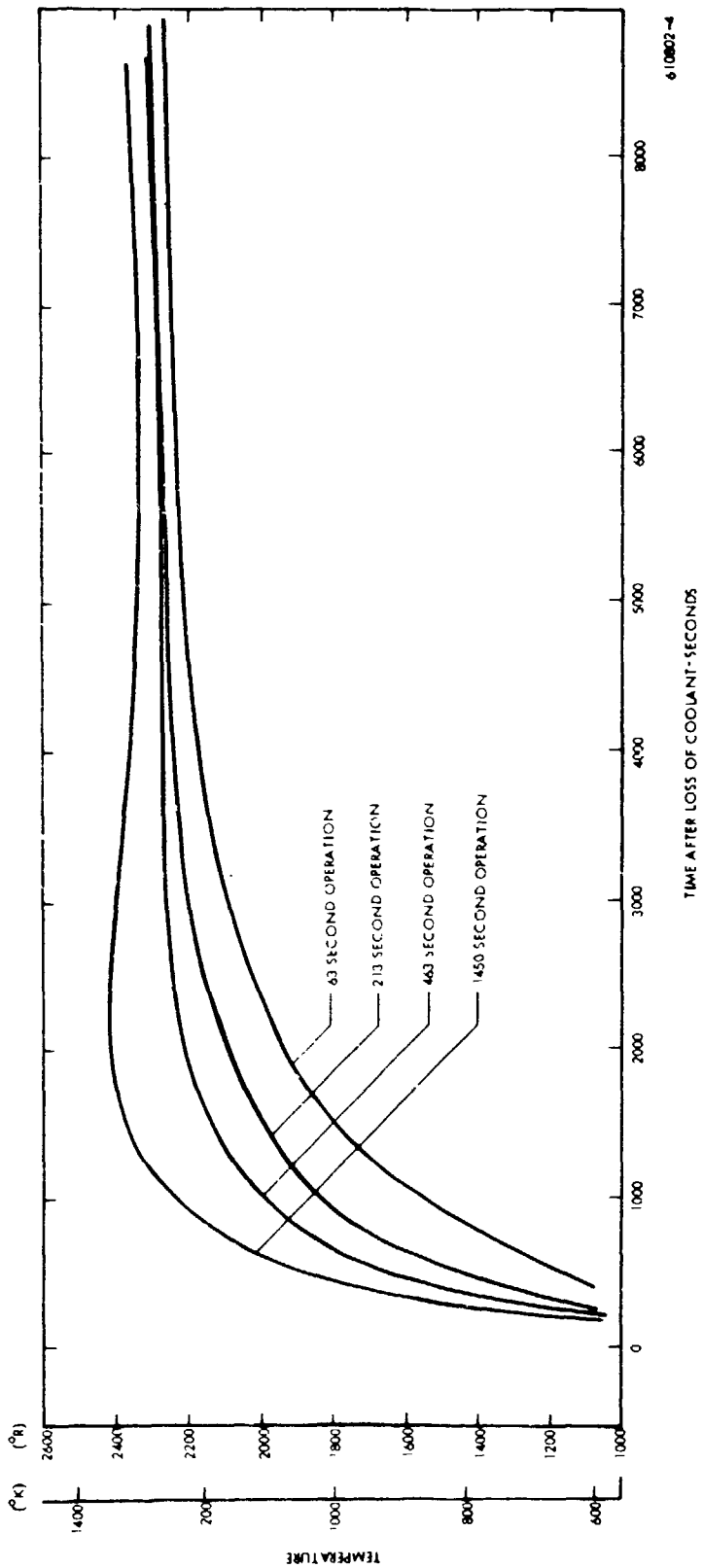

Figure 6-7. NERVA-NRX Core Support Plate Internal Temperature (Location 3) Following Loss of Coolant

The post-operational heating responses were evaluated using POST-OP[7], an advanced version of NOFLOW. The basic reactor model used in the NERVA heating analyses is shown in Figure 6-8. The heat transfer modes are, in general, identical with those considered for NRX. However, in the case of NERVA, the lateral support system was subjected to a considerably more detailed thermal examination.

In order to assess the effect of post-operational heating on NERVA integrity, the thermal response of the core support systems will be considered first. As in the case of NRX, NERVA is provided with two core support systems. The axial system consists of counterflow tie tubes attached to the core support plate and extending the length of the core. The tie tubes are cooled by a flow separate from that of the remainder of the reactor. (This flow system is described in Section 5.1 of this report.) While detailed analyses of the thermal response of these tie tubes have not yet been performed, it is felt that the NERVA tie tubes will also melt soon after failure.[4]

The NERVA lateral support system has been considerably changed from that which was used in the original NRX design. In the NERVA design, lateral support forces are transmitted to the core by segmented graphite seals acted on by graphite plungers which are in turn supported by Inconel springs recessed into the beryllium reflector structure. Axial motion of the seals is restricted by graphite spacers inserted into the inner surface of the beryllium reflector. Heat transfer from the spacers to the reflector is retarded by a layer of pyrographite tile or cloth resting between the surfaces. Figure 6-9 illustrates the design of this lateral support system. The heat transfer model used in the heating analyses is shown in Figure 6-10. In these analyses it was assumed that the temperature of the Inconel spring was identical with that of the beryllium reflector.

Post-operational heating analyses of the NERVA model indicates that the lateral support system of this reactor will be capable of supporting loads for substantially longer times after failure than will its counterpart in NRX. The effective lifetime of the NERVA lateral support system is determined by the lifetime of the beryllium reflector. Based on the

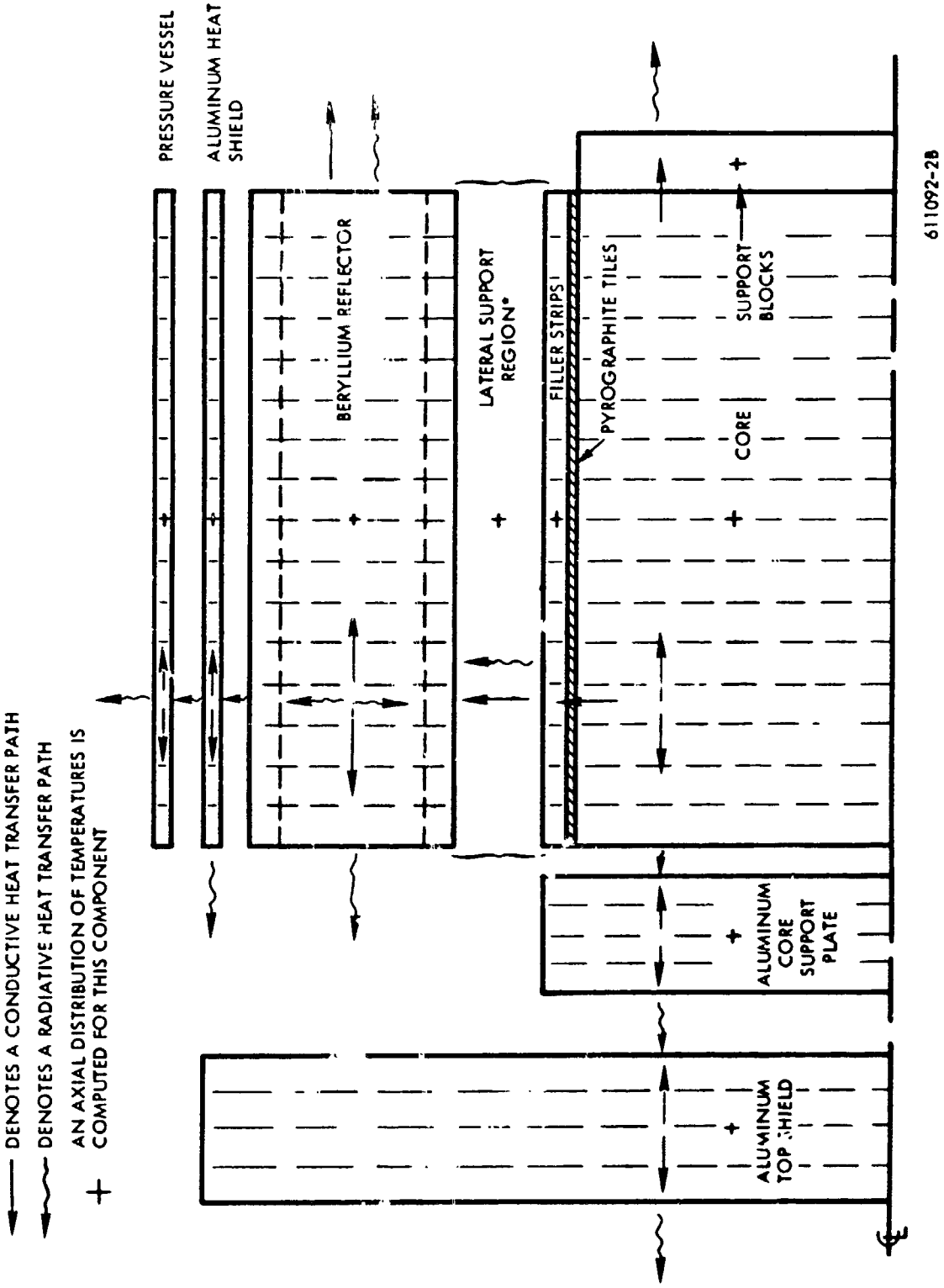

Figure 6-8. Basic Reactor Model - Schematic Drawing

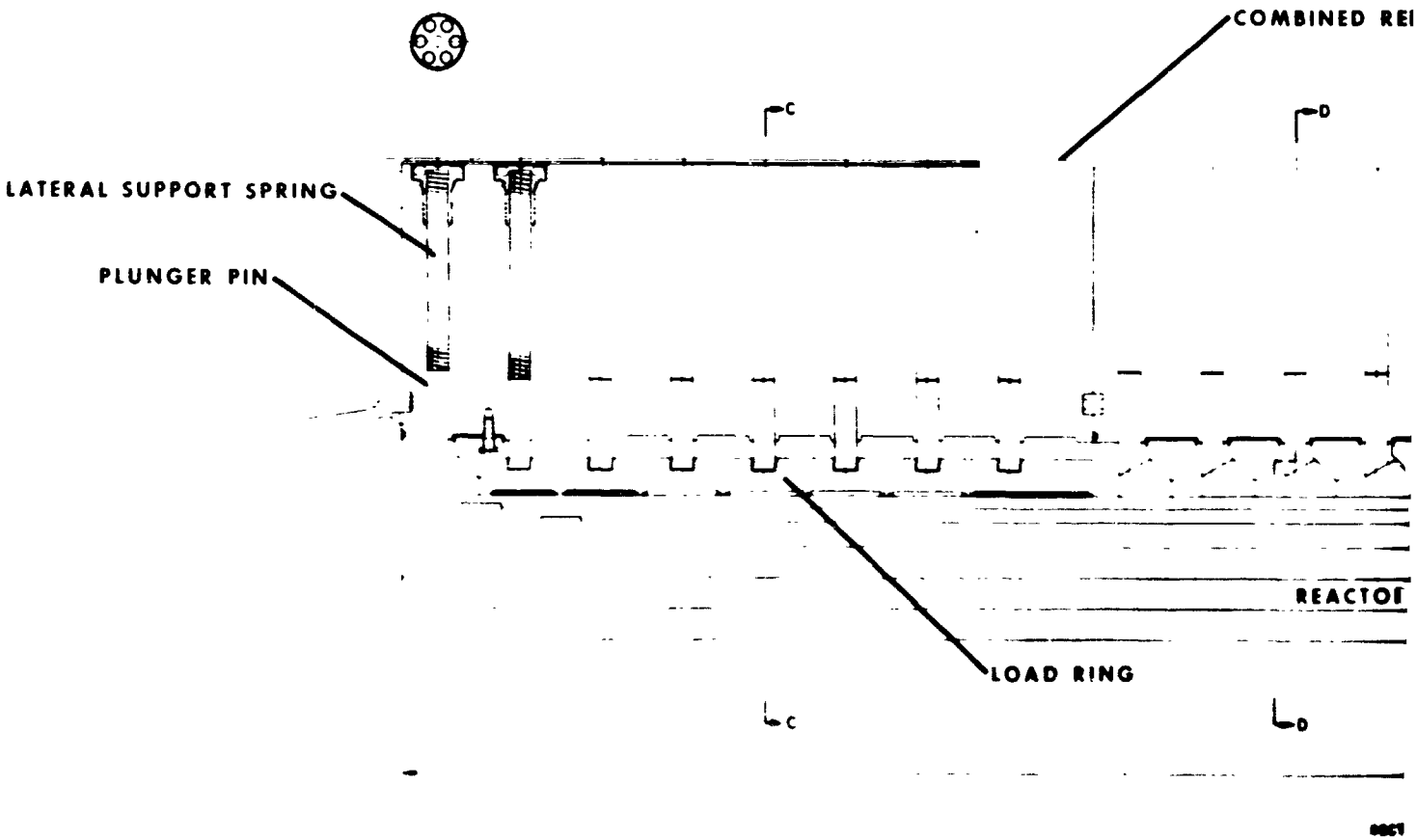
COMBINED RE
C
D
LATERAL SUPPORT SPRING
PLUNGER PIN
REACTOI
LOAD RING
C
D

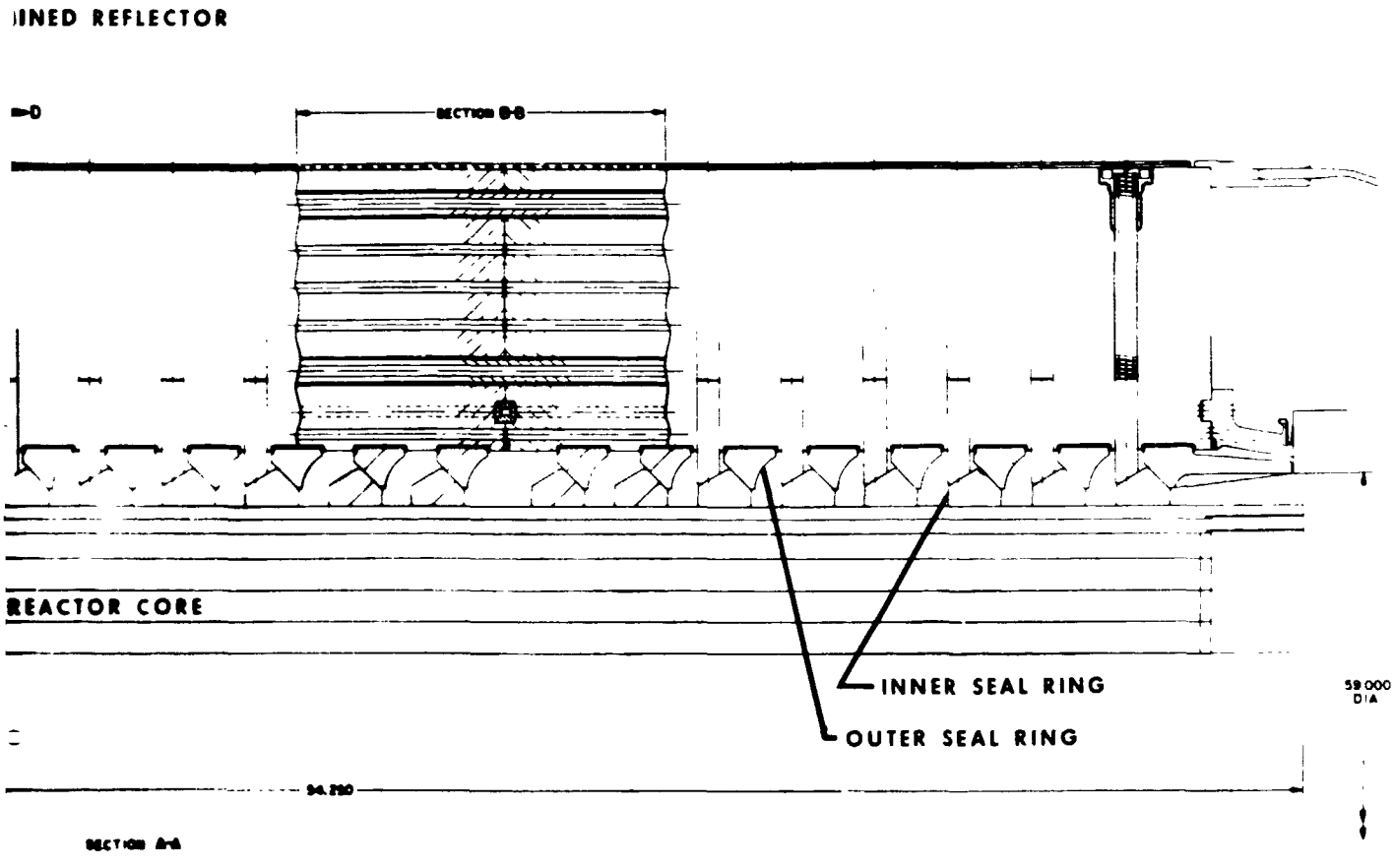

Figure 6-9. NERVA II Lateral Support System Hot Periphery Concept - Elevation

BLANK PAGE

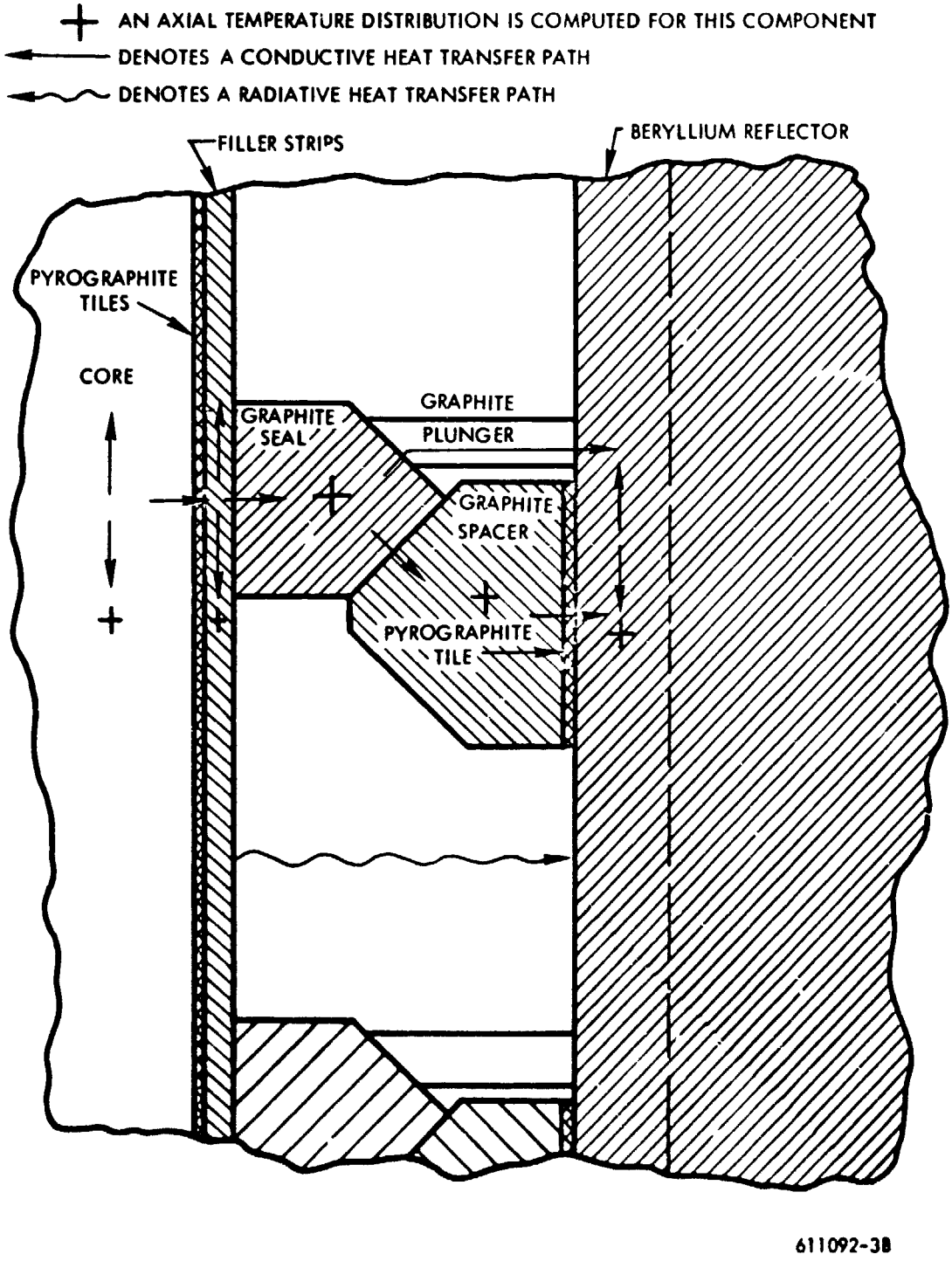

Figure 6-10. Heat Transfer Model for Lateral Support Region for NERVA Reactor

WANL Materials Manual, this component will have a tensile capability of 1000 psi up to 1960°R and of 500 psi up to 2250°R. An estimate of the bundling force in the reflector due to the core lateral support system is 400-500 psi. Thus, a measure of the effective lifetime of this system can be defined as the length of time after loss-of-coolant required for the beryllium reflector temperature to reach 2250°R.

Based on these criteria, it was found that for a 30-second operating period, the lateral support system would survive at least 40 minutes and, perhaps indefinitely after loss-of-coolant. For a 500-second operating period, the support system would endure at least 20 minutes.

As originally conceived[8] the core support plate region in NERVA would be quite similar in location and design to that in NRX. Thermal analyses indicated that the effective lifetime of the support plate in the two reactor designs would be essentially identical. For the 30-second operating period, the support plate would last about 600 seconds after loss-of-coolant. For 500 seconds operation, it would last 135 seconds.

In an attempt to prolong the effective lifetime of this component a thermal analysis was conducted on a postulated design in which the positions of shield and core support plate were interchanged. It was found that this design arrangement can prolong the effective lifetime of the core support plate to 435 seconds after loss-of-coolant.

As a result of these analyses it appears that the NERVA reactor, as presently conceived, will maintain integrity for relatively long periods after loss-of-coolant. In fact, if failures occurs early in the reactor operating period, core integrity may be maintained until such time as the reactor encounters the high aerodynamic loading and heating rate associated with re-entry. (This subject will be discussed in the subsequent section.) As far as ATS is concerned, it appears that some design modifications may be required to make the reactor capable of withstanding the loads associated with application of this countermeasure. Such modifications appear to be within the framework of present design concepts.

6.2.2 Re-Entry Behavior

If the reactor survives the effect of post-operational heating, it will eventually re-enter the Earth's sensible atmosphere where it will be decelerated and undergo the

combined effects of aerodynamic loading and heating. It is quite possible that as a result of these effects, reactor disassembly will be accomplished.

6.2.2.1 NRX Re-Entry Vehicle Definition

To evaluate the effect of re-entry forces on the integrity of the spent reactor its re-entry trajectory must be examined. This requires a mechanically and structurally well defined re-entry vehicle, which is, preferably, aerodynamically stable. Such a vehicle was defined for the NERVA engine[9] system. It consisted of the entire reactor assembly, the entire pressure vessel (dome and cylinder), and the nozzle assembly including the skirt, but had no external piping or fittings that protruded (beyond the diameter of the pressure vessel dome flange, and there were no other engine systems external to the reactor assembly).

Figure 6-11 shows a model representation of this re-entry vehicle. The NRX reactor served as a guide in defining this configuration. Testing of this model in a hypersonic wind tunnel demonstrated that the pictured re-entry vehicle is in fact aerodynamically stable. Therefore, this vehicle was selected for the re-entry analyses which are summarized in the following paragraphs. This configuration will henceforth be referred to as the NRX re-entry vehicle or the NRX R/V. In order to obtain such an R/V some separation mode must be defined, but presently, such definition is lacking; however, it is assumed this will ultimately be supplied by the flight system/engine contractors. For the purpose of the following discussion it is simply assumed that separation can be accomplished to produce such an R/V.

6.2.2.2 NRX Re-Entry Analysis

In order to assess the effect of re-entry loading and heating on the R/V, it is first necessary to evaluate the vehicle's trajectory. Moreover, this trajectory analysis must consider not only the translational motion of the vehicle but also its rotational motion about its center of gravity. This analysis requires the use of a six-degree of freedom trajectory program. Such programs were utilized in the analysis of re-entry behavior of the NRX R/V[10, 11]. However, even before such analyses can be performed, it is necessary to define a number of initial conditions which will play a large part in influencing the R/V's

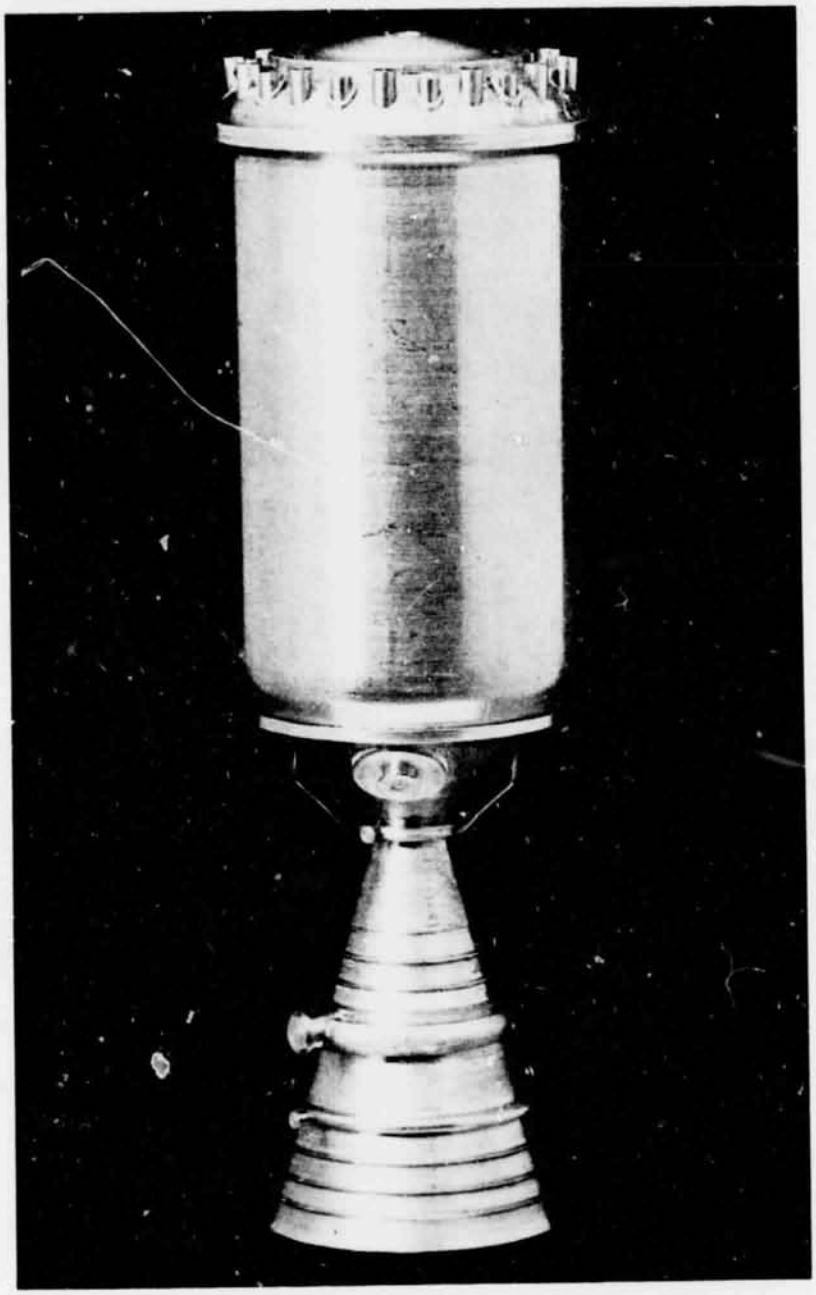

Figure 6-11. NERVA Re-Entry Vehicle

entire re-entry trajectory (i.e. conditions at time of failure). These conditions are: altitude, velocity, re-entry angle, vehicle roll rate, vehicle yaw rate, and vehicle pitch rate. The latter motions, i.e. yaw, pitch, and roll are expected to occur when the R/V is separated from the remainder of the nuclear stage.

In the re-entry analyses performed as part of the NERVA flight safety effort, two sets of initial failure conditions were examined as a function of different initial yaw, pitch, and roll rates, and are summarized in Table 6-1.

TABLE 6-1

INITIAL CONDITIONS EXAMINED IN NRX R/V RE-ENTRY ANALYSIS

	Case 1	Case 2
Geodetic Altitude	646,792.8 ft.	399,083 ft.
Inertial Velocity	23,743 ft/sec	25,682 ft/sec.
Path Angle	+0.226 degrees	-0.066 degrees

Case 1 corresponds to the type of initial re-entry conditions which a vehicle will experience in the event of failure during a sub-orbital start trajectory; Case 2, corresponds to the type of re-entry conditions experienced in the event of an orbital failure.

Table 6-2 notes the altitude at which the R/V will stabilize, i.e. cease rotating about its center of gravity, under the initial conditions described in Table 6-1 and under a variety of initial tumbling conditions.

Table 6-2 indicates that for a vehicle tumbling relatively rapidly, stabilization will be achieved below 300,000 feet. Since the NRX reactor will have lost both lateral and axial support shortly after loss-of-coolant (Section 6.2.1.1), it is to be expected that almost complete fuel element ejection will occur before the R/V is stabilized[6]. This observation is particularly true for orbital failures where a vehicle may spend from days to weeks in orbit prior to re-entering the Earth's atmosphere. In this case even if a vehicle is tumbling very slowly, element ejection is almost a certainty prior to re-entry.

TABLE 6-2

PREDICTED STABILIZING ALTITUDE AS A FUNCTION OF INITIAL RE-ENTRY CONDITIONS AND SEPARATION DYNAMICS

Failure Case	Reference	Rotational Rates			Stabilization Altitude (feet)
		Pitch	Yaw	Roll	
1	10	25	25	25	270,000
	10	50	50	50	270,000
	11	25	0	0	260,000
	11	1	1	1	345,000
2	10	25	25	25	280,000
	10	25	0	0	260,000
	11	25	0	0	270,000
	11	1	1	1	320,000

For the NRX R/V, early ejection of fuel elements during re-entry can be avoided only if vehicular tumbling is prevented. One means of preventing such tumbling is to spin stabilize the R/V subsequent to failure and separation. In such a case, disassembly is not anticipated until the R/V encounters maximum heating and loading. An analyses of the re-entry behavior of an R/V so stabilized, has been performed. The initial altitude, velocity, and flight path angle examined in this spin stabilized analysis correspond with those for Case 1 in Table 6-1. The initial pitch rate was assumed to be 0 degrees per second, the yaw rate to be -5 degrees per second, and the roll rate to be 360 degrees per second. The probable disassembly sequence is described in Reference 11 and is quoted below:

> "At 106,000 feet, the forward flange region on the windward side has melted and since the conduction of heat is very high in aluminum, and since the vehicle is spinning, it is expected that the melting will burn the pressure vessel through aft of the forward flange and failure will occur at 106,000 feet. The viscous shear forces acting counter to the inertial forces will separate the pressure vessel from the remaining machine. One modification that might alter this event is a possible asymetric burning on the very aft nozzle station (not examined in this study) which would cause a very large oscillation (flat spin) and cause

maximum heating to shift back on the center of the pressure shell. In any event, the shell will definitely burn through, but the burn through at the forward flange will cause an earlier disassembly because of the proximity of the dome end support ring and core support ring to the hot boundary layer gas following loss of the pressure vessel. Both of these rings are 0.1 inch titanium, and once the pressure vessel opens this area to the peak heat flux, these rings will heat and fail thermostructurally in a matter of seconds. At almost the moment the burn through occurs on the flange area, the dome closure at the front of the vehicle will melt and be collapsed by the air loads back over the small air gap onto the shield assembly. The shield assembly will transmit the entire airload onto the core support ring which will tend to buckle about the same time the support plate is exposed to the hot gases of the boundary layer. These phenomena, together with the tremendous positive shear and bending moments, will tear the whole front end shield assembly loose. The moment the dome end support ring and core support ring fail, the outer beryllium reflector will come loose. This will completely expose the core. The burnup and failure should be complete at 95,000 feet. At this time in the trajectory, the re-entry vehicle will have passed through the peak heating and deceleration loads and the core elements will not be subjected to any significant loads. There will be some additional heating. The core, however, has reached very high temperatures and practically all the hardware supporting the core has failed (i.e., tie rods, lateral support, aluminum barrel, etc.) and the whole machine should disperse at 95,000 feet as a cloud of pieces of varying size."

It appears that in all cases disassembly of the NRX R/V will occur either prior to or during re-entry. The resulting radioactive debris will consist of fuel elements. A description of this debris and its distribution is given in Chapter 7.0, and a summary of the types of radiological doses associated with it is given in Chapter 8.0.

6.2.2.3 NERVA Re-Entry

At present the NERVA re-entry vehicle has not been defined, and thus, re-entry analysis could not be performed. However, because of the longer endurance of the NERVA R/V lateral support system, it is expected that its disassembly behavior will differ considerably from that of the NRX R/V.

6.3 AUXILIARY THRUST SYSTEM (ATS)

The purpose of an auxiliary thrust system is to provide controlled disposal of the radioactive nuclear engine by utilizing some means of auxiliary thrust to perform either a retromaneuver to insure deep ocean impact, or a thrusting action to boost the system into a long-life orbit. In this context, the auxiliary thrust system encompasses all components and functions involved in the disposal of the aborted nuclear engine or stage. The application of an ATS as an acceptable countermeasure is based on the following two assumptions: (1) The radioactive nuclear engine system can be disposed of in deep ocean waters with no adverse radiological consequences to man (disposal by retromaneuver), and (2) If sufficient time is allowed for radioactive decay, the consequences of re-entry of debris of nuclear systems would be of the same degree as that for debris of non-nuclear systems (disposal by boosting maneuver).

Conceptual auxiliary thrust systems for NERVA application have been investigated by the Lockheed Missiles and Space Company[12]. Their studies included investigation of the feasibility of ATS for safe disposal of failed nuclear stages, investigation of effects of various parameters on safety performance specifications, development of a conceptual ATS design for NRX and NERVA sized nuclear stages, and analysis of ATS performance for these proposed flight mission models A summary of the results of their studies is presented in the following paragraphs.

6.3.1 System Requirements for ATS

To accomplish the goal of safe disposal, the ATS must have, in addition to the basic means of providing thrust to the stage or engine, the following characteristics and system functional requirements: high system reliability, attitude reference sensors and attitude control system, command and communication equipment, a means for separation of payload, and a means for controlled dumping of nuclear engine propellant. The auxiliary thrust requirements are discussed in Section 6.3.2; other characteristics are discussed below.

6.3.1.1 System Reliability

If the ATS is to be considered a primary safety countermeasure system, it must have a high system reliability comparable to the reliability required of the other prime countermeasures (such as an explosive destruct system). The reliability requirement is directly

determined by the level of risk acceptable for nuclear stage operations. As an example of reliability for a safety system, that specified for the Polaris destruct system is 99.9 percent reliability during flight. At present it appears that this reliability value is higher than can be presently met by certain of the ATS components.

To attain the necessary reliability, careful use of redundant design and performance capability is required. The ATS system will contain many components, failure of any one of which may cause loss of the system. Failure evaluation or malfunction analysis will be useful in determining system reliability. The use of redundancy for selected critical components can be so arranged as to increase the overall reliability. However, redundancy cannot be used for all components because of weight penalties introduced or because of the functional nature of the equipment. But with careful analysis of all potential failure modes of equipment and if failure patterns can be predicted with a high degree of certainty, it seems likely that the reliability requirements for an ATS system can be ultimately met.

6.3.1.2 Attitude Reference Sensors and Control Systems

It is important that the errors in the predicted ocean impact location (for retro application) or the errors in the predicted orbit lifetime (for boost application) be held to a minimum for successful use of ATS. To insure accurate disposal, it is imperative that the thrust system be oriented correctly at time of firing and kept on course during the firing. Thus, some form of attitude reference and control must be provided in order to aim the system correctly before firing. If the ATS is applied to the entire stage, the existing control system can be used for this purpose. However, if an "engine only" configuration were to be used, it would be difficult to provide a separate attitude control system due to space limitations and high radiation environment. LMSC investigated applicability of spin stabilization to the NERVA (Mw) "engine only" configuration as an alternate means of controlling impact location. At a spin rate of 10 radians/seconds due to thrust misalignment, loads due to acceleration at the engine periphery would be 10.9 g and at the ATS thrust motor center of gravity, 10.6 g. Because of these high loadings, and the likely increase in dispersion of the fuel elements upon ultimate break-up of the re-entering engine, it appears that spin stabilization is not promising for reliable ATS operation.

Any error in the velocity of the nuclear stage from that programmed for the controlled impact point may introduce a significant dispersion. Velocity errors could arise as a result of incomplete propellant dumping, unexpected loss of engine hardware, failure or off-design performance of one of the ATS rocket thrusters, etc. Thus, it is necessary that velocity sensing equipment be included, as well as a method of terminating the thrust when the desired velocity increment (retro) has been added. Thrust termination would probably not be used in the event of boost operations since any velocity increment added above that to satisfy minimum orbit lifetime requirements would increase the lifetime, thereby adding to the safety of the disposal.

6.3.1.3 Command and Communication Equipment

The requirement to maintain continuous knowledge of the location and behavior of the nuclear stage, and the capability of transmitting commands to the vehicle during all phases of powered flight is obvious. The selection and planned use of the ATS will be influenced by the characteristics of the Ground Communication and Tracking System (GCTS) available for the support of nuclear vehicle missions. The GCTS established for the Apollo program with appropriate modifications would probably be used for ground support of nuclear rocket flight missions. For proposed sub-orbital start missions, it appears that for the critical time periods when thrust failure would result in African impact and use of the ATS would be required, existing GCTS stations are out of range of the vehicle and mobile ground stations would be required for satisfactory communications and actuation of the ATS.

6.3.1.4 Payload Separation

Separation of the payload prior to initiation of the ATS is desirable. Separation reduces the weight to be accelerated by the ATS and permits separate recovery of a manned system and/or experiments. If the payload were not separated, the payload propulsion system could possibly be used in conjunction with the ATS to provide auxiliary thrust. However, the payload propulsion module may be insufficient as the only thruster, and addtional ATS rocket motors might be required. These motors must be mounted externally, which results in maximum heating and drag. Thus for the conceptual ATS design as proposed by LMSC, the payload was assumed to be separated prior to ATS firing.

6.3.1.5 Controlled Dumping of Hydrogen Propellant

Dumping the nuclear stage hydrogen propellant prior to firing of the auxiliary rocket motors is desirable to reduce the mass of the re-entry vehicle. If this propellant were dumped in a controlled manner so that the escaping hydrogen gas or liquid could provide usable thrust, the size of the ATS rocket motor could be reduced, thereby effectively reducing the weight penalty.

LMSC has examined the propulsion capabilities of the hydrogen as a mono-propellant both in the cold gas and liquid form. Venting the cold gas through an optimum nozzle yields a specific impulse of 76 seconds for inlet conditions of 40°R and pressure between 10 and 42 psia. For a lightly insulated propellant tank, hydrogen boil-off rate in orbit has been estimated at about an average of 950 pounds per hour. Based on this flow rate and an I_{sp} = 76 seconds, a thrust of 20 pounds could be generated. For an orbit start mission of an NRX sized engine with continuous thrusting until the supply of hydrogen was depleted, a total ΔV of 2000 feet per second, or more, could be applied to the nuclear stage. A disadvantage of such continuous thrusting is that most of the thrust would be applied at other than an optimum position in the orbit, and continuous pitch plane orientation would be required from the attitude control system. Pulsing the cold gas at the optimum trajectory point (apogee) would provide more efficient use of the ΔV to gain maximum orbit lifetime. The use of a cold gas system would not be useful for failures from sub-orbit starts, because of the low acceleration rates obtainable, and the short orbit lifetime at time of failure. However, even for boost operations, the cold gas propulsion does not appear to be practicable. Current efforts on propellant tank design emphasize a super-insulated, double-walled tank with the objective of minimizing hydrogen boil-off. Thus, the thrust actually available from boil-off would, in fact, be appreciably less than that mentioned above. Consequently, this approach for utilization of the hydrogen propellant holds little merit for a practical ATS system.

The venting of the liquid hydrogen provides a lower total impulse than the gaseous hydrogen. However, the large mass of liquid hydrogen available and the short action time make it desirable for both orbital and sub-orbital applications. For this application, the propellant is positioned in the forward end of the tank by application of a ullage thrust. A

24-foot diameter round hole in the center of the tank dome is then opened allowing the liquid hydrogen to be expelled followed by gaseous hydrogen under a decaying pressure gradient.

LMSC[12] has calculated the flow rates, thrust, and specific impulse for both the liquid and gaseous phase venting, and computed the ΔV attainable as a function of failure time for several hypothetical flight missions for NRX and NERVA size reactors. Figure 6-12[12] gives the ΔV impulse to the nuclear stage from propellant dump for various failure times following orbit startup of an NRX sized engine for a lunar transfer mission ("Mission Model I", see Section 8.2 for a summary description of this mission.) Figure 6-13[13] shows a similar curve for a vehicle powered by the NERVA (5000 Mw) engine on a flight mission of direct ascent to a 72-hour lunar injection. Total time of venting the hydrogen depends on failure time and will be in the range of 1 to 3 minutes for the case of Figure 6-12 and about 2 to 4 minutes for the case of Figure 6-13. As will be shown in Section 6.3.3, the ΔV impulse provided by propellant venting for early failure times provides better than one-half of the total ΔV required for successful ATS operation for the three flight missions described in Section 8.2.

6.3.2 ATS Conceptual Design

Several ATS system concepts which utilized either liquid-propellant systems or solid-propellant systems were explained. Only rocket motors which were presently operational or those late in their development stage were considered. Only LOX/LH_2 liquid propellant propulsion systems were considered because of their higher specific impulse.

Examination of the Saturn S-VI stage[14] showed that it would provide adequate ΔV capability for the three flight missions analyzed (Section 8.2). This stage contains approximately 21,500 pounds of propellant in three tanks and is powered by two RL-10A3 rocket engines. This stage could be used as part of the payload for certain nuclear vehicle configurations, in which case its use would not represent a payload loss. Because of the placement of the S-VI stage on top of the NERVA propellant tank, propellant dumping was not considered. Because of its restart capability, the S-VI stage could be used for both nuclear stage retro deceleration and then following separation from the SN stage, restarting of the S-VI engines for payload recovery.

An alternate liquid-propelled ATS module was examined, based on a scaled down version of the S-VI stage. This system would weigh 9020 pounds and be positioned so as to

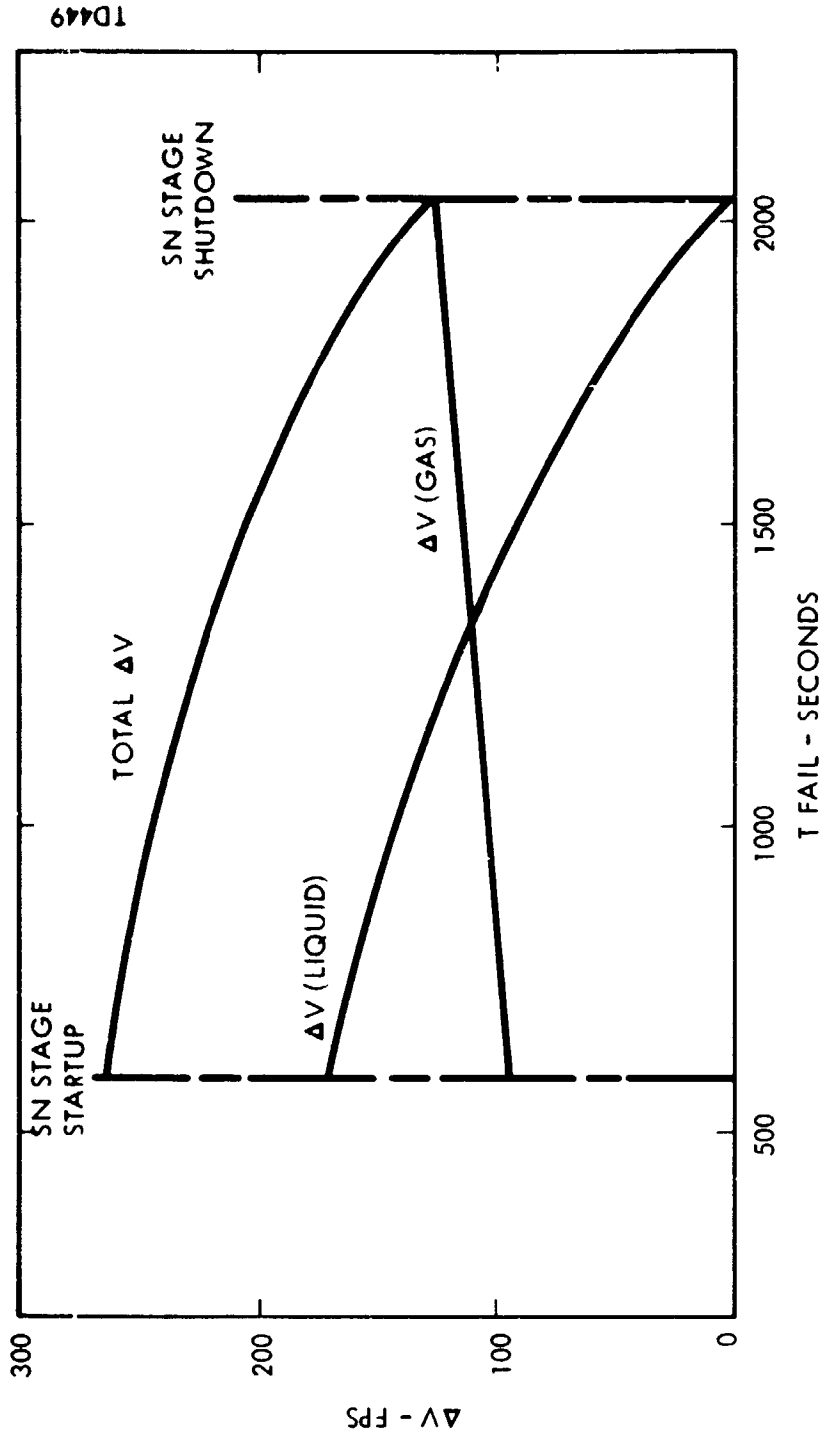

Figure 6-12. Delta V Impulse from Propellant Dump, Mission Model I

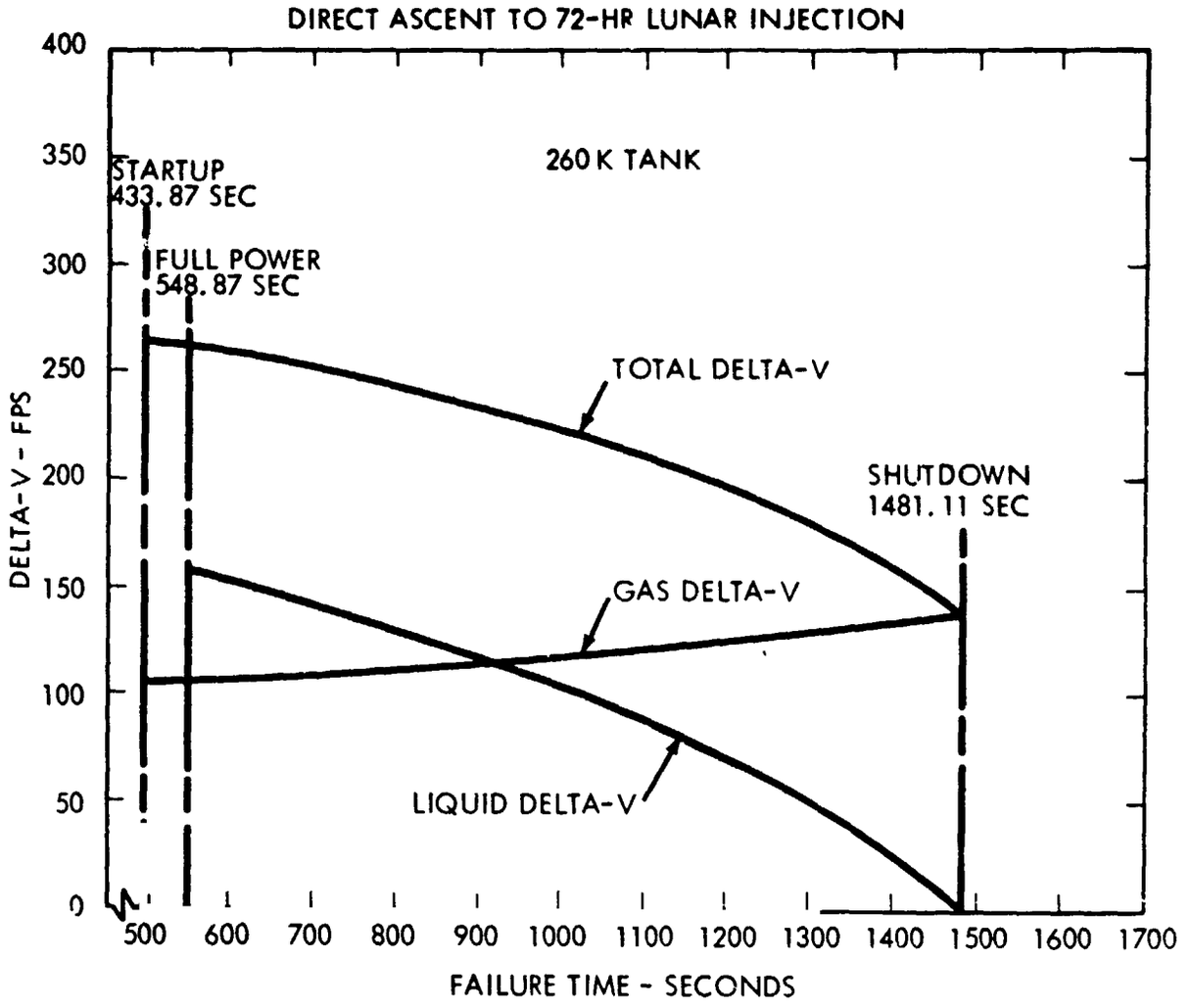

Figure 6-13. Delta V Impulse From Propellant Dump
NERVA (5000 Mw) Direct Ascent Lunar Mission

dispose of the SN stage only, with no-propellant dumping. Detailed analysis of this system was not performed, but the ΔV values appeared adequate for successful disposal.

A survey of available solid propellant rocket motors was made based on their specific impulse, weight, burning time, and size. Analysis of the ΔV requirements indicated that a ΔV of 200 to 250 fps would be adequate if the impulse available from dumping the stage liquid hydrogen were used to augment the ATS motors. To increase reliability, several rocket motors would be used so that a "one-engine-out" capability could be built into the system. Eleven of these motors appeared to meet the basic ATS requirements. Further analysis of the capabilities of these eleven, led to the selection of the two solid propellant motors shown in the table below:

Ballistic Nomenclature	Other Designations	CPIA Unit No.	Weight (lb)	Avg. Thrust (lb)	Burn Time (sec)	Vac I_{sp} (lb-sec/lb)	Propellant Weight Fraction	Application
24 DS 5850	XM-94 X25881	415	573.0	5888	24.0	281	0.877	Scout Fourth Stage
9.15 DS 5770	BE-3A4	416	214.1	5770	9.15	276	0.892	Athena Fourth Stage

The weights include allowances for mounting structure and thrust termination devices.

The final conceptual design chosen for the ATS utilized the above solid rocket motors, with thrust augmented by controlled venting of the liquid hydrogen nuclear stage propellant. Solid propellant rocket motors were chosen over a liquid propellant system on the basis of their high individual reliability, fast thrust rise time, and insensitivity to stage orientation and zero-g environment. Although liquid rocket systems can be made equally reliable, they require more complex plumbing and installation, and are not as easily canted in the event of an ATS engine failure.

The ATS rocket motors are mounted around the inside of the SN-stage instrument unit as shown in Figure 6-14. Each motor is swing mounted on a bracket, with the thrust vector aligned parallel to the vehicle centerline. If any motor fails, the opposing motor can be canted to direct its thrust through the cg of the accelerated mass. For this reason,

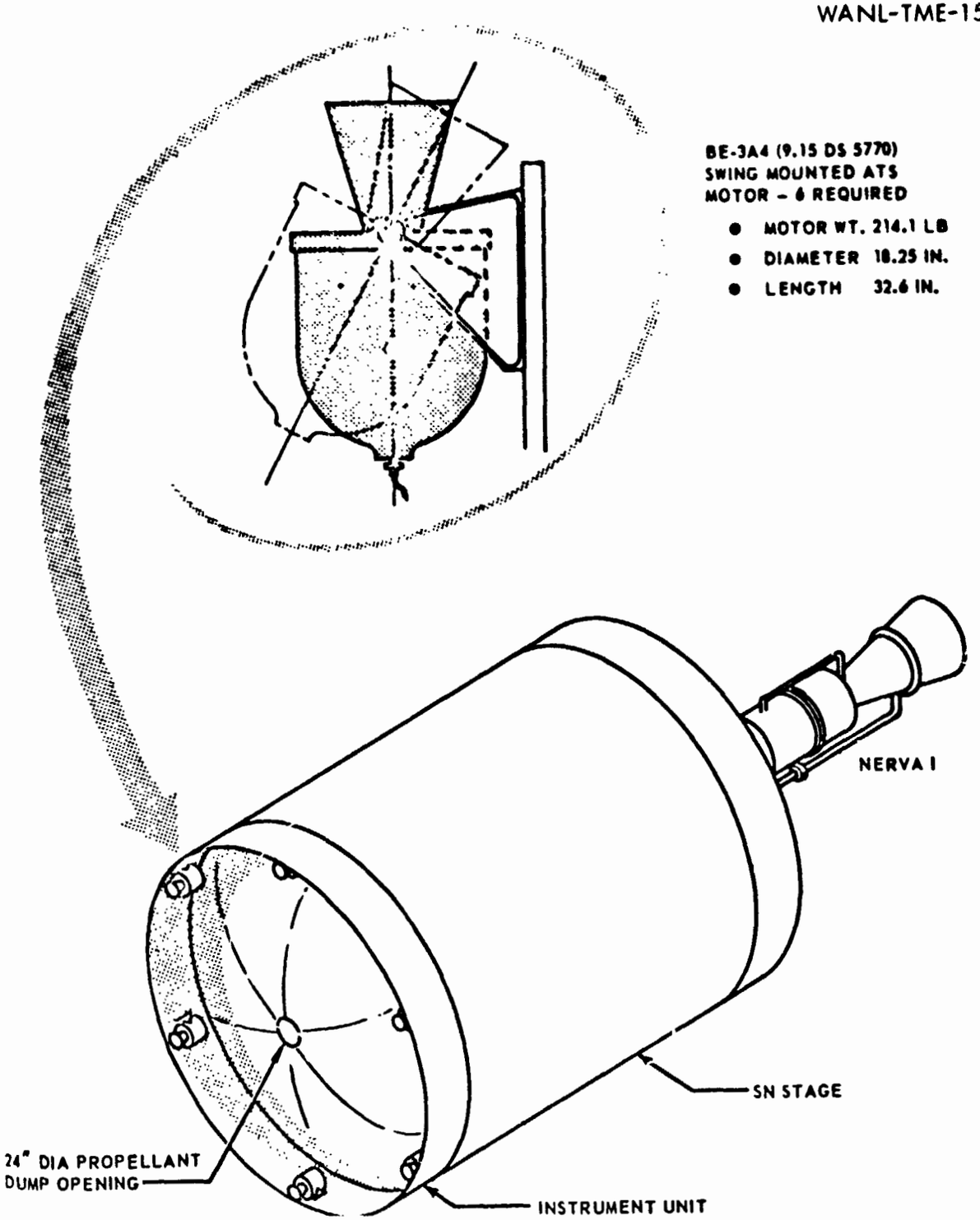

Figure 6-14. Arrangement of ATS Solid Propellant Motors for MM-1

only even numbers of motors are used; if odd numbers were considered, two motors would have to be canted to compensate for one engine out.

The ATS concept shown in Figure 6-14 is applicable only for a specific mission: a 100 nm orbit start lunar mission utilizing a NERVA - NRX sized engine ("Mission Model I", Section 8.2). The number of rocket motors required and the resulting ΔV impulse gained by use of these motors for all three mission models described in Section 8.2 are summarized in Table 6-3.

TABLE 6-3

ΔV CAPABILITY OF ATS SOLID PROPELLANT ROCKET MOTORS

Mission Model	Rocket Motor CPIA Unit No.	Number Required	Installed Weight (lb)	ΔV All Motors Firing (fps)	ΔV One Motor Out (fps)*	ΔV Two Motors Out (fps)
I	416	6	1146	238	198	159
II	416	8	1793	258	225	193
III	415	6	3588	325	270	215
III	416**	6	1146	123	103	75

* Design condition
** Alternate configuration for disposal into long-lived orbit only

6.3.3 ATS Safety Analysis

6.3.3.1 General Considerations

The use of an auxiliary thrust system to provide controlled disposal of a failed nuclear stage appears feasible utilizing the LMSC conceptual design for the ATS system. Analyses have been made for the three mission models (Section 8.2) to calculate, as a function of failure time, the ocean impact points for retromaneuver disposal and the orbit lifetime for a boost maneuver. The accident model chosen for these analyses was a loss-of-coolant without reactor disassembly until after completion of ATS application. It is then assumed that non-violent disassembly (0.0ΔV) occurs immediately after the ATS function. An intact fuel element is chosen as the reference size of core fragment upon which the impact locations or orbit lifetimes are based.

For calculation of the ability of the ATS to provide satisfactory disposal, a new ATS Chain Link was written for the LMSC Nuclear Flight Executive Program[12]. The program evaluates whether safe disposal can be accomplished by utilization of the basic parameters involved in ATS application such as ΔV capability, maximum and minimum coast time before application of thrust, maximum probable errors in velocity, and flight-path angle due to ATS thrust and alignment errors. The program operates by first calculating the maximum orbit lifetime of the nuclear stage that can be achieved with the on-board ΔV capability, with the ΔV applied at the coast orbit apogee. If this orbit lifetime (for a single fuel element) is less than a reference lifetime (chosen as 200 years for the LMSC analyses), the program then searches for a satisfactory ocean impact disposal location. The impact dispersion, defined by the distance between the undershoot and overshoot from the nominal impact location due to the maximum probable errors, is calculated and compared with acceptable deep water ocean areas. If the disposal area is not acceptable, the retro conditions are altered and the problem is re-run until an acceptable impact area is found. If no ocean disposal can be achieved, the ATS countermeasure would be considered ineffective for ocean disposal at that failure time. For those failure times in the mission trajectory at which the ATS is capable of boosting the stage to an orbit where fuel element lifetime exceeds the reference lifetime set in the program (200 years), ocean disposal locations are not determined. The following sequence of operations shown on the next page is typical.

The actual time for tank venting and vehicle alignment will vary with each mission model and with the failure time. For the LMSC analyses, a coast time of 60 seconds was selected as a nominal value of the elapsed time between failure and initiation of propellant dump.

Function	Estimated Time (sec)
Failure event	0.0
Detect and identify failure	6.0
Select disposal mode and transmit coarse alignment data	4.0
Orient stage (transmit fine alignment data during this period)	20 - 100
Separate payload	10
Apply ullage thrust	10
Vent SN stage propellant (monitor vehicle behavior and transmit final velocity requirement just prior to end of vent period)	60 - 180
Fire ATS rockets	10

6.3.3.2 Use of ATS for Controlled Ocean Impact

The ATS Chain Link was used to evaluate the capability of the ATS conceptual design to provide controlled ocean disposal by retromaneuver for the three selected mission models of Section 8.2. The results of these analyses are summarized in Tables 6-4, 6-5, and 6-6. For Mission Model III, the larger of the two ATS designs (270 fps + propellant dump impulse, Table 6-3) was used since the smaller design is inadequate except for orbital disposal.

The tabulated results show that each ATS design is capable of safe ocean disposal of the failed stage up to a fail time where a fuel element orbit lifetime of 200 years or greater can be obtained by boosting the stage at apogee. These analyses assume that sufficient time is available before reactor disassembly to permit coasting to apogee or beyond. It was shown in Section 6.2.1.1 that under loss-of-coolant conditions for the NRX reactor, tie rods melt within 30 seconds and the lateral support system fails within about 160 seconds leading to reactor

TABLE 6-4

MISSION MODEL I ATS SUMMARY DATA

(For an Onboard ΔV of 200 fps + Propellant Dump Impulse)

Fail Time After Launch (Seconds)	Prop. Dump Impulse (fps)	Orbit Lifetime (Years)[1]	Range Angle (Degrees)	Coast Time (Seconds)	Dispersion (nm)[2]	Impact Coordinates[3] Pt	Longitude	Latitude
600	262.62	0.025	54.3	60.0	474.2	1	-14.80	4.50
						2	-11.34	2.67
						3	-7.88	0.75
650	261.41	0.456	91.69	660.0	740.2	1	58.83	-27.41
						2	65.79	-28.01
						3	72.75	-28.26
700	259.24	10.43	119.27	2260.0	279.3	1	-174.37	13.72
						2	-172.18	14.67
						3	-169.98	15.61
750	256.95	35.74	121.37	2660.0	218.5	1	-153.55	22.67
						2	-151.65	23.18
						3	-149.74	23.66
800	254.66	81.77	125.15	2860.0	184.0	1	-143.07	25.79
						2	-141.40	26.08
						3	-139.72	26.35
1000	243.59	558.96	Impact disposal not checked when element orbit lifetime estimate esceeds 200 years.					
1200	230.24	2224.37						
1400	213.56	9380.22						

(1) Based on single fuel element - apogee boost
(2) Distance from Point 1 to Point 3
(3) Point 1 - Max. undershoot impact
Point 2 - Nominal impact
Point 3 - Max. overshoot impact.

TABLE 6-5

MISSION MODEL II ATS SUMMARY DATA

(For an Onboard ΔV of 225 fps + Propellant Dump Impulse)

Fail Time After Launch (Seconds)	Prop. Dump Impulse (fps)	Orbit Lifetime (Years)(1)	Range Angle (Degrees)	Coast Time (Seconds)	Dispersion (nm)(2)	Pt	Impact Coordinates (3) Longitude	Latitude
1050	292.27	0.0	31.49	60.0	131.0	1	-8.69	0.95
						2	-7.74	0.95
						3	-6.78	-0.11
1075	291.30	0.0	32.71	60.0	154.3	1	-5.88	-0.71
						2	-4.75	-1.33
						3	-3.63	-1.95
1100	290.34	0.008	33.35	60.0	188.2	1	-2.59	-2.64
						2	-1.21	-3.39
						3	-0.17	-4.14
1125	289.44	0.016	36.91	60.0	244.2	1	1.31	-4.93
						2	3.12	-5.88
						3	4.93	-6.84
1154	288.54	0.027	36.70	860.0	287.1	1	51.76	-26.00
						2	54.39	-26.42
						3	57.03	-26.80
1167.797	287.86	0.035	50.20	660.0	438.0	1	51.51	-26.01
						2	55.54	-26.64
						3	59.57	-27.15
1267.797	284.91	3.914	37.34	1660.0	274.5	1	98.99	-22.49
						2	101.24	-21.59
						3	103.50	-20.66
6600	280.92	12.92	120.45	2260.0	256.0	1	-173.74	23.47
						2	-171.48	24.02
						3	-169.22	24.54
6700	276.33	102.52	122.15	2860.0	175.9	1	-141.97	28.72
						2	-140.30	28.68
						3	-138.63	28.62
6800	271.46	298.34	Impact disposal not checked when element orbit lifetime estimate exceeds 200 years.					
7000	260.43	1217.82						
7200	245.84	4,18.74						

(1) Based on single fuel element - apogee boost
(2) Distance from Point 1 to Point 3
(3) Point 1 - Max. Undershoot impact
Point 2 - Nominal impact
Point 3 - Max. overshoot impact

TABLE 6-6

MISSION MODEL III ATS SUMMARY DATA

(For an Onboard ΔV of 270 fps + Propellant Dump Impulse)

Foil Time After Launch (Seconds)	Prop. Dump Impulse (fps)	Orbit Lifetime (Years)(1)	Range Angle (Degrees)	Coast Time (Seconds)	Dispersion (nm)(2)	Impact Coordinates(3) Pt	Longitude	Latitude
3462.712	325.26	11.328	107.21	60.0	490.8	1	-154.11	22.18
						2	-149.82	23.33
						3	-145.53	24.36
3500	324.72	16.165	112.57	2460.0	431.7	1	-1.93	-15.76
						2	1.56	-17.15
						3	5.04	-18.49
3550	321.79	330.09	Impact disposal not checked when element orbit lifetime estimate exceeds 200 years.					
3600	318.33	1652.08						
3800	300.82	31756.10						

(1) Based on single fuel element - apogee boost
(2) Distance from Point 1 to Point 3
(3) Point 1 - Max. undershoot impact
Point 2 - Nominal impact
Point 3 - Max. overshoot impact

disassembly shortly thereafter. The lateral support system of the NERVA (5000 Mw) reactor, based on the present conceptual design, may survive for periods up to 20 minutes or longer following a loss-of-coolant accident (Sectic- 6.1.1.2). The ability of the NERVA reactor system to maintain its integrity under the thrust forces of the ATS as a function of time after the loss-of-coolant accident has yet to be determined. However, for the NRX design, it appears that ATS disposal would be unsatisfactory for times later than 200 seconds following the loss-of-cooiant accident. Thus it can be seen that only for a very early failure time in the case of an NRX orbit start mission (MM I), will ATS be satisfactory for ocean disposal. For the sub-orbit portion of Mission Model II (NRX reactor), the ATS could be used for ocean disposal with delay times limited to stage orientation and payload separation events except for those times when approaching orbit injection (fail times later than 1150 seconds).

To insure successful use of ATS following a loss-of-coolant accident, integrity of the reactor must be maintained up to and during the time of application of the auxiliary thrusting action. Integrity can be improved by modifying the reactor design, or by providing emergency cooling. The use of such cooling will affect ATS system by the thrust resulting from the coolant flow. Velocity increments of the magnitude anticipated from core cooling will not materially affect the ability of the ATS to safely dispose of the stage, but will have definite effects on the coast trajectory and must be accounted for to minimize dispersion. Furthermore, since the coolant thrust is in opposition to the ullage thrust required for propellant dump, all coolant flow must be stopped prior to propellant dump initiation.

6.3.3.3 Use of ATS for Increasing Orbit Lifetime

For orbital disposal, the ultimate location at which the debris will impact is not predictable, and therefore it is essential that none of the re-entering fragments have sufficient fission product activity to cause a significant level of exposure. The acceptable activity level for an impacting element has not been quantitatively established. LMSC[12] has considered that an acceptable level would probably be less than 1 curie but greater than 0.01 curie.

The orbit lifetime obtained by ATS boost and the required decay time for the activity to drop to the reference level of 0.01 to 1.0 curie are shown in Figures 6-15, 6-16, and 6-17 for the three mission models. The advantage of coast time (up to the apogee point)

before firing the ATS on gaining longer orbit lifetime is illustrated in Figure 6-15. Thus, applying the ATS boost at the point of failure in Mission Model I, gives about twice the orbit lifetime of a fuel element had no ATS boost been applied. (It is assumed the intact stage is boosted, followed by disassembly with re-entry of elements of orbit lifetime as shown in the figures). However, if ATS boost could be delayed until apogee (a delay time of about 2600 seconds), the orbit lifetime could be increased by a factor of at least 500, insuring a final impact activity of less than 0.01 curie /element for all but the earliest failures. Thus, the importance of reactor integrity following a loss-of-coolant accident can be seen if ATS is to be useful for boosting to long-lived orbit.

For Mission Model II (Figure 6-16), it can be seen that during the sub-orbital portion of powered flight (up to 1167 seconds failure time), ATS boost is not particularly successful; even with ATS boost at apogee, the impact activity will be greater than 0.1 curie per element. However, for the orbital restart portion of powered flight, ATS boost will yield results similar to those of Mission Model I. For Mission Model III, ATS boost is needed only during the first 80 seconds of operation in order to insure that the impact inventory will be less than 0.01 curie per element.

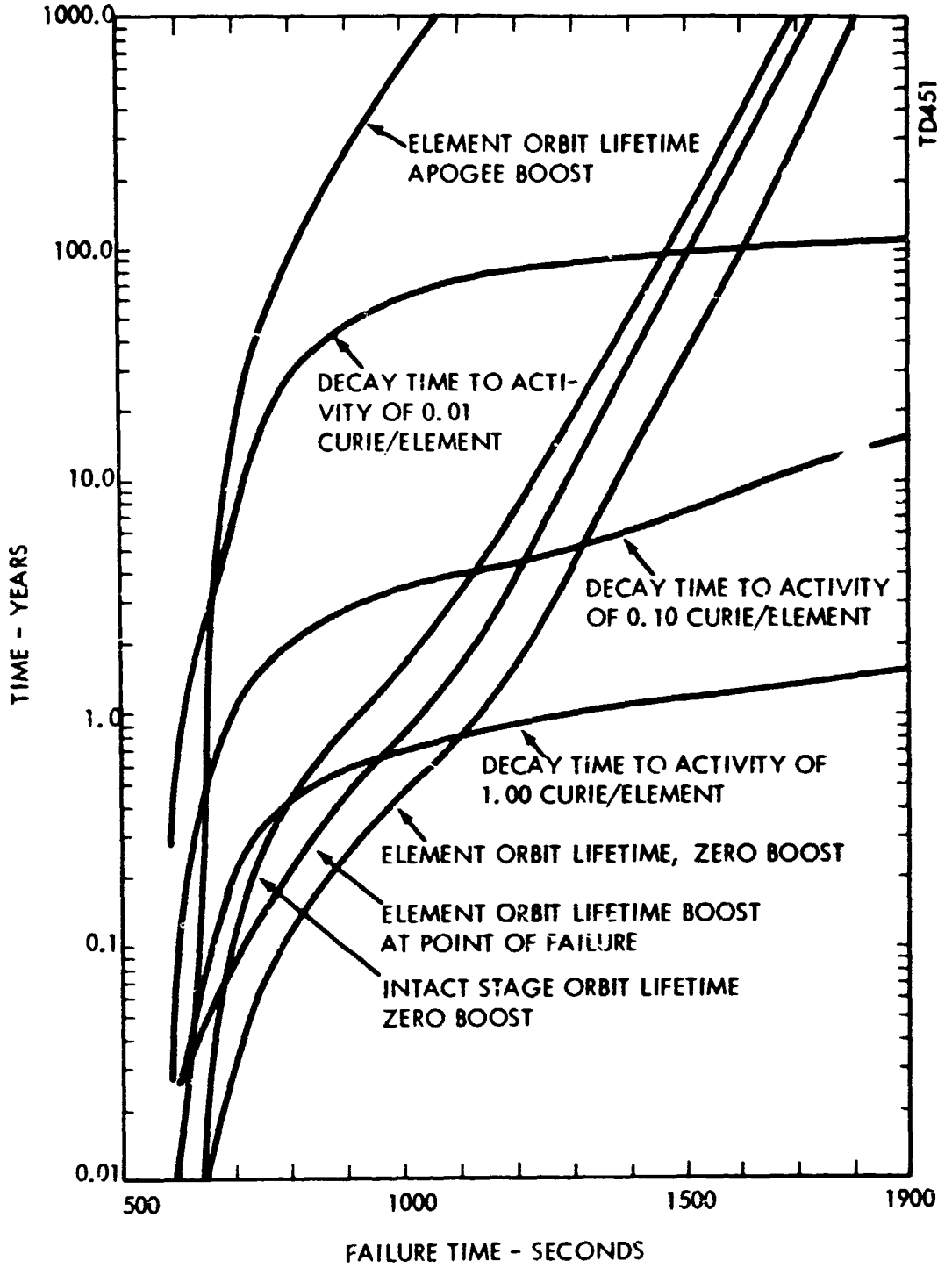

Figure 6-15. Orbit Lifetime and Decay Time versus Failure Time, Mission Model I

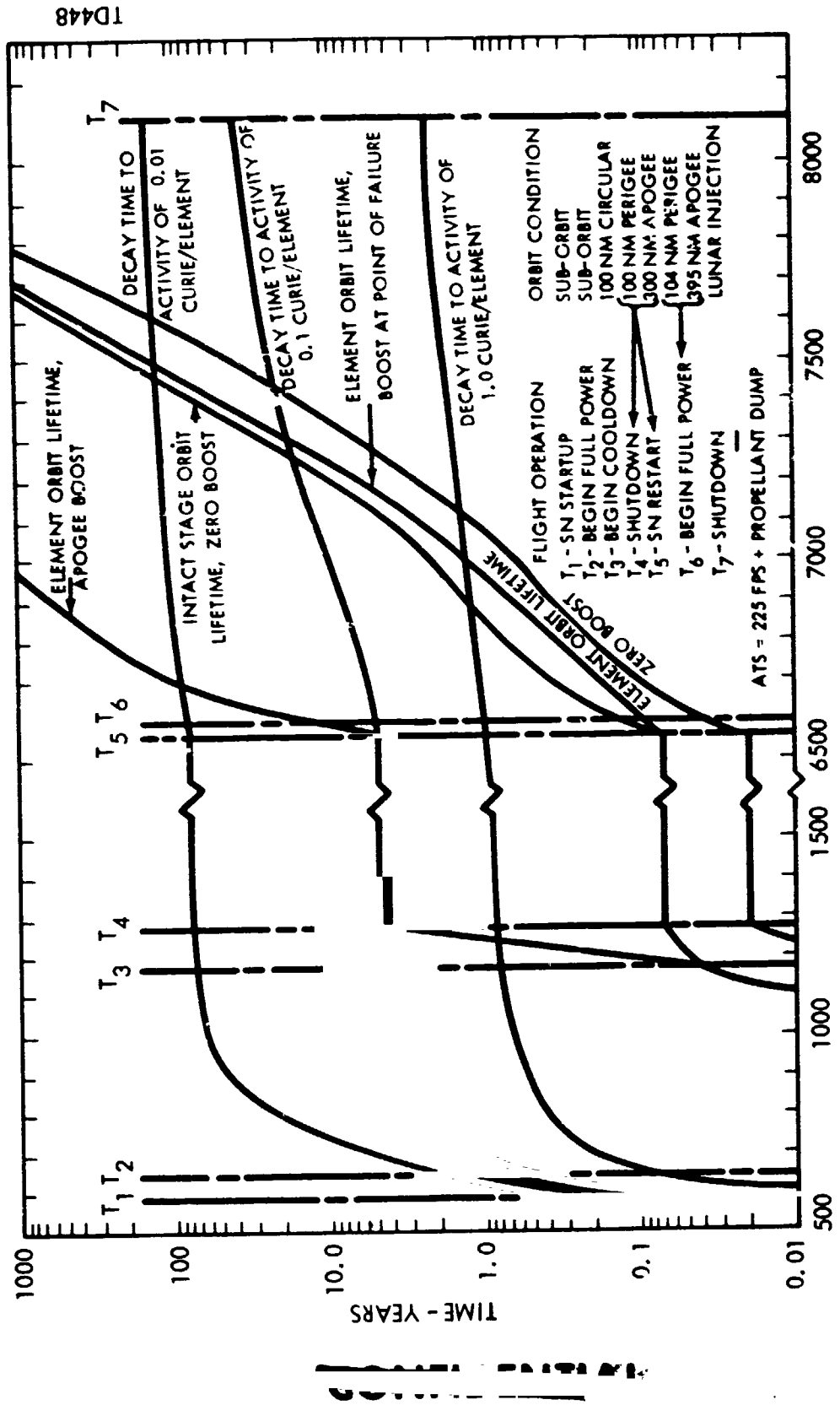

Figure 6-16. Orbit Lifetime and Decay Time versus Failure Time, Mission Model II

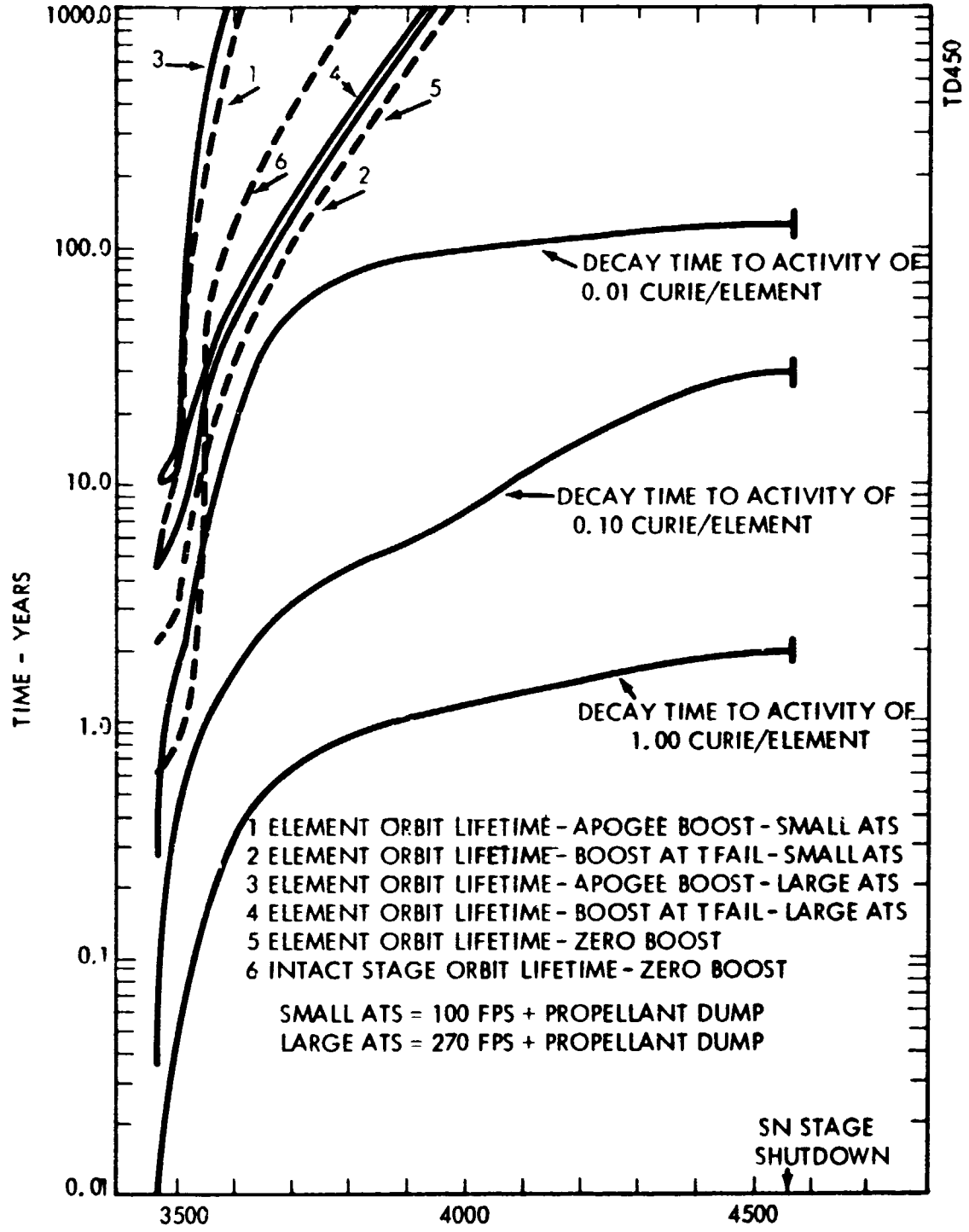

Figure 6-17. Orbit Lifetime and Decay Time versus Failure Time, Mission Model III

6.4 EXPLOSIVE DESTRUCT

The use of a reactor destruct system as a safety countermeasure has been considered from the inception of the ROVER Flight Safety Program. Of the various destruct systems considered, the use of high explosives to disassemble the core has probably received the greatest attention. Early in the ROVER Program many experimental studies were conducted to determine the feasibility of explosive destruct, to investigate basic information on core fragmentation, and to evaluate suitable ordnance hardware. A summary of these experiments was included in an earlier NERVA Source Term Report[15] and is not presented here. However, this section includes a summary of the recent work directed toward the design of a conceptual in-flight explosive destruct system and describes the results of safety analyses based on data obtained from recent destruct experiments.

6.4.1 In-Flight Destruct System

The definition of a conceptual design for an in-flight explosive destruct system was performed by Picatinny Arsenal[16] and is summarized in this section.

The following ground rules were formulated in establishing a conceptual design for an in-flight destruct system; they are based on the premise that satisfactory fragmentation of an NRX-sized reactor could be accomplished.

1. Four, 25-pound HE (high explosive) charges are required.
2. These charges must be equally spaced throughout the core.
3. A 105-mm projectile is adequate to hold the 25-pound charge.
4. A muzzle velocity of 1000 fps is required.
5. The four projectiles must be capable of defeating the target at an angle of about 36° from the vertical.
6. The four projectiles must be exploded simultaneously.

6.4.1.1 Overall System Description

The explosive destruct system will be located external to the NERVA thrust structure system between the propellant tank and the reactor. Four launchers of the closed-breech type will be mounted on the thrust cone at an angle of 36° to the vehicle axis as

shown in Figure 6-18. The destruct package will be activated either by ground command or by a signal from an internal sensing device. On receiving the signal, initiators in each of the four launchers will ignite the propellant and the chamber pressure will increase. When the chamber pressure within the launcher reaches 650 psi, shot-start rods, which hold the projectile within the launcher, will rupture, and at this time the projectile will begin to move. Simultaneously, recoil-absorbing material (a metallic honeycomb) located behind each launcher tube will begin to crush and collapse, allowing the tube to recoil. Pressure within the chamber will continue to increase until it reaches a maximum of 29,100 psi. The pressure will gradually decrease, and at 15,000 psi the projectile will leave the muzzle. At this time the projectile will have traveled 53 inches and will have reached a velocity of 1000 fps. The launcher tube will have recoiled 27 inches and will have attained a velocity of 250 fps. As the projectile moves forward, a firing wire unwinds from a bobbin located either at the launcher or the projectile base. When the projectile penetrates the reactor to a proper depth, an electrical signal will detonate the four charges simultaneously. In addition, a final fuzing system has been included in the design. This will function at a specified time after projectile firing and will detonate the projectiles before any projectile can pass completely through the reactor core. It will function regardless of the performance of the other systems. The total weight of the system has been estimated to be approximately 1500 pounds.

6.4.1.2 Component Description

Explosive selection. The selection of a particular explosive for the proposed destruct system depends to a large extent upon the capability of the explosive to resist the radiation effects associated with neutron fluxes. Tests were performed on a variety of explosives subsequent to their exposure to neutron flux environments in the GETR or during KIWI-TNT. The following tests were performed: explosion temperature, melting point, differential thermal analysis, gas volume release, and vacuum stability. As a result of their resistance to radiation effects, three explosives were selected as the best main charge candidates in the following order: TACOT (tetranitrodibenzotetraazapentalene), TATB (triaminotrinitrobenzene), and DATB (diaminotrinitrobenzene). Based on its radiation

Figure 6-18. NERVA Post-Operation Destruct System

resistance and thermal stability, TACOT was ultimately selected as the most promising explosive for a main charge. NONA (nonanitroterphenyl) was chosen as the most promising candidate for a booster material if one is necessary.

However, because of cost (TACOT costs $275/lb compared to $5.50/lb for DATB), all preliminary experiments were conducted using DATB. These preliminary experiments consisted of the preparation of appropriately sized explosive pellets by a press loading technique. Pellets as large as eighteen inches in diameter and five inches in height were successfully produced. In the APG-III test, which will be described later in this section, DATB was used as a main explosive charge.

Projectile description. The candidate projectile is a 105 mm - loaded shell weighing about 100 pounds and measuring 55 inches in length. Its nose is similar in design to an anti-tank shell. The shell nose, body, and base are all constructed of 4130 steel. This particular shell design was used in the APG-III tests which are described later.

The candidate shell was tested to determine its ability to penetrate a simulated core support plate. Tests at 1000 fps were unsuccessful since the tip of the projectile flattened on impact with the simulated plate. Motion pictures indicated excessive yaw at impact. Additional tests were performed with a projectile having a modified nose design and a higher velocity of 1500 fps; this projectile also failed to penetrate the target material successfully.

Additional tests are planned in which the projectile would be constructed of MT 1018 steel, and the target would be perforated to resemble the NERVA core support plate.

Propellant description. The propellant and its igniter must also be capable of withstanding the radiation environments to which they will be subjected. The propellant IB 7158 (DATB/Polystyrene) was found to be the best in the radiation environment and is being considered as the propellant in the launching system. Its composition will be optimized. Both black powder and ALCLO pellets are being considered for igniters.

Launching system. The proposed launching tube is a smooth bore cylinder, 111 inches in length. It has a small interior shoulder which serves to hold the projectile in place. An end cap closes the rear opening, and a shot-start rod holds the projectile tightly against the interior shoulder. The exterior surface of the launching tube is stepped slightly at a point near the muzzle to provide a surface which can bear against the front support ring which holds

the tube from moving forward. The tube is held from moving to the rear by a metallic honeycomb.

The launching tube is placed inside the guide tube which is a simple cylinder about 133-1/2 inches long. It has 5-1/4 inch inside diameter and a 135 mil thickness. It is threaded at its muzzle end where it mates with the front support ring. The middle section of the guide tube passes through and is welded to the rear support ring. The guide tube is attached to the thrust structure by means of struts connected to the front support ring and the rear support ring.

Trail cable. In order to detonate all four shells simultaneously, it has been proposed that a trail cable be used to connect each projectile with the firing unit. This cable system has not been developed to date.

6.4.2 Reactor Destruct Tests

6.4.2.1 LASL Experiments

During 1961 and 1962 LASL[17] performed experiments using cylindrical graphite configurations which approximated the KIWI designs on a one-third to one-tenth scale model. More recently, a one-ninth scale test was performed on a ROVER-type fuel assembly.[18] This test consisted of 33 ROVER-type fuel elements, 7 inches long, bundled together and placed around a single axial explosive. The assembly was placed in a 4 x 4 x 4 foot open top detonation chamber lined with neoprene rubber on three walls and Styrofoam on the fourth wall. The ground outside the container was covered with polyethylene sheeting to a distance of four feet from the detonation chamber. Following detonation, the debris within the container and on the polyethylene sheeting was collected and analyzed.

Particle size analyses were made using standard sieves, supplemented by microscopic analyses of the sieve samples. Loss of fuel beads was determined by counting the radioactivity of the debris samples with a gamma spectrometer. Selected density measurements were made using pycnometric methods.

Particles greater than 500 microns were primarily irregularly-shaped parallelepipeds broken along the axis of the coolant channels. The mass median particle diameter of the fragments based on the sieve analysis was 1125μ. The particle size distribution is shown in

Figure 6-19. Ten percent by weight of the fuel debris had a diameter of less than 100μ; 40 percent by weight had a diameter greater than 2500μ (0.1 inch). The confinement of the detonation chamber may have produced a smaller mass median particle size than a free dispersal destruct test. This was suggested by samples recovered from the Styrofoam which had a mass median particle diameter of 2700μ and did not include many of the fines that were present in the main samples.

6.4.2.2 Aberdeen Proving Ground Experiments

Two full-scale destruct tests of an NRX-size reactor core have been conducted by Aberdeen Proving Ground. The first test, APG-II,[19] used in the core mock-up a single 90° quadrant of depleted NERVA B-4 type fuel, with the remainder of the core constructed with solid graphite rods. The core was destructed with four 105 mm explosive projectiles, three of which were statically placed within the non-fueled quadrants; the fourth projectile was launched from a gun into the center of the depleted fuel elements. No differentiation of size distribution of the debris below 1/32 inch was made, which in that test constituted some 50 percent of the core material.

The best simulation of a reactor destruct thus far is from the June 1965 test at Aberdeen Proving Ground, designated as APG-III.[16, 20] The test was conducted by APG with assistance from the U. S. Naval Radiological Defense Laboratory[21] and the Sandia Corporation[22]. A NERVA-NRX engine, less the divergent section of the nozzle, was carefully mocked up. The reactor core was simulated with beaded fuel containing depleted uranium. The destruct was produced by detonation of four in-place projectiles. One quadrant of the reactor debris produced was collected, sieved, and weighed, and the gross particle size distribution obtained. The larger fragments of the pressure vessel, reflector, dummy control rods, and other engine components were also collected. Particle velocities were measured at several angles about the engine mockup, and extensive high-speed photographic coverage of the event was provided.

The results of this test produced data which are considered the best available to date in describing the characteristics of explosive destruct, and have been used in the analyses of destruct consequences. Therefore, the major results of the APG-III test are summarized below.

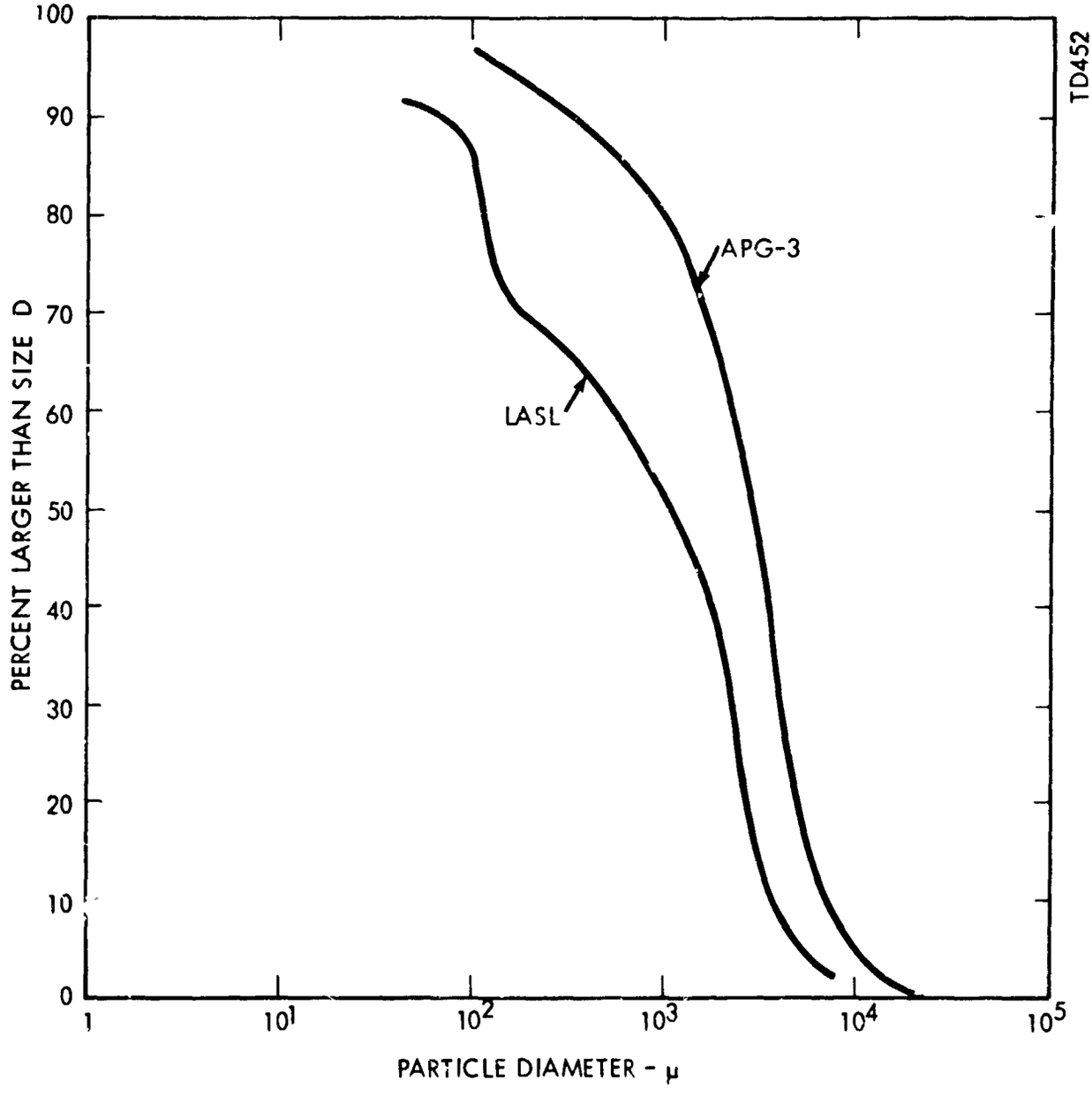

Figure 6-19. Percentage of Particles from Destruct Tests Larger Than a Given Diameter

The core material was fragmented into an exceedingly large number of fragments ($\sim 2 \times 10^{13}$), varying in size from 0.0034 mm (3.4 microns) to 26.9 mm and in weight from 1.02×10^{-10} grams to 16.0 grams. Of the total number of fragments, 99.974 percent were less than 0.105 mm in size class*, but this small debris comprised only 6.53 percent of the core mass. Thus, a relatively small number of fragments comprise most of the core mass and, hence, most of its radioactivity. In addition, analyses of the small material (< 0.105 mm in size class) indicated that these debris contained only 2.14 percent of the total core uranium. The particle size distribution is shown in Figure 6-19. The results of the LASL one-ninth scale test are also shown for comparison. The weight and number distributions are illustrated in Figure 6-20, which shows the accumulative weight of fragments versus size class, and in Figure 6-21 which depicts the accumulative number of fragments versus size class. It was found the presented area of the fragments could be defined by the relationship:

$$A = 1.08\, W^{2/3}$$

where A is expressed in mm^2 and W is expressed in grams.

The imparted fragment initial velocities were found to range from 0 to 2200 fps with no apparent relationship between velocity and size. Initial velocity was calculated by APG using standardized methods incorporating the effects of atmospheric drag. The fragment velocity distribution is shown in Figure 6-22 in terms of accumulative percentage of velocities as a function of fragment velocity. Measurement of the spatial distribution of the debris showed that most of the destruct debris was ejected out the sides of the reactor and was concentrated in four co-planar "jets" at right angles to each other and at right angles to the reactor longitudinal axis. The jets were located radially midway between the four explosive charges. The weight distribution of the graphitic material in these jets is shown in Figure 6-23. A fifth jet extended straight up along the reactor axis where the nozzle was blown off. The amount of material in this fifth jet was small in comparison to that in the four main radial jets. Analysis of the size distribution by APG personnel indicated that the

* Size class was evaluated by screening the debris through standard Tyler sieves. Size refers to the size of the small square openings in the sieve through which the particle could pass.

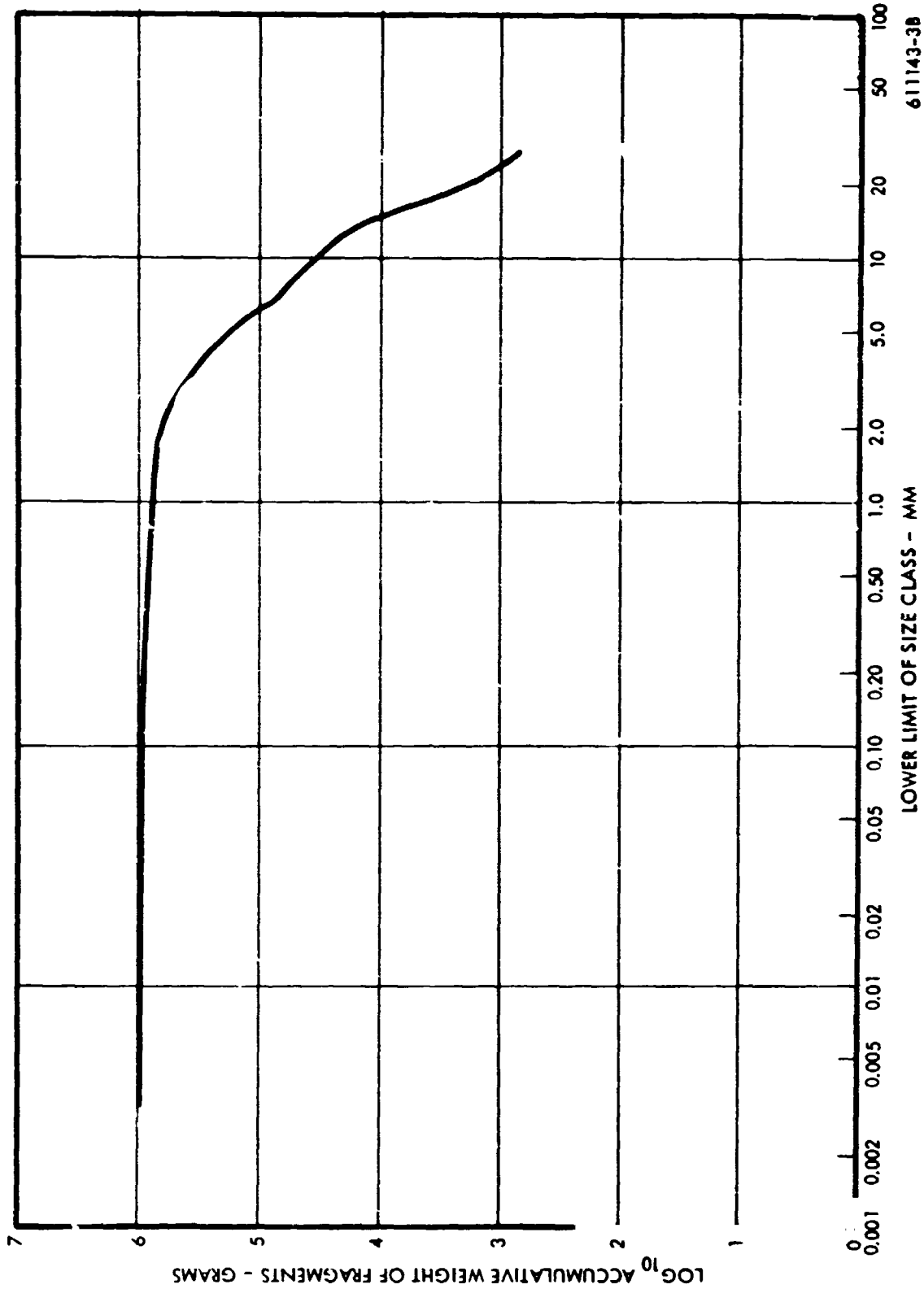

Figure 6-20. Accumulative Weight of Core Fragments versus Size Class

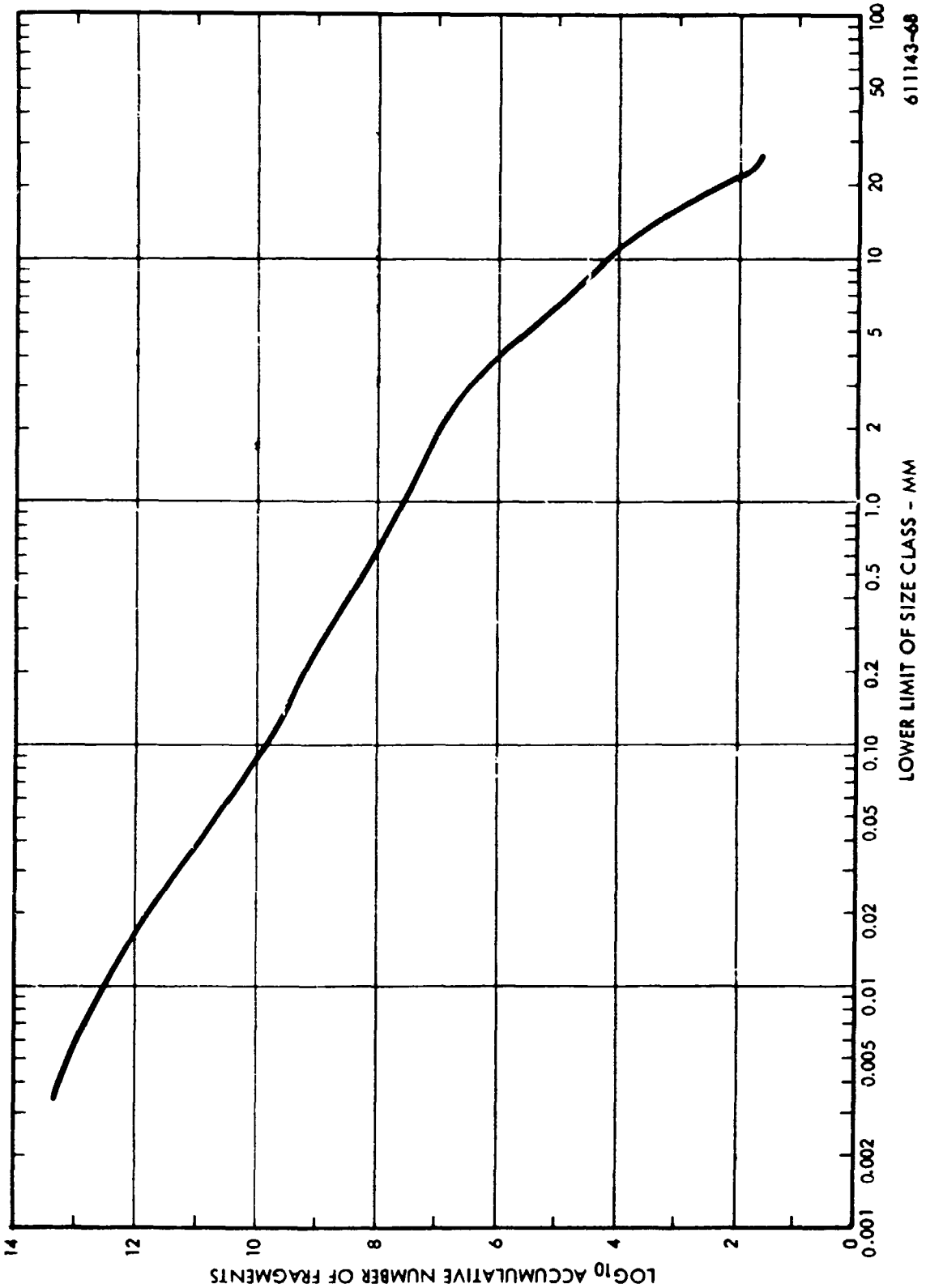

Figure 6-21. Accumulative Number of Core Fragments versus Size Class

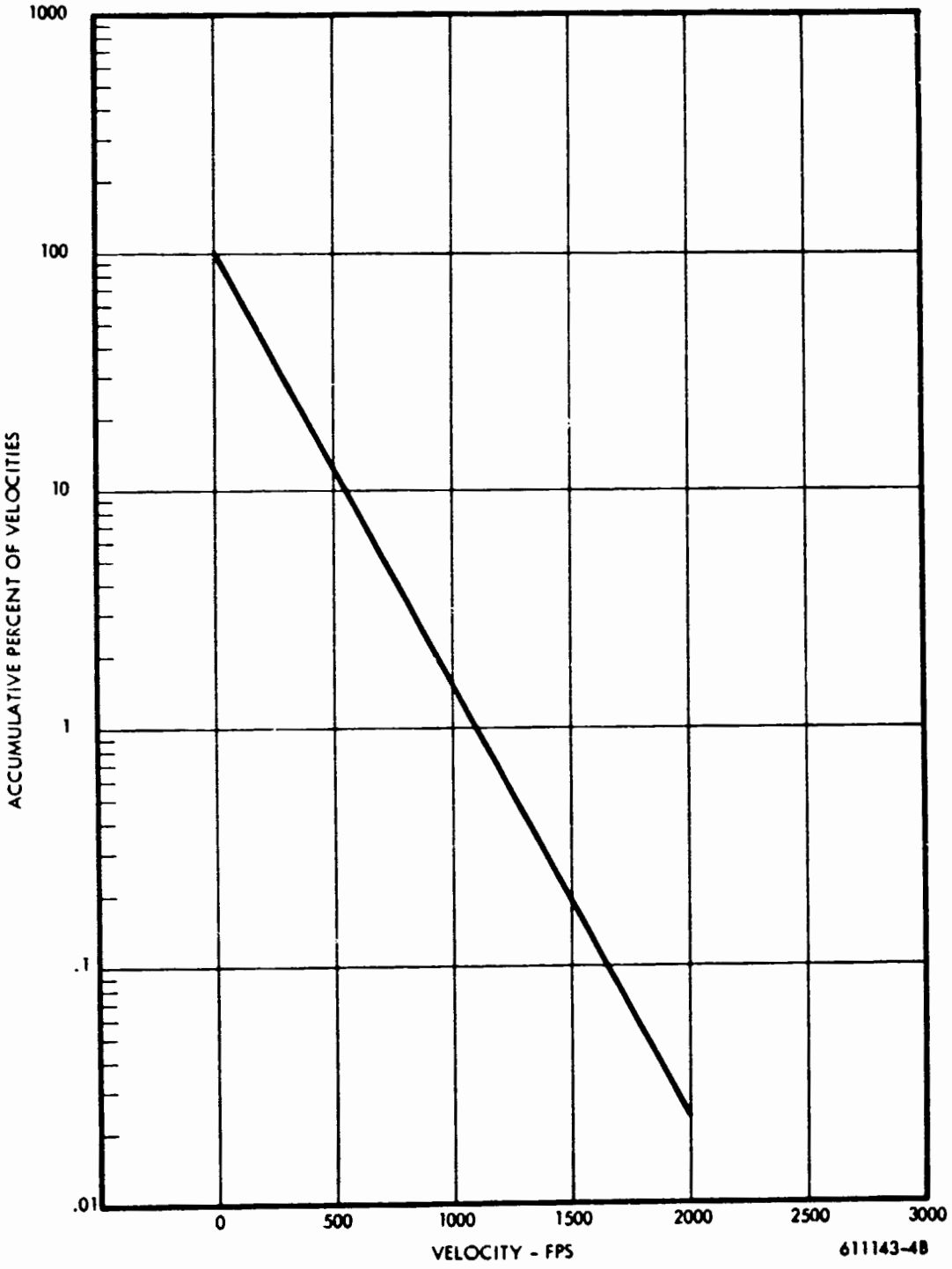

Figure 6-22. Accumulative Percent of Fragment Velocities versus Fragment Velocity

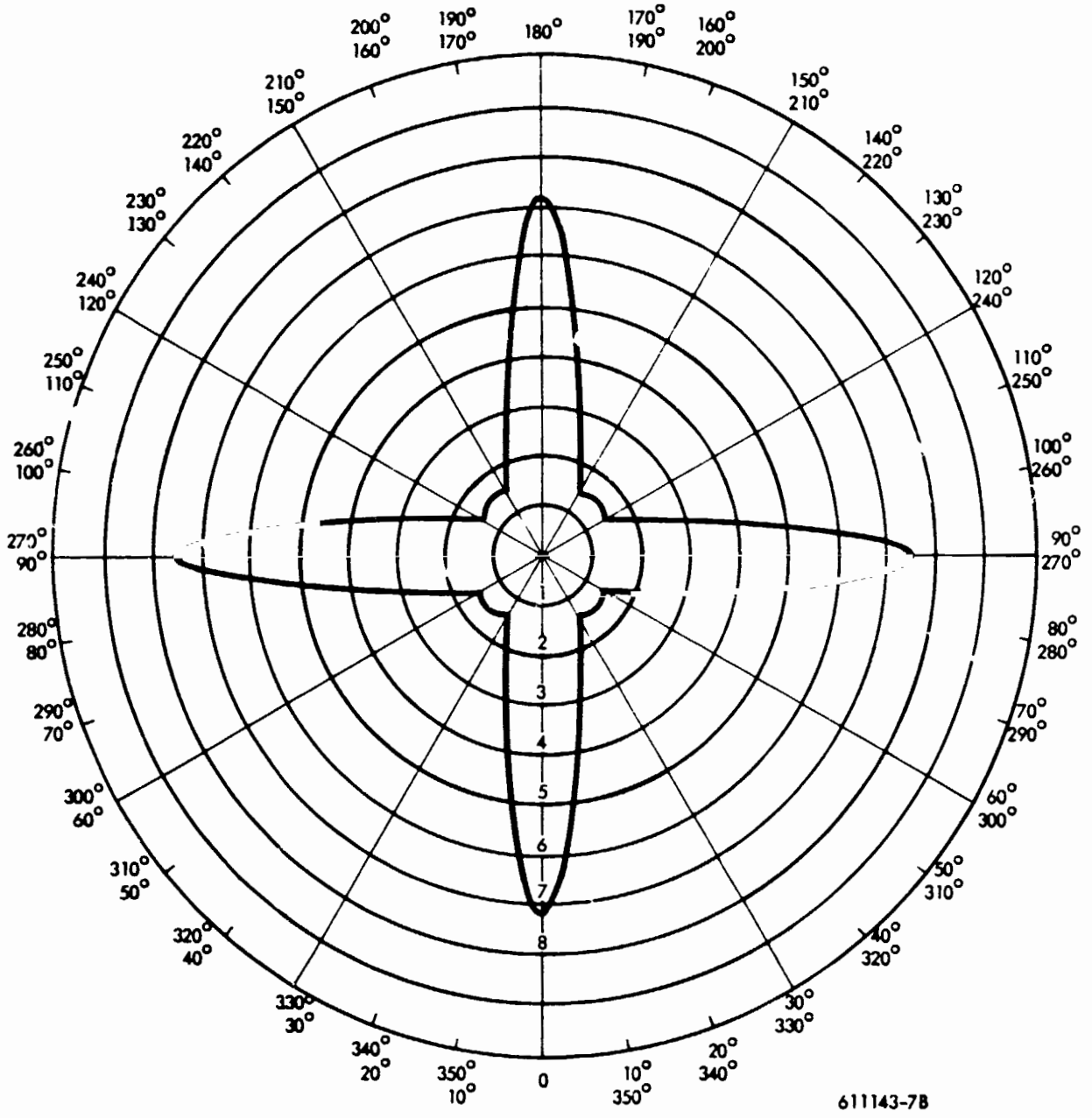

Figure 6-23. Percent of Graphite Weight versus Angular Interval

fragment mass and velocity were independent of angular distribution. However analysis of debris samples collected by the U.S. Naval Radiological Defense Laboratory, as reported in Reference 23, indicates that the size distribution of the material in the jets differs from that outside the jets. The mass median diameter of the material collected by USNRDL is shown in Figure 6-24. As can be seen, the size distribution varies depending on the sample location in relation to the jet location and distance. However for the destruct analyses made by LMSC and WANL (cf, Section 6.4.3) it was assumed the size distribution was independent of angular location.

At this point it should be noted that the flight configuration of a high explosive destruct system will not emplant the four charges parallel to the reactor axis. These charges must be placed at an angle to the axis because the design of the propellant tank and upper engine support structure preclude placing the projectile launchers directly above the engine. The effect of non-parallel charge emplacement cannot be predicted. Thus, it is not certain whether or not a similar jetting action will occur in a flight-configured destruct system. One cannot be certain that the fragment size distribution associated with this effect will remain unchanged.

6.4.3 Destruct Analyses

The analysis of an in-flight destruct countermeasure can be accomplished in three separate phases: (1) definition of the fragmentation and initial conditions of the debris resulting from the destruct action, (2) determination of the re-entry times, impact locations, and atmospheric interactions of the debris, and (3) evaluation of the interaction of the radioactive particles with the population in order to define probability of radiation exposure and population doses. The analytical models and analysis methods used by LMSC and WANL for the first two phases are described below. The expected population exposures resulting from the destruct countermeasure are presented in Chapter 8.0.

6.4.3.1 LMSC Analyses

LMSC analyzed the effectiveness of the destruct countermeasure[12] for the three hypothetical flight missions defined in Section 8.2. Their analytical approach was to

Figure 6-24. Mass Median Size versus Distance From Ground Zero And Position in Jet* APG-III

calculate for each mission as a function of failure time the following parameters for a suitable sample of destruct particles: the re-entry times and if possible, impact locations, fission product inventory of each particle at ground impact (correcting for losses by re-entry burnup and ablation), external gamma dose delivered by each particle at a fixed distance and dose exposure time period, the probability of exposure of the population to the particles, and the expected radiation dose to the population.

Destruct model. The particle size distribution of the destruct fragments as determined by the APG-III test was classified into twelve particle size groups for convenience in the analysis. The size range, the "average" particle diameter (log mean diameter), the weight fraction in each class, the particle density, and the weight fraction of each particle surviving re-entry (due to losses by burnup, Figure 3-8) are presented in Table 6-7. The APG-III particle velocity distribution data were divided into either five or ten velocity increment ranges. The increments are so spaced that each increment will have an equal probability that the velocity imparted to the particles by the destruct action will lie within that increment. The destruct model considered the distribution of all particle mass into the four jets, each jet comprising a solid cone angle of 20°. The model considers the vehicle (NERVA engine) axis is along the flight velocity vector at time of destruct such that the debris jets will be ejected perpendicular to the flight velocity vector. Only this one attitude position is considered and it is assumed the vehicle has not rolled or tumbled following failure and prior to destruct action. An alternate destruct model, which assumed a spherical mass distribution of fragments leaving the explosion center, was also used. This model was used for evaluating beta dose exposure potential since the particle deposition density on the ground could be derived with it. Evaluation of the maximum radioactivity that could be expected for the very small debris particles indicated that particles of size class 10, 11, and 12 (particles smaller than 31 microns log mean diameter) would have insufficient activity (due to small size and long terminal fall times for atmospheric re-entry) to introduce any biological effects even with multiple contacts. Thus particle classes 10, 11, and 12 were not considered in the LMSC analyses.

Calculations of the re-entry times, impact locations, fission product inventories, and population exposures were made using modified chain links and subroutines from the

TABLE 6-7

PARTICLE DATA FROM APG-III DESTRUCT TESTS

Size Class	Size Range Diameter (microns)	Log Mean Diameter (microns)	Particle Radius (cm)	Fraction in Class by Weight	Particle Density (gm/cm^3)	Fraction of Particle Surviving Re-entry
1	20,000 - 50,000	31,620.00	0.1581E+1	0.004	2.10	0.942
2	10,000 - 20,000	14,110.00	0.7055E+0	0.037	2.10	0.887
3	5,000 - 10,000	7,071.00	0.35355E+0	0.169	2.10	0.810
4	2,000 - 5,000	3,162.00	0.1581E+0	0.440	2.10	0.680
5	1,000 - 2,000	1,411.00	0.7055E-1	0.145	2.10	0.550
6	500 - 1,000	707.10	0.35355E-1	0.076	2.10	0.500
7	200 - 500	316.20	0.1581E-1	0.060	2.10	0.590
8	100 - 200	141.10	0.7055E-2	0.032	3.05	0.595
9	50 - 100	70.71	0.35355E-2	0.025	2.10	0.600
10	20 - 50	31.62	0.1581E-2	0.008	2.10	0.610
11	10 - 20	14.11	0.7055E-3	0.004	2.10	0.620
12	0 - 10	3.16	0.1581E-3	0.000	2.10	0.630
				1.000		

LMSC Nuclear Flight Executive Program. Because of the large number of re-entry analyses required for destruct analyses, the re-entry trajectory portions of the program were optimized to reduce computer running time. For the four-lobed (jet) destruct model, an array of 36 vectors define the initial particle locations in space. Five destruct velocity increments were used in the analysis, so that (36×5) 180 re-entry runs were required for each particle class for each failure time analyzed. A special subroutine was developed to compute the number of particles per square meter of a given size class and destruct velocity increment impacting the ground. This program along with special dose model calculations (Chapter 7.0) were used to calculate tissue dose from small beta-emitting particles.

Debris source strength and impact patterns. The source strength or impact inventory of the destruct debris is complicated by the fact that the destruct particles will be returning to earth at different times. The decay rate of deposited material at any time after failure will depend on how much material has been deposited by that time; particles with short re-entry times may have decayed significantly by the time the last destruct fragment returns to earth.

The deposited activity for destruct from a 100 nm orbit start mission of a NERVA-NRX powered vehicle (Mission Model 1, Section 8.2) after 143 seconds full power operation (fail time 786 seconds after launch) is shown in Figure 6-25. The overall decay of the reactor generated fission products is shown by the top curve; the other curves indicate the partitioning of the total source between orbit, atmosphere, and earth surface. Although the particles from destruct do not impact at the same time, the dose models used for calculation of population exposures (Chapter 7.0) assumed the interaction of the particles and the population begins as soon as the particle reaches the earth. For compatibility with these models, the "impact inventory" is then defined as the sum of the activities of the individual particles as each returns to the earth. Thus, the impact inventory for the case shown in Figure 6-25 was calculated as 7.09×10^5 curies, even though the maximum activity on the ground at any one time is only 1.6×10^5 curies.

The source strength of the different particle size classes will vary due to variation in particle mass, re-entry times, and extent of burnup suffered during re-entry.

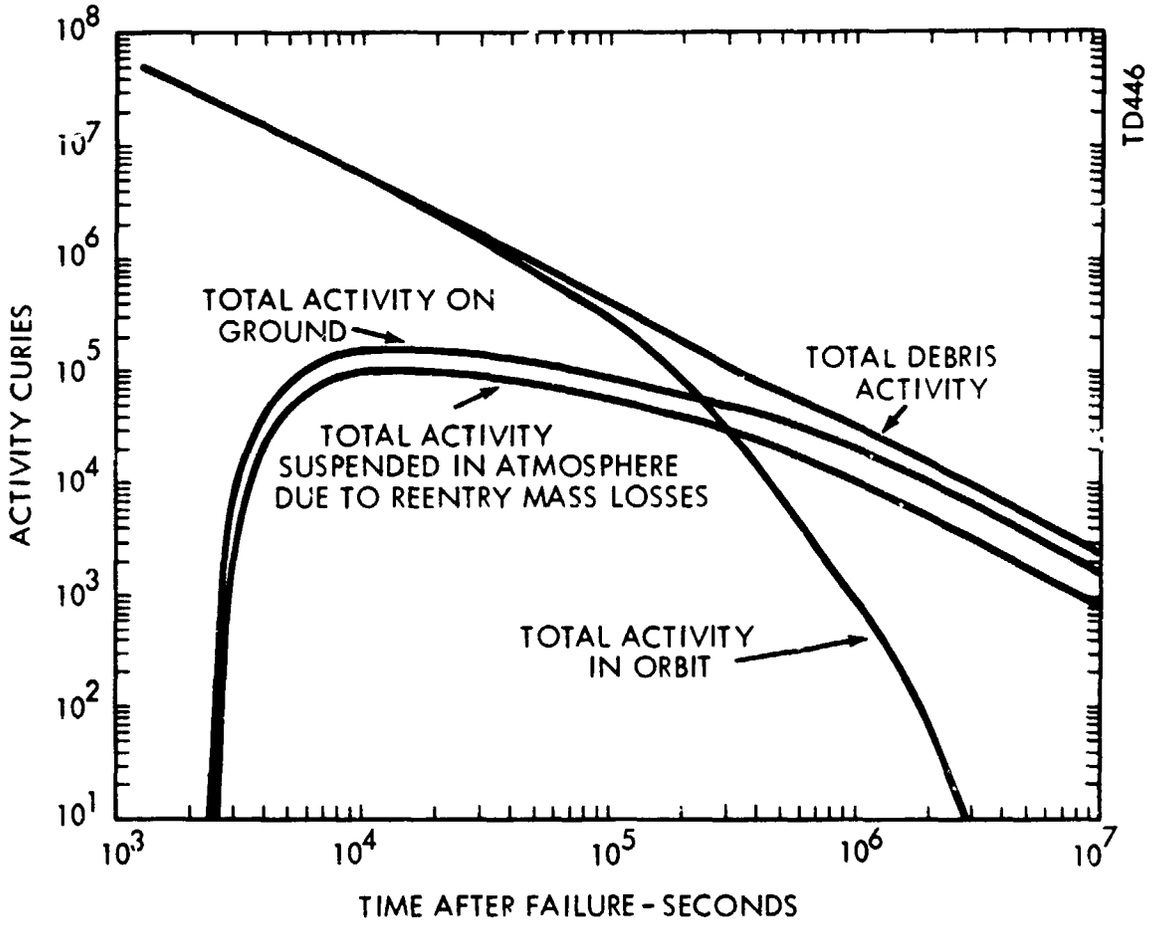

Figure 6-25. Activity Deposition From Destruct; Fail Time 786 Sec, MM-I

The ground impact inventory resulting from a destruct countermeasure at two failure times from an orbit start mission (MM I) and at one failure time from a sub-orbit start mission (MM II) is presented in Table 6-8. It can be seen that much of the activity is carried down by particle classes 3, 4, and 5. Class 4 accounts for over 50 percent of the activity during early failure times, when the dose delivery potential is the greatest.

The debris impact pattern or "footprint" for class 6 particles for a failure time of 1092 seconds for a sub-orbit start mission (MM II) is shown in Figure 6-26. The impact pattern for larger particle sizes shifts downrange and becomes less compact. Impact patterns for other sub-orbital failure times are shifted as would be expected. Earlier failures (before 1092 seconds) give more compact patterns further uprange. The converse is generally true for later failures. Impact patterns using the spherically-symmetrical destruct model are somewhat different than those formed using the lobed model, as would be expected. Two major differences were apparent: (1) the spherical model causes more particles to impact at short ranges because there are velocity vectors directed backward and downward; (2) the spherical model predicts a greater fraction of particles injected into orbit due to vectors directed forward and upward. In the lobed model, forward and backward vectors are not present for the assumed engine attitude at time of destruct.

The expected population whole body gamma doses and beta skin doses for the destruct countermeasures have been calculated based on particle exposure probability models (Chapter 7.0) and land population densities. These doses are presented in Chapter 8.0.

6.4.3.2 WANL Analyses

Westinghouse Astronuclear Laboratory has performed a study to determine the effect of gross changes in reactor attitude, failure time, and destruct initiation time on the amount of radioactive debris deposited on the African continent resulting from a sub-orbital destruct of a NERVA (5000 Mw) engine[24, 25]. No attempt was made to calculate population radiation doses resulting from the re-entering debris. Instead, the analysis was confined to establish the range of values of the destruct variables that would result in little or no contamination of Africa.

TABLE 6-8

ACTIVITY (CURIES) DEPOSITED BY PARTICLES OF DIFFERENT SIZES

Size Class	Mission Model-II Fail Time = 1092 Sec, Reactor Operating Time = 506 Sec			Mission Model-I Fail Time = 639 Sec, Reactor Operating Time = 52 Sec			Mission Model-I Fail Time = 786 Sec, Reactor Operating Time = 198 Sec		
	Activity Per Particle	Activity by Class	% In Class	Activity Per Particle	Activity by Class	% In Class	Activity Per Particle	Activity by Class	% In Class
1	4.773×10^{3}	5.73×10^{5}	0.7	2.739×10^{1}	3.29×10^{3}	0.5	2.45×10^{0}	2.94×10^{2}	.82
2	3.976×10^{2}	4.96×10^{6}	6.2	2.328×10^{0}	2.91×10^{4}	4.3	4.74×10^{-1}	5.81×10^{3}	.04
3	4.383×10^{0}	1.98×10^{7}	25.0	2.996×10^{-1}	1.36×10^{5}	20.3	1.144×10^{-1}	5.19×10^{4}	7.34
4	$3.10^{1} \times 10^{0}$	4.09×10^{7}	51.5	2.700×10^{-2}	3.56×10^{5}	52.9	2.33×10^{-2}	3.07×10^{5}	43.38
5	1.925×10^{-1}	9.40×10^{6}	11.8	2.014×10^{-3}	9.83×10^{4}	14.6	2.156×10^{-3}	1.05×10^{5}	14.84
6	1.31×10^{-2}	2.67×10^{6}	3.5	1.611×10^{-4}	3.28×10^{4}	4.9	4.573×10^{-4}	9.33×10^{4}	13.16
7	4.46×10^{-4}	8.03×10^{5}	1.0	$7.0[illegible] \times 10^{-6}$	1.26×10^{4}	1.9	5.324×10^{-5}	9.57×10^{4}	13.51
8	2.58×10^{-5}	1.92×10^{5}	0.2	4.304×10^{-7}	3.19×10^{3}	0.5	5.334×10^{-6}	3.95×10^{4}	5.58
9	4.42×10^{-7}	2.96×10^{4}	0.1	8.681×10^{-9}	5.81×10^{2}	0.1	1.408×10^{-7}	9.43×10^{3}	1.33
		7.94×10^{7}	100.0		6.719×10^{5}	100.0		7.086×10^{5}	100.0

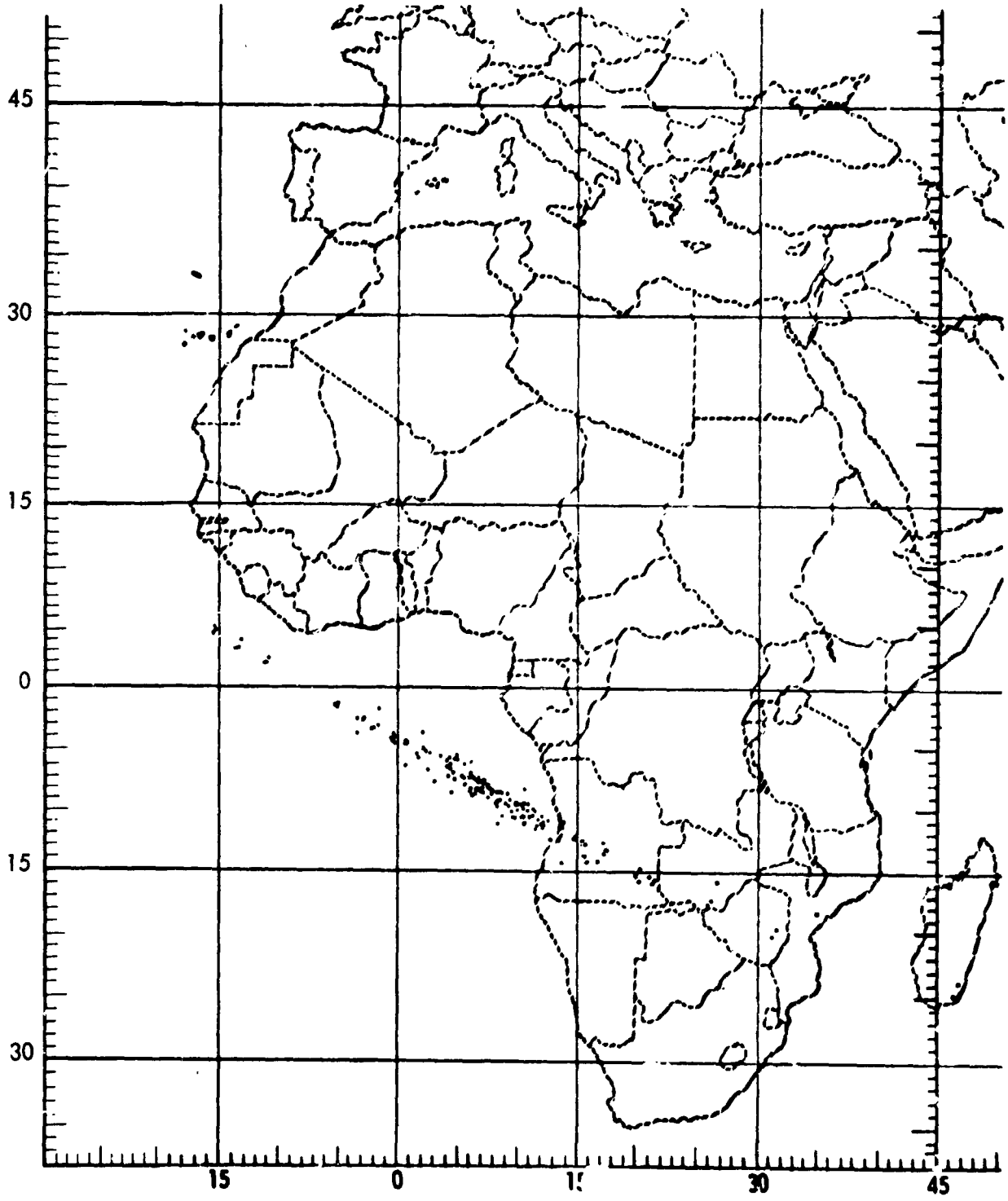

Figure 6-26. Class 6 Impact Pattern for Loaed Destruct Model - Sub-orbit Destruct of NRX Engine

Destruct model. The APG-III particle size distribution was classified into eight size groups, ranging between 13.5 mm to 0.105 mm. The upper and lower boundaries of each size group were chosen so that for each size class, the ballistic parameter did not differ by more than a factor of two. Particles smaller than 0.105 mm were not considered, since those smaller particles comprise only 6.5 percent of the total core mass, and contained only 2.1 percent of the total core uranium. The APG-III velocity distribution data were divided into six velocity increment ranges, varying from 0 to 900 fps. Higher velocities were not considered, since only 2 percent of the particle velocities originating from destruct were measured in the APG-III test to be greater than 900 fps.

The destruct model used considers the four jets ejected from the reactor to be co-planar and at right angles to the longitudinal axis of the reactor. This model differs from the LMSC destruct model in which the jets or lobes are considered to extend outward from the center of the reactor subtending a solid cone angle of 20°. Consultation with APG personnel[26] has confirmed that the concept of the debris being in a "destruct plane" which is perpendicular to the longitudinal axis closely approximates the actual geometry of the destruct action.

The analysis was predicated on the consideration that the vehicle may have assumed any combination of pitch, yaw, and roll when destruct occurs. Since the destruct debris is not formed in a spherically isotropic pattern, the attitude of the reactor at moment of destruct will affect the ground distribution of the debris. To define the orientation of the destruct plane it is necessary to define the pitch and yaw of the reactor's longitudinal axis. Initially, 13 different attitudes were selected for a screening analysis. Each of these attitudes was defined by selecting different combinations of pitch and yaw, in which the pitch and yaw angles were varied by 45° increments. In later analyses[25], pitch and yaw were varied by smaller increments to determine the sensitivity of debris impact location to slight changes in attitude. A third attitude variable examined was vehicle roll, since the distribution of debris in the destruct plane is non-isotropic. Three roll positions, 0°, 22.5°, and 45°, were examined for each of the 13 attitudes. Because of the symmetry of the

TABLE 6-9

FRACTION OF TOTAL CORE DEBRIS ON LAND FOR NERVA SUB-ORBIT START MISSION

Attitude	Pitch (Degrees)	Yaw (Degrees)	Fail Time					
			996 Seconds Roll Position			1006 Seconds Roll Position		
			0°	22.5°	45°	0°	22.5°	45°
1	0	0	0.1266	0.1355	0.1394	0.4101	0.3337	0.2949
2	45	0	0	0	0	0.6020	0.5878	0.5800
3	90	0	0.1365	0.1335	0.1338	0.2374	0.1699	0.1240
4	-45	0	0.1785	0.2273	0.2451	0.2139	0.1957	0.1207
5	0	45	0.1695	0.1799	0.1550	0.1246	0.1836	0.2576
6	0	90	0.1807	0.1192	0.1274	0.1227	0.1060	0.1815
7	0	-45	0.1714	0.1727	0.1791	0.1589	0.1458	0.2470
8	45	45	0.0596	0.0570	0.0571	0.2860	0.2655	0.3534
9	-45	+45	0.1993	0.1453	0.1450	0.1194	0.1958	0.1793
10	45	90	0.1850	0.1410	0.1377	0.1752	0.2231	0.1526
11	45	-45	0.0803	0.0736	0.0669	0.2850	0.2558	0.2173
12	-45	90	0.1698	0.1556	0.1473	0.1635	0.1821	0.2536
13	-45	-45	0.1882	0.2043	0.1466	0.1049	0.1289	0.2038

destruct pattern, larger roll angles using 22.5° angular increments would yield destruct patterns identical with those for the three roll positions examined.

The analysis model considered that explosive destruct action would be utilized only during those short time intervals of the total sub-orbit flight time during which failure would lead to land impact of the intact re-entry vehicle. Two failure times, 996 and 1006 seconds after launch, were selected. The time interval between these fail times bracket African impacts for the intact re-entry vehicle; earlier fail times would result in Atlantic ocean impact, whereas later failures would result in deep ocean disposal or impaction in an undetermined location. The effect of delaying destruct until the vehicle had re-entered to 400,000 feet altitude was also investigated for two different attitude cases.

A modified version of the WEREC Program[27] was used to predict the re-entry time and impact location of fractions of the core representing a definite particle size range, destruct velocity range, and destruct angle range. Land areas occupied by the debris representing a definite fraction of the core were calculated by a newly developed Computer program called DEFT (DEstruct FootprinT). The location, area, and ground density of the debris representing all fractions of the core were summed to define the total contaminated land area and debris density.

Debris impact patterns and source strength. In general, the footprint boundary for a given particle size-velocity class traces an elongated ellipse on the earth's surface, somewhat similar to the footprint obtained by the LMSC analysis. For many size and velocity groups, the downrange end of the ellipse is not closed, a condition indicating that some fraction of debris has been injected into orbit from the destruct action. However, the intent of this study was not to accurately define footprint boundaries, but to determine the extent of land contamination by the debris.

The fraction of core debris lying on land (Africa) as a function of reactor attitude for destruct at the two failure times is summarized in Table 6-9. The pitch angle is the angle between the reactor's longitudinal axis and the velocity vector with upward pitch considered positive; counterclockwise motion about the yaw axis is positive and is measured with respect to the velocity vector. Table 6-9 shows that while failure at 996 seconds for Attitude 2 results

in no land contamination, failure 10 seconds later at 1006 seconds in this same attitude results in a large fraction of the core impacting on Africa. In fact, this land fraction is the greatest for any of the attitudes studied. In general, those attitudes which result in the least fraction on land for failure at 996 seconds, result in the greatest fractions for 1006 second failures (e.g., Attitudes 1, 8, 11, as well as 2).

The effect of roll position on the amount of debris impacting Africa can be clearly seen from this data. Some attitudes introduce greater sensitivity to roll (e.g., 4, 4, 10) with the core fraction showing variations of as great as 35 percent. Other attitudes (e.g., 3, 8) exhibit very little change at different roll positions.

Evaluation of the total hazard potential of destruct must consider not only that debris which impacts on ocean and land areas, but also that portion which is injected into orbit. Such orbital debris eventually re-enters with impact in random locations between a $\pm$ 40 degree latitude band. Although the additional time provided by orbital decay reduces the radioactivity of the debris, the eventual possible land deposition of this debris leads to further potential radiological exposures. A pictorial representation of the core fractions on Africa, in the ocean, and that injected into orbit is presented in Figure 6-27.

This figure reveals that the later failure time (1006 seconds) results in a greater fraction of debris in orbit. This is to be expected since the vehicle has attained a greater velocity, which, when added to the destruct velocity imparted to the debris, results in a greater proportion of the fragment reaching orbital velocities.

The fission product inventory and gamma source strength of the destruct debris particles at ground impact time were calculated using the WANL Source Term Computer Program[28]. Rather than report the instantaneous activity or the gamma ray emission rate of the debris at ground impact, the following integrated four-day gamma energy, S, is used:

$$S = \int_0^4 3.456 \times 10^6 \, E_\gamma (t) \, dt$$

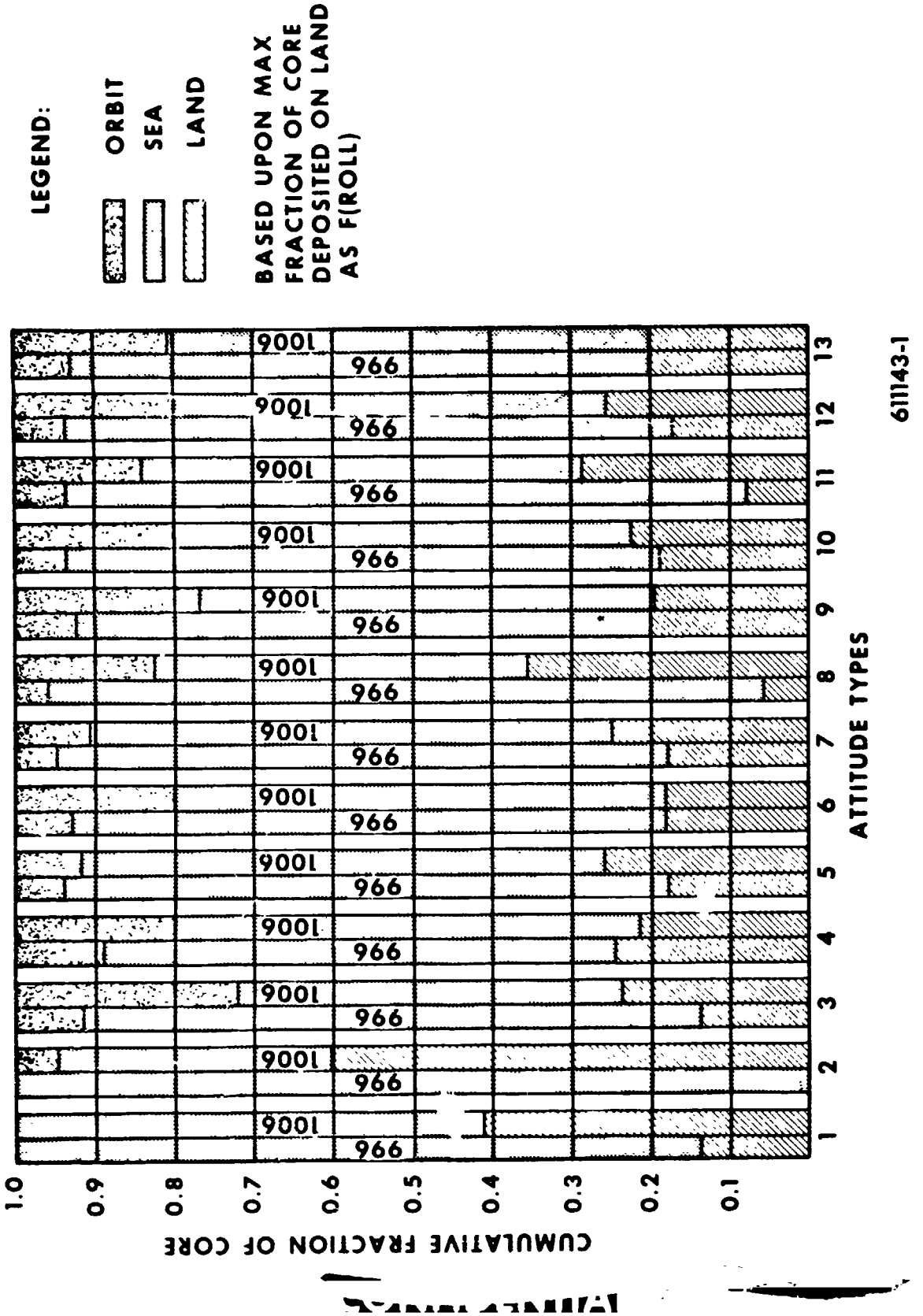

Figure 6-27. Cumulative Fraction of Core Deposited on Land, Sea and Orbit for Various Attitudes of Engine at Time of Destruct

where:

S = total four-day integrated gamma energy from particle, MEV

E_γ = gamma source strength of particle at ground impact time, MEV/sec

t = time, days

3.456×10^6 = number of seconds in four days

The value of S is determined by the Source Term Computer Program in which the function $E_\gamma(t)$, is integrated over 254 nuclides and seven gamma energy groups. The value of S is required as input to the MOREDO Computer Program (cf. Chapter 7.0) in order to calculate the dose to a mobile receptor. Although dose to the African population was not calculated in this study, the value of S, the integrated source strength of the particle, is a convenient parameter for use in comparing the effectiveness of different destruct attitudes and failure times in reducing the amount of debris impacting on land.

Particles of different size groups will have overlapping areas, thus reinforcing the ground activity. No attempt was made to define in detail the areas of overlap. Thus, the exact source strength gradients on the ground were not determined. However, the maximum and minimum source strengths that occur within the total area occupied by the debris due to the presence or absence of overlap were estimated.

The ground source strength (γ MEV/ft^2) for the 996 second failure case is shown in Figure 6-28. The shading used in these figures shows the maximum and minimum radioactivity, and also the range in the maximum and minimum values due to variation in roll position. The minimum source strength represents the general range of land contamination that would result regardless of vehicle roll position at time of destruct. It can be seen that roll can affect the maximum and minimum contaminations by a factor of two to three. However, variations between the maximum and minimum for any given attitude can be as great as a hundred-fold. The ground source strength for the 1006 fail case is similar to that shown in Figure 6-25, with the exception that Attitude 2 yields the largest source strength as might be predicted from the data of Table 6-9.

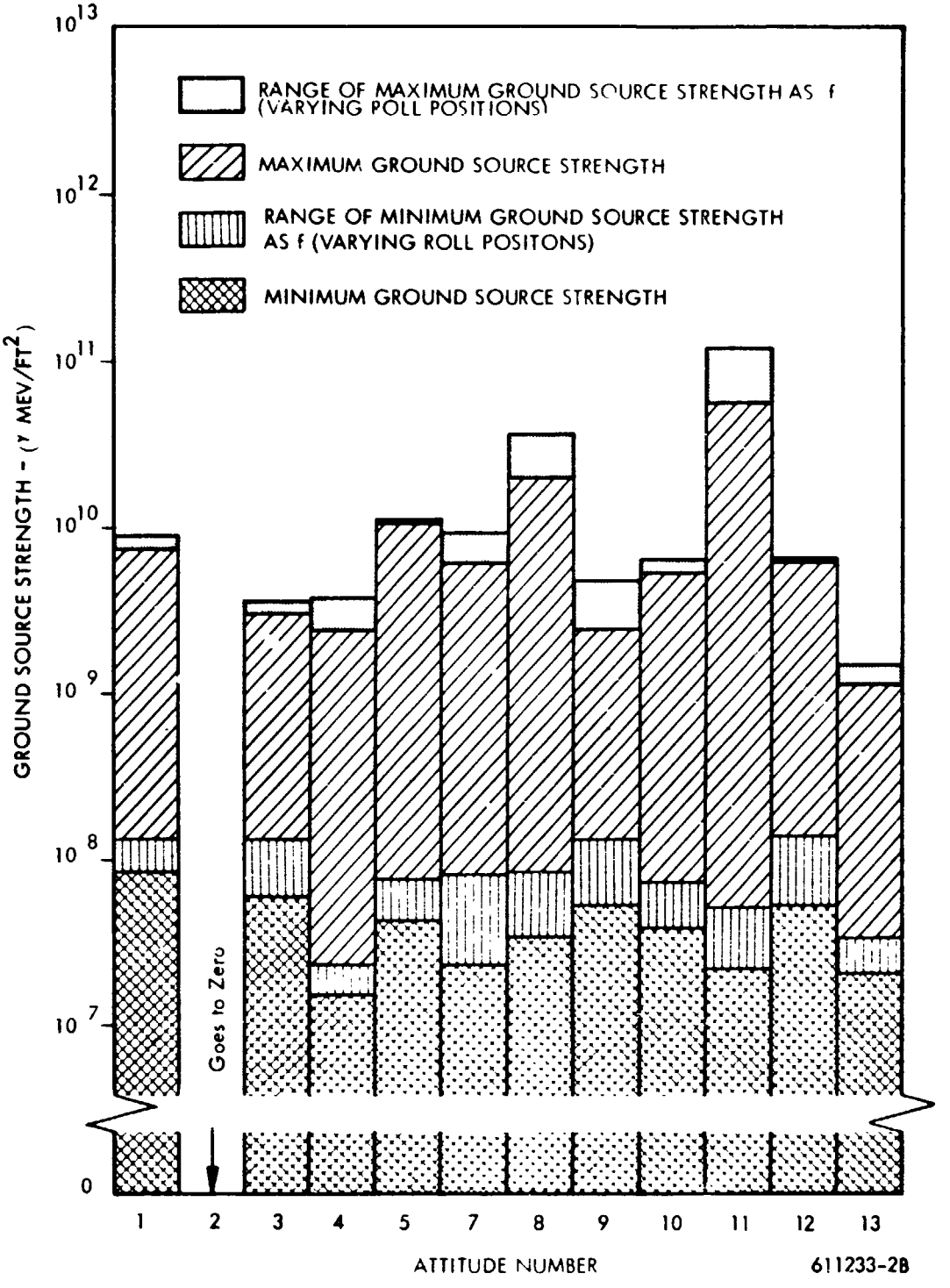

Figure 6-28. Ground Source Strength (γ MEV/ft^2) 996 Seconds Fail Time

The number of particles that impact on land for the varying particle size-velocity groups was computed to determine the particle ground density. For a given area, the greater the number of radioactive particles per unit area, the greater the probability of interaction between the populace and the debris. "Reciprocal" particle density (ft^2 per particle) was calculated since the normal particle densities (particles/ft^2) were always less than unity. Thus, reciprocal particle density can be considered as the area occupied by a single particle. The final ground particle density, as with ground source strength will depend on the extent of overlap of areas. Overlap boundaries were not determined, but only the maximum, minimum, and average densities are reported.

Reciprocal particle densities are shown in Figure 6-29. This figure shows that the average area occupied by a single particle is between 10^4 - 10^5 square feet. Hence, it can be assumed that a person will not interact with more than one particle. The data of this table, along with pertinent land areas and population data, could be used in the MOREDO mobile receptor dose model (Section 7.2.1) for estimating external whole body gamma dose to the African population.

It can be concluded, that with the exception of Attitude 2 at 996 seconds fail times, there does not appear to be any one attitude (of the 13 examined) that offers a significant improvement in land deposition of debris over another attitude.

Additional analyses, recently completed by WANL[25], have shown the amount of deviation in yaw and pitch from Attitude 2 values (pitch = 45°, yaw = 0°) that could be tolerated during the time span 996-1006 seconds, without land deposition occurring. This study has shown that between the time period 996 to 1000 seconds after launch, a narrow range of reactor attitudes exists from which destruct debris will indeed avoid the African continent. The allowable variation in attitude decreases rapidly with increasing fail time. Thus for failure at 996 seconds, the reactor attitude may vary within the approximate limits of 35° to 50° pitch and ± 5° yaw and all debris will miss Africa. (This assumes the maximum ΔV imparted to the debris particles by destruct action does not exceed 900 fps as was previously assumed in these analyses). For destruct at 1000 seconds after launch, the permissable attitude variation is narrowed to approximately 40° - 45° pitch, with no

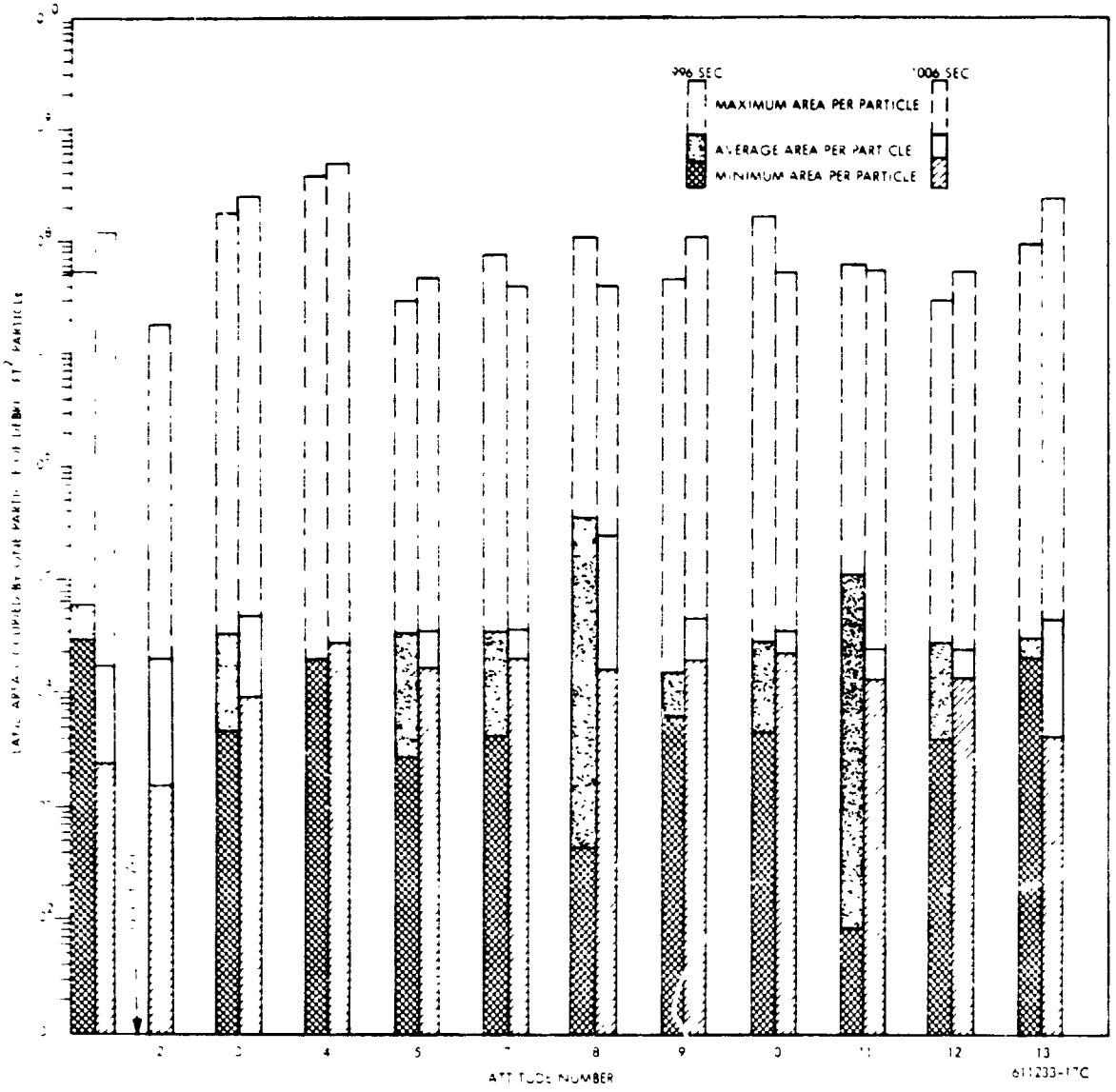

Figure 6-29. Particle Ground Density Resulting from Failure from Different Attitudes

variation from 0° yaw allowed. For failure times of 1002 seconds or later, no attitude appears capable of avoiding land impact.

The study revealed there is a significant influence of the destruct velocity imparted to the debris particles on the degree of attitude control required to insure avoidance of land impact. If the explosive destruct action could be modified in such a way as to reduce the upper limit of destruct velocities (a so-called "soft destruct"), then the attitude envelope yielding no land impact would be increased. Decreasing particle size also tends to increase the envelope of successful attitudes, but not nearly so markedly as will decreasing velocity. However, for the 1004 and 1006 fail times, it appears that a destruct action will result in some land impact.

The effects of delaying the destruct action following detection of flight failure were investigated. The potential benefits of delaying destruct action include: (1) reduction of core fission product inventory by diffusion during the delay time period (assuming no post-operational cooling) and (2) diminishing of debris injected into orbit by virtue of the reactor being at a lower altitude at time of destruct. The proportions of debris on land and in the ocean will also be changed from that of the immediate destruct case, and the delayed destruct action may produce more favorable conditions for reduction of potential radiological exposures of persons.

Delayed destruct following failure at 996 and 1006 seconds was considered to be initiated when the vehicle had reached an altitude of 400,000 feet. Delay time to reach this altitude was calculated to be 509 and 701 seconds for the 996 and 1006 failure times, respectively. It was assumed that the reactor remained intact during the delay time between flight system failure and initiation of destruct. It was further assumed that the core assembly and structural components were not significantly altered during the delay time, in order that the destruct action would yield the same results as an undamaged core. Two attitude positions of the engine at the time of delayed destruct, Attitudes 2 and 9, were selected for screening analysis. Attitude 2 (pitch = +45°, yaw = 0°) was chosen because immediate destruct at this attitude produced the best (996 seconds fail time) and the worst (1006 seconds fail time) results. Attitude 9 (pitch = -45°, yaw = +45°) was chosen on the basis that the core fraction impacting on land for immediate destruct varied the least for both failure times. The reduction

in core fission product activity was estimated assuming post-operational heating under loss-of-coolant conditions for the 509 and 701 second delay times. These estimates were based on previous NRX analyses utilizing the FIPDIF-NOFLOW computer program.

The results showed that for Attitude 2, delayed destruct offers no improvement. With the 996 second failure time, all debris is still ejected into the Atlantic Ocean. However, for the 1006 second failure time, delayed destruct causes an additional 10 to 12 percent of the core to impact on Africa. As was expected, the fraction of debris ejected into orbit was diminished--in this case to zero.

With Attitude 9, delayed destruct following failure at 996 seconds after launch resulted in significant improvement in reducing the hazard potential. The fraction of debris on land was reduced from about 16 percent to 0.2 percent or less, with the fraction injected into orbit reduced by about one-half. However, delayed destruct following failure at 1006 seconds significantly worsens the hazard potential, with the core debris fraction on land increasing by a factor of three from about 17 percent to greater than 50 percent.

The ground source strength (gamma MEV/ft^2) was calculated in the same manner as for the immediate destruct cases. Due to loss of fission products by diffusion, the integrated four-day gamma source strength of the debris is about a factor of two lower than the debris originating from immediate destruct. The average ground source strength for the delayed destruct cases are shown in Figure 6-30. Values for the immediate destruct cases are shown for comparison. As can be seen from this figure, for Attitude 2 (1006 seconds), the ground source strength is less than that for the immediate destruct, even though the core fraction on land is greater. This decrease can be attributed to the fission product diffusion inventory losses. However, for Attitude 9 (1006 seconds) this decrease in inventory due to diffusion does not compensate for the substantial increase in the core fraction deposited on land. Note that for Attitude 9 (996 seconds) the combined effect of less fraction on land and fission product diffusion substantially decreases the ground source strength in comparison with immediate destruct. Thus for this instance, delayed destruct markedly decreases the hazard potential.

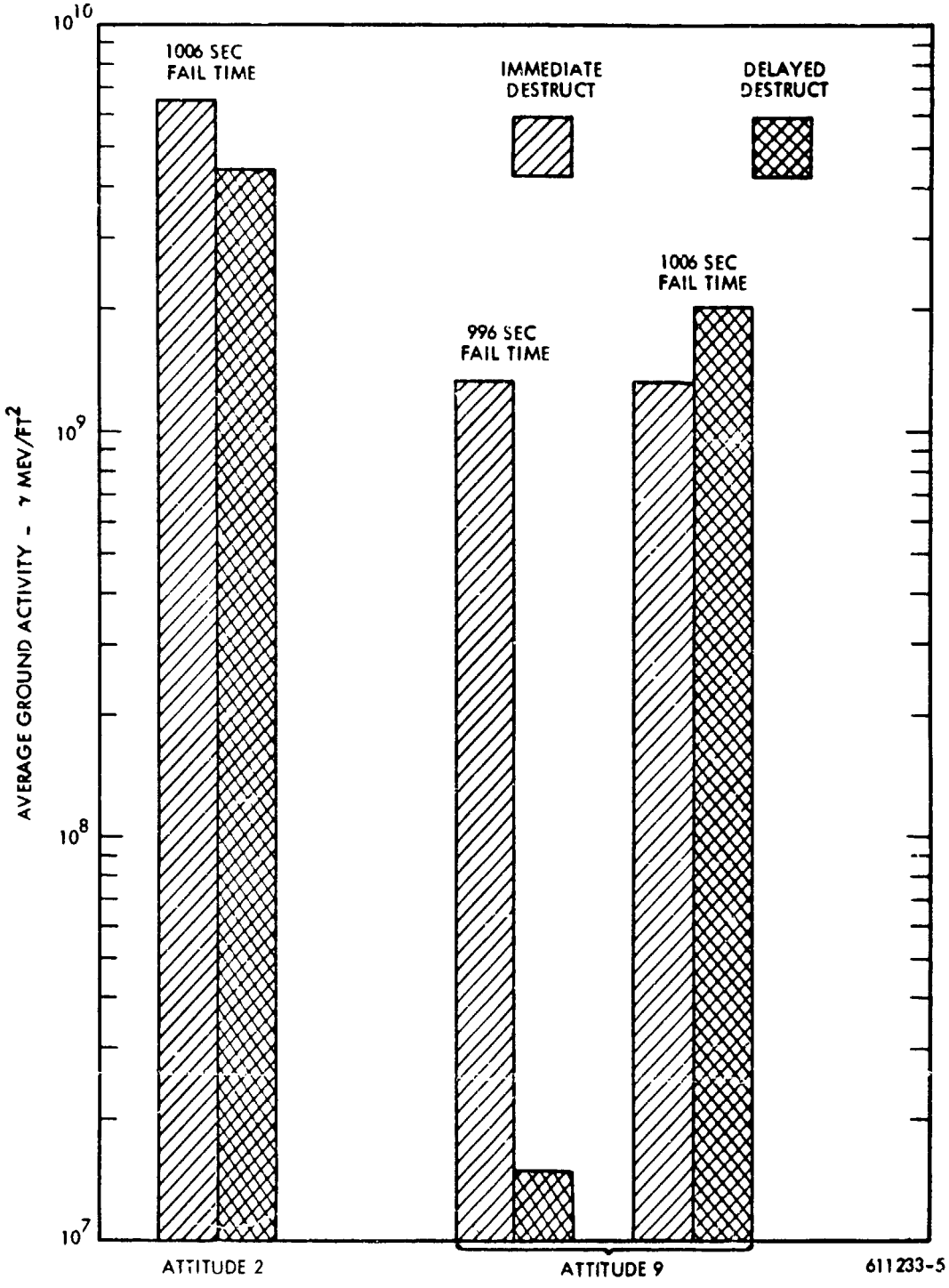

Figure 6-30. Comparison of Average Ground Source Strength for Immediate and Delayed Destruct

Based on the two attitudes studied, utilization of delayed destruct at failure times early in the 996-1006 second fail time spar may offer a significant reduction in the amount of debris reaching land. The converse appears true for late failure time of the 996-1006 time span. However, these general conclusions must be made with caution because of the limited analyses performed. In addition, if the accident model assumes a loss-of-coolant condition, the effect of post-operational heating on core integrity during the delay time prior to destruct must be evaluated in the destruct model.

6.5 NUCLEAR DESTRUCT

In addition to utilizing chemical explosives to fragment the NERVA core, it may be possible to achieve such fragmentation by a self-induced nuclear excursion. In addition to yielding small particles, such a safety countermeasure could offer the additional advantage of releasing large quantities of fission products to the environment. However, in order for an excursion to be effective in fragmenting the core, it is necessary that energy insertions be both large and rapid. The NERVA and NRX reactors, as currently designed, do not appear to have the inherent capability of undergoing such excursions as the result of reactor malfunctions.[29] It appears that malfunctions such as drum run out will result in no more severe consequences than core over-heating with subsequent thermal degradation of the reactor. Thus, to accomplish a self-induced destructive excursion, it will be necessary to devise some technique for rapidly inserting requisite reactivity.

6.5.1 Analytical Evaluations

At present there exist three computer programs which examine the response of NERVA type reactors to fast reactor transients. These are RAC[30], NERVEX[31] and NECKLACE[32]. The first two of these programs are similar in that they consider energy deposition within the core material to be uniformly distributed between the UC_2 and the graphite matrix. The programs evaluate the thermal, chemical, and mechanical response of the reactor core to the energy insertion rates associated with the excursion. In particular, they calculate pertinent physical parameters contributing to shutdown. NECKLACE on the other

hand considers the response of individual fuel beads to the reactor transient. Experimental evidence[33] indicates that in the event of a large rapid nuclear transient, these beads will rupture, a result which may lead to extensive core fragmentation and an eventual mechanism for reactor break-up.

6.5.1.1 RAC

There exist two versions of the RAC[29, 30] Computer Program. One uses a one-dimensional reactor model, and it performs its calculations in slab, cylindrical or spherical geometry. The other uses a two-dimensional reactor model, and it performs its calculations in the R-Z coordinate cylindrical geometry.

The computer program is concerned with the dynamic behavior of a graphite reactor under power transient conditions. In the code, the core is arbitrarily divided into a number of homogeneous segments, to each of which is assigned a fission or power density. Then for a given reactivity insertion (step or ramp), the program generates, as a function of time, fission energy in each segment, as well as the increasing fuel temperatures and graphite vapor pressures according to the heat content functions and vapor pressure data built into the program. In addition, each core segment is allowed to perform thermodynamic work on its neighboring segments through the interface of the segments. This work serves to relieve internal pressures associated with thermal expansion and/or vapor formation. In the event the reactivity insertions are large, this work sets the core into motion. Reactivity is decreased as the core expands.

6.5.1.2 NERVEX

The NERVEX[31] Program is similar to RAC; however, it considers only two dimensional, cylindrical R-Z geometry.

6.5.1.3 NECKLACE

The NECKLACE[32, 33] Computer Program examines the problem of heat conduction out of a UC_2 bead through its surrounding pyrographite coating into the graphite matrix. The problem uses spherical coordinates with allowance for an arbitrary number of zones arranged as nesting spherical shells, with the central volume of fuel being a sphere

In the NECKLACE Program all fission energy is initially deposited in the UC_2 bead. As the bead begins increasing in temperature, heat transfer begins through the pyrographite shell. Once the fuel reaches its melting point, it will be transformed into a liquid which will expand and also form a UC_2-C eutectic with the pyrocarbon coating. (As this eutectic is formed, provision must be made in the thermal conductivity calculations for the diminishing thickness of the pyrographite shell.) Competing with eutectic formation, will be vaporization of the fuel material (or the eutectic) during which the bead may experience very high internal pressures. What happens next will depend upon the extent to which the pyrographite coating has been degraded by UC_2-C eutectic formation. If considerable degradation occurs before vaporization becomes significant, heat transfer to the graphite matrix will occur much more rapidly, and vaporization will be suppressed. It is doubtful if core fragmentation will occur. However, if the energy pulse has been quite rapid or if the pyrographite coating is thick, vaporization should be large, and bead rupture accompanied by core fragmentation may occur.

One of the major problems encountered in using NECKLACE to perform excursion calculations is that of assessing the rate of UC_2-C eutectic formation. The basic kinetic and thermodynamic data needed to define the formation of this material are lacking. However, if this phenomena is neglected along with pyrographite weakening due to radiation damage and if it is assumed that no heat losses from the bead occurs, it is then calculated that 4×10^{14} fissions per gram UC_2 is required to fragment the fuel at room temperature. If the fuel is initially at 1350°C, 2.5×10^{14} fissions per gram U-235 are required.

6.5.2 Experimental Data

A number of experimental programs have yielded data on the energy requirements for core fragmentation. These experiments range in magnitude from small scale fuel tests in a variety of test reactors to the full scale KIWI-TNT test. The fuel tested in these experiments was NERVA type fuel with 100 micron UC_2 cores surrounded by a 25 micron pyrographite coating all dispersed in the graphite matrix. Actually, the UC_2 beads will range in diameter from 50 to 150 microns. Unless otherwise noted, this type fuel is discussed in the following paragraphs.

6.5.2.1 TREAT

In experiments in the TREAT[34] test reactor, small fuel samples experienced a total energy of 2.35 x 10^{15} fissions per gram U-235. The most rapid transient condition was 40 msec. No fragmentation was observed; however, photomicrographs showed considerable bead damage with the UC_2 being dispersed throughout the graphite matrix. While the energy of the experiment is in excess of that predicted by NECKLACE, the long transient probably allowed sufficient time for complete degradation of the pyrographite bead before substantial vapor pressures developed.

6.5.2.2 TRIG A

In order to obtain a shorter period, samples were tested in the TRIG A reactor.[33] Here a sample received a TRIG A pulse of 9.9-msec half width and a total exposure of 2.4 x 10^{14} fissions per gram U-235. No bead degradation was observed. It was concluded that breakup required either a still shorter period or a greater energy deposition or a combination of both.

6.5.2.3 SPERT-I Oxide Core

Fuel samples were next tested in the SPERT-I facility. Under conditions of 3.83 x 10^{14} fissions per gram U-235 (est.) and with a reactor period of 1.5 msec, no fragmentation was observed.[33] In fact, it was found subsequent to the test that a considerable number of intact beads still existed.

6.5.2.4 SNAPTRAN-3 External Fuel Sample Experiments

SNAPTRAN-3[33] was a destructive excursion performed 1 April 1964. Three NERVA fuel samples were placed about one inch from the outer vessel surface where it was estimated that the peak thermal neutron flux would exist. Three other samples were placed about 2.25 inches further out, in order to receive about one-half the peak flux. In this test the reactor period was 0.65 msec. The following three types of beads were used in the fuels tested:

1. A standard type fuel with a normal bead size distribution with core diameter ranging from 50 to 150 microns.

2. A beaded fuel with UC_2 beads ranging in diameter from 50 to 100 microns.

3. A beaded fuel with UC_2 beads ranging in diameter from 100 to 150 microns.

All the above beads had a 25 micron pyrographite coating.

Post excursion examination of the three different fuels in their two different locations, indicated only one of the fuel samples fragmented. Only the fuel sample containing UC_2 beads, 50 to 100 microns in diameter fragmented, and this occurred only for the particular sample placed closest to the outer vessel. However, photomicrographs did indicate that even for this sample, some beads failed to undergo fragmentation. An energy of approximately 10^{15} fissions per gram U-235 was estimated.

6.5.2.5 KIWI-TNT External Fuel Samples

During the KIWI-TNT test[33], which will be described later, a number of NERVA fuel specimens were placed external to the test reactor. The period of this test was 0.6 msec. As a result of the placement of the fuel samples, four different energy depositions were observed ranging from 3×10^{14} to 7×10^{15} fissions per gram U-235. In this test the following fuel variables were selected for examination: bead core size, bead core composition, bead coating thickness, prior exposure to radiation, and fuel ambient temperatures.

It was observed that for the standard NERVA fuel the only sample to fragment was that receiving 5×10^{15} fissions per gram U-235. For this case fragmentation was extensive and no bead structure remained, a result observed by photomicrographic examination. Less damage was observed for lower energy depositions. When samples were heated at 2400 to 2100°C and subjected to 7.7×10^{14} fissions per gram U-235, it was observed that UC_2 melted and the beads were damaged. While no fragmentation appeared to take place, there was considerable matrix damage in the sample heated to 2400°C. With lower energies, i.e. 3.4×10^{14} fissions per gram U-235, and identical temperatures, no matrix damage was observed nor did the pyrographite coating appear to be damaged.

As a result of these studies it appeared that for a reactor transient of 0.6 msec there exists a definite threshold in the energy required to fragment the NERVA fuel material

and that this threshold lies somewhere between 1.7×10^{15} and 5×10^{15} fissions per gram U-235. Moreover, it appears that this threshold may be diminished in the event the beads are heated prior to the excursion.

The experiments on beads of other geometries indicated that the fuel beads with larger than normal cores are damaged more easily than smaller ones, beads with thicker than normal coating show somewhat less damage than standard beads, and samples with a larger than normal bead volume fraction are fragmented more easily. In addition, it was observed that fuel samples which have been irradiated at full power show no increase or decrease in fragmentation sensitivity.

6.5.2.6 SNAPTRAN-2 External Fuel Sample Experiments

A number of NERVA fuel samples were placed external to the SNAPTRAN-2 excursion test.[33] The period of the excursion was 0.2 msec, a time much shorter than any experienced previously. However, the energy deposition was also diminished, being only 1.35×10^{14} fissions per gram U-235. Analysis indicated that the normal fuel underwent no appreciable damage, and only a trace of uranium migration was observed. However, for a fuel having beads 210 to 300 microns in diameter and a 50-micron pyrocarbon coating, some bead rupture was observed along with some matrix cracking for a flux position resulting in 8×10^{13} fissions per gram U-235.

6.5.2.7 The Full Scale KIWI-TNT Test

A full scale transient nuclear test was conducted on a KIWI* reactor on 12 January 1966. The basic KIWI design was used in this test reactor, however, tantalum neutron poison material normally used for shimming the reactor to the desired critical condition was removed to provide a greater excess reactivity. Changes in the hydraulic control drum motion system permitted much more rapid reactivity insertion rates. The lateral support system was also eliminated and the core was held together by bands.

Analysis of test results indicated a period of 0.6 milliseconds and a total fissions yield of 3.1×10^{20}.[29] The NERVEX program predicted a fission yield of 5.1×10^{20}

*The KIWI reactor is a predecessor of the NRX series of reactors.

fissions for the experiment;[35] RAC predicted a value of 10^{21} fissions.* In addition, data on overpressures indicated a kinetic energy release (i.e. the amount of heat energy transformed to mechanical energy) of 150 Mw sec. These data were then used to normalize the RAC code to make it more applicable for excursion predictions.

Subsequent to the test, radiochemical analyses were performed on fuel debris. It was found that the energy deposition in the test ranged from 4.5×10^{14} to 4.5×10^{15} fissions per gram U-235. This range in yields was due to fission peaking occurring in the center of the reactor and along the reflector. The lowest fission yields occurred at the reactor ends. It was found that fuel in these sections underwent 8.6×10^{14} fissions per gram U-235, and, moreover, that this fuel did not fragment. Fuel in the high fission yield section of the core underwent extreme fragmentation and vaporization.

6.5.3 Requirements for Nuclear Self-Destruct

On the basis of the above experimental programs, it appears the core fragmentation can be achieved if sufficient reactivity is added at a relatively rapid rate. The exact magnitude of reactivity required is still open to question. In order to help answer this question a parametric study was conducted to evaluate the total fission yield required as a function of both reactivity and reactivity insertion rate.[35] The study examined the 5000 Mw NERVA reactor and used the NERVEX computer program. The results are shown on Figure 6-31 where prompt excess reactivity inserted is plotted as a function of reciprocal insertion rate for constant fission yields. If one assumes on the basis of the aforementioned experimental results that 10^{15} fissions per gram are required for fragmentation, then, it follows that for the NERVA reactor a total fission yield of 1.21×10^{21} fissions will be required. Using the NERVEX results shown in Figure 6-31 and correcting for the fact that NERVEX predicts a fission yield of 5.1×10^{20} for KIWI-TNT whereas 3×10^{20} fissions were measured, it appears that an \$11 prompt or 1500 \$ per second ramp would be required for fragmentation. This value should be viewed only as an approximation and it will undoubtedly be modified when more refined data become available.

---

*Value was obtained from Figure 19 of Reference 29.

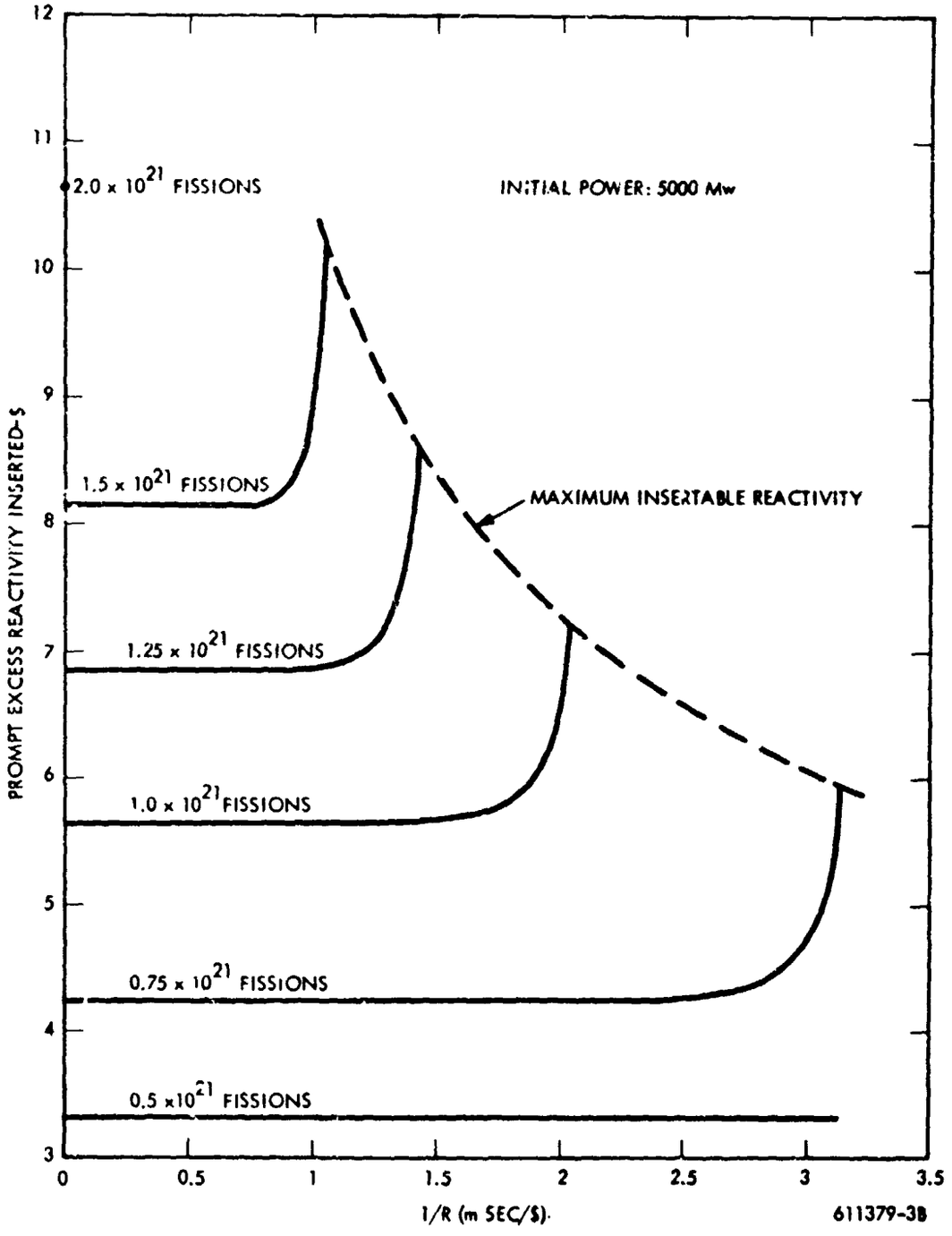

Figure 6-31. Total Prompt Excess Reactivity Inserted versus the Reciprocal of the Ramp Insertion Rate to Give the Number of Fissions Indicated

6.5.4 Techniques for Reactivity Insertion

In order that nuclear self-destruct may eventually become a practicable countermeasure system, it is necessary to devise some technique for achieving requisite reactivity insertion. A number of techniques for reactivity insertions have been examined analytically.[33] These include insertion of a projectile containing a moderating material such as U-235, H_2O, or polyethylene; maximization of reflector control, i.e., obtaining maximum reactivity insertions with either control drums or rods; and insertion of hydrogen or a hydrogenous material to the core. None of these techniques appears entirely infeasible; however, before they can be utilized, insertion requirements must be better defined and engineering problems associated in these methods must be solved.

6.6 REFERENCES

1. Nuclear Utility Services, Inc., A Preliminary Evaluation of the Environmental Safety Aspects of Nuclear Rocket Flight Operations, NUS-122, January 1963 (CRD)

2. Westinghouse Astronuclear Laboratory, Program Report on the Anti-Criticality Poison Wire System - Volume III - Part A, WANL-TNR-206, September 1965.

3. Call, D. W. and G. E. Parker, Selection of Material, Number and Distribution of Poison Wires for Anti-Criticality Poison Wire System, WANL-TME-603, November 1963 (CRD)

4. Trammell, M. R., Analysis of the Effects of Post-Operational Heat on a NERVA Reactor, WANL-TME-957, 1 October 1964 (CRD)

5. Cleary, J. D., W. C. McCune and M. R. Trammell, The Coupled NOFLOW-FIPDIF Computer Program, WANL-TME-1224, July 1965 (CRD).

6. Westinghouse Astronuclear Laboratory, ROVER Flight Safety Program - Preliminary Review - Volume II - Safety Analysis Report - Evaluation of Passive Re-Entry Approach, WANL-TNR-209, September 1965 (CRD).

7. Trammell M. R. and W. C. McCune, Evaluation of the Thermal Response of Three Proposed Reactor Designs to Post-Operational Heating Conditions, WANL-TME-1431, 1 June 1966 (CRD).

8. Westinghouse Electric Corporation, NERVA II Reactor Conceptual Design Report, WANL-TME-1315, October 1965 (CRD).

9. Grab L. H. and M. R. Trammell, Interim Report on the Re-Entry Behavior of the NERVA Reactor, WANL-TME-959, October 1964 (CRD).

10. Grob, L. H., and M. R. Trammell, Analysis of Re-Entry Behavior of a NERVA Vehicle, WANL-TME-1174, June 1965 (CRD).

11. Smith, S. O., Evaluation of NERVA-1 Passive Intact Re-Entry, General Electric Re-Entry Systems Department, Valley Forge Space Technology Center, DIN:5836-14-3, 18 August 1965.

12. Lockheed Missiles and Space Company, ROVER Flight Safety Program - Preliminary Review - Volume I - Evaluation of Destruct and Auxiliary Thrust Systems, LMSC-A778908, 30 March 1966 (CRD).

13. Lockheed Missiles and Space Company, Modular Nuclear Vehicle Study Mid-Term Presentation, LMSC-A829434, 15 September 1966.

14. NASA, Marshall Space Flight Center, Saturn 1B/S-VI Launch Vehicle for Voyager, Volume II, MTP-M-63-22, 20 October 1963.

15. Westinghouse Astronuclear Laboratory, NERVA Source Term Program, WANL-TME-178, September 1964 (CRD).

16. Picatinny Arsenal, ROVER Flight Safety Program - Preliminary Review - Volume III - Part B - Summary Report - Nuclear Rocket Countermeasures Post-Operational Destruct System, Picatinny Arsenal, Dover, N. J., December 1965.

17. Wackerle, J., A Feasibility Study of the Disposal of a ROVER Reactor with High Explosives, Los Alamos Scientific Laboratory, LAMS-2688, 3 July 1962 (CRD).

18. Los Alamos Scientific Laboratory, Particle Size Distribution from a One-Ninth- Scale ROVER Reactor Axial - HE Destruct, LA-3214-MS, 2 April 1965 (CRD).

19. Aberdeen Proving Ground, USATECOM, Feasibility Test of a Weapon Launched Destruct System for a Nuclear Rocket Engine, DPS-1060, September 1963 (CRD).

20. Dutschke, W., Engineer Design Test of NERVA Countermeasures (Full Scale), Aberdeen Proving Ground, Maryland, USATECOM Project No. 5-5-8410-02, Report No. DPS-1876, February 1966 (CRD).

21. U. S. Naval Radiological Defense Laboratory, The U. S. Naval Radiological Defense Laboratory (NRDL) Participation in the Collection of Debris from APG-III, The High Explosive Destruct of a Simulated NERVA Reactor at the Aberdeen Proving Grounds, Aberdeen, Maryland, on 22 June 1965, USNRDL-LR-116, San Francisco, California, 26 July 1965.

22. Berry, R. E., and J. P. Martin, ROVER/NERVA Destruct System Test Results, Aberdeen Proving Ground - 3 (Final Report), Sandin Laboratory, Albuquerque, N. Mexico, SC-RR-65-620, December 1965.

23. DeAgazio, A. W., Comparison of Nuclear and Explosive Destruct Concepts for Nuclear Engines, NUS Corporation, Washington, D. C., NUS-277, May 1966.

24. Westinghouse Astronuclear Laboratory, A Study of Land Areas Contaminated from a Sub-orbital Explosive Destruct of a NERVA Engine, WANL-TME-1448, 30 June 1966 (CRD).

25. Hargrove, H. G., The Effect of NERVA Engine Attitude on the Re-Entry of Destruct Debris, Westinghouse Astronuclear Laboratory, WANL-TME-1533, 17 October 1966 (CRD).

26. Personal Communication, L. G. Heppner, (Aberdeen Proving Ground) to H. G. Hargrove, (WANL) 1 March 1966.

27. Bridges, J. M., H. G. Hargrove and D. Hoecker, Summary Report on the Theoretical, Analytical and Experimental Studies Performed in the Investigation of the Re-Entry Burnup of NERVA Fuel, WANL-TNR-135, September 1963.

28. Brown, W. S., WANL Source Term Program Status Report, Volume II, WANL-TME-796, May 1964.

29. Los Alamos Scientific Laboratory, ROVER Flight Safety Program - Preliminary Review, Volume V - Safety Neutronics for ROVER Reactors, RFS-376 (LA-3358-MS), October 1965 (CRD).

30. Chezem, C. G. and W. R. Stratton, RAC, a Computer Program for Reactor Accident Calculations, Los Alamos Scientific Laboratory, LAMS-2920, 1963.

31. Call, D. W. and M. Roidt, NERVEX, A Two Dimensional Excursion Analysis Program, WANL-TME-1013, October 1964.

32. Chezem, C. G. and W. R. Stratton, NECKLACE - A Computer Program Concerning the Transient Temperatures of Fissioning Spheres Embedded in Graphite, LA-3115-MS, 1964.

33. Los Alamos Scientific Laboratory, Summary Report - Evaluation of the Self-Destruct Concept for Post-Operational ROVER Reactor Disposal - Volume III - Part C, RFS-425 (LA-3535-MS), April 1966.

34. Simmons, C. R., M. A. Vogel and A. Boltax, Transient Irradiation Experiments on NERVA Fuel Material, WANL-TNR-157, December 1963 (CRD).

35. Call, D. W., NERVA Nuclear Self-Destruct Safety Countermeasure, WANL-TME-1512, September 1966.

CHAPTER 7.0

RADIOLOGICAL CONSIDERATIONS IN NUCLEAR ROCKET FLIGHT SAFETY

Knowledge of the exact source term of the re-entering radioactive debris is necessary in order to evaluate the radiological safety problems of space nuclear propulsion systems. However to define the magnitude of these problems, it is necessary to know the extent and nature of the interaction of this debris with man and following such interaction, to estimate the manner and extent to which absorbed ionizing radiation would be distributed in man. A Radiological Effects Working Group was established within the ROVER Flight Safety Program for the purpose of developing radiological safety assessment methods and for acquiring data on the man-debris interactions associated with the use of nuclear propulsion systems. A comprehensive report presenting the analytical methods and experimental information obtained in the ROVER Radiological Effects Program up to April 1966 has been published by the United States Naval Radiological Defense Laboratory[1]. The information contained in that report, as part of the ROVER Flight Safety Preliminary Review documentation, has been used in the Safety Analysis Reports evaluating the use of passive re-entry[2] and evaluating destruct and auxiliary thrust system[3] countermeasures for NERVA powered space vehicles. Information abstracted from Reference 1 is presented in the following paragraphs. Equations and mathematical models defining the physical and radiological interactions of debris with humans, as derived in Reference 1, will not be repeated here. The major purpose of this section is to describe the factors considered, the assumptions made, and the limitations incurred in developing the means to assess the radiological safety aspects of nuclear rocket propulsion.

7.1 DEFINITION OF RADIOACTIVE DEBRIS

The characteristics of the re-entry debris depend on the re-entry mode under consideration. In the mission safety studies[2, 3], two basic re-entry modes have been considered: passive re-entry of an initially intact reactor and re-entry of debris resulting from the explosive destruct action of the reactor. Because the nature of debris is a factor in determining the applicability of the debris-man interaction models, the important characteristics of the debris for each re-entry mode are summarized below.

BLANK PAGE

7.1.1 Passive Re-Entry Debris

The disassembly and dispersal of the NERVA reactor under passive re-entry conditions have been described in Reference 2 and summarized in Section 6.2. It was shown that fuel elements will be ejected at some time following mission abort. The elements were assumed to be released as integral elements although breakage upon ejection is certainly not precluded. During re-entry and upon earth impact, the fuel elements may be further degraded, but the most probable fragment size has not been determined. The safety analysis of Reference 2 assumed that the fuel debris remained in the form of integral fuel elements. When information on passive re-entry fragment size becomes available, debris interaction models and dose exposure models can easily be modified to use the information.

Distribution and location of the debris on the earth's surface will depend on the flight mission and time of failure. For failures following orbit start-up, the earth area coverage is widely dispersed and impaction of debris will be in a random manner. For the launch azimuth restrictions in use at Cape Kennedy, impact location will lie in a band around the earth between 40°N latitude and 40°S latitude. For failures from sub-orbit start the debris impact location is predictable and will cover small areas, probably on the order of several square kilometers[2]. The radioactivity of the fuel and structural material debris will depend on the operational and post-operational history and was described in Chapters 3.0 and 4.0.

7.1.2 Destruct Re-Entry Debris

The APG-3 explosive destruct test[4, 5] of a simulated NERVA-NRX reactor has produced the best available information on the particle size distribution expected from explosive destruct. A summary of the APG-3 results was presented in Section 6.4. Particle sizes varied from 3 microns up to approximately 27 mm. To facilitate the handling of the particle size information in the physical interaction and radiological dose models, particle sizes have been categorized into twelve size ranges according to their diameter as shown in Table 7-1[1], and these size groups have been used by LMSC in their destruct analyses[3]. WANL has reduced the APG-3 data to eight size groups in their destruct analyses[6], neglecting particles smaller than 105 microns on the basis that particles below this size contained only 2.1 percent

of the total core uranium. The assumption is made that all particles in a given size range behave physically and biologically in essentially the same fashion as the geometric mean for that group.

Distribution and location of the debris on the earth's surface, as with the passive case, depends on the mission model and failure times. For destruct from orbit, a significant portion of the debris will have random impact location within the 40°N-40°S latitude band. For failure following sub-orbit start-up, typical destruct debris footprints have been described for the NRX[3] and NERVA[6] reactors. A further consideration of small sized fuel debris is the rate at which contained fission products may be eluted or dissolved in water or body fluids. Solubility tests performed at USNRDL[1] have shown that NERVA type fuel beads which have an intact pyrocarbon coating do not lose measurable activity when leached in water and simulated gastric juices. Measurement of fission product loss from uncoated and broken coated beads is in progress at USNRDL[1].

TABLE 7-1

DEBRIS SIZE CLASSES

Class	Size Range Diameter (Microns)	Log Mean Diameter (Microns)
12	0 - 10	3.16
11	10 - 20	14.11
10	20 - 50	31.62
9	50 - 100	70.71
8	100 - 200	141.10
7	200 - 500	316.20
6	500 - 1000	707.10
5	1000 - 2000	1,411.00
4	2000 - 5000	3,162.00
3	5000 - 10,000	7,071.00
2	10,000 - 20,000	14,110.00
1	20,000 - 50,000	31,620,00

7.2 DEBRIS EXPOSURE MODELS

The estimation of the biological interactions which may result from nuclear rocket engine failures is complicated by the random nature of the deposition of the debris in the biosphere. The exposure conditions for each possible receptor cannot be precisely predicted. A range of conditions exists which depends upon the impact location, abundance and size of debris, and the population density. Thus, the mathematical description of a dose to a receptor must include a factor which defines the probability that the receptor and the debris will interact in a certain manner. The assumptions of "worst case" exposures, where the receptor is at a fixed distance from the source for an exactly defined time with specified shielding conditions, is not representative of the exposure history of the great majority of the population that could be potentially affected by these sources. Thus probability functions and probability models have been developed to describe the interactions between the debris and the receptor. This probability combined with the radiological dose model for given exposure conditions then provides results describing the distribution of dose over the affected population group.

Several exposure routes exist by which humans may be subjected to ionizing radiation from the re-entered debris[1]. The following three primary exposure situations are summarized here: external whole body exposure to gamma radiation, external body (skin) exposure, and internal body exposure due to ingestion or inhalation of radioactive debris.

7.2.1 External Gamma Whole Body Exposures

An external whole body exposure model has been developed and is based on the premise that the receptors do not always remain stationary, but are free to move about in some manner. The details of one such model, MOREDO (Mobile Receptor Dose) have been described[1,7] and have been programmed for digital computer solution[8]. In the MOREDO model, the extent of a given individual's movements is assumed to be strongly dependent upon his age, occupation, and diurnal habits. It is assumed that each individual's movements can be described by a Gaussian frequency distribution of separation from an associated center of motion, the standard deviation of which describes the extent of movement. The associated population dose exposure is dependent on the juxtaposition of centers of motion (people) and radioactive particles. These are obtained by assuming that both the particle

and population distribution are described by the Poisson distribution law. The program utilizes two options depending on the radioactive particle density:

1. The particles are sufficiently dispersed on the Earth's surface that any given person is under the influence of only a single particle at least 95 percent of the time.
2. When the first option does not hold, the particles are described as an infinite plane source, and the dosage to the population on this plane is considered.

The MOREDO program is a complete radiological dose model, in that it not only considers exposure probabilities, but also calculates (from source term input data) the gamma dose distribution within the total population group, as well as the total population gamma dose. The MOREDO program was utilized in evaluation of the safety considerations of the passive re-entry of NERVA reactors[2].

A modified mobile receptor dose model has been developed by LMSC[3] since the MOREDO program is not compatible with LMSC's Nuclear Flight Executive Program used for mission safety analyses. The Lockheed model uses exposure probability assumptions similar to those in MOREDO and is also a complete radiological dose model, in that population doses are calculated.

A non-mobile receptor model has been used by LMSC in which the population interaction with a debris particle is based on a static immobile population as well as a source which remains stationary after impact. This concept has been used to develop the "exclusion area" model. This exclusion area is defined as that circular area around the given impact particle within which the gamma dose received by a person will equal or exceed a specified value in a given exposure period. Since a dose gradient exists relative to the exposure distance to the particle, the dose associated with an exclusion area applies specifically at the periphery of the circle. Those persons within the circular area will receive a dose greater than the specified numbers. The number of persons exposed depends on the population density at the impact point of the debris. The model has been programmed and is called the Lockheed Exclusion Area Code (LEAC)[9, 10]. The specified dose values and exposure period required to calculate the exclusion area are optionally selected input data.

7.2.2 Epidermal Contact

To define the interaction between the individuals and nuclear rocket debris via direct skin contact requires consideration of three factors: (1) the probability of direct contact and retention of the particles with the skin; (2) the probable exposure period during which the particle remains on the skin; and (3) the cultural habits of the persons with respect to such items as the fraction of time spent indoors, nature and extent of clothing, bathing frequency, and physical activity.

Equations for the probability of contact of particles with the skin have been derived[1]. The model relates the number of particles interacting with an individual to the number of particles deposited per unit ground area. The model considers the area of ground shielded by a standing man, and includes the effects of local winds at ground level. To calculate the mean number of particles striking and sticking to an individual, "impaction" and "sticking" efficiency factors are applied. Impaction efficiency corrects for those particles which travel around the body with the air flow rather than intercepting the body. The sticking efficiency allows for those particles that strike the body but bounce off.

The probable exposure period during which a particle remains on the skin indicates that the surface condition of the skin (mainly perspiration and oiliness) and physical activity of the individual are the most important parameters. From experimental work at ORNL an empirical relationship has been developed between average retention time and particle size[11]. For particles in the 40 to 1000 micron range, average retention time varies from about two hours for 1000μ particles up to about 10 hours for 40μ particles. Equations have then been developed to calculate the probability that N particles will strike and reside on an individual for at least some time t.

Further refinements to the probability models have included consideration of the cultural factors of the degree of clothing worn by individuals and the fraction of time spent outdoors. Four clothing patterns for potentially affected geographic areas have been identified[12] and estimates of the bare body surface exposed for each category have been calculated. These factors plus a term for the fractional time spent outdoors, then, have been included in the final equations for calculating skin contact probabilities. Because of the

complexity of these relationships, the equations are not reprinted here, but may be found in Reference 1, pages IV-13 to IV-21.

7.2.3 Internal Body Exposures

Two direct routes of exposure of internal body organs to radioactive particulate debris have been examined in detail: lung exposure and ingestion exposure. Indirect exposure by solubilized isotopes which enter man via the water or food chain have been investigated. However, it seems that the maximum organ doses probable by this means will not create a potential biological problem, with the possible exception of radioiodine[1]. Even for this case, to receive a significant thyroid dose a particle must be large (1000μ) and must be ingested within a short time compared to the radioiodine half life, and furthermore, the iodine must be completely dissolved from the particle during the time of passage through the gastrointestinal tract. Thus, the major effort has been limited to developing models for the direct exposure of the lung and the gastrointestinal tract.

7.2.3.1 Lung Exposures

Extensive mathematical models are developed in Reference 1 (pages IV-23 to IV-34) in order to estimate the probability of inhalation of particle and to determine the fraction of particles inhaled that actually reach the lungs. The following list summarizes those factors considered in arriving at a lung exposure model. Consult Reference 1 for details.

1. Direct inhalation of air suspended particles. This is limited to particles in the range of 0 to 10μ. Larger particles will not remain suspended in the atmosphere for significant times because of their higher settling velocity.
2. Impaction inhalation in which wind-driven particles up to 1 mm diameter can impact on the breathing zone. The model considers different impaction efficiencies for the nasal and mouth areas and also considers the fractions of inspired volume occurring by both nose and mouth. Nasal passages are considered to reject fragments greater than 100μ, and the mouth is assumed to trap all fragments larger than 1 mm.

3. The total inhalation exposure is partitioned to calculate the mean number of particles inhaled via the nose and mouth.
4. Only a fraction of the inhaled particles reach the lung. Particles deposited in the nasal passages and upper respiratory will be swallowed (ingestion exposure) rather than gaining access to the deep lung. Analytical relationships have been derived giving the retention in the lungs as a function of size for both nose and mouth entry. For mouth-breathed particles, the maximum particle size retained in the lung (assuming graphitic fuel particle of $\rho = 2.2$ gm/cm^3) is 15 microns. For nose-breathed graphitic particles, the maximum size retained in the lung is about 7 microns.
5. For those particles reaching the lung, a biological half life of 120 days is used as recommended by the ICRP[13] for insoluble materials.

7.2.3.2 Ingestion Exposures

Ingestion can occur by swallowing those particles trapped in the upper respiratory tract or by eating foods containing particles. The probability for ingesting a particle via the inhalation route is evaluated using the model determined for lung exposure, assuming the particles not reaching the lung are swallowed. A model for estimating the direct ingestion of particles retained on vegetable crops has been proposed[7] and considers such factors as retention efficiency of particles on the plants, crop areas required to feed one person, and a reduction factor for processing of the food (washing, peeling, etc.) prior to eating. The probability of a given sized particle reaching the gastrointestinal tract is calculated assuming the particle deposition density varies according to the Poisson distribution.

The average transit time of a particle through the gastrointestinal tract is taken as 31 hours as stipulated by the ICRP[13]. Experimental studies performed by the Argonne Cancer Research Hospital using insoluble ceramic spheres (30-40μ) yielded an average retention time of 30 hours[14]. LASL[15] experimental studies yielded a mean transit time of 34.5 hours.

7.3 RADIOLOGICAL DOSE MODELS

This section summarizes the various radiological dose models used to calculate either the gamma ray exposure or the beta and gamma dose from contact with a debris

particle. These dose functions when combined with the interaction probability models discussed in Section 7.2, provide a means for evaluating the dose received by the population for varying debris deposition patterns.

7.3.1 Beta and Gamma Energy Absorption in Tissue

The models that have been developed within the ROVER programs to calculate the beta and gamma energy deposition in tissue are summarized below. The geometric considerations for calculation of absorbed dose by the whole body or specific body organs is described in Sections 7.3.2 to 7.3.5 inclusive.

7.3.1.1 Beta Dose Calculational Models

Two models have been developed to calculate the beta dose rate from a debris particle[1]. One uses a modified point source function based on the work of Loevinger[16]. The second model, known as the Combined Berger Spencer (CBS)[17] model, considers both the degradation of the electron spectrum by the particle and finite absorber geometries. The use of the present CBS model is confined to single UC_2 fragments, although extensions to consider larger NERVA fuel fragments containing several UC_2 beads is in progress at USNRDL.

The CBS beta dose model treats the beta dose problem in three parts. The first part calculates the degraded beta particle spectrum at the surface of the particle. This is accomplished with the aid of three separate computer programs, each with its own separate function as follows:

1. Beta Spectrum Program[18] - computes the beta spectrum for each beta emitting nuclide.
2. Composite Beta Spectrum Program[19] - produces a point source spectrum for a specified mixture of fission products by summing the individual spectra with appropriate weighting for the activity of each contributing fission product nuclide. The contribution of each fission product nuclide to the mixture is determined from one of the fission product inventory abundance programs (cf. Section 3.1.1).
3. Beta Spectrum Degradation Program[20] - calculates the emergent degraded beta spectra, arising from beta particle energy degradation within the UC_2

particle due to scattering and absorption processes. This program uses analytical functions to approximate the Monte Carlo computation required for determination of the emergent spectra.

The second part of the CBS model calculates the energy dissipation by fast electrons according to the method of Spencer[21, 22]. The data of Spencer has been graphed, and a computer program performs linear interpolation to define an energy dissipation function. The third part of the CBS model applies the energy dissipation data to the emergent spectrum. The dose rate as c function of radial distance in tissue is summed over 24 energy intervals. This depth dose rate data is then integrated over a distance equal to the range of the beta particles to find the total beta energy emitted by the UC_2 particle, the average dose to a spherical volume, or the average dose delivered to a thin disk at any selected depth of tissue. An example of the CBS model output data has been plotted and is shown in Figure 7-1.

7.3.1.2 Gamma Dose Calculational Models

The gamma dose from an ingested particle is derived from multiple scattering calculations using a Monte Carlo method to calculate absorbed fractions. These absorbed fractions are the ratio of energy absorbed in a tissue volume to the total energy emitted, and have been calculated and tabulated for various anatomical models, source distributions, and gamma ray energies[23, 24]. The average absorbed dose is calculated by weighting the gamma spectra divided into seven energy groups and calculated by the fission product abundance programs, (cf. 3.1.1) to the approximate absorbed fraction values.

For external whole body gamma exposures, the decay energy is divided into seven energy groups. Separate dose conversion coefficients are calculated for the average gamma energy within each group and are used to convert gamma ray flux to absorbed dose rate (MEV/sec-cm^2 to rad/hr). Total dose is then obtained by summing over each energy group and integrating the dose rate over time.

7.3.2 External Whole Body Gamma Dose

The assumption is made that the effective height of the receptor is one meter above the debris particle deposition plane. Thus, the distance, d, from a particle point source to the effective height of the receptor is: $d^2 = 1 + r^2$, where r is the distance from the source

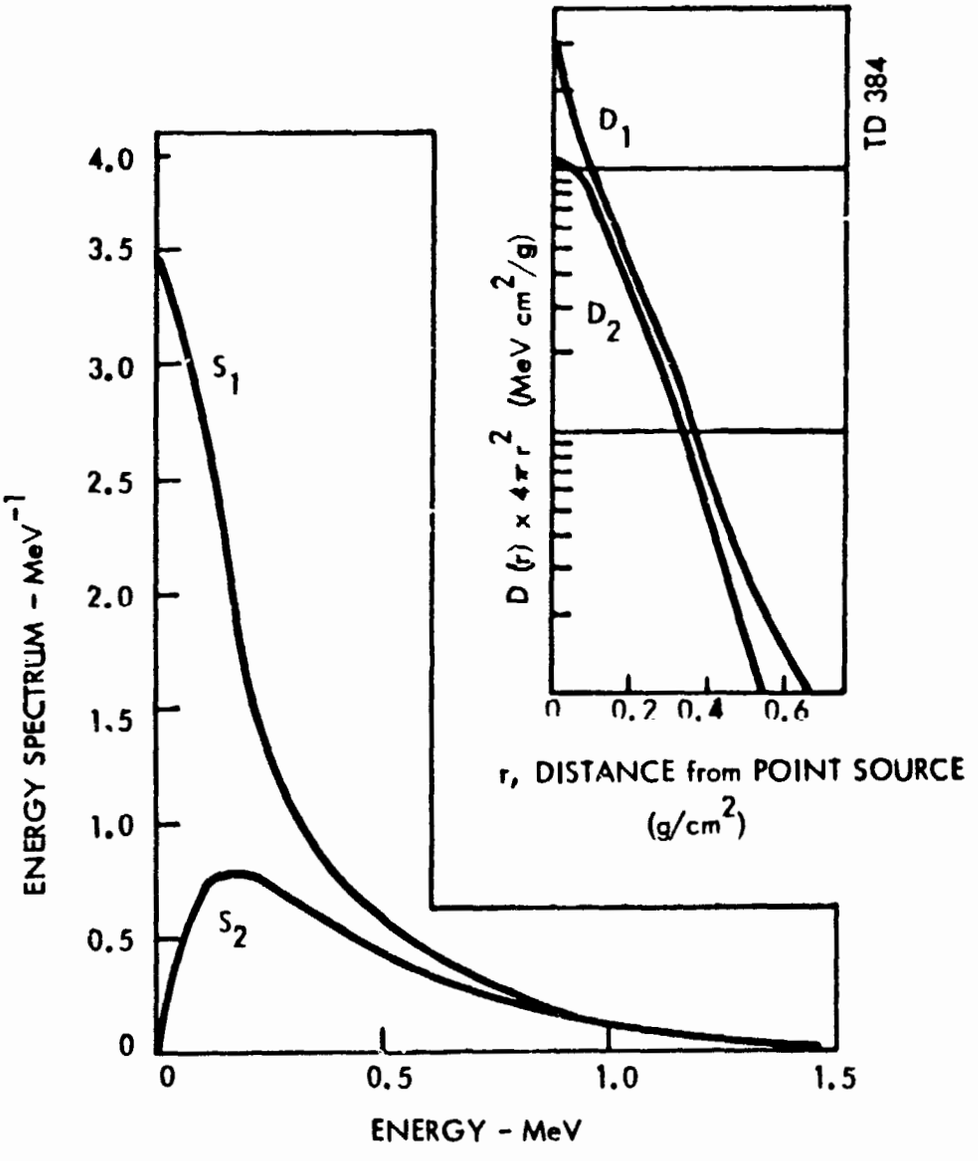

Figure 7-1. CBS Calculations of Beta Spectra and Dose Distributions

(S_1 is a fission product beta spectrum 10^6 seconds after fission normalized to 1 emitted electron. S_2 is the corresponding degraded spectrum from a UC_2 fragment (60μ radius). D_1 and D_2 are dose distributions in tissue, with the inverse square attenuation removed, as a function of distance r from a point source, for source spectra S_1 and S_2.)

at the base (at the feet) of the receptor. The gamma ray flux at a distance from a single particle is assumed to be attenuated in accordance with the inverse square law. Corrections for air absorption of gamma rays and gamma ray scattering (build up factor) are applied in the models.

The above factors are included in the LEAC, MOREDO and Lockheed mobile receptor dose models. The MOREDO program also includes a calculational model for exposure to multiple particles using a uniformly contaminated plane source dose model. However, the MOREDO program has a serious deficiency, in that it cannot account for the exposures to that segment of the population located in the area contiguous to the plane source. Such a situation arises in the case of passive re-entry following failure from sub-orbital start-up[2] in which the fuel debris is dispersed over a relatively small area of several square kilometers. In this case an approximate estimate of the additional population exposed outside of the plane source was made by calculating the number of persons located in isodose regions surrounding the finite plane source.

A comparison of the results obtained using the mobile receptor dose models and the stationary receptor model has been given in References 1 and 3. When the separation distance between the receptor and source(s) is small in comparison with the degree of movement of the receptor about his center of motion (σ value), the mobile receptor model gives significantly less dose than the stationary model. This is the region of most interest to safety analyses, since the larger doses arise from close proximity to the source. Conversely as the source receptor distance increases and becomes large in comparison with the standard deviation of motion, the results of the stationary and mobile models are about comparable. There is also a region, where the ratio s/σ is in the range of 1.0 to 2.0, in which the mobile dose model can yield a gamma dose greater than that calculated by the stationary model.

7.3.3 External Beta Skin Dose

Beta dose to the skin is calculated by integrating with respect to time the beta dose rate (Section 7.3.1.1) to a disk of skin. The disk area of the skin is taken as 1.0 cm^2, and the radiation sensitive layer of the skin is assumed to be 100 microns in depth. The biological effects of skin irradiation will vary with the area exposed, but the critical area,

if any, cannot be defined at this time. This model for calculation of beta dose per particle, coupled with the relationships defining probability of exposure of individuals to debris particles (Section 7.2.2), is used to determine the expected number of people receiving a dose equal to or less than a specified value.

7.3.4 Lung Dose

The total beta energy emitted from particles in the lung is assumed to be absorbed by the entire lung. Therefore the average dose is the total emitted beta energy divided by the ICRP lung mass (1000g) for a 70Kg man. Since particles retained in the lung are no greater than 10μ, corrections for particle self-absorption can be neglected, and the time integrated beta energy emission rate from a point source is applicable. Exposure period is calculated using a 120-day biological half life as recommended by ICRP.

Gamma dose to the lung is calculated by the method of absorbed fractions, assuming uniform distribution of the particles in the lung. A data table of absorbed fractions applicable to the lung is published in Reference 1, page VI-11.

Because of the small particle size retained by the lung, actual dose per particle to the lung is quite small. Using a nominal 10-minute run for an NRX reactor, and assuming minimum particle fall times, the lung dose per particle from a 14-micron graphite fuel particle and a 3-micron UC_2 particle was calculated as 8.5×10^{-7} rad and 2.5×10^{-5} rad, respectively[1].

7.3.5 Gastrointestinal Dose

The beta dose at a depth of 300 microns beyond the gut wall is calculated for an infinite medium using the CBS dose model. The 300-micron depth is chosen on the basis that the dividing crypt cells in the walls of the intestines are located at this distance. The beta dose to the lower large intestine is calculated using an average transit time of 18 hours; a 13-hour transit time is used for the passage of the particle through the upper intestine.

The gamma dose to the gastrointestinal tract is averaged over the entire gastrointestinal tract, assuming an ICRP 2000-gram mass for a 70-kilogram man. The method of absorbed fractions is used to determine the average energy absorbed (data table published in Reference 1). The entire transit time of 31 hours is used in determining the gamma dose.

Sensitivity analyses made by USNRDL[1] have shown that the direct ingestion route is more significant than the inhalation route for exposure of the gastrointestinal tract to radioactive particles. Direct ingestion from vegetable crops shows a large possible variation in the expected number of particles that could be ingested. However, a delay between deposition on the crops and time of ingestion would be expected, thereby reducing any potential hazard.

7.4 RADIATION EXPOSURE CRITERIA

Radiation protection standards have been established by the following major organizations: Internation Commission of Radiological Protection (ICRP), National Council on Radiation Protection and Measurements (NCRP) - USA, British Medical Research Council (BMRC), Federal Radiation Council (FRC) - USA, and the Atomic Energy Commission (AEC) - USA. Standards of the first three organizations listed are in the form of recommendations; those of the latter two have legal status.

The peacetime radiation protection standards can be divided into two general types: normal and emergency conditions. Although any radiological effects resulting from nuclear propulsion applications would be the result of an accident situation, the doses may not exceed normal population radiation exposure criteria for all but a very small percentage of the exposed population. Unfortunately, the established standards do not deal precisely with the interactions considered in the ROVER program. For example, irradiation of highly localized areas or volumes of tissue rather than entire organs is not covered by established criteria.

For normal peacetime operations, the FRC has published radiation protection guides for two classifications of persons: radiation workers and the general population. These guides are the same as promulgated by the AEC for their licenses and contractors. Tables listing these standards are not included in this report, but are available in the FRC staff reports[25, 26] and also in Reference 1, pages VII-4 to VII-5. Recommendations for the general population exposure limits in a peacetime emergency condition have been made by the FRC and BMRC. The FRC recommendations pertain to the contamination of human food products due to an acute

localized release of radioactivity. The standards are thus applicable to internal doses resulting from dietary intake of specific radionuclides (I^{131}, Sr^{90}, Cs^{137}). The FRC has not yet established equivalent standards for inhalation or direct irradiation. The BMRC has published emergency limits for both external[27] and internal[28, 29] exposures from accidents to members of the general population (also published in Reference 8, pages VII-8 and VII-9). However, these BMRC recommendations make no mention of the gastrointestinal tract doses which would result from ingestion or inhalation at the recommended limits. Thus, while the existing radiation exposure criteria do nor directly apply to nuclear rocket flight rations, some guidance is available for all but the gastrointestinal tract. It is concluded that further studies on this exposure route should be continued. In addition, radiation exposure criteria specifically applicable to the nuclear rocket program should be developed to aid in mission evaluation.

7.5 REFERENCES

1. U. S. Naval Radiological Defense Laboratory, (USNRDL), ROVER Flight Safety Program Preliminary Review, Vol. IV, Radiological Considerations in Nuclear Flight Safety, San Francisco, California, April 20, 1966 (U).

2. Westinghouse Astronuclear Laboratory, ROVER Flight Safety Program Preliminary Review, Vol. II - Safety Analysis Report - Evaluation of Passive Re-entry Approach, WANL-TNR-209, September 1965 (CRD).

3. Lockheed Missiles and Space Company, ROVER Flight Safety Program Preliminary Review, Vol. I - Safety Analysis Report - Evaluation of Destruct and Auxiliary Thrust Systems LMSC-A778908, March 30, 1966 (CRD).

4. Dutschke, W. Engineer Design Test of NERVA Countermeasures (Full Scale), Aberdeer Proving Ground, Maryland, USATECOM Project No. 5-5-8410-02, Report No. DPS-1876, February 1966.

5. Picatinny Arsenal, ROVER Flight Safety Program Preliminary Review, Vol. III-B - Post-Operational Destruct System, Technical Memorandum 1746, December 1965 (CRD).

6. Westinghouse Astronuclear Laboratory, A Study of Land Areas Contaminated fro a Sub-orbital Explosive Destruct of a NERVA Engine, WANL-TME-1448, June 30, 1966 (CRD).

7. DeAgazio, A. W., Dose Calculation Models for Re-entering Nuclear Rocket Debris, NUS-229, Revised, NUS Corporation, October, 1965.

8. Kim, Y.S., MOREDO - NUS Mobile Receptor Dose Programs, NUS Corporation, NUS-257, October 12, 1965 (U).

9. Lockheed Missiles and Space Company, Nuclear Vehicle Flight Safety Study, Phase III Report - Nuclear Flight Executive Program, LMSC A304973, Sunnyvale, California, January 31, 1964. (U).

10. Lockheed Missiles and Space Company, Nuclear Flight Executive Program Operating Manual, LMSC-A824882, July 15, 1966 (U).

11. Fish, B. R., et al., Environmental Studies: Radiological Significance of Nuclear Rocket Debris, Progress Report July 1 - December 31, 1964, ORNL-TM-1053, April 1965 (CRD).

12. Garcia, L. F., J.C. Keister, and J.F. Sitton, Demographic and Cultural Factors for Countries Between 40° North and 40° South, NUS-230, NUS Corporation, Washington, D. C., May 1965 (S).

13. Report of Committee II on Permissible Dose for Internal Radiation (1959), Pergamon Press ICRP Publication 2, 1959.

14. LeRoy, G. V., J. H. Rust and R. J. Hasterlik, The Consequences of Ingestion by Man of Real and Simulated Fallout, ACRH-102, Argonne Cancer Research Hospital.

15. Some Biological Aspects of Radioactive Microspheres, Bio-Medical Research Group, LA-3365-MS, Los Alamos Scientific Laboratory, August 1965.

16. Hine, G. J. and G. L. Brownell, Radiation Dosimetry, Academic Press, Inc. New York, 1956.

17. Ellett, W., M. Berger and O. Hogan, Dose Models for Evaluating the Radiation Hazard from Reactor Debris, Transactions of the American Nuclear Society, Vol. 8, No. 2, 1965.

18. Hogan, O. L., P. E. Zigman and J. L. Mackin, Beta Spectra II. Spectra of Individual Negatron Emitters, USNRDL-TR-802, United States Naval Radiological Defense Laboratory, December 1964 (U).

19. Hogan, O.L. and M. A. Hagan, Beta Spectra I. FORTRAN Program for Composite Spectra, USNRDL-TR-1033, U.S. Naval Radiological Defense Laboratory, March 28, 1966 (U).

20. Hogan, O.L., Beta Spectra IV. Fission Product Beta Spectrum Degradation by Uranium Carbide Particles, U.S. Naval Radiological Defense Laboratory, (In preparation).

21. Spencer, L. V., Theory of Electron Penetration, Phys. Rev. Vol. 98 p. 1597, 1955.

22. Spencer, L. V., Energy Dissipation by Fast Electrons, NBS Monogram No. 1, U. S. Dept. of Commerce, 1959.

23. Ellett, W., A. Calluhan and G. Brownell, Gamma Ray Dosimetry of Internal Emitters - Part I, Brit. Journal of Radiology, Volume 37, No. 433, p. 45, 1964.

24. Ibid, Part II, Volume 38, No. 451, p. 541, 1965.

25. Federal Radiation Council Staff Report No. 1, Background Material for the Development of Radiation Protection Standards, Supt. of Doc., GPO, May 1960.

26. Federal Radiation Council Staff Report No. 2, Background Material for the Development of Radiation Protection Standards, Supt. of Doc., GPO, September 1961.

27. British Medial Research Council, The Hazards to Man of Nuclear and Allied Radiations, Report Cmnd. 1225, Her Majesty's Stationery Office, London, December 1960.

28. Report to the Medical Research Council by its Committee on Protection Against Ionizing Radiations, Maximum Permissible Dietary Contamination after the Accidental Release of Radioactive Material from a Nuclear Reactor, Brit. Med. Jour., I, 967-969, 1959.

29. Report to the Medical Research Council by its Committee on Protection Against Ionizing Radiations, Maximum Permissible Contamination of Respirable Air after an Accidental Release of Radioiodine, Radiostrontium, and Cesium - 137, Brit. Med. Jour. 3, 576-579, 1961.

CHAPTER 8.0

SAFETY ANALYSIS OF SELECTED NERVA FLIGHT MISSIONS

For the analysis of the safety of nuclear rocket flight operations for any defined mission, it is necessary to obtain basic information on the following:

1. The kind and number of accidents that can be postulated,
2. An estimate of the accident consequences, and
3. The probability that an accident can occur.

The previous chapters of this report have summarized the available information in these three areas as applicable to potential NERVA flight operations. From an evaluation of this information an estimate of the safeness of the mission may be derived. This section summarizes the results of safety analyses that have been made in the ROVER Program for three reference nuclear vehicle flight missions. The relative saf- he missions and the effectiveness of the safety counterm ntitatively expressed in terms of the radiation dose received

8.1 MEASUREMENT OF SAFET'

In order to judge the safety of a nuclear rocket flight, a nuclear reactor, a nuclear engine, or in fact any device or operation, it is necessary to define some yardstick which quantitatively describes the "safeness" of the given device or operation. The term "Safety Index" has been used to define a parameter which can in some manner express the safeness of an operation.

Safety indices presently in use in the analyses of nuclear reactor safety and of missile range safety are generally indicative of the type of safety analysis performed. Safety analyses of land-based reactors have stressed the consequences of a reactor accident; thus the safety index examined frequently is the size of the "maximum credible accident". On the other hand, chemical rocket propulsion and range safety has emphasized accident

probability calculations, based on reliability data obtained from extensive test programs and from actual flight experience.

A number of safety indices for application to nuclear rockets have been proposed[1]. The most recent mission analyses for application of the NERVA engine (Section 8.2) have used two major safety indices as follows:

1. Maximum Population Exposure from Worst-Case Accident. The worst-case accident is defined as a failure at some instant in the flight trajectory which will result in the maximum fission product inventory impacting on land surfaces of the earth. The resulting radiation dose levels to the population are then calculated using appropriate population interaction models and radiological dose exposure models (cf. Chapter 7.0). This safety index is analogous to the maximum credible accident case for land based reactors, in that the accident (loss-of-coolant for the missions analyzed to date) is considered credible, but the probability of failure is neglected.

2. Expected Number of Persons Exposed to a Specified Dose Level for a Given Mission. Whereas, the above safety index is calculated on the assumption that the failure did in fact occur (at the worst point in flight time) this index considers the probability of failure during the entire flight time of the mission. This safety index is based on the nuclear stage and engine reliability estimates, and utilizes the failure probability function for the specific mission (cf. Section 5.2). The expected number of persons that would be exposed to a given dose (or dose range) as a result of the mission flight is equal to the integral of the product of the probability of failure per unit time and the expected number of people exposed for that failure time, integrated over the entire time interval of nuclear engine operation. Details on the derivation and application of this safety index are described in Reference 2.

Some additional safety indices have been used by LMSC in the safety analyses of explosive destruct and auxiliary thrust system countermeasures[2]. Their numerical values were calculated in the process of obtaining the two major indices described above.

Although these lesser indices provide a somewhat more detailed breakdown of the safety analysis results, the two major indices have been selected to represent parameters that summarize the relative safeness of selected flight missions[3].

8.2 MISSION DESCRIPTION

Work has been performed in the ROVER Flight Safety Program to evaluate the effectiveness of countermeasure techniques that might be employed to reduce the radiological consequences resulting from an in-flight failure of a nuclear powered rocket[2, 4]. The effectiveness of the countermeasure concepts has been determined for three hypothetical rocket vehicle flight missions employing a third-stage powered by a NERVA-type engine. Two of the missions employ a NERVA-I (NRX size, 1120 MW) engine. The third mission employs a nuclear stage powered by a NERVA (5000 MW) engine.

A brief description of each mission is presented below. A complete description of the flight vehicle, engine characteristics, and the mission model trajectory and performance data is presented in Reference 2. The numerical results of the safety indices which define the relative safeness of each mission and the effectiveness of the countermeasures are presented in Section 8.3.

8.2.1 Mission Model I - Orbital Startup of NERVA-I

Model I is defined as a 70-hour lunar-transfer mission involving orbital startup of a NERVA-I (1120 MW) powered nuclear stage at 100 nm without rendezvous. The ascent trajectory to 100 nm employs an MLV-Saturn V-I booster. After the boost phase which lasts 588 seconds, the nuclear stage is injected into a 100 nm orbit. After parking-orbit injection, the second stage (MS-II) of the booster is separated and decelerated to de-orbit velocity. The nuclear stage and payload coast in a parking orbit to allow time for checkout and to satisfy launch-window constraints. The nuclear stage is started and operated until injection energy for a 70-hour lunar transfer is achieved. The nuclear stage is then jettisoned, having delivered a payload of 144,000 pounds to injection. The NERVA engine operates for 1449.6

seconds in this mission. The trajectory simulation for this mission utilized instantaneous staging of the three vehicle stages. The nominal 90-minute parking orbit was omitted since it is of little interest to the analysis. A summary of the nuclear stage trajectory data as a function of time after launch is shown graphically in Figure 8-1.

8.2.2 Mission Model II - Sub-orbital Startup of NERVA-1

Model II is defined as a 70-hour lunar-transfer mission utilizing sub-orbital start of a NERVA-1 (1120 MW) powered nuclear stage. A MLV-Saturn V-1 delivers the nuclear stage and payload to an altitude of 91.5 nm. The booster operation lasts 586 seconds. At this point, the nuclear stage is started and operates for 581 seconds to a nominal altitude of 100 nm. Because of the shutdown transient thrust, the nuclear stage and payload enter an eccentric orbit having an apogee of 289 nm and a perigee of 100 nm. After orbit injection, the NERVA is pulse-cooled until the point of required restart. When launch-window constraints have been satisfied, the nuclear stage is restarted and operates for a time period of 1560 seconds until the injection energy for a 70-hour lunar transfer is achieved. This mission delivers a payload of 157,000 pounds to injection. The trajectory simulation included a propellant allowance allocated for after-cooling during park-orbit coast; however, the thrust pulses were not included, since shutdown causes the major perturbation on park-orbit eccentricity and the effect of after-cooling is relatively minor. The nuclear stage trajectory characteristics are shown in Figure 8-2.

8.2.3 Mission Model III-Utilizing NERVA Engine

Mission Model III, a Mars fly-by mission, requires three launches and involves the Earth orbit rendezvous (EOR) and assembly of an orbit launch vehicle (OLV) in space. The initial launch of the MLV Saturn V-1 and kick stage places a partially fueled nuclear propulsion module into a high earth orbit of 262 nm. After checkout of the nuclear stage in high orbit, a second launch vehicle and kick stage delivers the orbital tanker which provides the rest of the propellant for the nuclear stage. The third launch vehicle, a

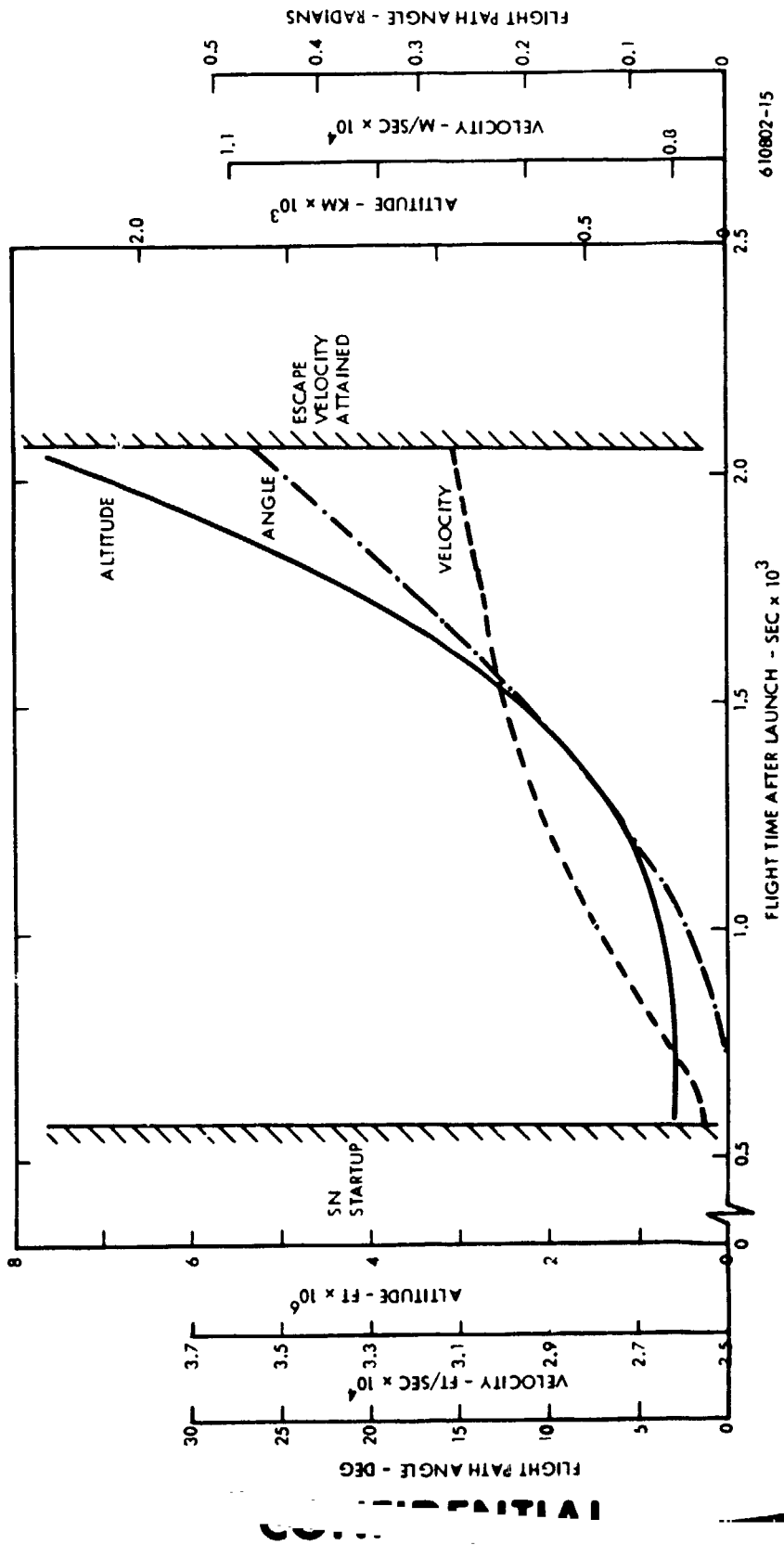

Figure 8-1. Trajectory Data of Nuclear Stage After SN Startup (Mission Model I)

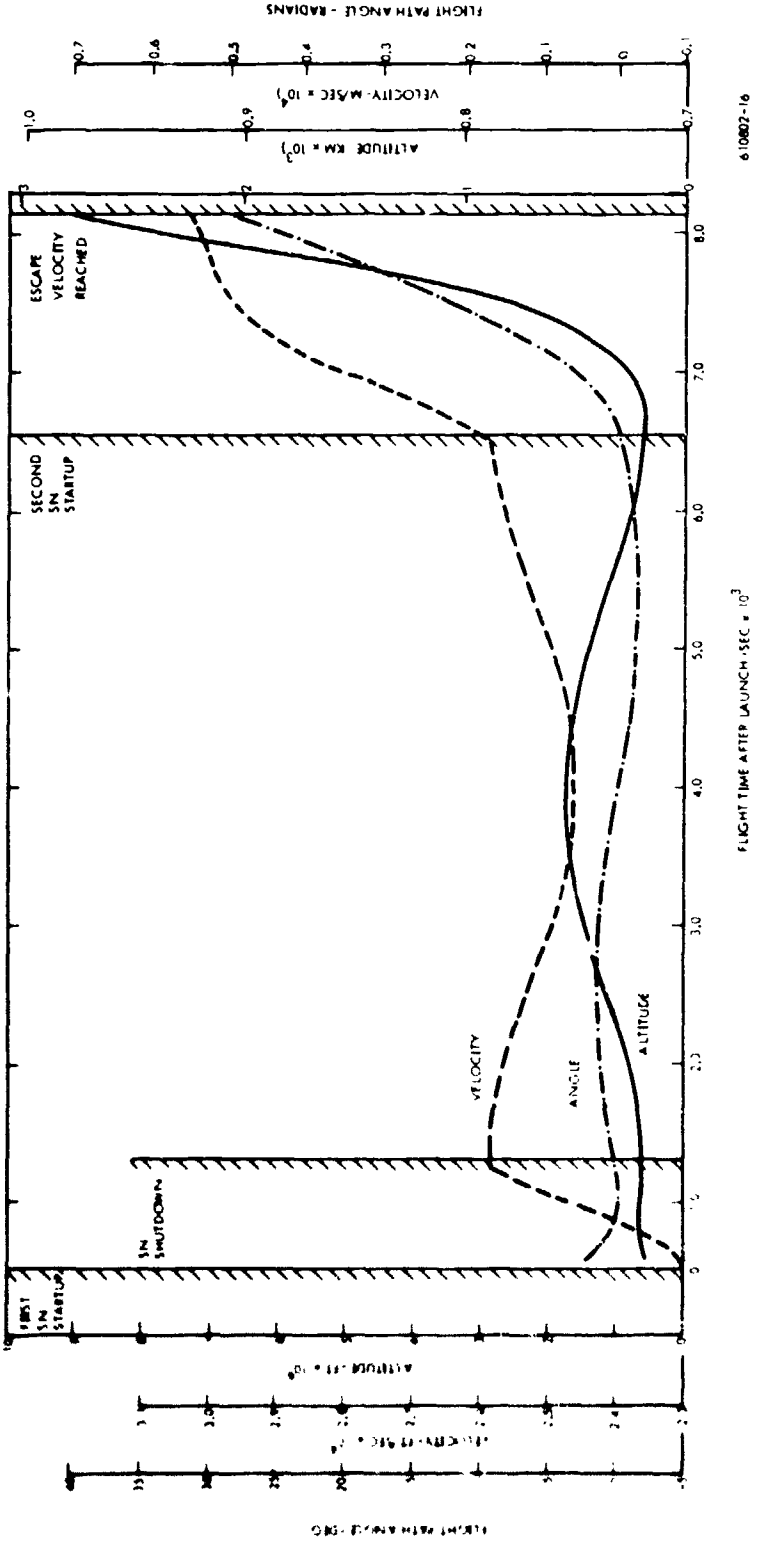

Figure 8-2. Trajectory Data of Nuclear Stage After SN Startup (Mission Model II)

conventional Saturn V booster, and kick stage deliver the interplanetary spacecraft and crew to the rendezvous orbit, where assembly of the OLV is completed. After assembly and check-out, the OLV coasts in orbit to satisfy launch window constraints. The nuclear stage is then started, and the NERVA engine operates until injection energy for the Mars transfer is achieved. The nuclear stage trajectory data are shown in Figure 8-3.

8.3 POPULATION DOSE EXPOSURES

The safety analysis of the passive re-entry approach and of the explosive destruct and ATS countermeasure systems for each of the above missions has been described in References 4 and 2, respectively. This section summarizes the radiation dose exposure to the general population as presented in these references. A direct comparison of the whole body gamma dose population exposures received under passive re-entry conditions and the exposures received following the destruct or ATS countermeasures has not been made, since different exposure models and analysis conditions were utilized. The WANL analyses (passive re-entry) used the MOREDO model, and considered the fission product inventory losses occurring by diffusion under loss-of-coolant conditions prior to actual passive disassembly of the reactor. The LMSC analyses utilized the exclusion area model for population doses and considered no depletion by fission product diffusion. Some exposures were also calculated by LMSC utilizing their mobile receptor dose model. The influence of using this alternate model is noted in the results below where data are available.

8.3.1 Passive Re-entry

The maximum population exposures for the worst case accident (Safety Index No. 1) for the three missions are summarized in Table 8-1. The number of persons exposed for the case of Mission Model II sub-orbit start is dependent on the tumbling rate of the reactor during re-entry, which affects the rate of ejection of the fuel elements out of the reactor. A slow tumbling rate results in a larger contaminated earth area with greater number of persons exposed. The expected number of exposures for Mission Model II reported in the

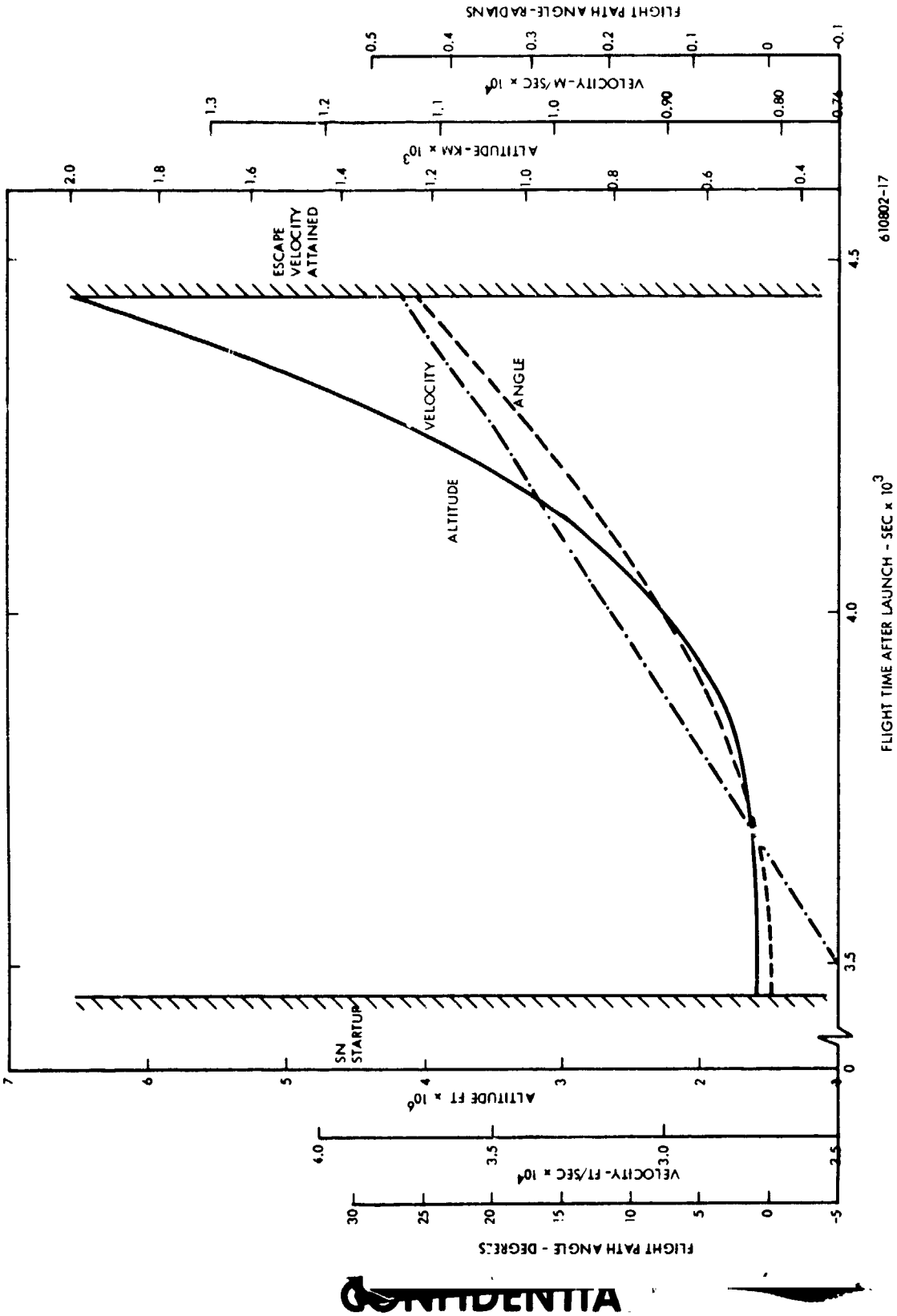

Figure 8-3. Trajectory Data of Nuclear Stage After SN Startup (Mission Model III)

TABLE 8-1

WORST-CASE POPULATION EXPOSURES FROM PASSIVE RE-ENTRY UTILIZING MOREDO DOSE MODEL

Mission		Ground Exposure Time	Probable Number of People Receiving Indicated Gamma Dose (Rems)						Man-Rems
			0.5-5	5-10	10-50	50-100	100-500	> 500	
I		4 days	106	0.489	3.52	0.580	< 0.04	< 0.04	9.05×10^2
		13 weeks	973	4.30	1.42	1.77	1.56	< 0.04	2.82×10^3
		1 year	1154	6.37	1.37	1.54	2.03	< 0.04	3.16×10^3
		30 years	1180	6.68	1.38	1.51	2.09	< 0.04	3.21×10^3
II	Suborbit	4 days	5050	260.1	179.4	87.3	63.4	3.69	$3.02 \times 10^{4**}$
		13 weeks	6550	336	198.9	84.9	88.5	6.18	$3.90 \times 10^{4**}$
		1 year	6885	354	207	84.7	90.9	7.15	$4.10 \times 10^{4**}$
		30 years	6910	357	208	84.6	91.3	7.32	$4.13 \times 10^{4**}$
	Orbit	4 days	3910	22.5	6.91	0.78	3.40	0.16	7.53×10^3
		13 weeks	13800	1480	676	10.6	2.18	3.92	4.60×10^4
		1 year	13600	1680	998	16.6	4.92	4.23	5.77×10^4
		30 years	13600	1690	1040	17.6	5.44	4.26	5.94×10^4
III		4 days	0*	0	0	0	0	0	0.103
		13 weeks	0	0	0	0	0	0	2.22
		1 year	0	0	0	0	0	0	7.59
		30 years	9.62	0	0	0	0	0	81.7

*Zero indicates a value less than 0.08 people.

**Includes only those exposures in the fuel element "plane source".

table are for the minimum tumbling rate (tumbling rate sufficient such that the core was emptied of elements when the re-entry vehicle reached 270,000 feet altitude.) The additional number of exposures external to the plane source are also included in the totals shown for the suborbit phase of Mission Model II.

Table 8-2 summarizes the expected number of persons exposed to varying dose ranges for the three missions (Safety Index No. 2). It can be seen that Mission Model II results in the greatest number of people receiving a significant dose. Note that when the probability of flight failure is considered (including the fact that only failures occurring within 7 percent of the total sub-orbital nuclear flight time result in African impacts) the expected number of exposures for the sub-orbit flight portion of the mission is very small. Thus it is the orbital portion of Mission Model II that introduces the possibility of exposing the greatest number of people to a significant dose.

Analyses of the uncertainties in the calculated values of population exposures have been made and these show that if the maximum positive uncertainties in the results were applied to the values of Table 8-I, the expected number of people exposed in each dose range would increase by not more than a factor of 2 to 3. Negative uncertainties could reduce the calculated number of exposures by as much as a factor of 100 or even greater. Thus, the analyses are considered conservative, in that the results are close to the upper limit of the possible population exposure.

Lockheed[2] has calculated the worst case exposures and the expected exposures resulting from "non-countermeasure action" using their exclusion area dose model. Their non-countermeasure case is analogous to the WANL passive re-entry approach in that no direct countermeasure action is taken at time of failure. The LMSC reference re-entry source material is considered to be 1626 fuel elements, released essentially at time of flight failure. The delay time in core disassembly and degradation time of the reactor under passive re-entry conditions due to post-operational heating has been neglected. Thus for failures from orbit start, the non-countermeasure case closely approximates the passive

TABLE 8-2

EXPECTED POPULATION EXPOSURES FROM PASSIVE RE-ENTRY UTILIZING MOREDO DOSE MODEL

Mission	Ground Exposure Time	Expected Numbers of People Receiving Indicated Dose (Rems)					
		0.5-5	5-10	10-48	50-100	100-500	> 500
I	4 days	2.65	0.0519	0.148	0.00171	0*	0
	13 Weeks	54.5	0.315	0.113	0.0996	0.0876	0
	1 Year	78.0	0.613	0.203	0.0853	0.130	0.00109
	30 Years	87.2	0.739	0.304	0.105	0.143	0.00122
II Slow Tumbling Rate	4 Days	0	0	0.0842	0.0509	0.0764	0.00771
	13 Weeks	0	0	0.0638	0.0503	0.0886	0.0164
	1 Year	0	0	0.0607	0.0511	0.0886	0.0188
	30 Years	0	0	0.0603	0.0513	0.0884	0.0192
II Fast Tumbling Rate	4 Days	0	0	0.00117	0.00221	0.0173	0.0180
	13 Weeks	0	0	0.000585	0.00186	0.0130	0.0234
	1 Year	0	0	0.000532	0.00181	0.0120	0.0244
	30 Years	0	0	0.000532	0.00181	0.0118	0.0246
II (Orbit Phase)	4 Days	168	1.01	0.206	0.0194	0.0880	0.0746
	13 Weeks	478	56.6	28	0.387	0.0590	0.179
	1 Year	483	58.0	37.5	0.619	0.134	0.193
	30 Years	489	58.7	38.4	0.504	0.299	0.196
III	4 Days	0	0	0	0	0	0
	13 Weeks	0	0	0	0	0	0
	1 Year	0	0	0	0	0	0
	30 Years	0.301	0	0	0	0	0

* Zero indicates less than 2×10^{-4} people.

re-entry approach. However, for failures from sub-orbit start (Mission Model II), the delay time in core disassembly and element ejection is important, and thus the non-countermeasure case does not accurately represent the true re-entry characteristics of the radioactive core debris.

The results for the worst-case exposures and for the expected exposures for the non-countermeasure case for all missions are presented in Tables 8-3 and 8-4, respectively. Comparison of these tables with Tables 8-1 and 8-2, show that, in general, the non-countermeasure case using the exclusion area dose model results in a lesser number of persons exposed than does the passive re-entry analysis using the MOREDO dose model. The Mission Model II sub-orbit, non-countermeasure, worst-case exposures are significantly greater than for passive re-entry, since the LMSC worst-case analysis resulted in impact of the fuel elements very close to the densely populated city of Nova Lisboa, Angola.

The Lockheed Mobile Receptor dose model[2] was applied to the analysis of the non-countermeasure case for Mission Model II. A comparison of results for the worst case accident is shown in Table 8-5. The mobile receptor results are based on the assumption the receptor has a standard deviation of 25 meters from his center of motion (i.e., the receptor has a probability of 0.606 of being within a circle of 25 meters radius about his center of motion; see Appendix C of Reference 2). The difference in the expected exposures for Mission Model II as calculated by the exclusion area and LMSC mobile receptor model is shown in Figure 8-4. It is not possible to compare the Lockheed mobile receptor exposures with those obtained by the MOREDO program because of differences between the two models.

8.3.2 Explosive Destruct

The maximum population exposures to whole body gamma doses for the worst-case accident are summarized in Table 8-6. Because of the large number of trajectory calculations required for destruct analysis, only the dose received in a 4-day exposure period was calculated. However, it would be expected that the variation of safety index values with increased dose exposure time should follow the same general trend as for the non-countermeasure case (Table 8-4). All analyses were made "lobed" destruct pattern with debris concentrated in four jets.

TABLE 8-3

WORST-CASE POPULATION EXPOSURES FROM NON-COUNTERMEASURE CASE UTILIZING EXCLUSION AREA DOSE MODEL

Mission		Ground Exposure Time	Probable Number of People Receiving Indicated Gamma Dose (Rems)						Man-Rems
			0.5-5	5-10	10-50	50-100	100-500	> 500	
I		4 days	7.70	0.425	0.344	0.043	0.034	< 0.01	48.2
		13 weeks	16.2	0.905	0.729	0.093	0.074	< 0.01	102.4
		1 year	19.4	1.085	0.850	0.109	0.085	0.011	128.7
		30 years	20.1	1.11	0.897	0.111	0.085	0.012	133.8
II	Suborbit	4 days	1.96×10^{6}	1.65×10^{5}	1.43×10^{5}	1.84×10^{4}	1.48×10^{4}	1.90×10^{3}	1.82×10^{7}
		13 weeks	2.23×10^{6}	1.93×10^{5}	1.70×10^{5}	2.17×10^{4}	1.78×10^{4}	2.22×10^{3}	2.13×10^{7}
		1 year	2.78×10^{6}	1.76×10^{5}	1.95×10^{5}	2.25×10^{4}	1.83×10^{4}	2.33×10^{3}	2.24×10^{7}
		30 years	2.31×10^{6}	1.98×10^{5}	1.79×10^{5}	2.31×10^{4}	1.85×10^{4}	2.35×10^{3}	2.23×10^{7}
	Orbit	4 days	117	6.70	5.46	0.67	0.53	0.067	6.48×10^{2}
		13 weeks	433	28.1	22.8	2.83	2.33	0.294	3.22×10^{3}
		1 year	503	33.7	26.9	3.46	2.75	0.343	3.78×10^{3}
		30 years	528	35.3	29.5	3.67	2.94	0.362	4.54×10^{3}
III		4 days	0*	0	0	0	0	0	0
		13 weeks	0.132	0	0	0	0	0	1.14
		1 year	0.344	0.018	0.015	0	0	0	2.29
		30 years	2.96	0.170	0.131	0.0165	0.013	0	19.7

* Zero indicates a value less than 0.01 people.

TABLE 8-4

EXPECTED POPULATION EXPOSURES FROM NON-COUNTERMEASURE CASE UTILIZING EXCLUSION AREA DOSE MODEL

Mission	Ground Exposure Time	Expected Number of People Receiving Indicated Gamma Dose (Rems)					
		0.5-5	5-10	10-50	50-150	150-450	450
I	4 days	0.340	0.018	0.015	0.0025	0.00029	0*
	13 weeks	2.03	0.112	0.087	0.014	0.0053	0.0014
	1 year	2.87	0.164	0.129	0.022	0.0075	0.0022
	30 years	5.13	0.290	0.224	0.038	0.013	0.0037
II	4 days	43.8	3.35	2.89	0.262	0.162	0.044
	13 weeks	89.6	6.70	5.32	0.903	0.318	0.086
	1 year	99.9	7.50	6.06	1.00	0.358	0.097
	30 years	105.0	7.50	6.72	1.11	0.377	0.101
III	4 days	0*	0	0	0	0	0
	13 weeks	0.00592	0.00026	0.00019	0	0	0
	1 year	0.0168	0.00760	0.00054	0	0	0
	30 years	0.203	0.0121	0.00823	0.00111	0.00033	0

*Zero indicates a value less than 1.0×10^{-4} people.

TABLE 8-5

COMPARISON OF EXCLUSION AREA AND MOBILE RECEPTOR DOSE MODELS - MISSION MODEL II NON-COUNTERMEASURE CASE

Failure Time	Dose Model	Probable Number of People Receiving Indicated 4-Day Gamma Dose (Rems)***						Man-Rems
		0.05-5	5-10	10-50	50-100	100-500	> 500	
1091.7 *	Excl. Area	4969	428	354	470	37.8	5.10	4.12×10^4
1092.3	Mobile Recep.	4120	440	577	160	53	< 0.01	5.98×10^4
1092*	Excl. Area	1.96×10^6	1.65×10^5	1.43×10^5	1.84×10^4	1.48×10^4	1.90×10^3	1.82×10^7
	Mobile Recep.	1.65×10^6	1.62×10^5	2.30×10^5	6.13×10^4	2.04×10^4	1.05×10^2	2.34×10^7
6553**	Excl. Area	117.0	6.70	5.46	0.67	0.53	0.067	6.48×10^2
	Mobile Recep.	176	28	16	<0.01	<0.01	< 0.01	1.17×10^3

*Failure from Sub-orbit Start Phase of Mission Model II.
**Failure from Orbit Start Phase of Mission Model II.
***Assumes Failure Does in Fact Occur at Indicated Failure Time (Seconds) After Launch.

TABLE 8-6

WORST-CASE FOUR-DAY POPULATION EXPOSURES FROM EXPLOSIVE DESTRUCT COUNTERMEASURE

Mission	Probable Number of People Receiving Indicated Gamma Dose (Rems)						
	0.5-5	5-10	10-50	50-100	100-500	500	Man-Rems
I	0.876	0*	0	0	0	0	2.50
II Suborbit	4640	222	221	12.7	1.19	0.068	2.57×10^4
Orbit	300.8	3.67	1.05	0.0170	0.0128	0	2.92×10^2
III**	0.148	0.009	0	0	0	0	0.986

*Zero indicates a value less than 0.01 people.

**Results for 30 year exposure period. 4 day, 13 week, 1 year dose periods result in less than 0.01 people exposed.

TABLE 8-7

WORST-CASE BETA SKIN DOSE POPULATION EXPOSURES FROM EXPLOSIVE DESTRUCT COUNTERMEASURE

Mission	Probable Number of People Receiving Indicated Beta Skin Dose (Rods)						
	10-100	100-600	600-2000	2000-4000	4000-10,000	10,000 to 30,000	30,000 to 100,000
I	930	94	0*	0	0	0	0
II Suborbit	10,000	3400	1040	350	270	130	30
Orbit	No Data →						
III	No Data. Maximum beta dose (1 cm^2 skin disk) possible is less than 10 rods.						

*Zero indicates a value less than 0.01 people.

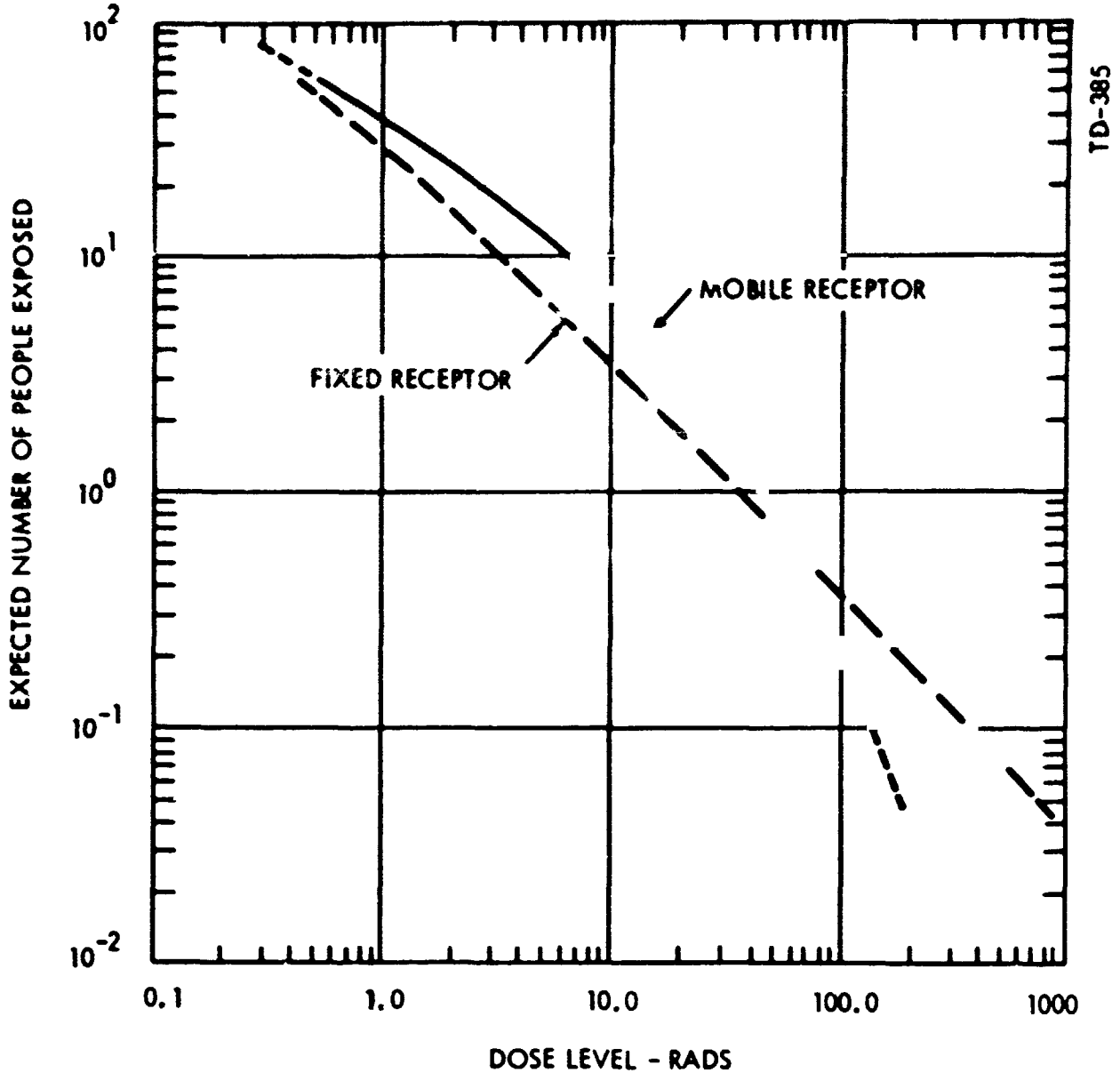

Figure 8-4. Expected Exposures versus Dose Level for Entire Mission Model II. Mobile Receptors with Center of Motion = 25 Meters (Non-Countermeasure Case)

The beta dose skin exposures for the worst case are summarized in Table 8-7. The values represent the dose delivered to a 1 cm^2 disk of skin. The skin depth dose (at 100μ depth) was also calculated, and the results generally were about 100 times as high as the disk dose. Data are insufficient to determine which of the two methods of representing dose from a particle will be of greater value in correlating biological damage. The gastro-intestinal tract interaction probabilities were analyzed, but were found to be small (less than a factor of 3000) in comparison with skin contact exposure probability. The dose levels for gastrointestinal exposures are generally near those for skin (within a factor of about 2), so that additional exposures by this route are considered negligible.

The expected population exposures for each mission (Safety Index No. 2) are summarized in Table 8-8.

8.3.3 Auxiliary Thrust System

Safety indices analogous to those defined for the passive re-entry (or non-countermeasure) and destruct have been defined[2]. The basic assumption for deriving the ATS safety indices is that when the ATS operates properly, zero exposures result; when it does not, the number of exposures and inventory are nearly identical to those of the non-countermeasure case.

The reliability of the ATS system is used to calculate both the exposures given a failure (given failure at maximum impact inventory for Safety Index No. 1) and the expected number of exposures for the entire mission (Safety Index No. 2). If the reliability of the ATS at some time, t, is R_t, then $(1-R_t)$ is the probability that the ATS will not work. Thus, the expected number of exposures given a failure is merely:

$$N_{ats} = N(1 - R_t) = (1 - R_t) \sum_{i=1}^{n} N_i$$

where:

N_{cts} = number of exposures given a failure when the ATS system is carried

N = number of exposures given a failure in the non-countermeasure case

n = the number of regions in which impact occurs

TABLE 8-8

EXPECTED 4-DAY POPULATION EXPOSURES FROM
EXPLOSIVE DESTRUCT COUNTERMEASURE

Mission	Expected Number of People Receiving Indicated Gamma Dose (Rems)					
	0.5-5	5-10	10-50	50-150	150-450	450
I	0.0573	0.0221	0.000596	0*	0	0
II	70.1	1.32	0.58	0.0413	0.0085	0.0002
III	0	0	0	0	0	0

*Zero indicates a value less than 1.0×10^{-4} people.

Astronuclear Laboratory
WANL-TME-1506

Similarly, if the ATS reliability is assumed to be constant throughout the flight, the expected exposures for the entire mission will be:

$$E_{ats} = (1 - R_t) E_{non\text{-}countermeasure}$$

A reliability of $R_t = 0.95$ was assigned by LMSC[2] in the safety analysis of ATS operation. This reliability was assumed to be constant throughout the missions. Thus the calculated exposures values for ATS operation are equal simply to the values of the non-countermeasure case exposures (Tables 8-3 and 8-4) times (1-0.95); that is, the expected ATS exposures are 1/20th of the non-countermeasure exposure values. These expected ATS exposures for the worst-case accident and for the entire mission are tabulated in Tables 8-9 and 8-10, respectively. Values for Mission Model II by the mobile receptor model are included for comparison.

8.3.4 Nuclear (Self) Destruct

A detailed safety analysis of the nuclear destruct countermeasure concept as applied to the three mission models has not been made. However, a preliminary study was made by the NUS Corporation to present a comparison of the radiological consequences between the high explosive destruct and nuclear destruct concepts[5]. The analysis is based on experimental data obtained from the APG-3 and KIWI-TNT experiments, and utilizes the exposure probabilities and radiological dose models that are summarized in Chapter 7.0 of this report.

The characteristics of the fuel debris following nuclear and explosive destruct will exhibit several differences. The most important differencesin the characteristic that will affect population exposures are the size and number distribution of particles, the fission product inventory lost by vaporization, and the fission product distribution in the debris particles.

The NUS analysis considered a sub-orbital start mission of an NRX-size reactor, with failure and destruct occurring 1090 seconds after launch (nearly identical to Mission Model II). The radiological doses are derived from consideration of the particle ground density and the fission product activity per particle. For explosive destruct, the inventory of fission products was assumed uniformly distributed throughout the particle volume. For nuclear destruct, the

TABLE 8-9

WORST-CASE 4-DAY POPULATION EXPOSURES FROM ATS COUNTERMEASURE

Mission		Dose Model	0.5-5	5-10	10-50	50-100	100-500	> 500	Man-Rems
I		Excl. Area	0.385	0.0213	0.0172	0*	0	0	2.41
II	Sub-orbit	Excl. Area	9.80×10^4	8.25×10^3	7.15×10^3	9.20×10^2	7.40×10^2	95	9.10×10^5
		Mobile Recep.	8.25×10^4	8.10×10^3	1.15×10^4	3.07×10^3	1.02×10^3	5.25	1.17×10^6
	Orbit	Excl. Area	5.85	0.335	0.273	0.0335	0.0265	0	32.4
		Mobile Recep.	8.80	1.40	0.80	0	0	0	58.7
III**		Excl. Area	0.148	0.009	0	0	0	0	0.986

*Zero indicates a value less than 0.01 people.

**Results for 30 year exposure period. 4 day, 13 week, 1 year dose periods result in less than 0.01 people exposed.

TABLE 8-10

EXPECTED 4-DAY POPULATION EXPOSURES FROM ATS COUNTERMEASURE

Mission	Dose Model	0.5-5	5-10	10-50	50-150	150-450	450
I	Excl. Area	0.0170	0.00090	0.00074	0.00013	0*	0
II	Excl. Area	2.19	0.168	0.145	0.0131	0.0081	0.0022
	Mobile Recep.	2.31	0.278	0.299	0.0392	0.0040	0.00022
III**	Excl. Area	0.01017	0.000606	0.000415	0	0	0

*Zero indicates a value less than 1.0×10^{-4} people.

**Results for 30 year exposure period. 4 day, 13 week, 1 year dose periods result in less than 0.01 people exposed.

fission products were assumed uniformly distributed over the surface of the particle, and using graphical data from the TNT test on number versus size distribution the inventory per particle was calculated.

Explosive destruct results in a large proportion of very small particles, with maximum particle size of 26.9 mm. Nuclear destruct (TNT Test) created a lesser total number of particles, but with a significant number of fragments (ca 9600) in the 56 to 100 mm size range. These larger fragments account for approximately 96 percent of the total activity of the fragments.

The safety analysis showed that the external whole body gamma dose exposures resulting from nuclear destruct are at least 50 times greater than those which could occur from explosive destruct. The population dose and the average individual dose for persons exposed in Africa are:

	Man-Rad	Rad/Person
Explosive Destruct	3.2×10^3	0.054
Nuclear Destruct	4.4×10^5	7.5

Analysis of gastrointestinal tract doses shows the explosive destruct system offers less dose for a given exposure probability than does the nuclear destruct. This analysis considered a two-thirds depletion of the fission product inventory due to vaporization in the case of nuclear destruct based on the KIWI-TNT results. However, any loss of fission products condensed on the surface of the nuclear destruct debris during re-entry has been neglected. An appreciable loss by ablation or burn-up during re-entry could significantly affect the above conclusions. The reactor operating and post-operational temperature effects may significantly alter the particle size and the size distribution for either destruct system. In addition, the explosive destruct tests conducted to date do not adequately reproduce conditions that exist at time of destruct with a flight configuration system. Similarly, the data from KIWI-TNT does not provide adequate data as to the capabilities and requirements for nuclear destruct. Thus, a comparison of the radiological consequences to the population due to the two destruct countermeasures cannot be evaluated with a high degree of confidence.

8.4 REFERENCES

1. Lockheed Missiles and Space Company, Preliminary Guidelines for the Preparation of Nuclear Vehicle Flight Safety System Performance Specifications, LMSC A664243, Sunnyvale, California, July 1964 (U).

2. Lockheed Missiles and Space Company, ROVER Flight Safety Program Preliminary Review, Vol. I, Safety Analysis Report - Evaluation of Destruct and Auxiliary Thrust Systems, LMSC - A778908, March 30, 1960 (CRD).

3. Space Nuclear Propulsion Office - Washington, Format for Presenting Final Results -- Volumes I and II, Memorandum from R. S. Decker, Chief, Safety Branch, SNPO, August 13, 1965.

4. Westinghouse Astronuclear Laboratory, ROVER Flight Safety Program - Preliminary Review, Volume II, Safety Analysis Report - Evaluation of Passive Re-entry Approach (U), September 30, 1965 (CRD).

5. DeAgazio, A. W., Comparison of Nuclear and Explosive Destruct Concepts for Nuclear Rocket Engines, NUS Corporation, Washington, D. C., NUS-277, May 1966 (U).

12